

**Investigating the role of lymph node
stromal cells and miR-132 in regulating
TLR4 agonist adjuvant efficacy**

Anne Leonor Marie Thuery

PhD

University of York

Biology

December 2015

Abstract

Lymph nodes (LNs) are highly organized structures containing adaptive and innate immune cells supported by a network of specialized stromal cells. These stromal cells provide the structural basis for immune cell migration, localization and specialized microenvironments for effector function through the production of specific chemokines. Crosstalk between stroma and haematopoietic cells is important in regulating the efficacy of the immune response in part through their plastic response to inflammation and capacity to generate specialized structures, including germinal centres (GCs). The mechanisms driving tissue remodelling and GC formation in LNs are unclear. Understanding the timing and molecular mechanisms leading to stromal cell reorganization will help generate novel vaccination strategies that can control and regulate immune responses. An adjuvant is a non-antigenic substance that when added to vaccines, enhances the immune response to inoculated antigens. TLR agonists have been shown to be potent second-generation adjuvants. TLR4 agonist adjuvants induce rapid LN remodelling through the loss of B cell follicles and the formation of a ring-like structure in the cortex; surprisingly this was not due to a loss of CXCL13 production by the stromal cells. After forming this ring, large numbers of new B cell follicles appear in the LN paracortex. The molecular mechanisms leading to this reorganization was investigated. TLR4 activation and signalling has to be tightly controlled to avoid uncontrolled inflammation and enable tissue repair. miRNAs constitute a key component in a negative feedback loop in innate immune responses. Deficiency in a TLR4-induced miRNA leads to an altered immune response and changes to adjuvant induced tissue remodelling. By using a simple antigen challenge model, it was possible to determine a novel molecular mechanism controlling LN remodelling and vaccine efficacy.

Table of Contents

Abstract	2
Table of Contents	3
List of Figures	9
List of Tables	13
Acknowledgments	14
Declaration	15
Chapter 1: Introduction	16
1.1. Structure of adult murine lymph nodes	16
1.2. Function of adult murine LNs	17
1.2.1. Lymph node entry and exit.....	19
1.2.2. Immune response within LNs	20
1.3. Development of stromal networks	22
1.3.1. Lymphoid stromal organizer cells.....	22
1.3.2. FDC differentiation and role	24
1.3.3. FRC development and role.....	24
1.3.4. MRC development	25
1.4. Role of stroma in immune responses	27
1.5. LN changes during inflammation	28
1.5.1. LN hypertrophy	28
1.5.2. LN remodelling	29
1.6. TLR signalling pathways	30
1.7. Adjuvants in biology	31
1.7.1. Principles of vaccination.....	31
1.7.2. The discovery of adjuvants.....	32
1.7.3. Aluminium-based adjuvants	33
1.7.4. Novel adjuvants: TLR4 agonist adjuvants.....	34
1.7.5. Other adjuvants	35
1.8. MicroRNAs: regulators of the immune response	37
1.8.1. miRNAs biogenesis.....	38
1.8.2. miRNAs function	40
1.8.3. miR-132	40
1.9. Summary and aims	43
1.10. Hypothesis	43

1.11. Specific aims	43
Chapter 2: Materials and Methods	45
2.1. Reagents.....	45
2.2. Animals	50
2.3. Adjuvant immunizations.....	50
2.4. Sample collection.....	51
2.5. Enzymatic digestion of lymph nodes.....	51
2.6. FRC culture and treatment of cells.....	52
2.7. Bone Marrow Dendritic Cell isolation and culture.....	52
2.8. Flow cytometry procedure	52
2.8.1. Surface marker antibody staining	52
2.8.2. Intracellular staining.....	53
2.8.3. Viability determination	53
2.8.4. Quantifying cell numbers	53
2.9. Cell sorting	59
2.10. Immunohistochemistry	59
2.10.1. Sample preparation and cryosectioning.....	59
2.10.2. Immunofluorescent staining.....	59
2.10.3. Confocal imaging.....	60
2.10.4. Image quantification.....	60
2.11. Antibody ELISA	62
2.11.1. Sample preparation	62
2.11.2. Measuring serum antibody titres	62
2.11.3. Measuring serum antibody avidity	62
2.12. Quantitative PCR.....	63
2.12.1. RNA extraction.....	63
2.12.2. Total complementary DNA synthesis.....	63
2.12.3. Specific miRNA complementary DNA synthesis.....	63
2.12.4. Primer design	64
2.12.5. qPCR reaction	64
2.12.6. Melt curve	65
2.12.7. qPCR analysis	65
2.13. CD11c+ cells depletion.....	67
2.14. TNF α inhibition	67
2.15. Statistics.....	67
Chapter 3: TLR4 agonists induce LN remodelling.....	68

3.1. Introduction	68
3.1.1. Initiation of LN hypertrophy.....	68
3.1.2. LN architecture changes	69
3.1.3. Summary.....	69
3.1.4. Aims	69
3.2. Establishing a model of adjuvant mediated LN remodelling	70
3.3. Effect of adjuvants on LN remodelling.....	73
3.3.1. Treatment induces LN hypertrophy.....	73
3.3.2. Treatment induces an increase in immune cells.....	73
3.3.3. Treatment effect on B and T cell zones	76
3.3.4. Stroma in lymph node remodelling	79
3.4. Rapid lymph node hypertrophy	83
3.4.1. Quantifying immune cell populations.....	83
3.4.2. Early remodelling of B cell follicles.....	83
3.4.3. Effect of treatment on stromal architecture	87
3.4.4. Quantifying stromal cell populations.....	87
3.5. Role of lymphocytes in LN expansion	91
3.6. Role of CD11c expressing cells in LN expansion	91
3.7. Summary of findings.....	94
3.8. Discussion	94
3.8.1. TLR4 adjuvants drive LN hypertrophy and remodelling	94
3.8.2. Immunization leads to changes to LN structure and cell numbers	95
3.8.3. TLR4 adjuvants drive a dissolution of B cell follicles.....	95
3.8.4. Initiation of LN expansion.....	96
3.8.5. Conclusion.....	97
Chapter 4: miR-132 is a regulator of the immune response	98
4.1. Introduction	98
4.1.1. Macrophages in LNs.....	98
4.1.2. Role of LN MRCs	99
4.1.3. MicroRNAs effect on the immune response in LNs.....	100
4.1.4. miR-132 in regulating the immune response.....	100
4.1.5. Summary.....	101
4.1.6. Aims	102
4.2. Stroma responds to TLR stimulation	102
4.2.1. Expression of TLRs by stromal cells.....	102
4.2.2. Enzymatic isolation of mouse LN stromal cells	102
4.2.3. TLR4 expression in FRCs.....	102

4.2.4.	FRCs respond to a wide range of TLR agonists.....	106
4.2.5.	TLR mediated gene expression in FRCs.....	106
4.3.	TLR4 signalling regulates cytokines and miR-132 expression	109
4.3.1.	Gene expression in FRCs.....	109
4.3.2.	LPS treatment of isolated B cells.....	109
4.3.3.	Decreased response in miR-132 ^{-/-} FRCs to TLR stimulation	109
4.4.	Loss of miR-132 modulates LN structure	113
4.5.	Adjuvant induced hypertrophy in miR-132^{-/-} mice.....	113
4.5.1.	Treatment induces an increase in immune cells.....	113
4.5.2.	miR-132 regulates B cell follicle remodelling	113
4.5.3.	Role of miR-132 in stromal remodelling	114
4.6.	Remodelling kinetics in miR-132^{-/-} mice	122
4.6.1.	Dissolution of LN architecture	122
4.6.2.	Normal stromal networks in miR-132 ^{-/-} mice.....	122
4.7.	Immunization effect on macrophages	128
4.8.	Marginal reticular cell network remodelling.....	128
4.9.	MRC differentiation into FDCs.....	132
4.10.	Role of TNFα in follicle structure	136
4.11.	Analysis of miR-132 mediated transcription	136
4.11.1.	Dendritic cell regulation by miR-132.....	136
4.11.2.	Treatment effect on gene expression in total LNs.....	137
4.12.	Remodelling at 6 months post boost.....	137
4.12.1.	LN structure 6 months post boost.....	137
4.12.2.	LN structure 3 day boost post 6 months post boost.....	137
4.13.	Haematopoietic and stromal contribution to remodelling.....	143
4.14.	Summary of findings.....	146
4.15.	Discussion	146
4.15.1.	Stromal cells respond to TLR stimulation.....	146
4.15.2.	miR-132 is up-regulated in LNs upon stimulation.....	147
4.15.3.	miR-132 deficiency leads to changes in LN structure	147
4.15.4.	Macrophage and MRC migration in miR-132 ^{-/-} mice.....	149
4.15.5.	MRC differentiation and potential mechanisms of remodelling	150
4.15.6.	TNF α is critical in B cell follicle formation but not remodelling	151
4.15.7.	LN structure 6 months after immunization	151
4.15.8.	Stromal and haematopoietic contribution of miR-132	151
4.15.9.	Conclusion.....	152

Chapter 5: Consequence of TLR4 mediated remodelling on the immune

response	153
5.1. Introduction	153
5.1.1. Effect of LN hypertrophy on B cell follicles	153
5.1.2. GC formation	153
5.1.3. Plasma cells and antibody production	157
5.1.4. Summary	158
5.1.5. Aims	158
5.2. Adjuvant effect on AICDA expression in total LNs	159
5.3. Immune cell analysis	159
5.4. OVA specific antibody production	164
5.4.1. Antibody titration at day 24	164
5.4.2. Rapid antibody production post treatment	164
5.4.3. Antibodies at 6 months, 3 days post boost	164
5.4.4. Antibody production in chimeras	165
5.5. Summary of findings	170
5.6. Discussion	170
5.6.1. GLA-SE treatment leads to an increase in AICDA and specific cell types	170
5.6.2. miR-132 deficiency leads to a rapid formation of GCs and production of antibodies	171
5.6.3. Absence of miR-132 leads to a polarization of the immune response	172
5.6.4. miR-132 has no role on the memory response	172
5.6.5. Conclusion	173
Chapter 6: General Discussion	174
6.1. Summary of findings and relevance	174
6.1.1. TLR4 adjuvants induce rapid LN remodelling	174
6.1.2. MiR-132 is a regulator of the immune response to adjuvants	174
6.1.3. Consequence of LN remodelling on the immune response	175
6.2. Conclusion and schematic of miR-132 role in remodelling	175
6.3. Outstanding questions and future work	179
6.3.1. Role of MRCs	179
6.3.2. MiR-132 effect on the breadth of the immune response	179
6.3.3. Effect of miR-132 inhibition on other microRNAs	179
6.3.4. TLR4 as a target	182
6.3.5. Determining which cell types are indispensable in LN remodelling	182
6.3.6. How do changes in LN help develop better adjuvants?	183
Definitions	184

Bibliography..... 191

List of Figures

Figure 1.1: Lymph node structure and organization.....	18
Figure 1.2: Different stages of LN formation.	23
Figure 1.3: LN stromal cells and their interactions with immune cells.	26
Figure 1.4: miRNA synthesis and function within a cell.....	39
Figure 1.5: miRNAs regulate TLR4 signalling.....	42
Figure 1.6: Schematic illustrating the specific aim of the project.	44
Figure 2.1: Accucheck beads were used to determine cellularity and a live-dead marker to determine viability.	55
Figure 2.2: Gating strategies for identifying stromal cell subsets.	56
Figure 2.3: Gating strategies for identifying adaptive immune cell types.	57
Figure 2.4: Gating strategies for identifying innate immune cell types.....	58
Figure 2.5: Cell profiler B cell follicle quantification pipeline.	61
Figure 2.6: Melt curve analysis to confirm product specificity plots fluorescence vs Derivative fluorescence.	66
Figure 3.1: LN architecture when treated with antigen/adjuvant complexes in the flank.	71
Figure 3.2: LN architecture when treated with antigen/adjuvant complexes in the hock.	72
Figure 3.3: Effect of different adjuvants on lymph node size.....	74
Figure 3.4: Effect of adjuvants treatment on immune cells.	75
Figure 3.5: Dynamic remodelling of the LN when treated with different antigen/adjuvant complexes.....	77
Figure 3.6: Quantification of histology results with Cell Profiler.	78
Figure 3.7: Architecture of the reticular network in mouse LN, and the dynamic remodelling when treated with antigen/adjuvant.....	80
Figure 3.8: Flow cytometry profiles of lymph node stromal subsets freshly isolated from lymph nodes of individual mice.....	81

Figure 3.9: Effect of adjuvants on stromal cell and endothelial populations.....	82
Figure 3.10: Time course of OVA/GLA-SE vs. OVA/Alum and the effect on immune cell types.	84
Figure 3.11: LN architecture at different time points.	85
Figure 3.12: Quantification of histology results with Cell Profiler.	86
Figure 3.13: Stromal network architecture in mouse LN when treated with OVA/Alum.	88
Figure 3.14: Stromal network architecture in mouse LN when treated with OVA/GLA-SE.....	89
Figure 3.15: Time course of OVA/GLA-SE vs. OVA/Alum and the effect on stromal cell types.	90
Figure 3.16: Architecture of the reticular network in Rag ^{-/-} mouse LNs, and the dynamic remodelling when treated with antigen/adjuvant.....	92
Figure 3.17: CD11c expressing cell effect on remodelling when treated with antigen/adjuvant.....	93
Figure 4.1: Expression of Toll Like Receptors by stromal cells.....	103
Figure 4.2: Flow cytometry profiles of lymph node stromal subsets freshly isolated from lymph nodes of individual mice after culturing.....	104
Figure 4.3: LPS treatment effect on TLR4 expression in FRCs.....	105
Figure 4.4: Effect of different TLR agonists on cultured FRCs' gene expression.	107
Figure 4.5: FRC response is TLR mediated.....	108
Figure 4.6: Effect of TLR4-agonist adjuvants on isolated FRCs gene expression or on total LN.....	110
Figure 4.7: Role of miR-132 in B cells response to adjuvants.	111
Figure 4.8: Effect of TLR4-agonist adjuvants on WT or miR-132 ^{-/-} cultured FRCs gene expression.	112
Figure 4.9: Comparison of WT and miR-132 ^{-/-} naïve LNs.....	115
Figure 4.10: Effect of adjuvants on adaptive cell populations in WT and miR-132 ^{-/-} mice at day 24.....	116

Figure 4.11: Effect of adjuvants on innate cell populations in WT and miR-132 ^{-/-} mice at day 24.....	117
Figure 4.12: B and T cell zones in WT vs. miR-132 ^{-/-} mouse LN.	118
Figure 4.13: Quantification of histology results with Cell Profiler.	119
Figure 4.14: Architecture of the stromal network in WT vs. miR-132 ^{-/-} mouse LNs...	120
Figure 4.15: Effect of adjuvants on stromal cell populations in WT and miR-132 ^{-/-} mice at day 24.....	121
Figure 4.16: Effect of adjuvants on immune cell populations in WT and miR-132 ^{-/-} mice at days 3 and 7.....	123
Figure 4.17: LN architecture when treated with antigen/adjuvant complex at days 3 and 7.....	124
Figure 4.18: Quantification of histology results with Cell Profiler.	125
Figure 4.19: LN stroma network when treated with antigen/adjuvant complex at days 3 and 7.....	126
Figure 4.20: Effect of adjuvants on stromal cell populations in WT and miR-132 ^{-/-} mice at days 3 and 7.....	127
Figure 4.21: Close up of the architecture in mouse LNs when treated with antigen/adjuvant at day 24.	129
Figure 4.22: Effect of adjuvants on miR-132 expression in MRCs and on MRC expansion in WT and miR-132 ^{-/-} mice.....	130
Figure 4.23: Close up of the architecture in mouse LNs when treated with antigen/adjuvant at day 24.	131
Figure 4.24: Quantification of MRC kinetics.	133
Figure 4.25: Investigating CXCL12 and CXCL13 expression in total LNs and in MRCs.....	134
Figure 4.26: Investigating CXCR5 expression in B cells by flow cytometry.	135
Figure 4.27: Role of TNF α in regulating the remodelling process.....	138
Figure 4.28: Role of miR-132 in Bone Marrow DCs response to adjuvants.....	139
Figure 4.29: Role of miR-132 in stromal and immune cells' response to adjuvants....	140

Figure 4.30: Analysis of LNs 6 months post immunization.	141
Figure 4.31: Analysis of LNs boosted for 3 days 6 months post immunization.....	142
Figure 4.32: Flow cytometry on reciprocal Bone Marrow Chimeras to study the stromal vs. haematopoietic contribution of miR-132.	144
Figure 4.33: Histology on reciprocal Bone Marrow Chimeras to study the stromal vs. haematopoietic contribution of miR-132.....	145
Figure 5.1: The Germinal Centre reaction.	156
Figure 5.2: Effect of TLR4-agonist adjuvant on AICDA expression in WT and miR-132 ^{-/-} mice.....	160
Figure 5.3: Effect of adjuvants on B cell populations in WT and miR-132 ^{-/-} mice at day 24.....	161
Figure 5.4: Effect of adjuvants on cell populations in WT and miR-132 ^{-/-} mice at days 3 and 7.....	162
Figure 5.5: Germinal centre formation post immunization in WT and miR-132 ^{-/-} mice.	163
Figure 5.6: Antibody titration and avidity in WT and miR-132 ^{-/-} mice.	166
Figure 5.7: Antibody production in WT and miR-132 ^{-/-} mice after 3 or 7 days of OVA/GLA-SE treatment.	167
Figure 5.8: Antibody production in 6 month prime and boost mice.....	168
Figure 5.9: Antibody production in reciprocal bone marrow chimeras.....	169
Figure 6.1: Schematic of changes to LN structure in WT mice upon OVA/GLA-SE treatment.	177
Figure 6.2: Schematic of changes to LN structure in WT mice upon OVA/GLA-SE treatment.	178
Figure 6.3: The “stop and wait” model.....	181

List of Tables

Table 1.1. List of licensed adjuvants.	37
Table 2.2. Adjuvants	45
Table 2.3. Vaccines	45
Table 2.4. Primary antibodies	46
Table 2.5. Secondary antibodies	48
Table 2.6. Primers	49

Acknowledgments

I would like to thank the many people who have helped me in these years for the preparation of my thesis.

I am extremely thankful to my supervisor Dr. Mark Coles for his encouragement and guidance. I would like to express my gratitude to my training advisory panel, Professor Norman Maitland, Professor Antal Rot and Dr. Adrian Mountford for their advice, support and critical eye. I am grateful to everyone in York and particularly in the CII for making this a wonderful place to work. I would like to particularly thank Amy Sawtell for aiding me upon starting, the Kaye lab for their helpful suggestions and support, Elizabeth Gothard, my deskmate, for her statistics help and everyone else in the Coles lab. I would not have been able to do this work without the help of Rita Pinter and the rest of the BSF staff and also the Technology Facility.

This thesis was possible thanks to the European Commission and is part of the Marie Curie Initial Training Network funded under Framework Programme 7. I am deeply grateful to everyone that was part of the network for their help and support. It was a great opportunity to have other people that could offer support and advice.

Finally, I would like to thank my friends and family and particularly Olivier Preham for always being there and being understanding and giving me the courage to finish this thesis.

Declaration

I, Anne Leonor Marie Isabel Thuery, declare that this thesis is a presentation of original work and I am the sole author. This work has not previously been presented for an award at this, or any other, University. All sources are acknowledged as References.

Chapter 1: Introduction

1.1. Structure of adult murine lymph nodes

Secondary Lymphoid Organs (SLOs) such as the spleen or lymph nodes (LNs) are specialized immunological tissues that facilitate efficient high affinity immune responses. LNs are located throughout the body in strategic lymphatic drainage points and contain an abundance of haematopoietic cells. LNs are found at the interface between the blood and lymphatic systems and enable the initiation of the immune response as they bring Antigen-Presenting Cells (APCs) presenting antigen in contact with circulating lymphocytes. The main entry points for lymphocytes into the LNs is through High Endothelial Venules (HEVs) formed from blood vessels [1]. Lymphocytes circulate through the LNs and exit through the HEVs after surveying the LNs and then enter the blood. LNs permit the efficient detection of infection or tissue damage by bringing lymphocytes and antigen together. LNs are composed of the cortex, the paracortex and the medulla [2]. B cell follicles, which are the sites of high affinity antibody production, are found in the cortex [3]. The paracortex is composed of the T cell zone, where interactions between Dendritic Cells (DCs) and T cells happen [4]. The medullary sinus makes up the medulla where cells exit the LN, antigen is cleared from the LN and plasma cells reside. LNs are highly organized structures; stromal cells create the scaffold within the LN on which immune cells migrate, and provide compartmentalized architecture that is required for protective immunity [5].

The localization of immune cells within these structures results from chemokine expression by different stromal cell populations. Fibroblastic Reticular Cells (FRCs), or T cell zone stroma, express CCL19 and CCL21 that bind to the common receptor CCR7 which is highly expressed on T cells and on activated DCs forming the paracortex of the LN [6, 7]. FRCs secrete extracellular matrix that provides the network for cellular interactions, form conduit structures and surround the blood vascular network. In contrast, B cells reside in follicular structures in the outer cortex with a stromal network that matures into Follicular Dendritic Cells (FDCs) that express high levels of CXCL13 [8]. In the subcapsular zone, closely associated with the lymphatic endothelial vessels, Marginal Reticular Cells (MRCs) support macrophages, Lymphoid Tissue inducer cells (LTi), Natural Killer cells (NK), NKT cells and $\gamma\delta$ T cells, which are primed to respond to infection [9-11]. These different stromal cell networks can be visualized through the expression of Reticular Fibroblasts and Reticular Fibres (ER-TR7), smooth muscle actin

and desmin on FRCs, Complement Receptor 1 and 2 (CR1/CR2 or CD21/35) on FDCs and Receptor Activator of Nuclear Factor kappa-B ligand (Rank-L) or Mucosal Vascular Addressin Cell Adhesion Molecule-1 (MAdCAM-1) on MRCs [9-11]. These populations and their localization are shown in Figure 1.1 [6].

1.2. Function of adult murine LNs

LNs are important organs required for the proper development of an immune response leading to pathogen clearance. By bringing the different factors required in close contact, LNs increase the chances of specific immune cells recognizing the antigen [1]. Efficient immune responses are facilitated by LN architecture, characterized by the T cell and DC domain and the B cell domain. Until recently, the mechanisms that control the efficacy of the immune response were thought to be mediated by the interactions between leukocytes. In the past couple of years, it has been shown that non-haematopoietic cells such as lymphoid stroma and the lymphatic and blood vasculatures play important roles in modulating the immune response [12].

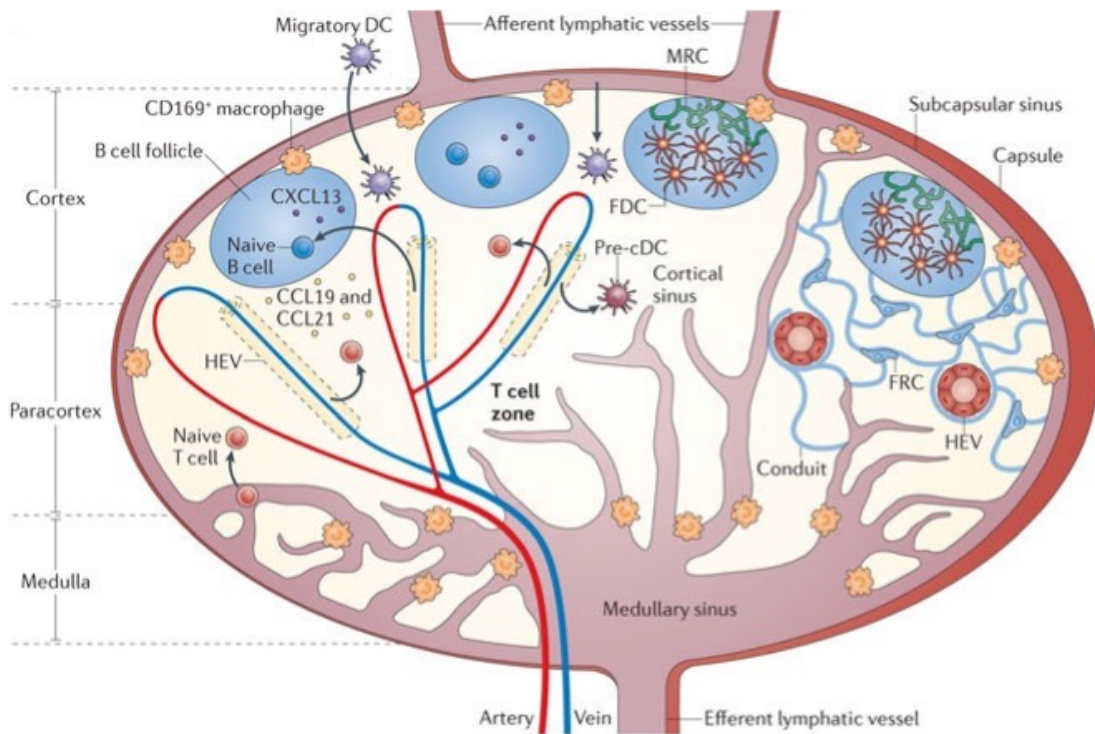


Figure 1.1: Lymph node structure and organization.

LNs are divided into three distinct regions, the cortex, the paracortex and the medulla. FRCs express CCL19 and CCL21 that bind to CCR7, which is expressed by T cells and activated DCs that accumulate in this region to form the paracortex. FDCs express CXCL13 that binds to CXCR5, which is found on B cells to form the cortex. Adapted from Förster, R et al., *Nature Reviews Immunology*, 2012.

1.2.1. Lymph node entry and exit

Cells traffic into LNs through the blood, through HEVs, or through afferent lymphatic vessels. Naïve lymphocytes enter through HEVs into the LNs. HEVs are composed of Blood Endothelial Cells (BECs). In order to cross the HEV endothelium, lymphocytes bind L-selectin (CD26L) on their surface to HEV glycoproteins, also called Peripheral Node Addressins (PNAd) that enables lymphocytes to roll on the endothelium surface [13]. Lymphocytes then bind CCL21, CXCL12 and CXCL13, which enables extravasation and entry into the parenchyma [1, 5]. HEVs produce CCL21, whereas FRCs and FDCs produce CXCL12 and CXCL13 respectively. These chemokines are then transported to the endothelial surface by transcytosis [14]. Lymphocytes bind these chemokines causing receptor signalling. This leads to integrin activation and extension of Lymphocyte Function-associated Antigen-1 (LFA-1) on lymphocytes and binding to Intercellular Adhesion Molecule (ICAM)-1 or 2 on HEVs causing cell arrest [1]. Lymphocytes then migrate along the HEV lumen until a suitable point of entry is found for cells to transmigrate through the endothelium and enter the LN. HEVs are important in the regulation of lymphocyte entry into the LNs. Pockets holding lymphocytes have been found to form between endothelial cells. More cells are held in these pockets during an immune response when lymphocyte egress is blocked. It is thought that when lymphocytes exit the LN through the lymphatic sinuses, cells are released from these pockets in order to maintain homeostasis [15].

Cells migrating from tissues in the periphery enter through the afferent lymphatic vessels. During inflammation, lymphatic vessels increase expression of cell-adhesion molecules promoting cell entry. DCs enter lymphatic vessels through a chemokine dependent manner; CCL21 produced by Lymphatic Endothelial Cells (LECs) binds to CCR7 expressed by DCs. CCL21 forms a gradient for the DCs to migrate along to reach the vessels from which they enter the LN into the sub-capsular sinus [16, 17]. DCs then follow CCL19 and CCL21 gradients through the LN into the T-cell zone. The atypical chemokine receptor CCRL1 binds CCL21, leading to cells internalizing and degrading this chemokine, thereby maintaining low quantities of CCL21 in the cortex helping maintain the gradient. Mice lacking CCRL1 lose this gradient; therefore DCs can't migrate into the paracortex [18].

Cells exit the LNs through the medullary sinus into efferent lymphatic vessels where they regain circulation. This process of egress from the LN is dependent on Sphingosine-1-Phosphate (S1P). Lymphocytes express S1P Receptor 1 (S1PR1), which

probes for S1P that is released into the lymph by LECs, thus stimulating entry into the sinus [19, 20]. In the absence of S1PR1 expression, lymphocytes are unable to exit the LN through the cortical sinus causing blood lymphopenia [21].

1.2.2. Immune response within LNs

The immune system is composed of two major types, the innate immune system and the adaptive immune system. The innate immune response is an evolutionary older defence strategy that provides immediate defence against infection but no long-lasting protective memory. The adaptive immune response creates immunological memory after the immune reaction to a specific antigen. This acquired immune response is specific for a particular antigen and requires highly specialized cells [22, 23].

Once pathogens have penetrated tissues, there is an acute local inflammatory response with recruitment of innate cells such as neutrophils, monocytes and macrophages. In most cases, these cells then surround the pathogen in a phagosome and kill the ingested pathogen with mechanisms involving oxidants such as nitric oxide. After this event of phagocytosis, macrophages and DCs internally process the digested pathogen then display fragments of it to their surface, which participates in antigen presentation [24]. These APCs are important for the innate immune response but also for the adaptive immune system as they contribute to T-cell activation within the LNs. Antigen is transported to the draining LNs either through the lymph or within activated APCs. DCs are guided to the paracortex by the chemokines CCL19 and CCL21, which bind to the receptor CCR7. It has been shown that CCR7 expression is critical for DCs to migrate in response to inflammation [6].

DCs exposed to antigen change into mature APCs. During an immune response, DCs migrate and remain near HEVs, increasing the probability of naïve T cells recognizing the antigen on their surface. Maturation of DCs involves up-regulation of Major Histocompatibility Complex II (MHCII), CD80/86 and chemokine receptors such as CCR7, enabling them to migrate from peripheral tissues into the draining LNs [25]. DCs in the LN present MHCII restricted antigens to T cells, which recognize these with their T Cell Receptor (TCR). This interaction is the first signal required for T cell activation. CD80/86 molecules then bind to CD28 on T cells, further stimulating T cells. These signals trigger the expression of CD40L on T cells that binds CD40 on DCs, in turn stimulating cytokine release by DCs, further activating T cells. Depending on the cytokine produced by DCs, determined by the type of antigen, the naïve T cells

differentiate into different T Helper (T_H) subsets: T_H1 , T_H2 , T_H17 , Regulatory T cells (T_{reg}), Follicular Helper T cells (T_{FH}) or Follicular Regulatory T cells (T_{FR}) [26]. Upon activation T cells undergo clonal expansion during which they differentiate into either effector cells migrating to the site of infection or into memory cells for protective immunity [27]. There are two types of memory T cells, Central Memory (T_{CM}) or Effector Memory (T_{EM}). T_{CM} cells enter and patrol LNs through CD62L and CCR7 expression, whereas T_{EM} cells lack these molecules and instead produce effector cytokines [28]. T_{FH} cells are defined by high CXCR5 expression. These cells migrate to B cell follicles where they are essential for B cell activation and for the formation of Germinal Centres (GCs) [29]. Activation of CD8 T cells requires interaction with mature DCs. CD4 helper T cells license the DCs to give activating signal to naïve CD8 T cells. Licensing involves CD40-CD40L signalling. CD8 T cells differentiate into Cytotoxic T Lymphocytes (CTL) through IL-2, IL-12 and IFN γ production by CD4 T cells. After being activated, CD8 T cells go through clonal expansion and differentiate into either memory CD8 T cells or CTLs [30]. CTLs are specialized in killing cells, which is important for fighting intracellular pathogens and tumours [31].

Naïve B cells reside in follicles in the cortex of the LN. Once their B Cell Receptor (BCR) binds a specific antigen, B cells migrate to the interface between B cell follicle and T cell zone where they present antigen to CD4 T cells. T cells that recognize the antigen through the TCR provide survival and proliferation signal for B cells through CD40-CD40L interactions. The type of immunoglobulin produced by B cells is dictated by the different cytokines secreted by T_H1 and T_H2 cells. T_H1 cells stimulate IgG2a production, whereas T_H2 cells stimulate IgG1 production. After encountering antigen, B cells differentiate into GC B cells, memory cells or plasma cells [32]. GC B cells proliferate and undergo somatic hypermutation of the variable region of their BCR and Ig class switch recombination, increasing the affinity of the immunoglobulin-antigen binding. T_{FH} cells are essential for the survival and proliferation of GC B cells. Antibodies that are self-reactive are eliminated in a FAS dependent process by negative affinity selection. Plasma cells migrate to lymphoid tissues and produce protective antibodies [33].

1.3. Development of stromal networks

There are various mesenchymal-derived stromal cell subsets that are indispensable for immune homeostasis and LN function [5]. Mesenchymal cells require interaction with haematopoietic cells in order to differentiate into the different stromal subsets found in the LN [34].

1.3.1. Lymphoid stromal organizer cells

LNs start to develop at embryonic days 11 and 16. At these early stages of development stromal cells can already be found and they are required for the formation of LNs [34, 35]. Evidence indicates that retinoic acid produced by neurons can act on mesenchymal stromal cells stimulating the production of the chemokine CXCL13. However, CXCL13 is not required for LN development nor is retinoic acid likely to be the only mechanism inducing CXCL13 production [36]. CXCR5+ haematopoietic cells are attracted to the developing CXCL13 gradient in the LN anlagen. These cells originate from foetal liver progenitor cells and are called LTis. [37] LTis were thought to have the capacity of differentiating into B cells, T cells, NK cells or DCs, although it is now thought that true LTis are terminally differentiated effector cells rather than being common lymphoid progenitor cells [38]. LTis express lymphotoxin $\alpha 1\beta 2$ (LT $\alpha 1\beta 2$), which binds to the LT β Receptor (LT β R) expressed by mesenchymal stromal cells. The initiation of lymphotoxin expression is believed to be dependent on RANK/RANKL signalling. The LT $\alpha 1\beta 2$ /LT β R signalling promotes the differentiation of mesenchymal stromal cells into Lymphoid Tissue organizer cells (LTos) [39, 40]. LTo cells then up-regulate the chemokines CXCL13, CCL19 and CCL21, Interleukin-7 (IL-7), as well as adhesion molecules (Vascular Cell Adhesion Molecule-1 (VCAM-1), ICAM-1 and MAdCAM-1) [41], leading to an increased recruitment of cells as well as promoting their survival [42]. LTos differentiate into different stromal cell populations through LT β R signalling.

A few days after birth, LNs are colonized by lymphocytes that interact with the stromal cells and drive their survival and functional maturation [43]. Stromal cells differentiate into different subsets depending on the cell types they interact with. The accumulation of lymphocytes leads to a rapid increase in LN size and to the formation of distinct T and B cell areas [44]. The process of LN formation is illustrated in Figure 1.2 [41].

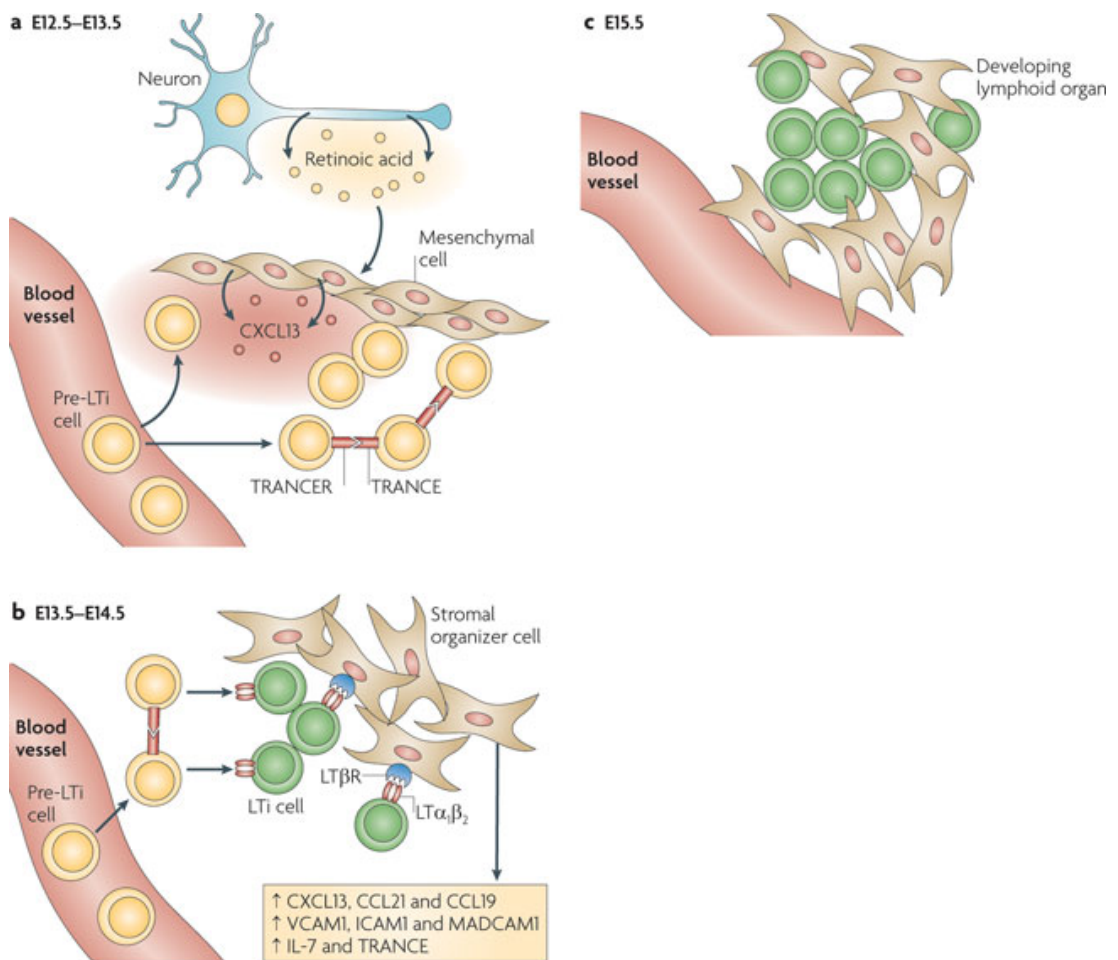


Figure 1.2: Different stages of LN formation.

At embryonic day 12, retinoic acid stimulates mesenchymal cells to produce CXCL13. This chemokine then attracts LTi precursor cells, which start to form clusters. These events facilitate signalling through RANK/RANL-L. This leads to LT $\alpha_1\beta_2$ expression by LTi cells leading to their maturation. LT $\alpha_1\beta_2$ interacts with the LTR found on stromal cells leading to their activation where they produce chemokines and adhesion molecules. These molecules attract more haematopoietic cells to the cluster leading to LN formation. Adapted from Mebius, RE et al., *Nature Reviews Immunology*, 2010.

1.3.2. FDC differentiation and role

The interaction between LTis and stromal cells triggers the formation of follicles. After birth, B cells colonize the LN and form clusters in the cortex of the LN. This entry of B cells is essential for the expression of FDC markers that can be found seven days after birth [45]. Differentiation into FDCs requires $LT\alpha 1\beta 2$ and Tumor Necrosis Factor α (TNF α) production by B cells; these chemokines activate the NK κ B pathway [46, 47]. The B cell area contains a conduit system ensheathed by FDCs. This happens after alteration of the network whereby FDCs replace FRCs around the conduit network [48]. Maturation of stromal cells into FDCs expressing CXCL13 is dependent on B cells. FDCs require TNF α and lymphotoxin produced by B cells [49]. Lymphotoxin is essential for the survival of FDCs [46]. FDCs in turn produce B cell Activating Factor (BAFF), which is required for B cell survival and CXCL13 which attract B cells into the follicle [50]. FDCs express CD21/35, enabling the capture and display of antigen on their surface to B cells [51]. FDCs also have an essential role in the formation of GCs [3]. GCs possess a light zone composed of FDCs that is located in the Subcapsular Sinus (SCS), and a dark zone where B cells go through rapid proliferation. The dark zone extends towards the T cell zone and contains CXCL12-producing stromal cells. FDCs maintain GC by promoting B cell survival [52].

1.3.3. FRC development and role

FRCs ensheath the conduit system and form the framework within the paracortex. ER-TR7 production is stimulated by interaction between stromal cells and T cells [11]. FRCs express the chemokines CCL19 and CCL21, which are chemoattractants for T cells and DCs. Heparin sulphate residues bind CCL21 to FRCs thus guiding DCs and T cells by haptotaxis along the network [5]. DC migration on FRCs is also mediated by the expression of C-type Lectin receptor (CLEC-2) on DCs, which binds to podoplanin (gp38) on FRCs. Absence of CLEC-2/gp38 interactions leads to a defect in developing T-cell responses as well as in DC migration [53]. FRCs guide both T cells and DCs facilitating an efficient immune response. IL-7 expressed by FRCs is critical for the survival of naïve T cells [54]. Lymphocytic Choriomeningitis Virus (LCMV) has been shown to lead to a reduction in FRC numbers and in IL-7 expression causing the host to be unable to respond to secondary infections [55]. In LNs lacking FRCs, after infection with inactivated influenza virus, there is a defect in T cell activation and disorganized GCs. Studies in which FRCs were ablated showed LNs with a loss of rigid B and T cell

compartments, abnormal T cell numbers, and there was a loss of specific CD4 and CD8 responses to viral infections [56]. However, FRCs are only required for naïve lymphocytes, as when FRCs were depleted during an immune response, there was no loss of activated cells or a failure to clear viral infections [57]. FRCs localized in B cell follicles have been found to produce BAFF helping maintain B cells homeostasis. This illustrates the key role for FRCs in promoting immune cell survival and activation while also establishing the important architecture required for the function of the LN. FRCs ensheath the conduits that connect the lymphatic vessels with the HEVs. This network permits the entry of molecules such as chemokines, cytokines and soluble antigen into the LN [58, 59].

1.3.4. MRC development

MRC differentiation is dependent on $LT\beta R$ and $TNFR1$ signalling [60]. MRCs are found in the SCS region of the LN, on the outer margin at the edge of B cell follicles. These cells resemble FRCs but express RANK-L and MAdCAM-1, and not CCL21. The FDC marker CD21/35 is also absent from these cells and they express CXCL13 at lower levels than mature FDCs. MRCs are important in B cell migration and entry of DCs and memory lymphocytes into the LN. [61]. During an immune response, MRCs act as precursor cells that have the potential to differentiate into FDCs [62].

These different stromal cells and their localization are illustrated in Figure 1.3 [63].

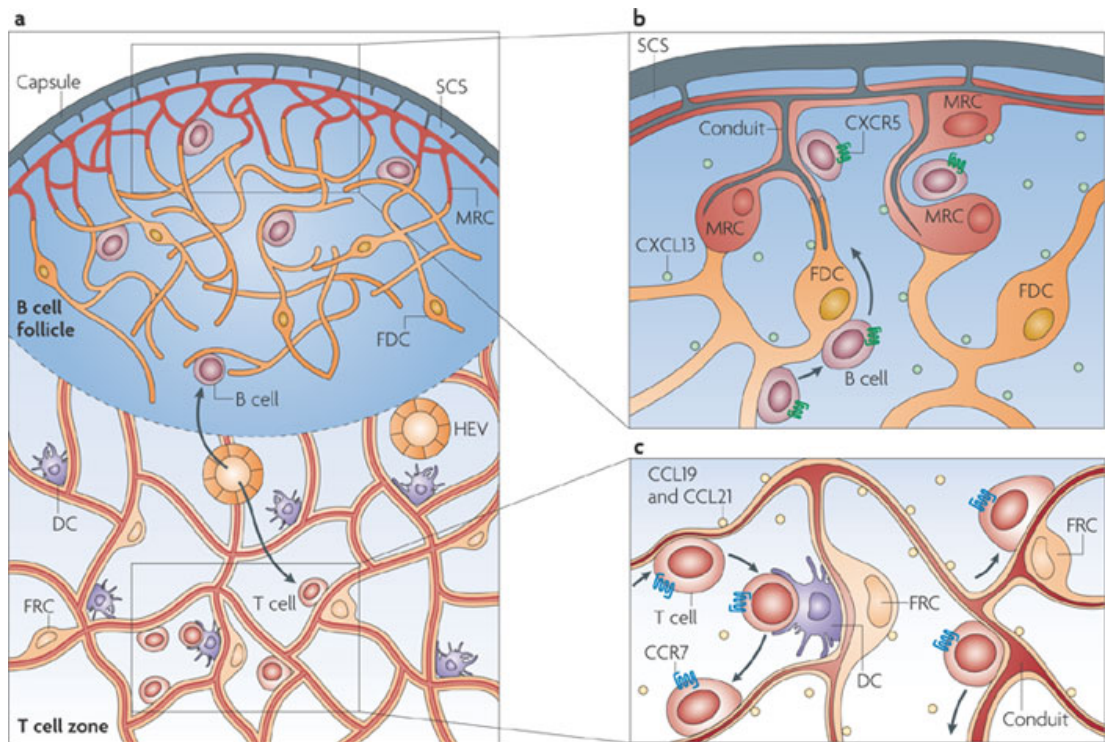


Figure 1.3: LN stromal cells and their interactions with immune cells.

Lymphocytes enter LNs through HEVs where they encounter FRCs. B cells migrate along the FRC network following the CXCL13 gradient towards the B cell follicles. T cells and DCs migrate along the FRC network within the T cell zone. B cells migrate in the B cell follicles in response to CXCL13 produced by FDCs and MRCs in search of antigen. T cells meanwhile traffic around the T cell zone following CCL19 and CCL21 gradients and interact with DCs. DCs present antigen to T cells. Adapted from Germain, RN et al., *Nature Reviews Immunology*, 2009.

1.4. Role of stroma in immune responses

The crosstalk between stroma and haematopoietic cells is important in regulating the immune response within the LNs. Stromal cells regulate immune responses in many different ways controlling cell positioning, motility and survival, but are also plastic in responding to localised inflammation. Stromal cells are able to change their chemokine expression patterns during inflammation leading to changes in cell trafficking and lymphocyte entry into the LN [64]. Self-reactive T cells are eliminated in the thymus; however, a small percentage escape central tolerance. A number of mechanisms regulate pathological T cell activation including regulatory T cells, regulatory DCs and stromal cell presentation of self-antigens, in the absence of co-stimulation, helping to enforce peripheral tolerance [65]. Under inflammatory conditions, LECs express cell adhesion molecules, which promote the entry of DCs into the LNs [66]. FRCs promote T cell survival by producing IL-7 [4], contribute to peripheral T cell tolerance by presenting self-Ag [67], and secrete Vascular Endothelial Growth Factors (VEGFs) which stimulates HEV growth [68]. FDCs control B cell homeostasis and survival by secreting BAFF [3]. FRCs, LECs and BECs are able to up-regulate MHCII on their surface in an inflammatory context [69]. During an immune response, there is a down-regulation of CCL19, CCL21 and CXCL13 by stromal cells resulting in a change in trafficking of lymphocytes and APCs. This reduction occurs at the peak of the immune response and aids the accumulation of specific cells. However, this event leads to a lessened reaction to a secondary antigen when the primary response has started [64]. The chemokines CCL19 and CCL21 promote T-cell activation and enhance T-cell interactions with APCs. CCL19 and CCL21 are also important in the stimulation of DC maturation, antigen presentation, endocytosis and promoting the extension and probing of dendrites [70-72]. DCs associated with FRCs have the capacity of taking up antigens found in conduits and presenting it to T cells [59]. FDCs promote GC formation. Light zone FDCs express CXCL13 and dark zone FDCs express CXCL12; these chemokines are critical for the different stages of B cell maturation. B cells migrate rapidly between the light and dark zones of GCs following the chemokine patterns. Thus, FDCs are critical in the control of B cell response and memory [3, 73]. It has recently been discovered that there is a dormant population of stromal cells that helps regulate B cell follicles during the immune response [74]. LECs and FRCs have also been shown to suppress inflammation. DC maturation and function is suppressed by LECs [75] and FRCs produce nitric oxide which blocks the proliferation of activated T cells [76, 77].

Suppression of T cell proliferation by FRCs requires Interferon- γ (IFN- γ) produced by activated T cells and is also dependent on direct contact between activated FRCs and T cells. This regulation is crucial, as it is a way to avoid tissue destruction and undesirable stimulatory effects [76]. Certain pathogens such as LCMV directly target and infect FRCs in the LNs [78]. *Leishmania major* infects ER-TR7 fibroblasts in LNs [79]. Ebola, Marburg and Lassa viruses infection of FRCs and endothelial cells leads to LN cell apoptosis [80, 81]. The contraction phase of the immune response is when a large percentage of effector cells die. This Antigen Induced Cell Death (AICD) returns the LN to its original state ready for future responses. CCL19 and CCL21 promote AICD in effector T cells [77].

1.5. LN changes during inflammation

1.5.1. LN hypertrophy

During an immune response there is an increase in lymphocytes entering and a reduction of lymphocyte exiting the LN leading to LN hypertrophy. In order to accommodate the increase in cells into the LN, there is vasculature remodelling and growth. The expansion of these capillaries enables the increased entry of nutrients and oxygen into the LN. The first two days correspond to the initiation phase, where proliferation of BECs leads to an increase in the HEV network. This proliferation is dependent on VEGF produced by FRCs [68]. There is also rapid proliferation and growth of HEVs due to increased VEGF expression by FRCs upon LT β R stimulation by CD11c expressing cells [82]. Pro-inflammatory cytokines promote the up-regulation of cell adhesion molecules expression on HEVs [83]. Inflammation leads to an increase in CCL21 expression by HEVs leading to an increase in blood flow through the LN [84]. The reticular network expands in response to inflammation as well and follows the same kinetics as HEVs [68]. LN remodelling and hypertrophy occur differently according to the type of infection.

Inflammation leads to the growth of lymphatic vessels through the LN leading to changes in its structure. Lymphangiogenesis permits an expansion in DCs and activated myeloid cells in LNs [85]. Growth of lymphatic vessels leads to an increase in the size of the medulla to accommodate the augmented number of cells. In some inflammation models, lymphangiogenesis was shown to be dependent on B cells. In mice lacking T cells or myeloid cells, the process of lymphangiogenesis is intact; however, this process does not occur in mice lacking B cells. Blockade of VEGF-2 or VEGF-3 as well as

LT β R leads to a decrease in lymphatic growth and remodelling [85, 86].

After infection of LNs, cell egress is blocked due to a down-regulation of S1PR1 expression on lymphocytes. The increase in cells entering the LN and the block of the exit causes a rapid accumulation of cells in the LN. This block in T cell egress is critical as it permits T-cell activation and effector T-cell expansion. When T cells are activated, CD69 is expressed at high levels and binds to S1PR1 on the surface of T cells leading to its internalization. When the immune response is in its contraction phase, CD69 expression is lost and S1PR1 is re-expressed which allows T cells to exit the LN following the S1P gradients on the lymphatic vessels [87, 88].

1.5.2. LN remodelling

During an immune response, LNs go through structural changes that differ according to the antigen. LN remodelling involves an increase in B cell follicles that can be found in the paracortex of the LN. Remodelling of inflamed LNs that increase in size is closely linked to stromal cell expansion and namely proliferation of FRCs [89]. Structural changes and growth of the reticular network occurs in response to lymphocyte accumulation. Appropriate immune response requires the stromal network to remodel and proliferate following an increased influx of cells. The homeostatic situation involving FRCs, DCs and T cells is disrupted once an antigen is detected in the LN. Depending on the model studied, FRCs either proliferate or stretch [89, 90]. Unpublished work from the Coles' lab showed that during *S. pneumonia* infection, FRCs stretch. LN architecture is critical to have an efficient immune response. This structure-function link of LNs was determined in mice that conditionally lack LT β , as this deficiency leads to a reduced LN structure integrity [91, 92]. These studies illustrate a dependent relationship between LN organization and the immune response towards viruses. Mice that lack CCL21 and CCL19 (plt/plt), and CCR7^{-/-} mice were found to have malformed T cells zones but are still able to mount potent T cell responses to LCMV [93, 94] but possess weaker responses to *Listeria monocytogenes* [95, 96]. Cytomegalovirus infection leads to a decrease in CCL19 expression and infection with the vaccinia virus leads to a decrease in CCL21 [64]. These chemokines are critical in LN structure so a decrease leads to a disorganization of LN structure. This mechanism of loss of structure is necessary in excluding naïve T cells from the inflamed LN [88] and also the decrease in these chemokines prevents AICD in T cells [97]. Changes in LN structure reduce lymphocyte compartmentalisation and enhances interactions that

are needed for an appropriate immune response. Impaired stromal networks cause an altered LN architecture leading to lymphocytes being in the wrong area. Responses to a secondary infection are not altered during an infection that does not affect stromal cells [55]. Changes to the homeostatic LN architecture occurs in response to lipopolysaccharide (LPS) [64] or of specific adjuvants, e.g. Complete Freund's Adjuvant (CFA) [10]. This change in LN architecture during an immune response in most cases does not alter the adaptive immune response. The virulence of *Salmonella typhimurium* is linked to LPS induced down-regulation of CCL21 and CXCL13 leading to changes in LN architecture and cell trafficking [98].

1.6. TLR signalling pathways

Toll-Like Receptors (TLRs) are part of the Pattern Recognition Receptor (PRR) family. TLRs are evolutionarily conserved and are members of the type-1 transmembrane receptor family. They are part of the innate immune system and are able to bind specifically to highly preserved molecules from pathogens. Ten TLRs have been identified in humans and twelve in mice. TLRs can be found expressed on diverse cell types including innate immune cells such as macrophages and DCs but also epithelial and endothelial cells. Bacterial LPS is specifically recognized by TLR4 and its activation promotes pro-inflammatory cytokines production. LPS was discovered as a ligand for TLR4 through the LPS-induced endotoxin shock in mice resulting from loss of function mutations of TLR4 [99]. TLRs have an extracellular Leucine-Rich Repeat (LRR) domain important for ligand recognition, a single transmembrane helix and an intracellular Toll/Interleukin-1 Receptor-like (TIR) domain required for signal transduction [100]. LPS Binding Protein (LPB) initially binds LPS and transfers it to CD14, a membrane protein that lacks an intracellular domain so associates with TLR4 to form a functional LPS complex. The MD-2 protein associated with the extracellular domain of TLR4 is also required for correct LPS binding. LPS is split into monomeric molecules by CD14 enabling recognition by TLR4/MD-2 [101]. LBP and CD14 have been shown to not be essential for TLR4/LPS signalling but to enhance the signalling [102].

Once there is ligand binding, TLR4 receptors homodimerize through TIR domain interactions. Through homophilic interactions between the TIR domains, adapter molecules are recruited. There are different adapter molecules which are essential in TLR4 signalling; Myeloid Differentiation Factor 88 (MyD88), TIR-domain-containing

adapter protein (TIRAP), TIR-domain-containing adapter inducing interferon- β (TRIF) and TRIF-Related Adapter Molecule (TRAM) [100]. MyD88 is composed of an N-terminal death domain and a C-terminal TIR domain that anchors to TLR4's TIR domain. Activation of the TIRAP-MyD88 pathway initiates intracellular signalling that regulates NF- κ B activation and inflammatory cytokine production. Intracellular signalling following TLR4 activation also activates the TRIF-TRAM pathway, activating the Interferon Regulatory Factor 3 (IRF3) transcription factor leading to the up-regulation of Interferons (IFNs), TNF α and stimulatory molecules. TNF α then activates the NF- κ B pathway [103].

1.7. Adjuvants in biology

1.7.1. Principles of vaccination

Vaccination is the most effective method of preventing infectious diseases that we possess. It aims to generate a de novo immune response to a pathogen in order to provide long-term protection against infection. Immunization aims to get the best protection with limited side effects due to inflammation. In most cases, vaccines are developed in order to protect an entire population against the infectious disease. Edward Jenner is the pioneer of vaccination as he showed through experiments that it was an effective way of protecting against the disease. In the 18th century he used cowpox infection to prevent smallpox. Since then, many vaccines have been developed and are commonly used and many more are being designed or are in trials.

The first vaccines contained live attenuated viruses or the whole pathogen. Attenuated vaccines are produced by inactivation or by passaging in culture until the virulence is reduced but the organism is still viable. Exposure to high temperatures inactivates pathogens, which enables the production of whole-pathogen vaccines [104]. These two methods are still found in vaccines, although they are known to have some reactivity and can have diminished potency or efficacy. In recent years, modern vaccines contain purified antigen in suspension rather than the whole pathogen. This improves vaccination efficacy and decreases the chance of adverse reactions. However, the limitation to purified antigens is that there are a reduced number of epitopes, and therefore limits the potential immune receptor range from immune cells.

Vaccination relies on the proper stimulation of the adaptive immune response in order to get long lasting immunity against the pathogen. This process is dependent on the maturation of APCs, which leads to adaptive cell activation. It has been determined

that the diminished efficacy of purified vaccines to induce immunity is due to an inability in promoting APC maturation [105]. The ability of B cells to mature and differentiate leading to immune memory is dependent on T_H cells. APCs present antigen to CD4 T_H cells. There are different types of activated T_H cells, which release cytokines specific to their population (T_H1, T_H2 and T_H17) leading to efficient pathogen clearance. A T_H1 response is necessary for the clearance of intracellular pathogens, T_H2 for extracellular parasites and T_H17 for bacteria and fungi [106]. Immune response mechanisms vary greatly according to the pathogen. Manipulating the immune response and more importantly the type of response can overcome some of the obstacles facing designing potent vaccines.

1.7.2. The discovery of adjuvants

An adjuvant is a substance that when added to vaccines, stimulates an increase in the immune response to inoculated antigens, while not possessing any specific antigenic effect [107]. For example, a tetanus vaccine contains small quantities of *Clostridium tetani* toxin adsorbed in aluminium (Alum) hydroxide [108]. The adjuvant effect was discovered in the 1920s as vaccines lost efficacy when produced under clean conditions. In the 1920s, it was discovered that horses had higher antibody titres when they developed an abscess at the site of injection. The generation of abscesses to unrelated substances along with the diphtheria toxoid increased the immune response [109]. The adjuvant potential of aluminium-based compounds was demonstrated in 1926 with diphtheria toxin [110]. In 1936, Freund developed one of the most potent adjuvants; CFA that is a water-and-oil emulsion containing inactivated mycobacteria. CFA causes severe reactions and is considered too toxic for human use, while under Home Office guidance can only be administered once in mice [111].

Immunostimulatory adjuvants present conserved Pathogen-Associated Molecular Patterns (PAMPs) such as LPS, double-stranded RNA (dsRNA) or unmethylated CpG DNA, which are recognized by PRRs including TLRs. The ten functional TLRs have evolved to recognize specific PAMPs. This recognition can trigger and shape a response from the adaptive immune system [112]. Additional mechanisms of how adjuvants work include increasing the vaccine antigens half-life, modifying the presentation of antigens by the MHC on APCs, improving antigen delivery and presentation, on intracellular signalling within APCs, modulating co-stimulatory signal recognition by T cells or inducing cytokine production [113]. Though adjuvants are commonly used,

their mechanism and function is still incompletely understood.

1.7.3. Aluminium-based adjuvants

To this day, aluminium-based adjuvants are the most commonly used in human vaccination; including diphtheria-tetanus-pertussis [108], human papillomavirus and hepatitis vaccines. The original aluminium-based adjuvant originated in the 1920s and was called aluminium phosphate. In the 1920s it was believed that aluminium was an effective adjuvant as it allowed antigen to remain in the body for longer, which was termed the depot effect [110]. Up to a year after vaccination, traces of Alum can be found at the injection site. This effect was considered dogma for 60 years and only recently has research into aluminium salts, referred to as Alum in this project, started but the mechanisms still remain unclear. Vaccines containing alum are prepared by having the antigen in suspension be adsorbed to aluminium hydrogel [114]. Alum also activates innate immune cells resulting in a T_H2 immune response [115]. Aluminium salts support antigen uptake and presentation by macrophages [116]. Antigen uptake by DCs and B cells is greater in an antigen/alum mix than antigen alone, and Alum increases CD86 expression in DCs [117]. It was thought that Alum might function as a PAMP and induce signal through a particular or several TLRs; however, *Myd88^{-/-}* mice produced normal IgG1 quantities in response to aluminium-adsorbed antigen [118]. Mice deficient for both *Myd88* and *TRIF* had normal antibody responses compared to control mice upon vaccination with antigen/alum [119]. Alum promotes the release of cytokines such as IL-1 β through the NLR family, Pyrin Domain containing 3 (NLRP3) inflammasome and adaptor protein Apoptosis-associated Speck-like protein containing CARD (ASC), which activates caspase 1. Inflammasomes are a pathogen recognizing system essential for protection. The ATP receptor P2X, that has a role in NLRP3 inflammasome stimulation, was not linked to IL-1 β production [120, 121]. Aluminium salts are thought to activate the NLRP3 inflammasome through two different ways. The first is that phagocytic cells take in aluminium salt particles, which leads to damage and rupture of lysosomes and antigen and enzyme release, such as cathepsin B, into the cytoplasm. This event causes to NLRP3 inflammasome activation [122]. The second way is an indirect activation linked to aluminium salt toxicity leading to Damage Associated Molecular Patterns (DAMPs) release, namely uric acid resulting in activating NLRP3 inflammasome [117]. Aluminium salts are known to induce strong antibody responses. Alum preferentially induces IL-4, which promotes T_H2 cells that stimulates B cell antibody production of the IgG1 and IgE subtypes [123, 124]. IL-4

inhibits T_H1-type responses. The increase in GR1+ IL-4 producing cells in the spleen is promoted by Alum six days following immunization. These cells are also found at the site of injection shortly after immunization and are able to stimulate B cells [125].

Oral or intranasal immunization of Alum is not possible due to the formation of antigenic deposits [126] and has been found to be unusable with DNA-based vaccines [127]. Another limitation found with Alum is the strong T_H2 bias of immune responses that limits the development of vaccines against certain pathogens requiring a T_H1 response.

1.7.4. Novel adjuvants: TLR4 agonist adjuvants

Gram-negative bacterial components such as LPS, which binds to TLR4 and its co-receptor CD14, are potent adjuvants but their clinical use is not possible as they induce a high fever. LPS stimulates a plethora of cells to produce cytokines and chemokines that control APC trafficking and maturation. Uncommonly, LPS can be delivered at a site different than the site of immunization and still retain its adjuvant properties [126].

Monophosphoryl Lipid-A (MPL-A) was developed as a less toxic derivative of LPS and it contains only the Lipid A portion which is responsible for LPS' adjuvant effect but also its toxicity. It is derived from LPS from *Salmonella minnesota*. Removing a phosphate group, a sugar moiety and an ester-linked fatty acid group diminishes the toxicity of Lipid A but does not affect its adjuvant function [128]. Although MPL-A interacts with TLR4, it has been found that the adjuvant effect can occur in cases where TLR4 is absent [119]. MPL-A activates TRIF rather than NF κ B directly leading to production of pro-inflammatory cytokines, namely IL-1 β , IL-12 and INF γ . MPL-A stimulates T_H1 immune responses including CTLs and the production of antibodies against the complement and the IgA subtype [129].

Combination adjuvants that simulate different parts of an immune response may produce a better immune response, as a pathogen stimulates different pathways. MPL-A's use in combination with aluminium oxyhydroxide, called AS04 is approved in Europe and is found in a Hepatitis B vaccine and the human papillomavirus vaccine, Cervarix [113]. Formulations of Alum and MPL-A enhance memory response; studies have shown that Alum prolongs the cytokine production after immunization at the injection site [130].

Glucopyranosyl Lipid Adjuvant-Stable oil in water Emulsion (GLA-SE) is a synthetic TLR4 agonist oil-in-water emulsion that was developed by the Infectious Disease

Research Institute (IDRI) [131]. GLA-SE is a potent adjuvant that induces a T_H1 response and activates the inflammasome with early IL-18 and IFN γ production [132]. Squalene oil-in-water emulsions enhance the immune response generated by TLR agonists [133]. Formulation is key in adjuvant development and in modulating their activity. An influenza vaccine H5N1 with GLA-SE as an adjuvant has passed phase I clinical trials [134]. Adjuvants have different effects on the immune system and should be chosen according to the desired immune response for the vaccine [135].

1.7.5. Other adjuvants

See Table 1.1 for a list of licenced adjuvants.

Emulsions

Water-in-oil-emulsion adjuvants such as Incomplete Freund's Adjuvant (IFA) or CFA were never validated for their use in humans due to the strong toxicity. These types of adjuvants work through depot formation at the injection site and stimulate antibody production [136]. These adjuvants are mostly used for terminal conditions such as cancer as they are considered toxic. Since then there have been new versions of emulsions such as Montanide emulsions, which is in clinical trials for studies against prostate cancer and ovarian cancer [137, 138]. There are also oil-in-water emulsions, which activate innate inflammatory responses through APC recruitment and activation. These emulsions are less reactive than the water-in-oil emulsions and have been used successfully in vaccines such as the seasonal influenza vaccine FludTM [139]. Water-and-oil emulsions are known to stimulate a T_H1 response whereas the oil-in-water emulsions a T_H2 response [140].

Liposomes and virosomes

Liposomes are lipid layers in synthetic nanospheres that are capable of encapsulating antigen and act as presenters of antigen [141]. The efficacy of these adjuvants is dependent on the lipid layer number, electric charge, molecular composition and preparation [142]. Licenced vaccines contain virosomes, which are similar to liposomes but contain empty envelopes of the influenza virus. This adds envelope glycoproteins to the adjuvant considered to aid in the uptake of antigen by cells. Virosomes are composed of stable membrane lipids and viral fusion proteins [143]. This type of adjuvant mimics virus infectivity without the risks involved with attenuated viruses and

can deliver the antigen directly into the cell cytosol [127]. Virosomes stimulate both T_H1 and T_H2 responses [129].

Saponins

Saponins derived from the bark of the *Quillaja saponaria* tree have been commonly used in medicine. Saponins such as QS21 promote antigen presentation by APCs, induce CTL production, and stimulate both a T_H1 and T_H2 response but are considered quite reactogenic [144]. The problems of QS21, most importantly the residual lytic activity found at the immunization site can be overcome by the addition of MPL-A, which has a synergic effect [139]. Saponins are also used in Immune Stimulating Complexes (ISCOM) formulations, which are structures containing antigen, cholesterol, phospholipid and saponin. Vaccines containing ISCOM stimulate both T_H1 and T_H2 responses [145].

TLR2 ligands

There are many derivatives of TLR2 ligands, gram-positive cell wall components that have been used in experimental vaccines. For example, a vaccine against Lyme disease was developed with OspA from *Borrelia burgdorferi* as an adjuvant [146]. The synthetic compound Pam2Cys enhances cell mediated immunity and antibody responses in a vaccine for *Listeria monocytogenes* [147].

CpG adjuvants

Prokaryote DNA contains unmethylated CpG dinucleotides recognized by the innate immune system, as they are ligands for TLR9 found in intracellular vesicles of cells. These sequences are specific to a type of species and in humans there are two types of motifs that have been described, type K and type D. The type K motifs promote B cell and monocyte proliferation and IgM, IL-10 and IL-6 production. Type D motifs activate DCs and stimulate TNF α and IL-8 secretion [148]. Vaccines containing CpG motifs induce a T_H1 response. These motifs can induce a strong immune response to weak antigens such as malarial antigens [148]. Many experimental vaccines contain CpG motifs against pathogens such as *Listeria monocytogenes* [149].

Bacterial toxins

Bacterial toxins have been studied as vaccine adjuvants due to their strong immunogenicity and specific receptors. Pertussigen derived from pertussis toxin has been used as an adjuvant as it augments IgE levels and increases sensitivity to antigen

and the immune response in the case of the trivalent childhood vaccine for diphtheria, pertussis and tetanus [150]. Heat-labile enterotoxin from *E.coli* enhances mucosal immunity, stimulates both T_H1 and T_H2, and has been shown to be safe and to enhance the vaccine against *Campylobacter* [151]. Cholera enterotoxin is similar to heat-labile enterotoxin but stimulates T_H2 responses and elicits strong mucosal immunogenic responses. Cholera enterotoxin has also been linked to strong side effects and diarrhoea in humans [152].

Cytokines

Cytokines can also be found in the modern classifications of adjuvants. Their use is particularly studied in the formulation for DNA vaccines where the cytokines can be expressed in the same vector as the antigen [153]. Cytokines could provide a less toxic way of enhancing vaccine efficacy. For example, inclusion of either IL-2 or IL-12 in a DNA vaccine with the sequence of the HIV antigen produces a strong T_H1 immune response [129].

Table 1.1. List of licensed adjuvants.

Adjuvant name	Type of adjuvant	Description
Alum	Mineral salts	Enhances T _H 2 type humoral immune responses and antigen stability.
MF59 (Novartis)	Oil-in-water emulsion	Used in influenza vaccines and activates humoral and cell-based immunity.
Virosomes (Berna Biotech)	Liposomes	Enhances humoral and cell-based immunity.
AS03 (GSK)	Oil-in-water emulsion	Used in influenza vaccines and activates humoral and cell-based immunity.
AS04 (GSK)	Alum-absorbed TLR4 agonist	Used for HPV and hepatitis-B vaccines. Activates humoral and cell-mediated immunity.

1.8. MicroRNAs: regulators of the immune response

MicroRNAs (miRNAs), discovered in 1993, are small highly conserved non-coding RNAs of about 18-25 nucleotides that function as important post-transcriptional regulators of gene expression [154]. They belong to the non-coding RNA family consisting of, transfer RNAs (tRNAs), small interfering RNAs (siRNAs), small nuclear RNAs (snRNAs), and ribosomal RNAs (rRNAs). Each miRNA targets several hundred different mRNAs and acts to regulate mRNA levels to control protein content of the cells. They are able to modify cellular functions such as proliferation, differentiation,

signalling, metabolism and apoptosis, and also functions such as inflammation [155].

1.8.1. miRNAs biogenesis

miRNA transcription is very similar to that of mRNA. Their genomic sequence can be found in introns or in inter-genic regions where they are transcribed by RNA polymerase II or RNA polymerase III into primary miRNAs measuring hundreds of base pairs in length. miRNAs are never located in exonic regions as this would lead to the loss of the mRNA transcript. Primary miRNAs possess a stem-loop secondary structure and the mature miRNA sequence is located within one or both stem strands [156]. Transcripts can go through a post-transcriptional modification by adenosine deaminases modifying adenosine into inosine leading to changes in the transcript's base pairing and potentially to structural changes. The pri-miRNA is spliced capped and polyadenylated in a similar way to that of mRNAs.

There are two endonuclease steps required for maturation of miRNAs. The RNase II enzyme called Drosha associates with the RNA binding protein DGCR8 making it capable of cleaving pri-miRNAs. Within the nucleus, Drosha processes the transcripts and cleaves them to 70 base pairs thus becoming precursor miRNAs. Flanking pri-miRNA sequences are released from the stem-loop precursor by Drosha cleavage. Drosha cleaves the 5' and 3' parts of the miRNA structure, while DGCR8 interacts with the primary miRNA and molecularly determines the correct cleavage sites [157].

Exportin 5 and Ran-GTP export these precursor miRNAs into the cytoplasm [158]. The RNase III processing enzyme Dicer associated with a RNA-binding domain protein Tar RNA Binding Protein (TRBP) cleaves the loop region of the precursor miRNAs leading to mature miRNAs of their final length of between 18 and 25 base pairs [159]. After this cleavage, RNA helicases unwind the secondary hairpin structure of the precursor miRNAs.

Single stranded miRNAs enter the RNA-Induced Silencing Complex (RISC) facilitating mRNA repression [160, 161]. One mature strand miRNA is loaded into the RISC complex, the other strand, called the star strand is usually degraded but in some cases is loaded in the RISC complex at the same frequency as the other strand. When both strands are capable of entering the RISC complex, the nomenclature is different, 5p is the miRNA from the 5' end of the stem loop and 3p is from the 3' end [162]. miRNAs can have differential strand usage depending on the cell type and state [163]. Figure 1.4 illustrates miRNA biogenesis [154].

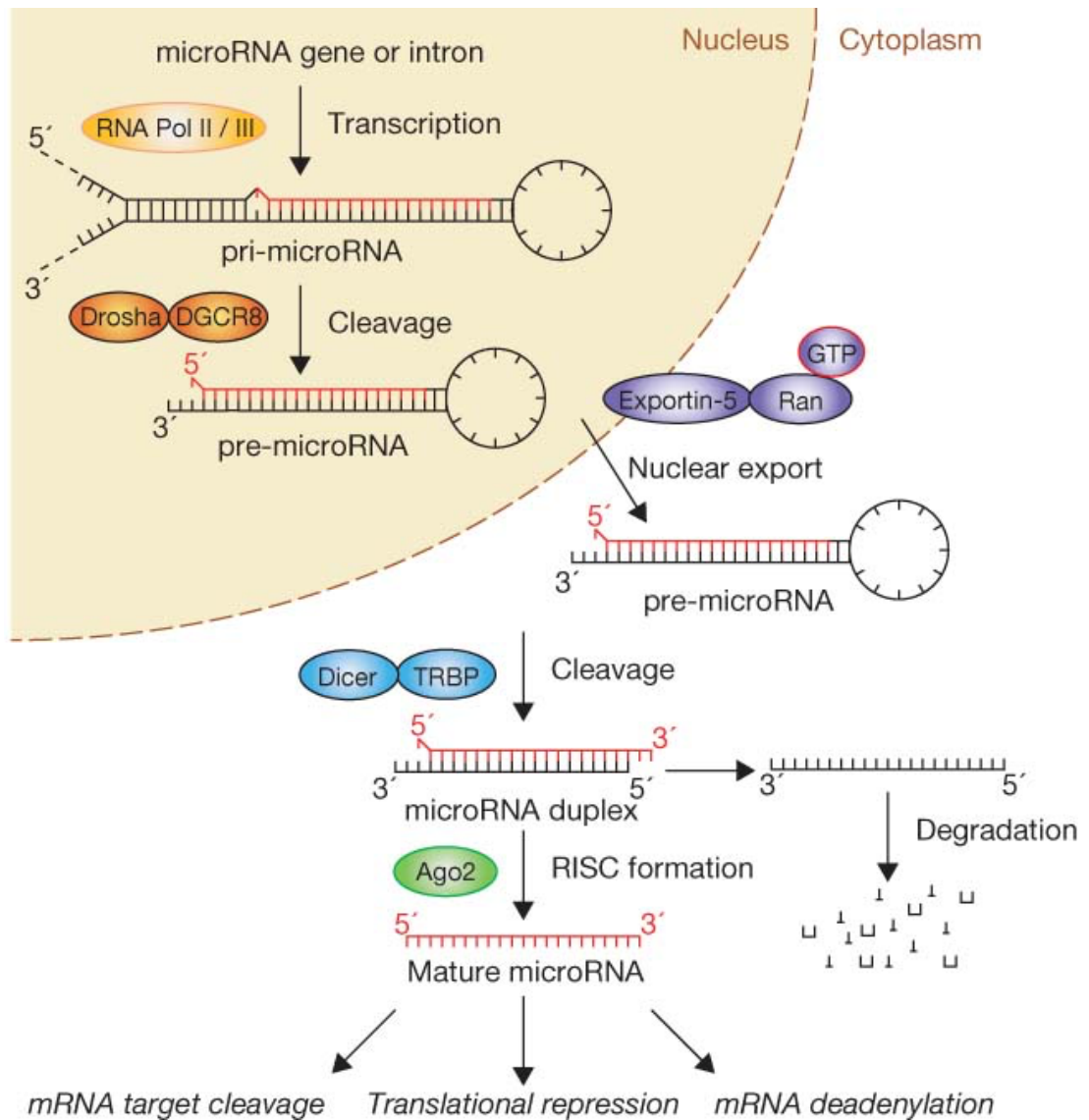


Figure 1.4: miRNA synthesis and function within a cell.

MicroRNAs are encoded within an intronic region of a gene or from an intergenic region. They are then transcribed by RNA polymerase II into primary transcripts or primary miRNA respectively. Primary miRNA is processed into pre-miRNA by the ribonuclease Drosha and DGCR8. This is the result of splicing from primary mRNA. Pre-miRNA is then processed by Dicer to form the functional miRNAs. The RISC complex forms around the miRNAs to enable the binding to the target gene leading to an inhibition of translation or mRNA degradation. Adapted from Miyaki et al. *Nature Reviews Rheumatology*, 2012.

1.8.2. miRNAs function

Mature miRNAs are loaded into RISC. The RISC loading complex is composed of the RNase Dicer, TRBP, Protein Activator of PKR (PACT) and argonaute 2 (Ago2). TRBP and PACT aren't essential for cleavage but act to stabilize and facilitate it [164]. Argonaute proteins in this RISC complex carry out endonucleic cleavage of mRNAs by miRNAs. The argonaute family in humans is composed of 4 members, but only Ago2 possesses enzymatic activity [165]. Argonaute proteins possess a Piwi Argonaut and Zwiille (PAZ) domain that enables their binding to the stem-loop structure of pri-miRNAs and to mature miRNAs present in the RISC complex [166]. The PIWI domain of argonaute proteins is composed of an RNase H domain enabling the splicing activity [167]. miRNA interactions with mRNAs occur at the 3' untranslated region (3'UTR) through imperfect base-pairing, this improves the chances for a miRNA to have multiple binding sites within a single mRNA and to many different mRNAs. The seed region consisting of a region of 6-8 nucleotides at the 5' end of miRNAs is essential for interactions between miRNAs and mRNAs. It is thought that the 5' end is necessary for target identification and that the 3' end is necessary for modulating repression of mRNAs. AU rich areas close to the seed region contribute to miRNA efficacy [168].

miRNAs' control of mRNA levels may not be as efficient as proteosomal degradation but allows a strong inflammatory response that can then be slowly modulated. A perfect match between a miRNA and its target leads to cleavage and degradation of the mRNA. However, if the interaction with the target involves more mismatches, this leads to an inhibition of translation [169]. The mRNA fragments formed after cleavage go through standard degradation.

1.8.3. miR-132

MicroRNAs regulate the strength and timing of TLR responses and signalling. miRNAs can regulate TLR expression, TLR signalling proteins, target transcription factors, target TLR signalling regulators, and target cytokine mRNAs. Two microRNAs, miR-132 and miR-212 form a miRNA cluster that has been shown to have a role in inflammation. miR-132 is highly expressed in the brain [170-173] and induces neuronal growth and dendritic plasticity [174]. miR-132 and miR-212 are encoded on chromosome 17 of the human genome and chromosome 11 in mice and is transcribed by cAMP-Response Element Binding protein (CREB) in neuronal cells [175] and by Repressor Element 1 Silencing Transcription factor (REST) in non-neuronal cells [176]. The same primary

transcript gives rise to miR-132 and miR-212 and this cluster possesses similar mature sequences and the same seed region but miR-132 is preferentially expressed [173].

TLR activation and signalling must be controlled to avoid excessive and sustained inflammation and tissue damage. miRNAs form a key factor in a negative feedback loop of the innate immune system [177]. There are several miRNAs induced by TLR activation that target mRNAs encoding the TLR signalling system [178]. This is illustrated in Figure 1.5 [112]. Due to miR-132's dual role in inflammation and brain functions, it has been dubbed "NeurimmiR" [179]. Several targets for miR-132 are known, including mediators involved in neurological development, synaptic transmission, inflammation and angiogenesis. miR-132's transcription is stimulated by TLR4 agonists and up-regulated at early stages of infection [180]. Different cell types including stromal fibroblasts express miR-132, and in mammary stroma this miRNA inhibits the Matrix Metalloproteinase 9 (MMP-9). Mice lacking miR-132 are unable to have proper epithelial-stroma interactions and therefore lack the ductal overgrowth that is required for mammary glands development [181]. miR-132 is induced in bone marrow (BM) and splenocytes of mice treated with LPS and represses acetylcholinesterase (AChE) expression. AChE is a key regulator of peripheral inflammation [180]. Heparin-Binding Epidermal-like Growth Factor (HB-EGF) involved in cell proliferation and migration as well as wound healing is repressed in mast cells by miR-132 [182]. In NK cells, miR-132 regulates IL-12 signalling by repression of Signal Transducer and Activator of Transcription 4 (STAT4) [183]. miR-132 is up-regulated during virus infections such as with Human Cytomegalovirus (HCMV) which could be a way for the virus to evade the immune response. This is further explained by the fact that upon virus stimulation, miR-132 regulates p300 that plays an important role in starting the antiviral response [184].

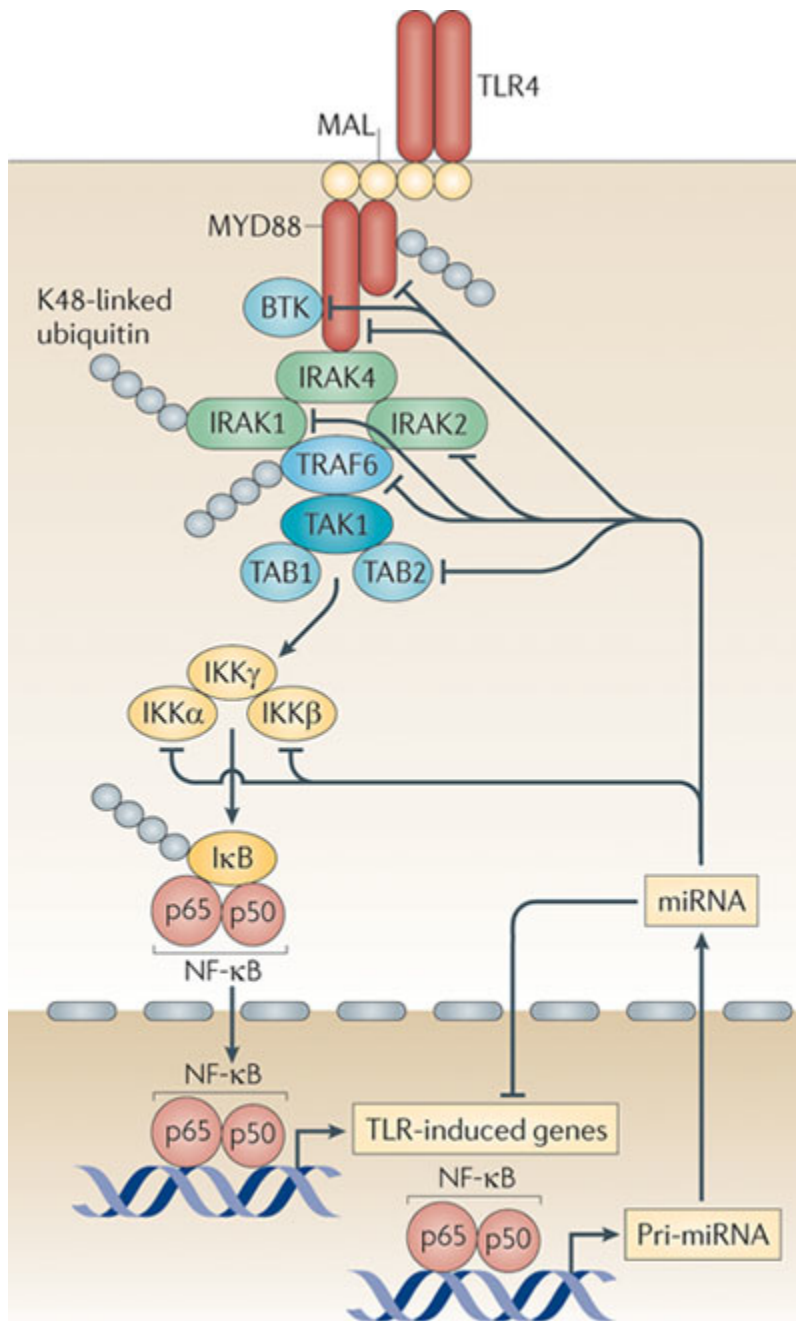


Figure 1.5: miRNAs regulate TLR4 signalling.

The TLR4 signalling pathway uses the adaptor molecule MyD88 to initiate NF κ B dependent gene transcription. TLR activation and signalling must be tightly controlled to avoid extreme inflammation and enable tissue repair. Proteasome degradation is one such mechanism, another is mediated by miRNAs. miRNAs bind to the 3' untranslated region of specific mRNA target sequences to inhibit gene synthesis of the signalling pathway or of cytokines. Adapted from O'Neill, L. et al., *Nature Reviews Immunology*, 2011.

1.9. Summary and aims

Stromal cells provide the structural basis for lymphocyte and DC migration and localization, providing specialized microenvironments for their homeostasis and function. Although stromal cell gene expression and function has been studied under homeostatic conditions, less is known about the behaviour of stroma during inflammation or the process leading to rapid stromal cell remodelling. During the early stages of a pathogen driven immune response, LNs rapidly enlarge which results from the vascular remodelling and increase in the rate of T and B cell influx. This can in part explain changes observed in the stromal network; however, adjuvant treatment has been shown to drive new stromal architecture for the immune response to take place. The aim is to determine the role of LN architecture in vaccine efficacy.

Using adjuvants, TLR agonists and infection models the timing and molecular mechanisms leading to stromal cell reorganization and changes in cytokine and chemokine expression was addressed. Rapid changes in inflammatory gene expression and cytokine production by LN stroma were observed both in *in vitro* stromal cell cultures and in adjuvant administration *in vivo*. A schematic showing the aim of the work undertaken is illustrated in Figure 1.6.

1.10. Hypothesis

The working hypothesis of my project is that adjuvant efficacy is not only dependent on DC activation and on antigen maintenance but on LN stromal cell remodelling. Specifically, the aim is to determine the molecular mechanisms of stromal cell activation and remodelling in response to TLR4 agonism. By developing a better understanding of these processes, we hope to create improved vaccines through the manipulation of stromal cell network organization leading to efficient cell interactions to optimally prime the immune response.

1.11. Specific aims

- Investigate stromal remodelling and LN expansion following immunization.
- Determine the mechanisms and cell changes behind LN remodelling.
- Analyse the role of miR-132 in regulating LN remodelling.
- Determine mechanisms by comparing miR-132 deficient mice with WT mice
- Investigate what miR-132 deficiency means functionally upon immunization.

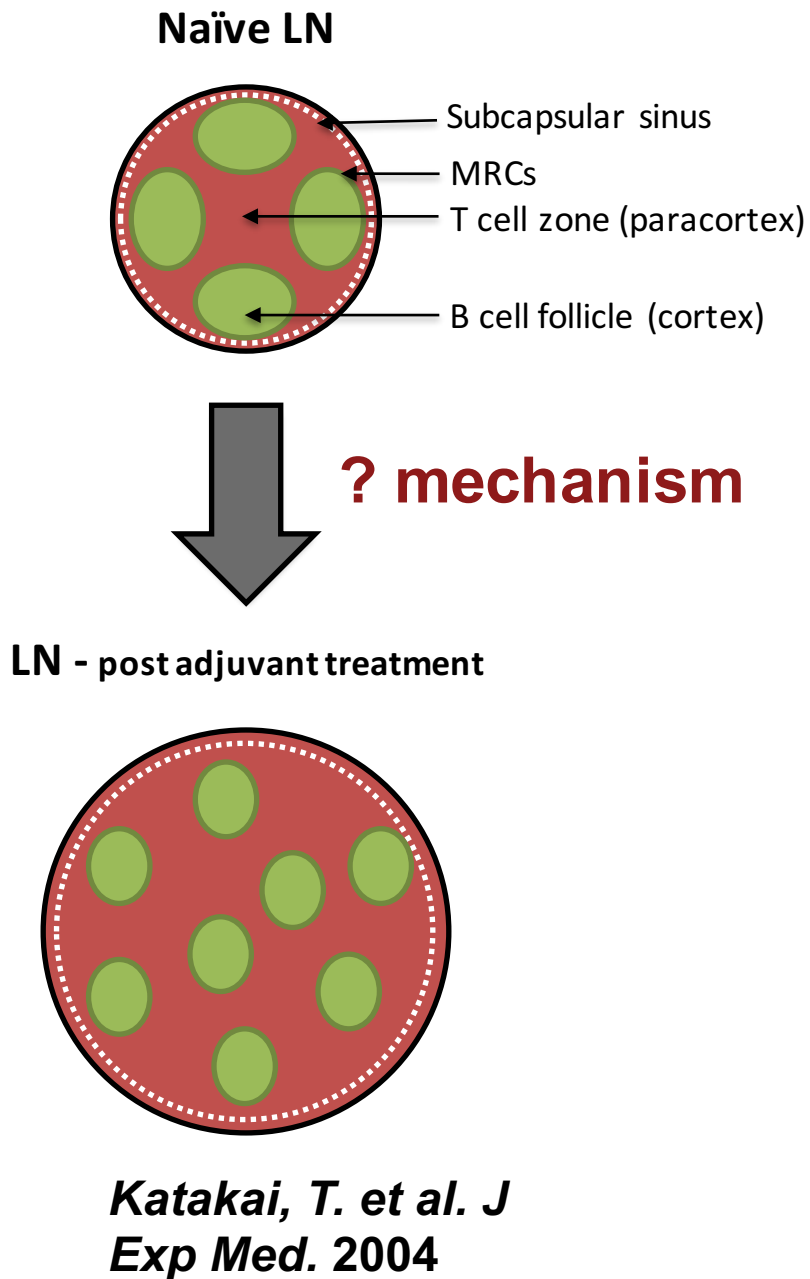


Figure 1.6: Schematic illustrating the specific aim of the project.

LN's have been shown to remodel during an immune response to adjuvants [11]. The mechanisms underlying how LN's rapidly change their architecture in response to immunization are still unknown.

Chapter 2: Materials and Methods

2.1. Reagents

Table 2.2. Adjuvants

Adjuvant name	Manufacturer	Catalogue number
Imject Alum (formulation of aluminum hydroxide and magnesium hydroxide)	Thermo Scientific	77161
Freund's Adjuvant, Complete (CFA)	Sigma Aldrich	F5881
Glucopyranosyl lipid adjuvant-stable oil in water emulsion (GLA-SE)	Infectious Disease Research Institute (IDRI)	IDRI-EM031
Freund's Adjuvant, Incomplete (IFA)	Sigma Aldrich	F5506
Sigma Adjuvant System. (Monophosphoryl Lipid-A (MPL-A) and Trehalose Dicorynomycolate (TDM)).	Sigma Aldrich	S6322
Second generation lipid adjuvant – stable oil in water emulsion (SLA-SE)	IDRI	IDRI-EM030
Formulated oil-in-water emulsion (W/OE)	IDRI	IDRI-EM582

Table 2.3. Vaccines

Vaccine name	Manufacturer	Catalogue number
Engerix B	Glaxo Smith Kline (GSK)	NDC 58160-821-05
Fendrix	GSK	AFENA015AR
Inactivated Influenza Vaccine (TIV)	Sanofi Pasteur	J8371-1

Table 2.4. Primary antibodies

	Fluorophore	Clone	Host	Isotype	Manufacturer	Use
B220	FITC	RA3-6B2	Rat	IgG2a	eBioscience	IHC, FC
	BV421				Biolegend	FC
CD3	eFluor 660	17A2	Rat	IgG2b	eBioscience	IHC
	PE-Cy7				Biolegend	FC
CD4	Pacific Blue	RM4-5	Rat	IgG2a	Biolegend	FC
CD8	APC-Cy7	53-6.7	Rat	IgG2a	Biolegend	FC
CD11b	PE-Cy7	M1.70	Rat	IgG2b	Biolegend	FC
CD11c	AF 647	N418	Hamster	IgG	eBioscience	FC
	BV421	HL3		IgG1	BD Biosciences	
CD19	PE-Cy7	eBio1D3	Rat	IgG2a	eBioscience	FC
	APC-Cy7	6D5			Biolegend	
CD21/CD35	eFluor 450	4E3	Rat	IgG2a	eBioscience	IHC, FC
CD31	APC	390	Rat	IgG2a	eBioscience	FC
	FITC					IHC, FC
CD44	APC	IM7	Rat	IgG2b	Biolegend	FC
CD45	FITC	6D5	Rat	IgG2b	Biolegend	IHC,

	PE					FC
CD95	PerCP eFluor 710	15A7	Mouse	IgG1	eBioscience	FC
CD169	FITC	MOMA-1	Rat	IgG2a	Serotec	IHC, FC
CXCR5	BV421	L138D7	Rat	IgG2b	Biolegend	FC
	PE					
ER-TR7	Purified	ER-TR7	Rat	IgG2a	Abcam	IHC
FDCM2	Purified	FDC-M2	Rat	IgG2a	Immunokontakt	IHC
Foxp3	PE-Cy7	FJK-16s	Rat	IgG2a	eBioscience	FC
ICAM	Pacific Blue	YN1/1.7.4	Rat	IgG2b	Biolegend	FC
IgD	FITC	11-26c	Rat	IgG2a	eBioscience	IHC, FC
GL7	eFluor 660	GL7	Rat	IgM	eBioscience	FC
gp38	eFluor 660	8.1.1	Hamster	IgG	eBioscience	FC
	AF 488					
Ly6C	PE	HK1.4	Rat	IgG2c	Biolegend	FC
Ly6G	AF 647	1A8	Rat	IgG2a	Biolegend	FC
Lyve-1	Purified	Poly	Rabbit	IgG	AngioBio	IHC
MAdCAM-1	AF 488	MECA-367	Rat	IgG2a	Biolegend	FC
	Biotin					
Meca-79	AF 488	Meca-79	Rat	IgM	eBioscience	IHC

MHCII	eFluor 450	M5/114. 15.2	Rat	IgG2b	eBioscience	FC
NK1.1	PE	PK136	Mouse	IgG2a	Biolegend	FC
PD-1	APC-Cy7	29F.1A1 2	Rat	IgG2a	Biolegend	FC
PNA	Biotin	Lectin from <i>Arachis hypogaea</i>			Sigma	IHC
RANK-L	Purified	IK22.5	Rat	IgG2a		IHC
SIGN-R1	APC	22D1	Hamster	IgG	eBioscience	FC
VCAM	APC	429	Rat	IgG2a	Biolegend	FC

Table 2.5. Secondary antibodies

	Fluorophore	Host	Manufacturer	Use
Streptavidin	eFluor 450		eBioscience	FC
	PE-Cy7			
	AF 594		Invitrogen	IHC
	AF 647			
Rat IgG	AF 488	Goat	Invitrogen	IHC
Rabbit IgG	AF 647	Goat	Invitrogen	IHC
Mouse IgG	Alkaline phosphatase (AP)	Goat	Sigma Aldrich	ELISA
Mouse IgG1	Alkaline phosphatase	Goat	Southern Biotech	ELISA
Mouse IgG2c	Alkaline phosphatase	Goat	Southern Biotech	ELISA
Mouse IgA	Alkaline phosphatase	Goat	Southern Biotech	ELISA
Mouse IgE	Alkaline phosphatase	Goat	Southern Biotech	ELISA

Table 2.6. Primers

Gene	Forward Primer	Reverse Primer
AICDA	GCCACCTTCGCAACAAGTCT	CCGGGCACAGTCATAGCAC
CXCL12	CAGAGCCAACGTCAAGCA	AGGTACTCTTGGATCCAC
CXCL13	CATAGATCGGATTCAAGTTACGCC	TCTTGGTCCAGATCACAACCTCA
HPRT	AGGAGTCCTGTTGATGTTGCCAGT	GGGACGCAGCAACTGACATTTCTA
HTRA1	AGTGGGTCAGGATTCATCGTA	GTGACCACGTGAGCATTGT
IL-1β	AACCTGCTGGTGTGTGACGTTT	CAGCACGAGGCTTTTTTGTGT
IL-22BP	TCACTCCATGGTGGGAAACAAA	CGCAGTAGCTGGAATGAGGT
IL-6	GGGACTGATGCTGGTGACAA	CGCACTAGGTTTGCCGAGTA
MMP-9	GTCCAGACCAAGGGTACAGC	ATACAGCGGGTACATGAGCG
TLR4	AGTGGGTCAAGGAACAGAAGCA	CTTTACCAGCTATTTCTCACC
TNFα	CTGTAGCCCACGTCGTAGC	TTGAGATCCATGCCGTTG
Gene	Assay name	Manufacturer
RNU6	U6 snRNA	Applied Biosystems
miR-132	Has-miR-132	Applied Biosystems

2.2. Animals

All mice used were maintained at the University of York Biological Services Facility (BSF). Mice were purchased and housed at the BSF under-pathogen free conditions. All mice used were between 6 to 10 weeks of age unless otherwise stated. B6.Rag2KO.CD45.1Cg, B6.CD11cCreTg and Rosa26iDTRfl and miR-132^{-/-} [185] mice were bred at the BSF. B6CD11cCreTg mice were crossed with Rosa26iDTRfl mice to generate B6.CD11cCreTg.Rosa26iDTRfl mice [186]. All mice were kept in micro-isolator cages in the vivarium under standard laboratory conditions with an artificial 12hrs dark/light cycle, and fed on a standard irradiated rodent diet with autoclaved water *ad libitum*. Sentinel mice were housed with experimental mice and tested for pathogens every three months. Animal care and protocols were in accordance with the European Union regulations and performed under a United-Kingdom Home Office licence. Immunized mice were treated following a randomized block design to remove the nuisance factor. In this case, the cage is considered the blocking factor. Another person who was blind to the treatment and to the aim of the experiment treated the mice to remove bias.

2.3. Adjuvant immunizations

Different adjuvants and vaccines (Table 2.1 and 2.2) were used and tested following two different immunization protocols. Mice were either immunized subcutaneously in the flank with 100µl or in the hock [187] with 25µl of Ovalbumin (OVA) (Sigma Aldrich) at 0.1mg/ml in a mixture of adjuvant diluted in Phosphate Buffered Saline (PBS). Different adjuvants were used following these two methods: Alum (Imject Alum, Pierce chemicals co.), MPL-A+TDM (Sigma), GLA-SE (IDRI), CFA or IFA (Sigma). Vaccines used clinically were tested, the Hepatitis B Virus (HBV) vaccines Fendrix (GSK) containing aluminum hydroxide and MPL-A, and Engerix B (GSK) that contains aluminum hydroxide only; and finally the seasonal Inactivated Influenza Vaccine (TIV) (Sanofi Pasteur) adsorbed in aluminum hydroxide. These vaccines were kindly provided by Prof. Charles Lacey and were diluted 1:2 in PBS and injected into mice subcutaneously in the flank.

Two to three weeks after the first challenge, mice were immunized with the same emulsion. Mice immunized with CFA were boosted with IFA or not at all. Four days later, inguinal LNs (iLNs) or popliteal LNs (pLNs) were isolated for analysis.

2.4. Sample collection

Blood was removed by cardiac puncture while the mice were anesthetized with isoflurane using heparin (Sigma Aldrich) coated syringes. Mice were then cervically dislocated to confirm death by a second method. When serum wasn't needed, mice were schedule 1 killed using increased concentrations of CO₂ and then cervically dislocated. Popliteal and inguinal LNs were removed and placed in Fluorescence-Activated Cell Sorting (FACS) wash, PBS containing 0.5% Bovine Serum Albumin (BSA) (Sigma Aldrich) and 2mM Ethylenediaminetetraacetic Acid (EDTA) (Sigma Aldrich).

2.5. Enzymatic digestion of lymph nodes

The digestion protocol was adapted from Fletcher A. et al. [188]. For flow cytometry or cell culture, LNs from mice were dissected and placed in RPMI-1640 media (Life Technologies). LNs were then pierced once with fine forceps and incubated with freshly made enzymatic mix containing 0.2mg/ml Collagenase P (Roche), 0.8mg/ml Dispase (Roche) and 0.1mg/ml DNaseI (Roche) in RPMI-1640. The tubes were then incubated at 37°C in a thermomixer with gentle mixing. After 20 minutes, LNs were carefully pipetted, releasing most leukocytes as it disrupted the capsule. Large fragments were then allowed to settle and the enzymatic mix was removed and added to 3 ml of cold FACS wash or cell culture media (α MEM (Life Technologies), 10% Foetal Calf Serum (FCS) and 5% L-glutamine) and centrifuged at 300g for 5 minutes at 4°C. The enzymatic mix was then added to the digestion tube, the contents mixed using a pipette and incubated for 10 minutes at 37°C in a thermomixer with gentle mixing. After the incubation, cells were mixed vigorously, after the fragments were again allowed to settle, the supernatant was removed and added to the previously spun cell pellet and centrifuged again. By this time, the fragments left over were fat and the LNs are digested. Cells were filtered through 70 μ m cell strainers, counted using a hemocytometer and plated at 500,000 cells/cm² or used for flow cytometry/cell isolation. For FRC culture, α MEM medium supplemented with FCS was used and after 24hrs post plating, cells were washed to remove non-adherent cells. Cells were incubated at 37°C with 5% CO₂.

2.6. FRC culture and treatment of cells

Total LN cells were cultured at 37°C with 5% CO₂ until a pure population of FRCs was obtained. When there was a pure population of FRCs, cells were plated at appropriate cell concentrations and treated with TLR agonists and incubated at 37°C with 5% CO₂. TLR agonists (Invivogen) were used at the concentration that was indicated by the manufacturer and adjuvants were used 1:1000.

2.7. Bone Marrow Dendritic Cell isolation and culture

Bones were removed from mice and cleaned. Bones were gently flushed and the bone marrow was collected into a petri dish. The cell suspension was transferred to a tube using a narrow gauge needle and through a cell strainer to remove debris. Cells were diluted to 2x10⁶ cells/ml with complete medium and 1ml of cells were distributed into 6-well plates. Medium containing 40ng/ml of murine recombinant Granulocyte Macrophage Colony-Stimulating Factor (GM-CSF) (Peprotech) was prepared and 1ml added to each well (final concentration of GM-CSF at 20ng/ml). Thereafter, 3, 6, 8 and 10 days later, media was removed and replenished with fresh medium containing GM-CSF. At day 11, cells were used for experiments and treated with TLR agonists (Invivogen) according to manufacturer's indication.

2.8. Flow cytometry procedure

2.8.1. Surface marker antibody staining

The single cell suspensions from the digested LNs were transferred into V-Bottom 96-well plates. Cells were resuspended in freshly made Fc block containing TruStain fcX a rat anti-mouse CD16/32 antibody (Biolegend) and rat IgG (Sigma) and incubated on ice for 10 minutes. The plates were then spun for 5 minutes at 4°C at 300g and the supernatant was discarded. The antibody staining mix containing the primary antibodies diluted in FACS wash was added to the cells and incubated 25-30 minutes on ice in the dark. Unstained controls and single stain controls prepared at the same concentration as in the master mix were also prepared. The antibodies used are listed in Table 2.3. Cells were washed three times, in cases where it was necessary the cells were incubated in the appropriate secondary antibody for 25-30 minutes on ice. Cells were then washed three times, resuspended in 150µl FACS wash and transferred to micro tubes (Titertube micro test tubes, Bio-Rad) containing 50µl of AccuCheck counting beads (Life Technologies). The samples were run on a Beckmann Coulter CyAn ADP flow cytometer machine

using the Summit software. Data acquired was analysed using the FlowJo software (Tree Star).

Gating strategies for identifying different cell types are shown in figures 2.2, 2.3 and 2.4.

2.8.2. Intracellular staining

In cases where the marker to be analysed was intracellular and did not require stimulation (e.g. FOXP3), following Fc block and surface staining, the cells were incubated in fixation/permeabilisation solution (eBioscience) for 30 minutes. The cells were washed twice in 1X permeabilisation buffer (eBioscience). Cells were then stained with the antibody master mix diluted in the permeabilisation buffer for 30 minutes on ice. The cells were washed twice and transferred to micro tubes.

2.8.3. Viability determination

After cell surface staining, cells were resuspended in PBS containing 4',6'-diamidino-2-phenylindole (DAPI) at a 1:5000 dilution and incubated 5 minutes on ice. Cells were then washed and transferred to micro tubes. The samples were run on a Beckmann Coulter CyAn ADP flow cytometer with the acquisition boost turned off. DAPI enters dead cells that have membrane permeability, this makes it possible to discriminate between live and dead cells as shown in Figure 2.1. For cells having undergone stimulation for intracellular staining, a viability dye eFluor 780 (eBioscience) was added to the master mix containing the surface marker antibodies instead of DAPI.

2.8.4. Quantifying cell numbers

To accurately calculate total cellularity of samples, AccuCheck counting beads were used. Prior to adding the beads to the micro tubes, the counting beads were thoroughly mixed. The cell and bead suspension was mixed before running on the flow cytometer. To ensure accuracy and that the beads were mixed properly, the counting beads consist of two types of beads that have different fluorescent intensity in the PE channel and should be at a ratio of 50:50 for the cell count to be accurate, but 45:55 was considered acceptable. Figure 2.1 illustrates how the counting beads appear on a flow cytometer plot. In order to calculate cell number, the beads were gated on along with the cell population of interest. The following calculation provided by Life technologies enabled cellularity determination:

$$\text{number of cells}/\mu\text{l} = \frac{\text{number of events (beads)}}{\text{number of events (cells)}} \times \text{number of beads}/\mu\text{l}$$

The number of beads per microliter was provided with the counting beads and varied between batches of beads.

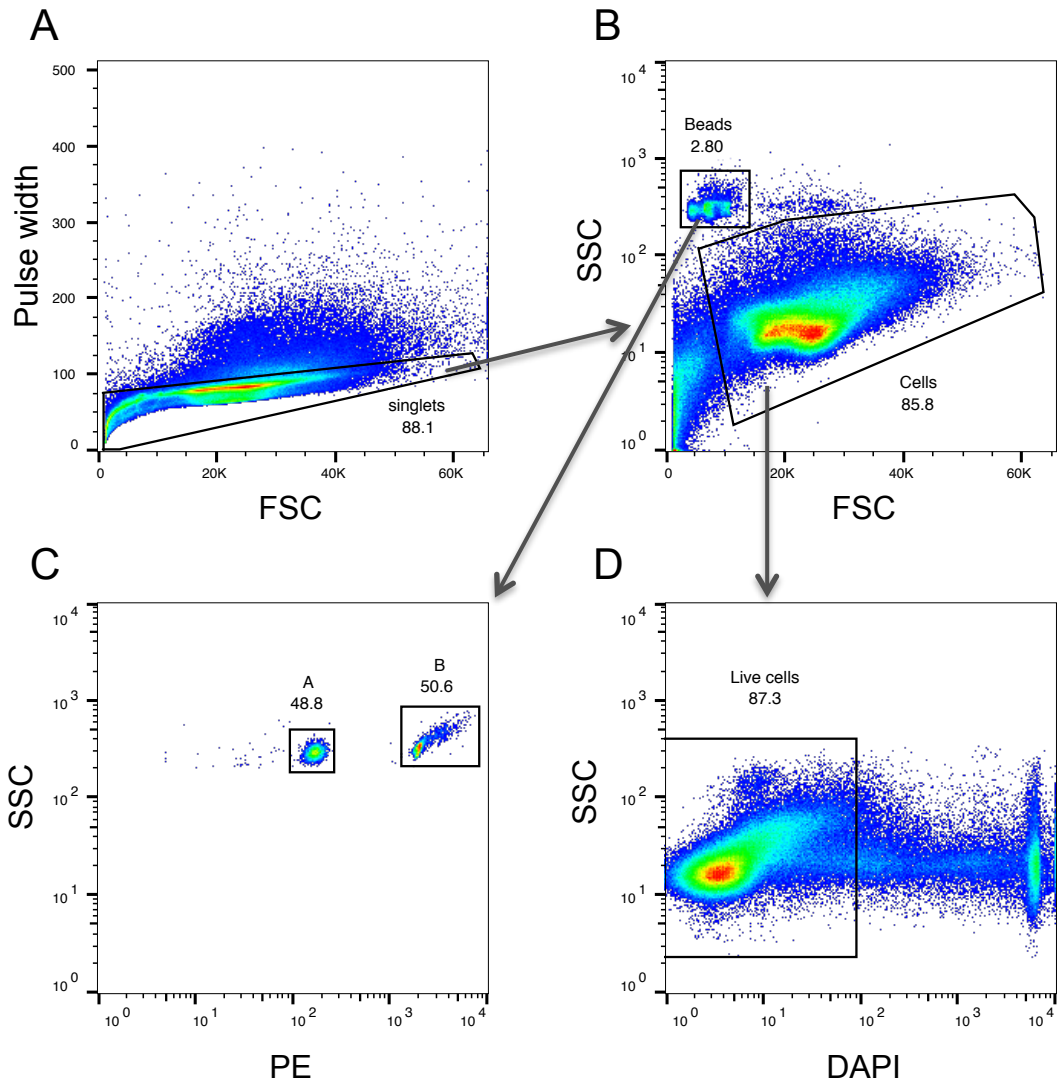


Figure 2.1: Accucheck beads were used to determine cellularity and a live-dead marker to determine viability.

Representative flow cytometry plots are shown here. **A:** Singlet discrimination was done by using the Pulse width. **B:** After staining, AccuCheck counting beads were added to the samples. The beads have a high side scatter (SSC) and a low forward scatter (FSC) that enables the easy distinction between the beads and the cells. **C:** The beads have different intensities in the FL2 channel; this helps distinguish the two sets of beads that need to be at a ratio near 50:50 to be deemed accurate. **D:** The live-dead stain with DAPI only stains the dead cells as the membranes are no longer intact.

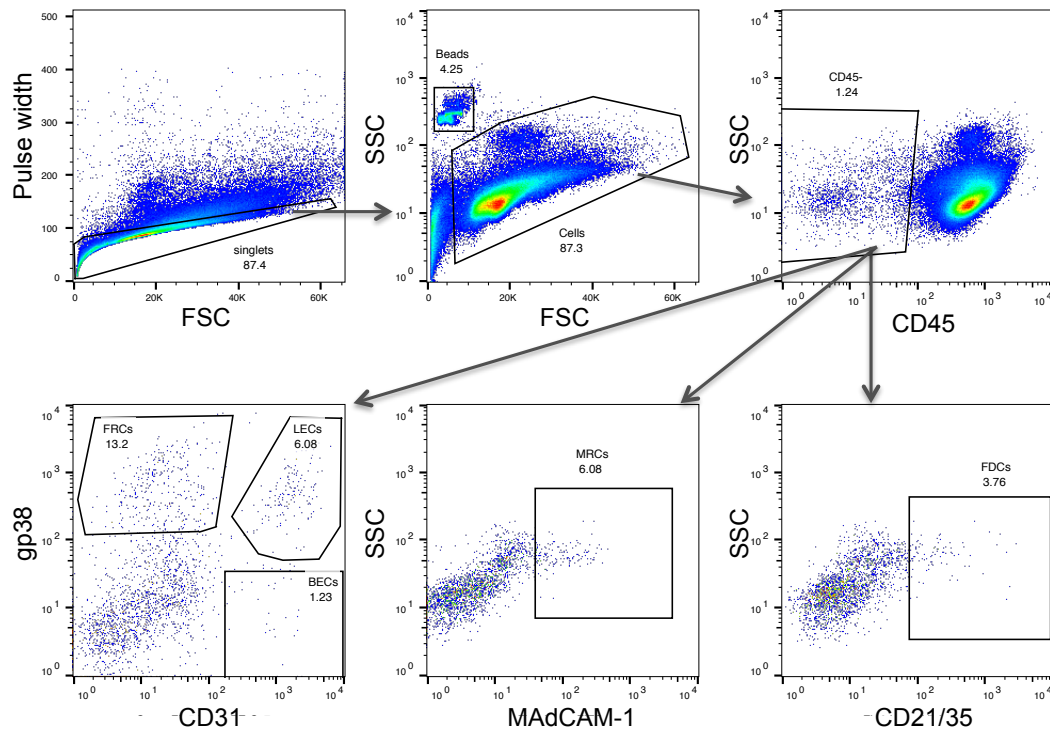


Figure 2.2: Gating strategies for identifying stromal cell subsets.

Representative flow cytometry plots are shown here. Singlet discrimination was done by using the Pulse width. Within CD45 negative cells it is possible to distinguish different cell types by using different markers. FRCs (CD45-gp38+CD31-), LECs (CD45-gp38+CD31+), BECs (CD45-gp38-CD31+), MRCs (CD45-gp38+MAdCAM-1+) and FDCs (CD45-gp38+CD21/35+).

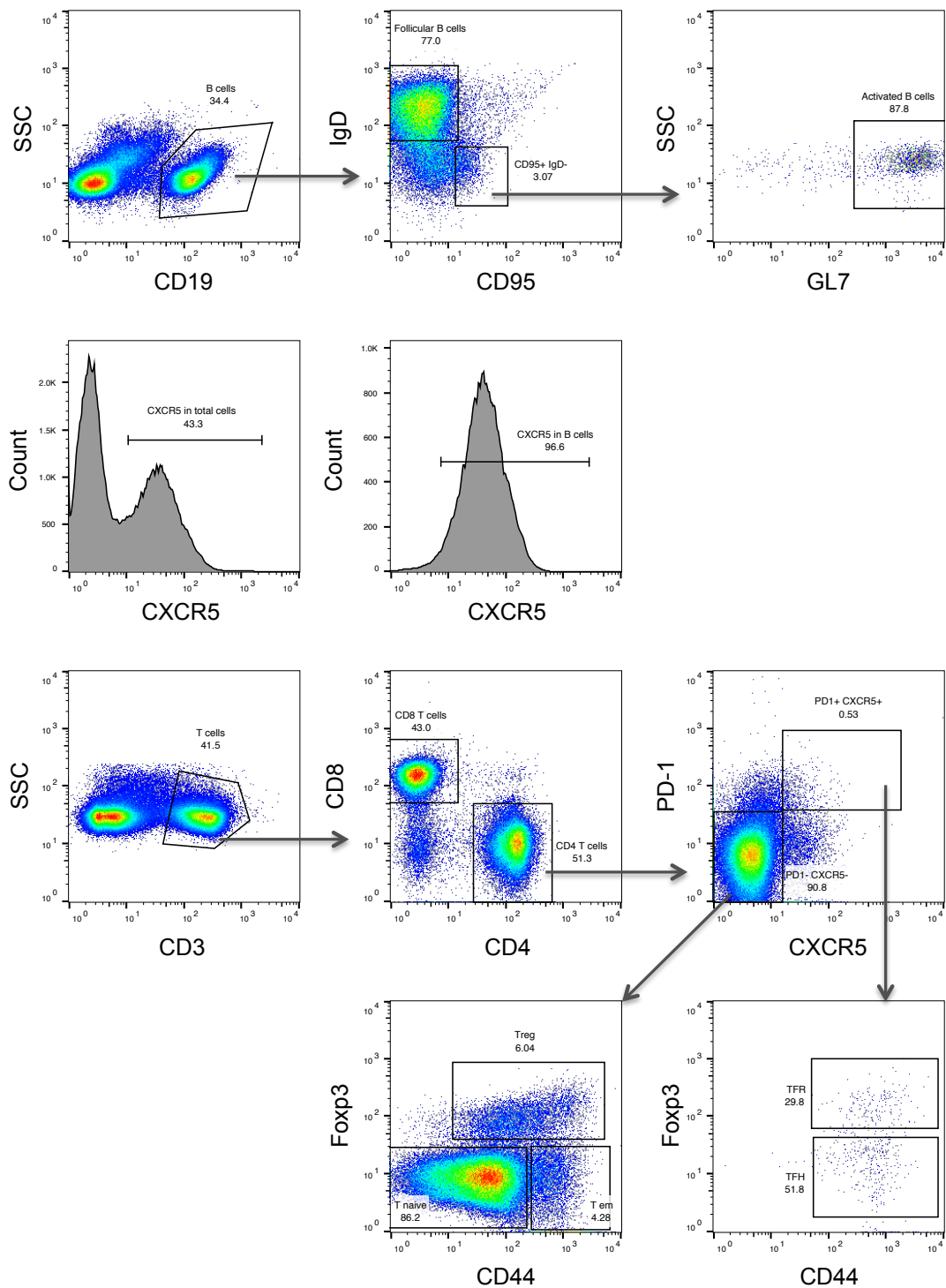


Figure 2.3: Gating strategies for identifying adaptive immune cell types.

Representative flow cytometry plots are shown here. Singlet discrimination was done by using the Pulse width. Different cell types can then be distinguished using different markers. Follicular B cells (CD19+IgD+CD95-), and Activated B cells (CD19+IgD-CD95+GL7+). CXCR5 is expressed in cells. T cells can be subcategorized as CD4+ and CD8+. Follicular Regulatory T Cells (CD4+PD1+CXCR5+Foxp3+CD44+), Follicular Helper T Cells (CD4+PD1+CXCR5+Foxp3-CD44+), T regulatory cells (CD4+PD1-CXCR5-Foxp3+CD44^{int}), T effector memory cells (CD4+PD1-CXCR5-Foxp3-CD44^{high}), T naïve cells (CD4+PD1-CXCR5-Foxp3-CD44-).

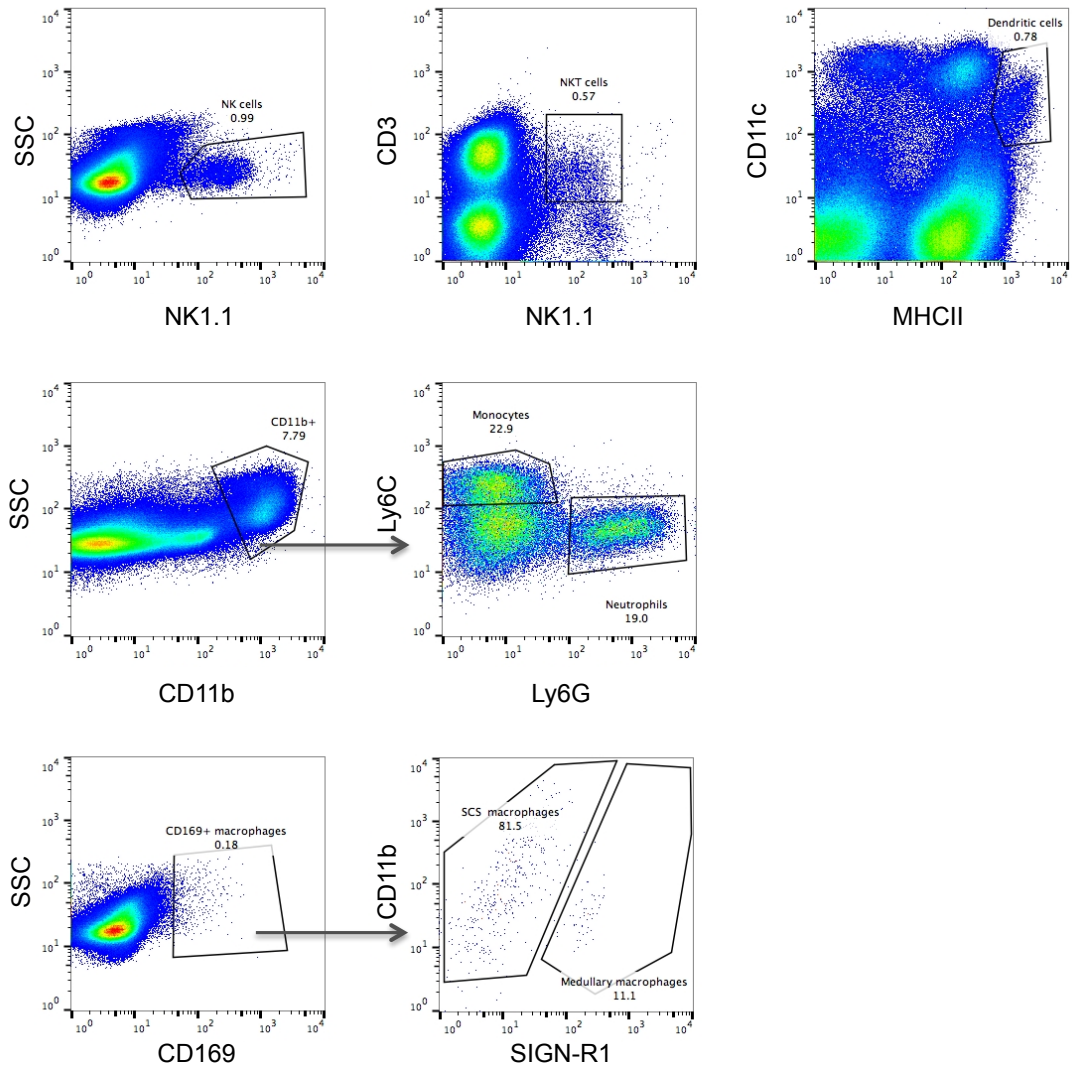


Figure 2.4: Gating strategies for identifying innate immune cell types.

Representative flow cytometry plots are shown here. Singlet discrimination was done by using the Pulse width. Different cell types can then be distinguished using different markers. NK cells (NK1.1+), NKT (NK1.1+CD3+), DCs (CD11c+MHCII^{high}), neutrophils (CD11b+Ly6C^{int}Ly6G^{high}), monocytes (CD11b+,Ly6G-Ly6C^{high}), Macrophages (CD169+), subcapsular sinus macrophages (CD169+SIGNR1+) and medullary sinus macrophages (CD169+SIGNR1-).

2.9. Cell sorting

To isolate specific cells from the draining LN, five mice were treated and their LNs were pooled to ensure sufficient cell numbers would be sorted. Samples were processed as described in section 2.5 and stained for flow cytometry as described in section 2.8. The staining was undergone in 15ml falcon tubes instead of 96 well plates. Before sorting, the cells were passed through a 40 μ m cell strainer to ensure there were no cell clumps and resuspended at a density of 10⁷ cells/ml in FACS buffer. Cells were sorted using a Beckman Coulter MoFlo Astrios machine into tubes coated with FCS. A post-sort sample was run to check that the purity was above 95%. Cells isolated were spun down and used for quantitative PCR (qPCR) analysis of genes.

2.10. Immunohistochemistry

2.10.1. Sample preparation and cryosectioning

LNs removed from mice were snap frozen in cryomoulds in Tissue-Tek™ CRYO-OCT Compound (Sakura) and stored at -80°C. 6 μ m sections were cut using a cryostat (Leica 1850) at -15°C onto labelled poly-L-lysine coated slides. Sections were air-dried for an hour and then stored at -20°C.

2.10.2. Immunofluorescent staining

Slides were removed from the freezer and left on the bench to reach room temperature for 30 minutes. Slides were then fixed with cold acetone for 10 minutes. The sections were circled with an Immedge pen (Vector Laboratories) and rehydrated by washing three times in PBS for 5 minutes. Samples were then incubated with blocking buffer containing 5% Goat serum and 1.5% Triton X-100 (Sigma Aldrich) for an hour. The serum chosen was dependent on the species the secondary antibody was raised in. Sections were then stained in the blocking buffer containing the diluted antibodies (Table 2.3) for one hour at room temperature. As a control conjugated isotype controls were used to check specificity of staining. Slides were then washed in PBS three times. When the primary antibody was purified or biotinylated, a secondary antibody (Table 2.4) incubation step was performed at room temperature for an hour. The slides were then washed in PBS again and dried. Prolong gold (Life technologies) was added to each section and mounted in SLS Coverslips No 1.5 22x64 mm. After incubating the slides overnight at 4°C, nail varnish was used to seal the coverslip onto the slide. All stained slides were stored at 4°C.

2.10.3. Confocal imaging

Sections were then examined using a Zeiss 710 confocal microscope on a fully motorised invert microscope and the Zen 2009 software. The microscope has five independent lasers and seven laser lines (405, 458, 488, 514, 561, 594 and 633 nm). LNs were imaged using the 10x objective, and tile scans were performed to image the whole tissue. The images were taken at 1024x1024 pixels with an average of 16. Images obtained were analysed using the image-processing package Fiji and the images were further processed using Photoshop (Adobe CS4).

2.10.4. Image quantification

The images obtained from stained sections (e.g. sections stained for B and T cells) were quantified by using Cell Profiler image analysis software (www.cellprofiler.org (Broad Institute)). This software works by creating a pipeline allowing sequential algorithms to be applied to image stacks. The “LN image analysis pipeline” first sets the specific channels to black and white, then it blurs the images permitting the software to distinguish B cell areas or T cell areas depending on which channel has been set to black and white (Figure 2.5).

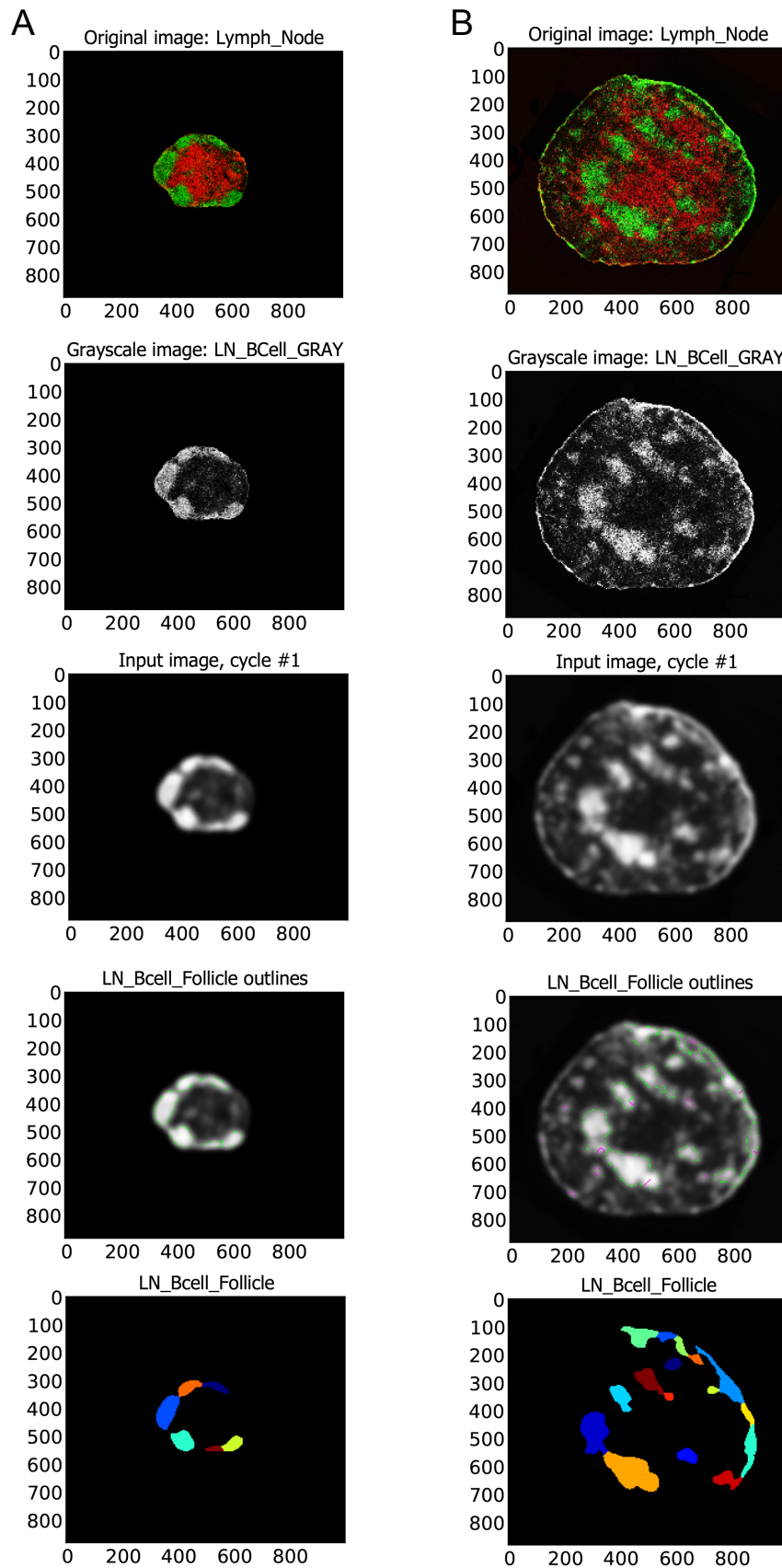


Figure 2.5: Cell profiler B cell follicle quantification pipeline.

A: Illustrates the pipeline used on a PBS treated LN and **B:** An OVA/GLA-SE treated LN. The green fluorescence staining the B cells is changed to black and white and blurred. The objects are then identified and quantified.

2.11. Antibody ELISA

2.11.1. Sample preparation

Blood removed from mice by cardiac puncture was spun down at 300g for 10 minutes to isolate the serum. Immediately following centrifugation, the supernatant was transferred to a new tube. Samples were stored at -80°C and maintained at 4°C during Enzyme-Linked Immunosorbent Assay (ELISA) experiments.

2.11.2. Measuring serum antibody titres

To determine serum antibody titres, direct ELISAs were performed. The OVA antigen is bound to the multiwell Nunc immunoplate (Thermo Scientific) at 20µg/ml in Carbonate/Bicarbonate buffer (Sigma Aldrich) for 2 hours at room temperature. The plates were washed 3 times with PBS/0,05%Tween (PBS/T) and then blocked in PBS/2.5%BSA for 2hrs at room temperature. After which, the plates were washed 3 times with PBS/T. The serum was diluted at 1:300 in PBS/T, added to the plates and then serially diluted 1:3 and incubated overnight at 4°C. After washing the plates with PBS/T, secondary antibodies were added to plates (see Table 2.4) diluted in PBS/T and incubated for 2hrs at room temperature. The plates were washed and the BluePhos Microwell Substrate (Insight Bio) was added and left to react for 1hr at room temperature. The reaction was stopped by adding the Alkaline Phosphatase Stop Solution (Insight Bio). The plates were then read at 595nm in a Bio-Rad Microplate reader. The antibody titre was calculated as the serum dilution needed for a pre-determined optical density.

2.11.3. Measuring serum antibody avidity

To determine serum antibody avidity, direct ELISAs were performed. The plates were treated in the same way as described in paragraph 2.11.2 until serum was to be added. The serum was diluted 1:2000, added to plates and incubated overnight at 4°C. The plates were washed 3 times with PBS/T and prepared dilutions of sodium thiocyanate (NaSCN) of 3M, 2.5M, 2M, 1.5M, 1M, 0.5M, and 0.25M were added to the wells. The plates were washed and the secondary antibodies were added to the wells and incubated for 2hrs at room temperature. The plates were washed and the BluePhos Microwell Substrate (Insight Bio) was added and left to react for 1hr at room temperature. The reaction was stopped by adding the Alkaline Phosphatase Stop Solution (Insight Bio). The plates were then read at 595nm in a Bio-Rad Microplate reader. The avidity index

is the NaSCN concentration at which 50% of the bound antibodies are eluted off.

2.12. Quantitative PCR

2.12.1. RNA extraction

Isolated cells were spun down at 300g for 5 minutes at 4°C, supernatant was removed and cells were lysed using QIAzol Lysis Reagent (Qiagen) and disrupted by vortexing the cells for one minute. The homogenate was incubated at room temperature for 5 minutes and the lysates were stored overnight at -80°C. RNA was extracted from cells following the Qiagen miRNeasy mini or micro kit protocol. These kits enable the purification of total RNA, including RNA of 18 nucleotides and upwards. The micro kit was used for the sorted stromal cells that were in low quantity. The micro kit is designed for small numbers of cells and elutes in a final volume of 14µl. The RNA quantity and quality was determined by using a nanodrop spectrometer. The 260/280 ratio of the sample had to be above 1.8 to not be considered contaminated. RNA samples were then stored at -80°C and kept at 4°C at all times during experiments.

2.12.2. Total complementary DNA synthesis

RNA was diluted in nuclease free water to a final volume of 10µl at known quantities determined by the nanodrop. If samples had a yield that was too low, which was the case for sorted stromal cells, RNA was left undiluted and 10µl was directly used. The master mix was added to the diluted RNA samples and contained 4.2µl H₂O, 2µl Reverse Transcriptase (RT) buffer, 0.8µl dNTP mix, 2µl RT Random Primer, and 1µl MultiScribe Reverse Transcriptase from the High Capacity cDNA Reverse Transcription Kit (Applied Biosystems). The samples were retro-transcribed in a thermo cycler PCR machine (SensoQuest). The conditions were 10 minutes at 25°C, two hours at 37°C and finally 5 minutes at 85°C. The samples were maintained at 4°C when handled and 80µl of nuclease free water was added to the samples before storage at -20°C.

2.12.3. Specific miRNA complementary DNA synthesis

Levels of mature miRNAs were determined using commercially available probes from Invitrogen. The reverse transcriptase procedure was followed as described. Two microliters of RNA was added to the master mix containing 8.16µl nuclease free water, 1.5µl RT buffer, 0.15µl dNTPs, 0.19µl RNase inhibitor, 2µl of miR-specific RT

probe and 1µl Multiscribe Reverse Transcriptase from the TaqMan MicroRNA Reverse Transcription Kit (Life Technologies). The samples were retro-transcribed in a thermo cycler PCR machine (SensoQuest). The conditions followed were 5 minutes at 4°C, 30 minutes at 16°C, 30 minutes at 42°C and 5 minutes at 85°C. The samples were maintained at 4°C when handled and stored at -20°C.

2.12.4. Primer design

Primers for SYBR green qPCR were designed using the NCBI Blast software to be between 18 and 24 nucleotides and ordered from Sigma. This length enables the primers to have adequate specificity and to bind to the template at the annealing temperature. To decrease the possibility of genomic DNA amplification, primers were designed to span an exon-to-exon junction. Primers had a melting temperature in the range of 60°C, a GC content of 50% and possessed no possible secondary structure as this would reduce the primer availability in the reaction. The amplicon product length is of 100-200 base pairs. Upon arrival, primers were hydrated with nuclease free water to a concentration of 100nM, a 10nM working stock for each primer was then made and stored at -20°C.

Taqman probes for miR-132 and the internal control RNU6 were ordered from Invitrogen.

2.12.5. qPCR reaction

Power SYBR Green PCR Master Mix or TaqMan Universal PCR Master Mix, no AmpErase UNG (Life Technologies) were used for qPCR. Each sample was run in duplicate and *Hprt* (hypoxanthine phosphoribosyltransferase) or *Rnu6* (U6 small nuclear RNA) were used as endogenous control genes. The qPCR mix was composed of 12.5µl of one or the other PCR Master Mix, 1µl of forward primer, 1µl of reverse primer, and 6.5µl H₂O for total cDNA or 9.5µl H₂O for specific miRNA. 4µl cDNA or 2µl specific miRNA were added to the MicroAmp Optical 96-well reaction plate (Applied Biosystems) along with the prepared master mix. Control samples for the qPCR reaction containing no cDNA or no RT reaction were included in the plates. The reaction was run on an Applied Biosystems 7300 real time PCR machine. The qPCR reaction was composed of the activation step consisting of heating the plate to 50°C for two minutes, followed by 95°C for 10 minutes. The data collection step was 40 cycles of a step at 95°C for 15 seconds, followed by one minute at 60°C. The qPCR reaction was followed by a melt curve that is described below.

2.12.6. Melt curve

After the SYBR green qPCR reaction, a melt curve analysis was done to assess that the assay produced a single amplicon. The final product is exposed to a temperature gradient from 50°C to 95°C while the fluorescence is analysed. The temperature at which the double stranded DNA melts into single stranded DNA leads to a decrease in fluorescence as the dye dissociates. The peak number is a reflection of the amplicon number. Therefore, primers producing a single peak are considered specific. This is illustrated in Figure 2.6.

2.12.7. qPCR analysis

After the reaction was finished, the threshold was placed automatically at 0.2Rn (which is the fluorescence signal normalized to a reference dye signal) in the linear part of the curve. This enabled the collection of Threshold cycles (Ct) that is the cycle number at which the fluorescence reaches threshold. The average Ct values and standard deviation were calculated from the duplicate raw Ct values for each sample. The values for each gene analysed were normalized to Ct values for *Hprt* or *Rnu6* for each sample giving the Δ Ct values. The $\Delta\Delta$ Ct values were then calculated using a control sample as calibrator and subtracting every sample's Δ Ct from the control sample. The fold change, or relative quantity was calculated as $2^{-\Delta\Delta Ct}$.

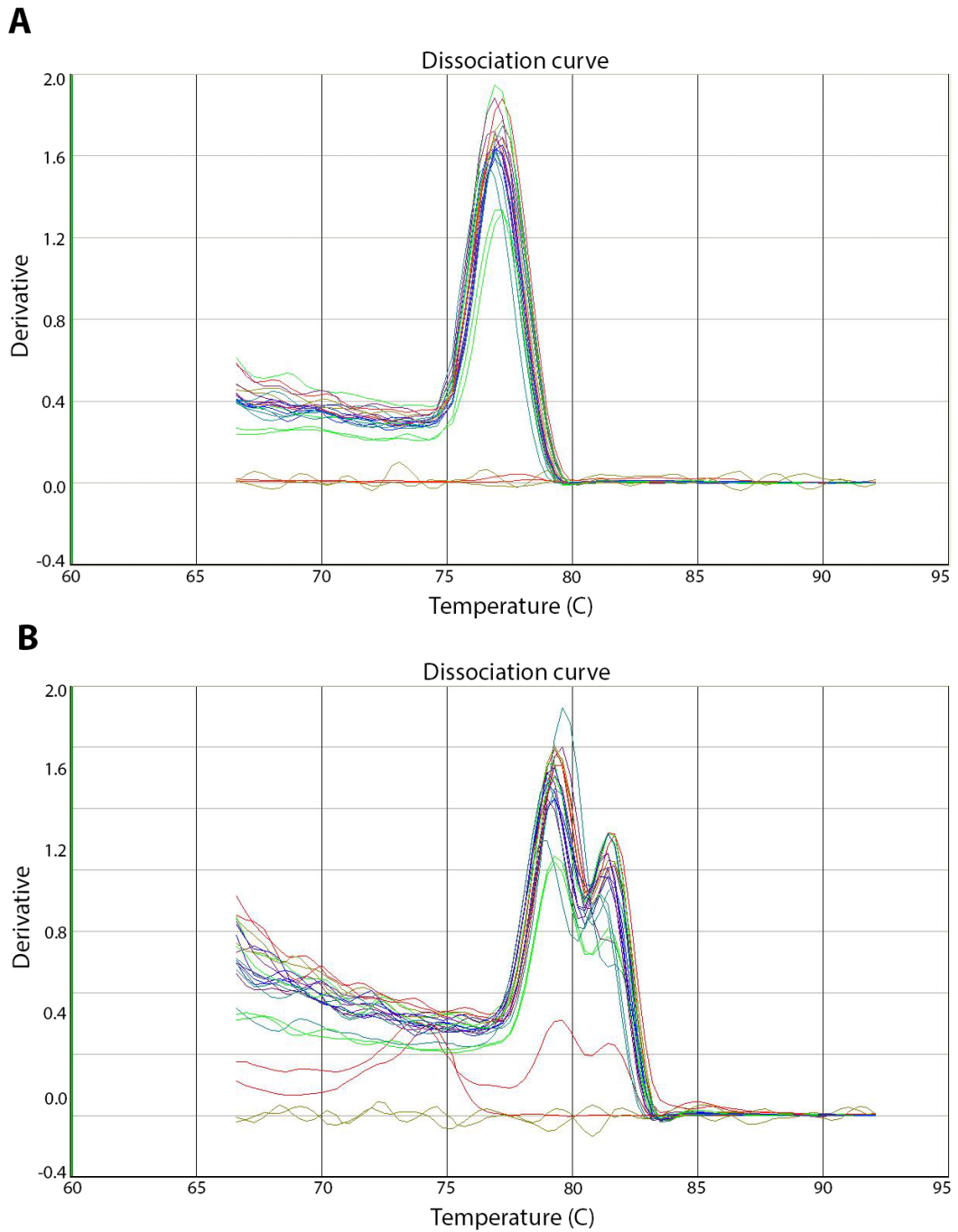


Figure 2.6: Melt curve analysis to confirm product specificity plots fluorescence vs Derivative fluorescence.

A: A single peak illustrates the specificity of the product amplified whereas **B:** shows there are two peaks and that the amplification was not product specific.

2.13. CD11c+ cells depletion

B6.CD11cCreTg.Rosa26iDTRfl mice express the primate Diphtheria Toxin Receptor (DTR) in all cells that have expressed CD11c. Diphtheria toxin (DTx) is harmless to the mice but specifically eliminates cells that express the DTR upon DTx administration [186]. 100ng of DTx (Sigma) diluted in PBS was administered intraperitoneally. After 24hrs after DTx treatment, mice were immunized with OVA/GLA-SE for 48hrs. pLNs were then analysed by flow cytometry.

2.14. TNF α inhibition

B6CD45.1 and miR-132^{-/-} mice were administered 2.5mg/ml *InVivo*Mab anti-TNF α (BioXCell) in 100 μ l intraperitoneally. 72hrs post treatment, mice were sacrificed and LNs were analysed by histology.

2.15. Statistics

Statistical analysis was done using the software GraphPad Prism. When comparing the effect of one parameter, such as a treatment, a one-way ANOVA was done to check the variances followed by a Tukey's or Dunnett's multiple comparison test and when comparing the effect of genotype and treatment a two-way ANOVA was done followed by a Tukey's or Dunnett's multiple comparison test. When comparing two groups a standard unpaired t-test was done. Data was then plotted on graphs with bars illustrating the mean values and error bars representing the Standard Error of the Mean (SEM).

Chapter 3: TLR4 agonists induce LN remodelling

3.1. Introduction

3.1.1. Initiation of LN hypertrophy

The innate immune response modulates LN microenvironments leading to changes in lymphocytes and DCs recruitment. This increases the chance of T cells interacting with APCs, thus initiating the adaptive immune response. The increase in lymphocyte and DC recruitment leads to an increase in LN size supported by an increase in stromal cells. “Inflammation induced recirculation” is the term used to refer to naïve lymphocytes being recruited into draining LNs from the site of infection [189]. In homeostatic conditions, lymphocytes regularly enter the LNs through HEVs from the blood. The cellular entry into LNs is dictated by chemokines produced by stromal cells, namely CCL19, CCL21 and CXCL13. HEVs express chemokines and adhesion molecules permitting the extravasation of cells into the LN [1]. Mice lacking certain adhesion molecules possess a deficiency in immune cell entry and in the formation of immune responses [190, 191].

During an immune response, T and B cell numbers increase while cell egress is shut down, enabling the rapid accumulation of cells [192]. Rapid changes to the stromal networks have to occur during the first few days of the immune response to facilitate the increase in cell numbers and drive an efficient immune response. Right after an infection, lymphatic vessels expand leading to an increase in APC entrance into the LN from the periphery [85]. Early stages of expansion are associated with an increase in LN neo-vascularisation, leading to an increase in blood flow to and from the LN. After antigen stimulation the HEV network increases in length. This increase in vascularity is not only due to vasodilatation but to proliferation of BECs [193]. HEVs proliferation in draining LNs is thought to be induced by DCs facilitating immune cell interactions and LN hypertrophy [194]. Although there are more HEVs, the growth is proportional to the increase in LN size; therefore the density of HEVs remains the same. Vasculature expansion is initiated by DCs that produce IL-1 β stimulating VEGF production by FRCs [68, 195]. Further expansion of the LN architecture is dependent on T and B cells [82]. Cell egress through S1PR signalling is blocked in a CD69 mediated process so that there can be rapid lymphocyte accumulation in the LN. Early presence of DCs and trapping of lymphocytes results in FRC expansion [89]. CLEC-2 expressed by DCs interacts with podoplanin on FRCs leading to a reduction in FRC contractility, thus

enabling FRCs to stretch to accommodate the increase in LN size [90]. Further expansion of the FRC network depends on interaction with T cells through lymphotoxin and LIGHT [89]. Changes in the LN architecture are regulated by the reticular network through TNFR and LT β R signalling [11].

3.1.2. LN architecture changes

Changes in LN architecture are dependent on the type of infection or immunization. Immune cell compartmentalization in LNs has been shown to be disrupted during an immune response. In some studies, this has been shown to be due to direct targeting of FRCs or to certain pathogens causing a down-regulation of CCL21, CCL19 and CXCL13 [55, 64]. Immunization with OVA/CFA or injections of DCs has been shown to lead to BECs proliferation illustrating the plasticity of these stromal cells and that BECs can be regulated by DCs [194]. It has been shown that in the case of LCMV infection, LN expansion is not facilitated by VEGF but by LT β production by B cells [196]. Immunizations with LPS and CFA both lead to changes in LN architecture and in changes to T and B cell zones [11, 98]. Repeated CFA delivery has been shown to potently stimulate LN hypertrophy, reorganisation of B cell follicles and blood and lymphatic vasculature angiogenesis [11].

3.1.3. Summary

In response to an infection or immunization, LNs rapidly expand to accommodate the rapid influx of innate and adaptive immune cells. To understand the molecular mechanism controlling this process it was important to identify and validate an appropriate model to investigate changes in LN architecture following adjuvant immunization.

3.1.4. Aims

- Establish an adjuvant-based model to investigate LN remodelling, defined as changes in LN architecture namely B cell follicles appearing in the paracortex.
- Investigate the effect of long-term treatment on LN architecture and on stromal cells.
- Investigate the dynamics of LN hypertrophy.
- Determine the role of lymphocytes and CD11c⁺ cells in LN hypertrophy.

3.2. Establishing a model of adjuvant mediated LN remodelling

Many different systems have been previously used to stimulate immune responses in draining LNs, thus it was necessary to identify and characterise a system that potently and reproducibly induced LN remodelling. Previous work analysing LN stromal remodelling was based on repeated footpad administrations of CFA [11]. Even though delivery of CFA drives high affinity antibody responses and tissue remodelling, it is toxic in humans and repeated administration cannot be done in the UK due to ethical concerns resulting from uncontrolled tissue inflammation. Therefore, different adjuvants and routes of administration were tested, focusing initially on subcutaneous delivery in the mouse flank, which drains to the inguinal LNs (iLNs). This injection was difficult to consistently reproduce, leading to high variation and limited LN remodelling (Figure 3.1). To test the effect of clinically approved vaccines on LNs, the HBV vaccines Fendrix (GSK) that contains aluminium hydroxide and MPL-A, and Engerix B (GSK), which contains aluminium hydroxide only; and finally the seasonal Inactivated Influenza Vaccine (TIV) (MASTA) adsorbed in aluminium hydroxide were injected. Immunizations led to a doubling in LN volume; however, although B cell follicles did increase in size they remained in the cortex.

An alternate technique to footpad administration was then used for the rest of the project called hock immunization [187]. Hock immunizations are done by subcutaneous injection with adjuvant/antigen complex in the region just above the ankle proximal to the Achilles tendon. The draining LN is mainly the popliteal LN (pLN) and small amounts of antigen/adjuvant complex drives immune response in the medial iliac LNs and to iLNs [197]. Injecting adjuvants in this site provides enlarged LNs with no impairment on the mouse's mobility, as it is a non-weight bearing structure. Adjuvants were administered at day 0, mice were then boosted at day 21 for three further days before sampling the pLNs at day 24. Immunization led to an enlargement of pLN when compared to the PBS treated mice (Figure 3.2). The strongest response was observed in MPL-A+TDM treated mice where the pLNs were massively enlarged and B cell follicular remodelling was observed. The synthetic TDM contained in the Sigma Adjuvant System is an analogue of the TDM of the tubercle bacillus. TDM is known to activate the immune response through the Mincle receptor and through TLR2. Inject Alum is formulated as a mix of aluminium hydroxide and magnesium hydroxide and will be referred to as Alum. From these results, the focus of all subsequent experiments was on TLR4 agonists using the pLN model.

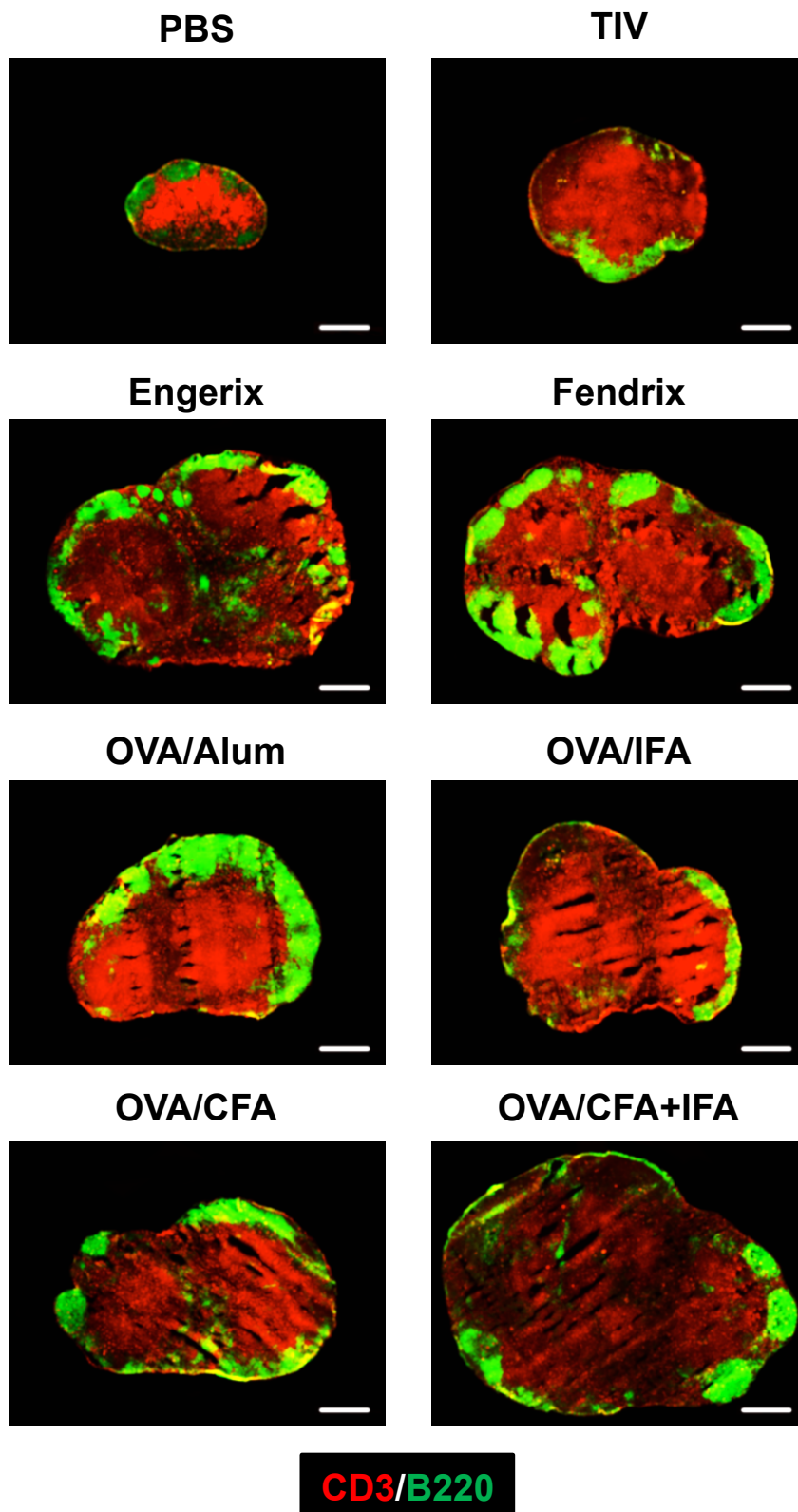


Figure 3.1: LN architecture when treated with antigen/adjuvant complexes in the flank.

Immunizations with OVA in combination with different adjuvants induce dynamic change of the LN. Frozen sections of the inguinal LN from B6CD45.1 mice injected in the flank. PBS, TIV, Engerix, Fendrix, OVA/Alum, OVA/IFA, OVA/CFA, and OVA/CFA+IFA immunized mice were stained with antibodies against CD3 (T cells) and B220 (B cells). Scale bar: 500 μ m.

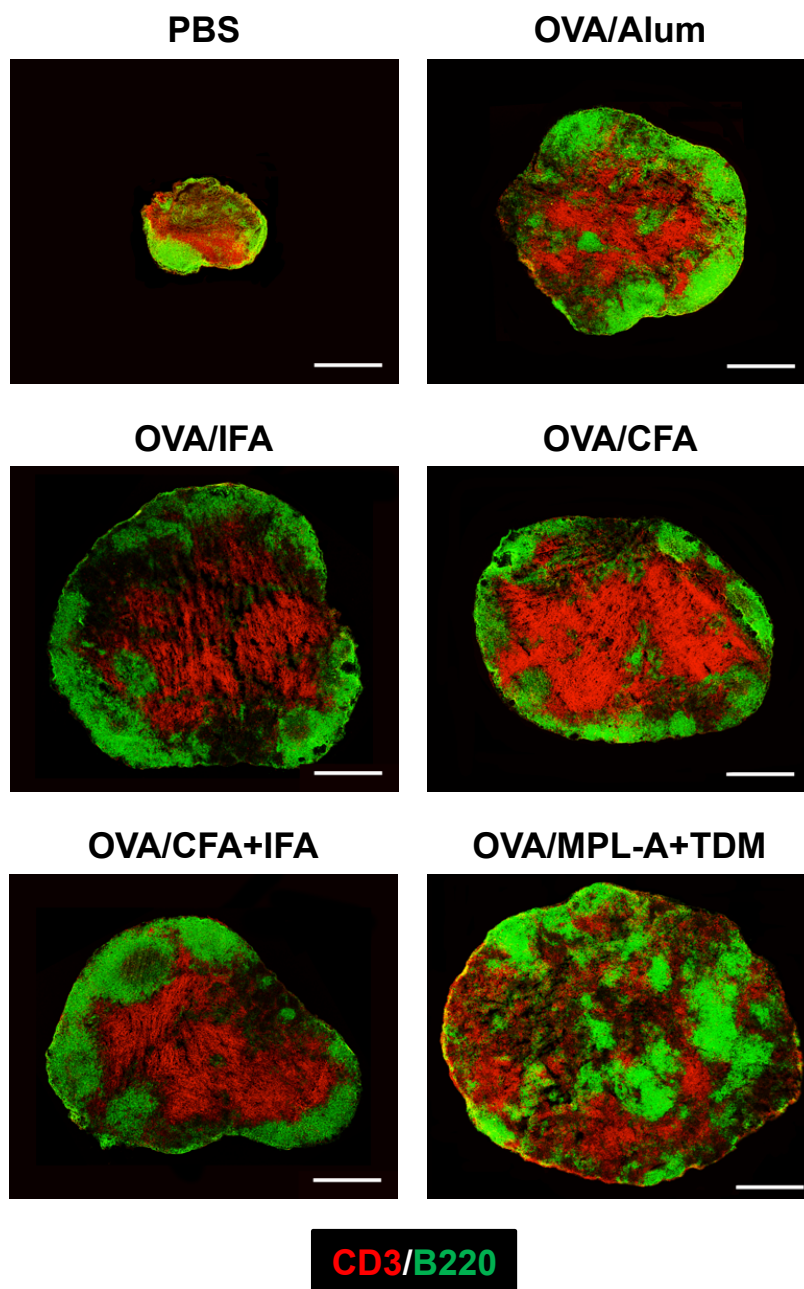


Figure 3.2: LN architecture when treated with antigen/adjuvant complexes in the hock.

Immunizations with OVA in combination with different adjuvants induce dynamic change of the LN. Frozen sections of the popliteal LN from B6CD45.1 mice injected in the hock. PBS, OVA/Alum, OVA/IFA, OVA/CFA, OVA/CFA+IFA, and OVA/MPL-A+TDM immunized mice were stained with antibodies against CD3 (T cells) and B220 (B cells). Scale bar: 500 μ m.

3.3. Effect of adjuvants on LN remodelling

3.3.1. Treatment induces LN hypertrophy

The mice were injected in the hock for three weeks with TLR4 agonist adjuvants, then boosted for three further days before sampling the pLNs (Figure 3.3). To quantify LN enlargement LNs were digested and absolute cell number were compared (Figure 3.3A). Treatment with OVA/MPL-A+TDM led to a 2-fold increase in total cellularity compared to a 4-fold increase in cellularity in OVA/GLA-SE injected mice. This shows a significant increase in total cellularity after injection of OVA/GLA-SE. To determine how changes in cell numbers correlated with changes in LN volume, LNs were weighed (Figure 3.3B) and frozen sections from LNs were cut from the centre for the LN and the area of each section was quantified (Figure 3.3C). The images obtained from separate experiments were quantified by using Cell Profiler image analysis software (www.cellprofiler.org). This image analysis package works by creating a pipeline allowing sequential algorithms to be applied to image stacks. The “LN image analysis pipeline” first sets the specific channels to black and white, then it blurs the images permitting the software to distinguish B cell areas. Using this approach, the images were analysed for LN area. OVA/MPL-A+TDM injected LNs had 3-fold increase in weight, whereas treatment with OVA/GLA-SE led to a 12-fold increase in weight. A 6-fold increase in total LN area was also observed upon OVA/GLA-SE stimulation. As a TLR4 agonist adjuvant, GLA-SE is significantly more potent in inducing LN hypertrophy compared to MPL-A+TDM. For all subsequent experiments we focused on GLA-SE as a TLR4 agonist adjuvant.

3.3.2. Treatment induces an increase in immune cells

To determine if the expansion observed resulted from selective expansion of specific cell types during hypertrophy, LN cell populations were quantified by flow cytometry (Figure 3.4) after treatment with adjuvants. Alum was used here as a control as it is to this day the most commonly used in vaccines. Treatment led to a significant increase in all cell types analysed, both with OVA/Alum and with OVA/GLA-SE when compared to PBS. OVA/GLA-SE treatment led to a significant increase in total cellularity, B cells, T cells, CD4 T cells, CD8 T cells and NK cells compared to OVA/Alum. Analysis of macrophages (subcapsular and medullary) showed no significant difference in OVA/Alum and OVA/GLA-SE treated mice. There was a significant reduction in the number of DCs in OVA/GLA-SE stimulated in comparison to OVA/Alum.

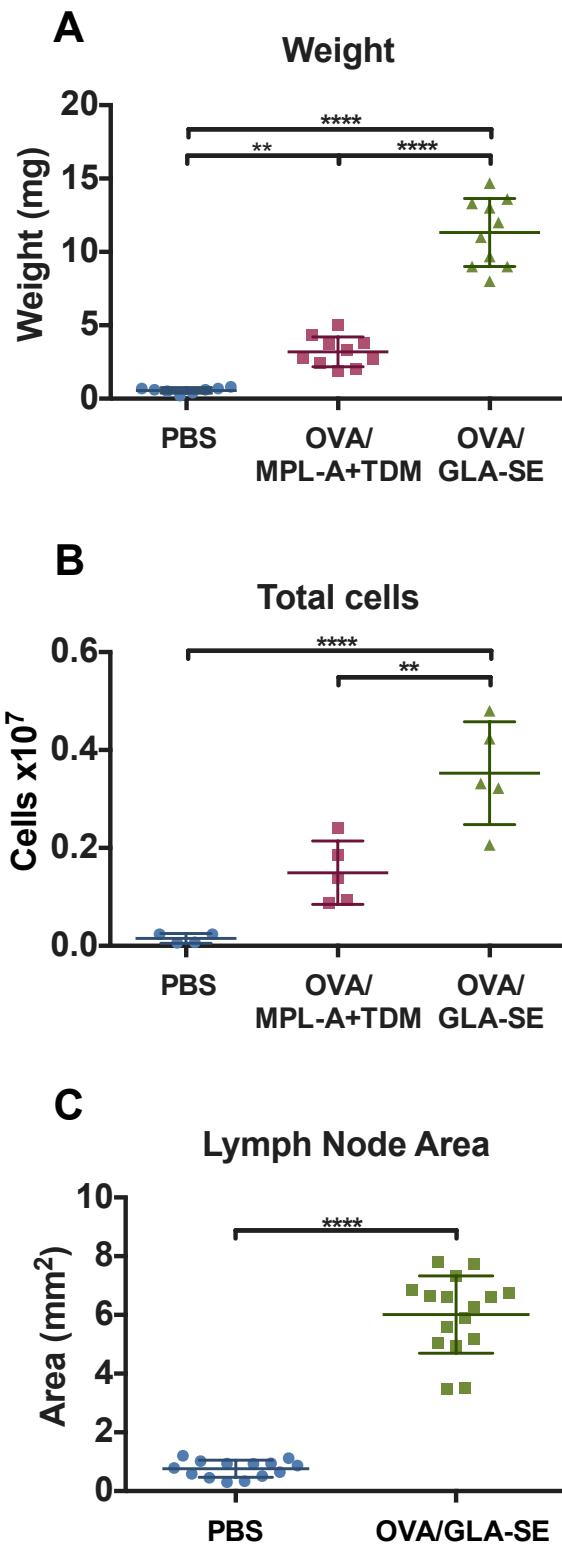


Figure 3.3: Effect of different adjuvants on lymph node size.

Mice were treated with PBS, OVA/MPL-A+TDM or OVA/GLA-SE for 3 weeks then boosted with the same solution for a further 3 days. LNs from mice were digested and stained for flow cytometry or stained for histology and LN size was measured using Cell Profiler. **A:** Weight, **B:** Total cells, and **C:** Lymph Node Area. AccuCheck counting beads from Invitrogen were used to get an accurate cell count. Data are cell number +/- SEM with A: N=10 and B: N=5 mice. One-Way ANOVA followed by multiple comparison Tukey's test. C: N=16 student t-test: *P ≤ 0.05, **P ≤ 0.01, *** P≤0.001, ****P ≤ 0.0001.

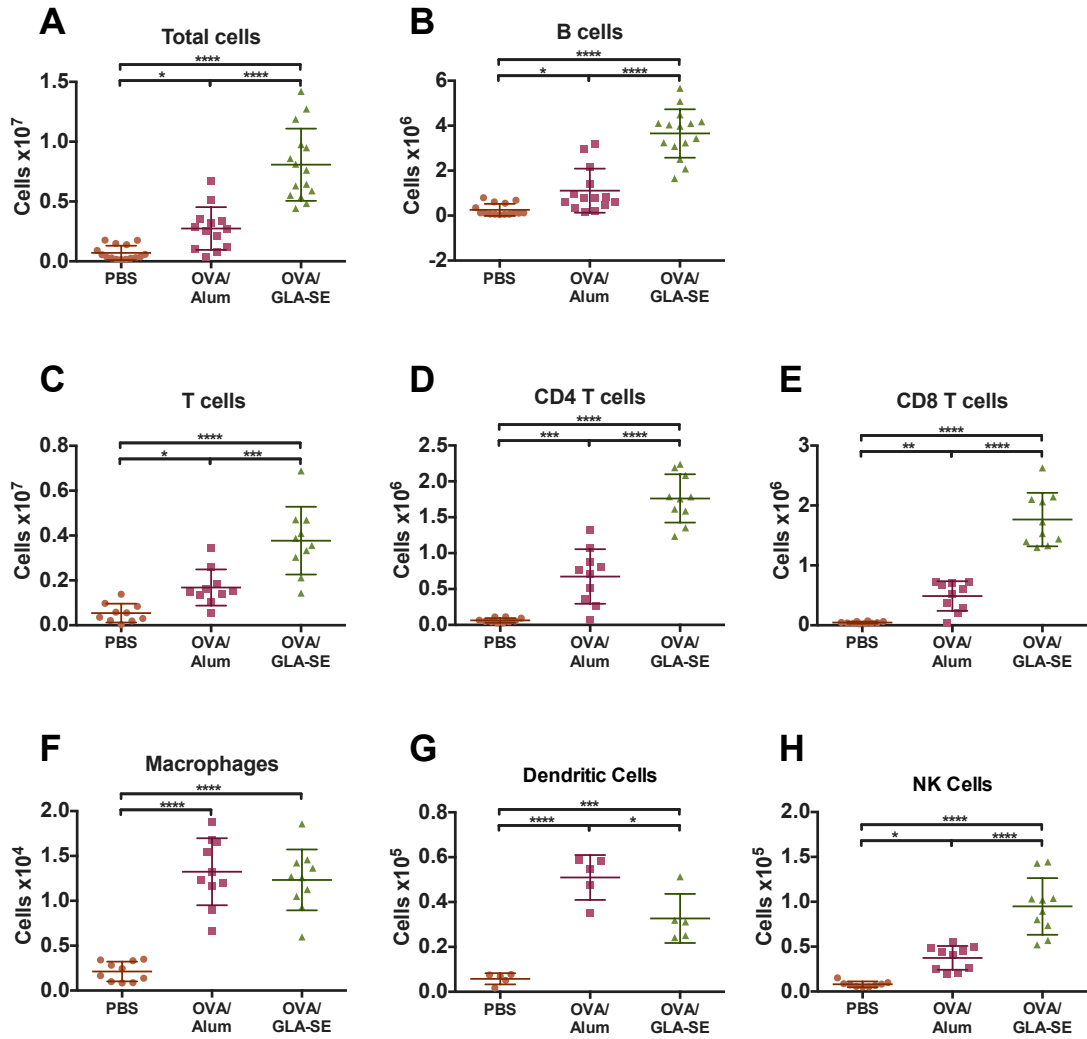


Figure 3.4: Effect of adjuvants treatment on immune cells.

Mice were treated with PBS, OVA/Alum, or OVA/GLA-SE for 3 weeks then boosted with the same solution for a further 3 days. LNs from mice were digested and stained for flow cytometry. **A:** Total cells, **B:** B cells (CD19+), **C:** T cells (CD3+), **D:** CD4 T cells (CD4+), **E:** CD8 T cells (CD8+), **F:** Macrophages (CD169+), **G:** Dendritic Cells (CD11c+MHCII+), and **H:** NK cells (NK1.1+). AccuCheck counting beads from Invitrogen were used to get an accurate cell count. Data are cell number +/- SEM with N=10 or 5 mice from 2 separate experiments. One-Way ANOVA followed by multiple comparison Tukey's test: *P ≤ 0.05, **P ≤ 0.01, *** P≤0.001, ****P ≤ 0.0001.

3.3.3. Treatment effect on B and T cell zones

Immunofluorescent stained tissue sections from popliteal LNs from long-term experiments (24 days; prime and boost) were analysed by confocal microscopy using antibodies specific for B cells and T cells (B220/CD3 respectively) (Figure 3.5). For the control PBS treated mice, the LNs were small with distinct B and T cell zones. Treatment with OVA/MPL-A+TDM led to an increased size but with still distinct B and T cell zones whereas OVA/GLA-SE led to remodelling and B cell follicles found in the cortex. The water-and-oil emulsion is a control for GLA-SE as it is the basis for this adjuvant but doesn't contain the TLR4 agonist. Treatment with OVA/water-and-oil emulsion led to an enlargement of the LNs with bigger B cell follicles. Due to the effect of the water-and-oil emulsion on LN structure and it being the basis of GLA-SE, this adjuvant should have been added as an additional control. OVA/Alum and OVA/IFA treated mice had LNs that were bigger and had larger follicles.

The images obtained from separate experiments were quantified by using Cell Profiler image analysis software. Using this approach, the images were analysed for LN area, follicle area and follicle number (Figure 3.6). Analysis from cell profiler correlated with the images obtained and with the flow results. OVA/GLA-SE leads to a 6-fold increase in LN area, a 1.5-fold increase in follicle area and a 3-fold increase in follicle number. OVA/Alum leads to a significantly less potent LN hypertrophy and increase in B cell follicles.

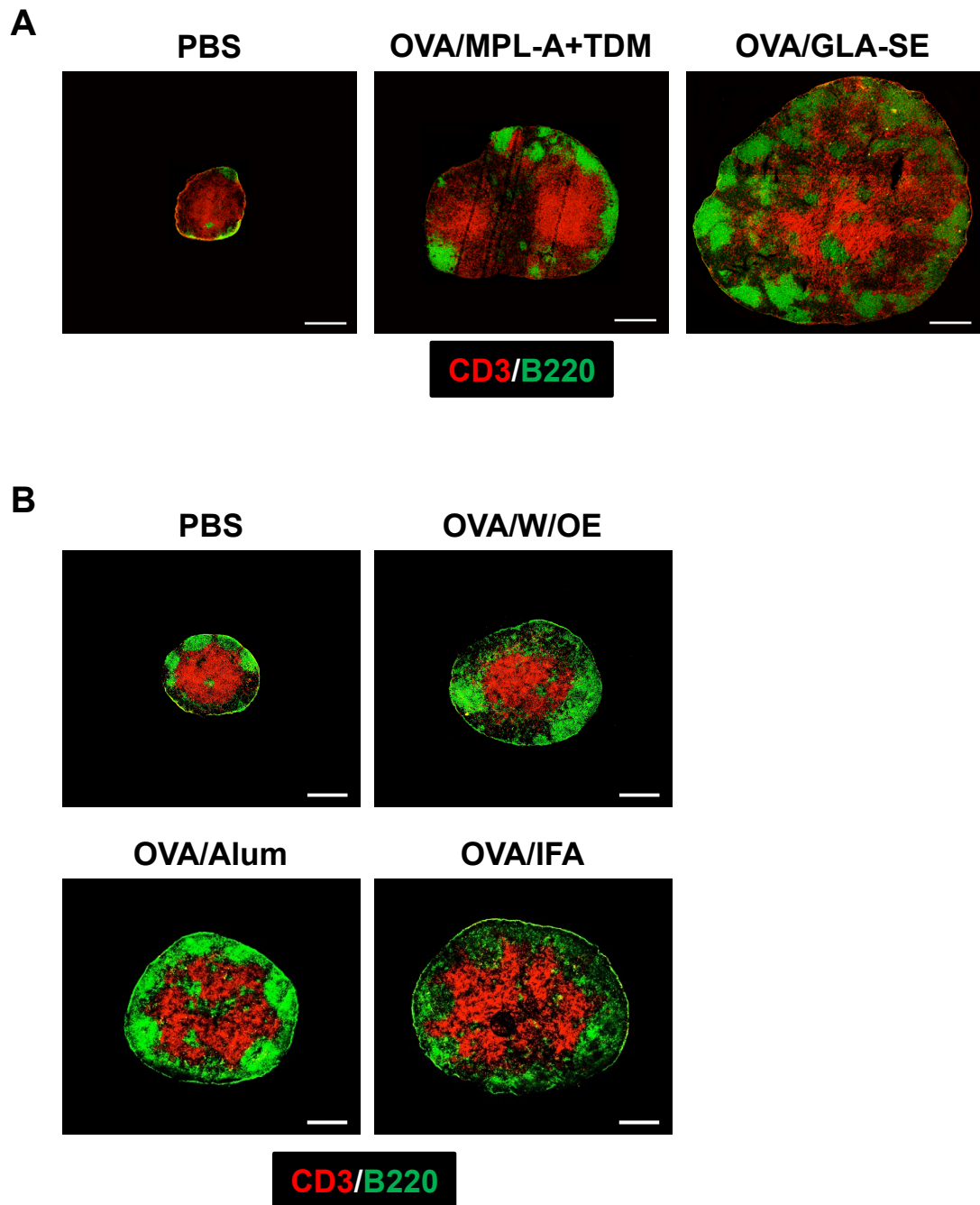


Figure 3.5: Dynamic remodelling of the LN when treated with different antigen/adjuvant complexes.

Mice were treated with PBS, OVA/Alum, or OVA/GLA-SE for 3 weeks then boosted with the same solution for a further 3 days. **A:** Frozen sections of the popliteal LN from PBS, OVA/MPL-A+TDM, and OVA/GLA-SE and **B:** Frozen sections of the popliteal LN from PBS, OVA/Water-and-oil emulsion, OVA/Alum, and OVA/IFA immunized mice were stained with antibodies against CD3 (T cells), B220 (B cells). N=5 mice, 2 slides/LN, representative image was chosen. Scale bar = 500 μ m.

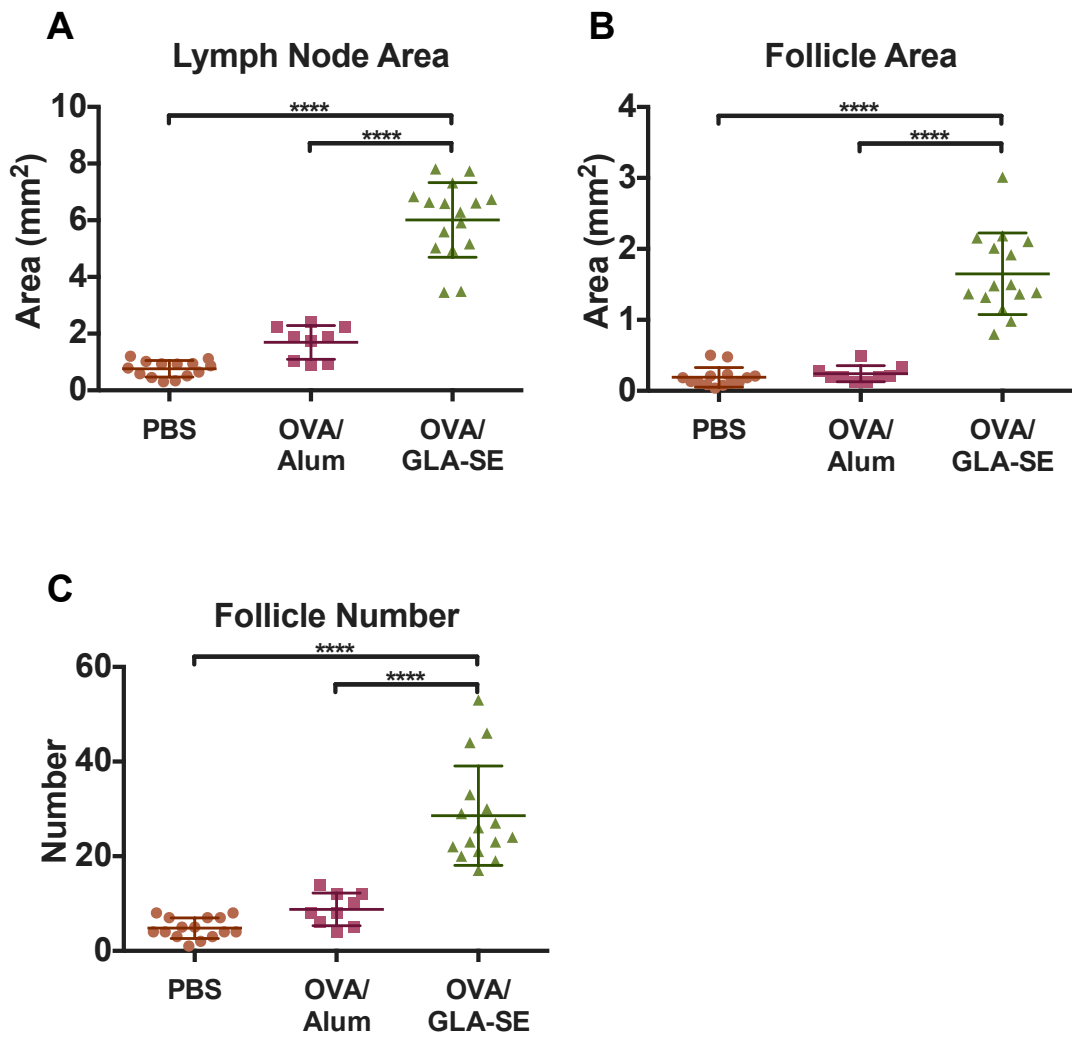


Figure 3.6: Quantification of histology results with Cell Profiler.

Frozen sections of the popliteal LN from PBS, OVA/Alum, or OVA/GLA-SE immunized mice were stained with antibodies against CD3 and B220. Images obtained were then run through a Cell Profiler pipeline to get the **A**: Lymph node area, **B**: Follicle Area, and **C**: Follicle number. N=15 from 3 separate experiments. One-Way ANOVA followed by multiple comparison Tukey's test: * $P \leq 0.05$, ** $P \leq 0.01$, *** $P \leq 0.001$, **** $P \leq 0.0001$.

3.3.4. Stroma in lymph node remodelling

Stromal cell networks support lymphocytes and DCs in LNs through producing chemokines, cytokines and an extracellular network on which lymphocyte can migrate and interact with APCs. Thus, stromal cell networks were characterised in sections using antibodies specific for LN reticular network (ER-TR7), FDC (FDCM2), and vascular networks (Lyve-1 (lymphatic vasculature) and Meca79 (HEVs)) (Figure 3.7). Immunizations with the TLR4 agonist adjuvants OVA/MPL-A+TDM and OVA/GLA-SE leads to pLN enlargement. The stromal network, as shown with the CD21/CD35 and ER-TR7 staining, mirrors the B and T cell distribution (as shown in Figure 3.5) and illustrates the LN remodelling. Treatment induced an expansion into the cortex of the LNs by the lymphatic vessels and an increase in the blood vasculature.

To quantify non-haematopoietic cells, LNs were processed using a reproducible low mortality enzymatic digestion protocol [188] (Figure 3.8). This method permits the analysis of the different major subsets of LN stroma by using the markers CD45, podoplanin (gp38) and CD31. Additionally, MRCs were identified and isolated by using MAdCAM-1 as a marker, and the FDC population using the CD21/35 marker. Treatment with OVA/GLA-SE leads to a significant increase in non-haematopoietic cells, FRCs, MRCs, LECs and BECS compared to both PBS and OVA/Alum treated LNs (Figure 3.9). This is consistent with the process of LN hypertrophy driving vasculature and stromal remodelling.

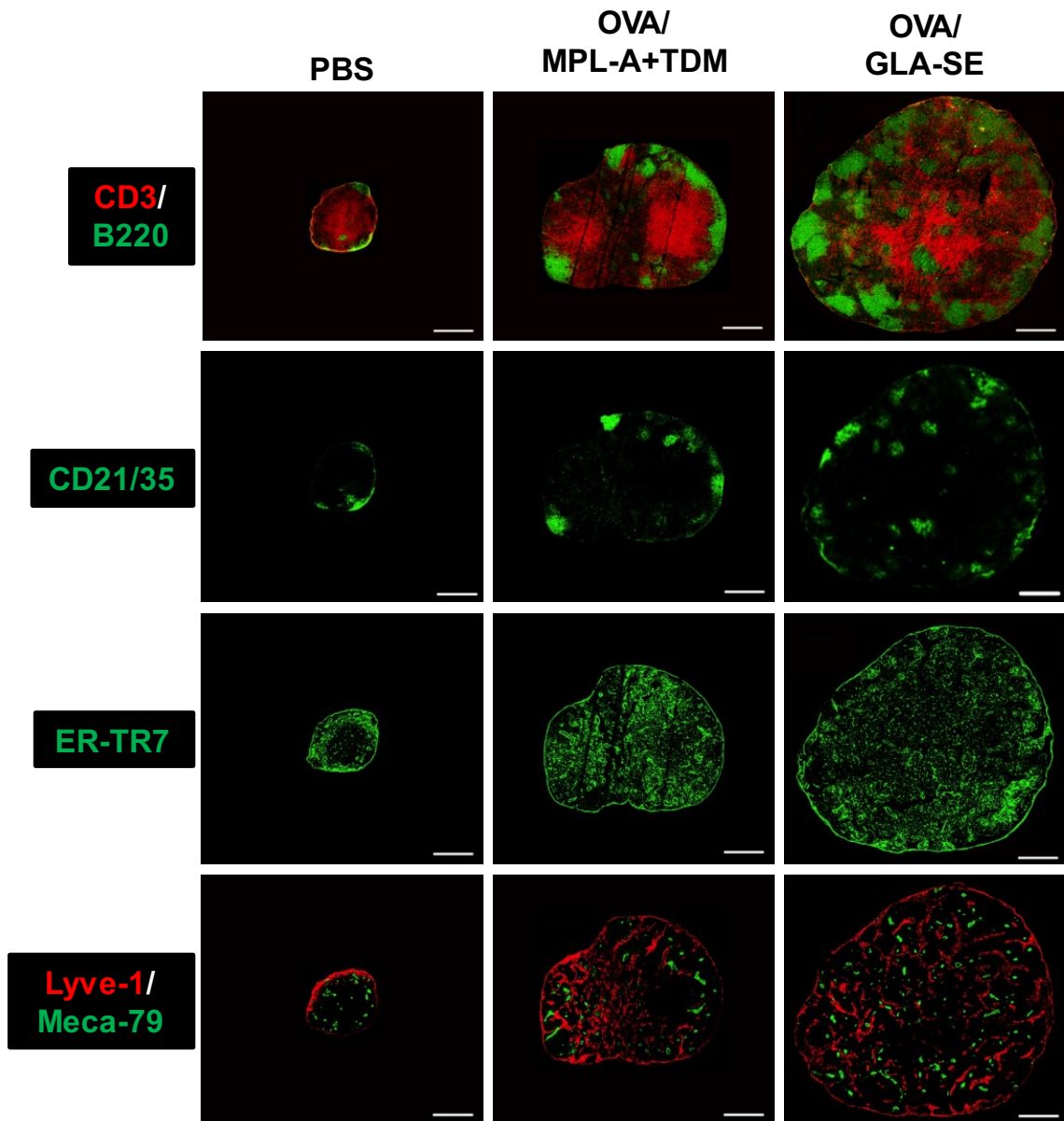


Figure 3.7: Architecture of the reticular network in mouse LN, and the dynamic remodelling when treated with antigen/adjuvant.

Mice were treated with PBS, OVA/Alum, or OVA/GLA-SE for 3 weeks then boosted with the same solution for a further 3 days. Immunizations with OVA in combination with different adjuvants induce dynamic change of the LN. Frozen sections of the popliteal LN from PBS, OVA/MPL-A+TDM, or OVA/GLA-SE immunized mice were stained with antibodies against CD3 (T cells), B220 (B cells), CD21/35 (FDCs), ERTR7 (Reticular network), Lyve-1 (Lymphatic vessels) and Meca-79 (HEVs). N=5 mice, 2 slides/LN, representative image was chosen. Scale bar = 500 μ m.

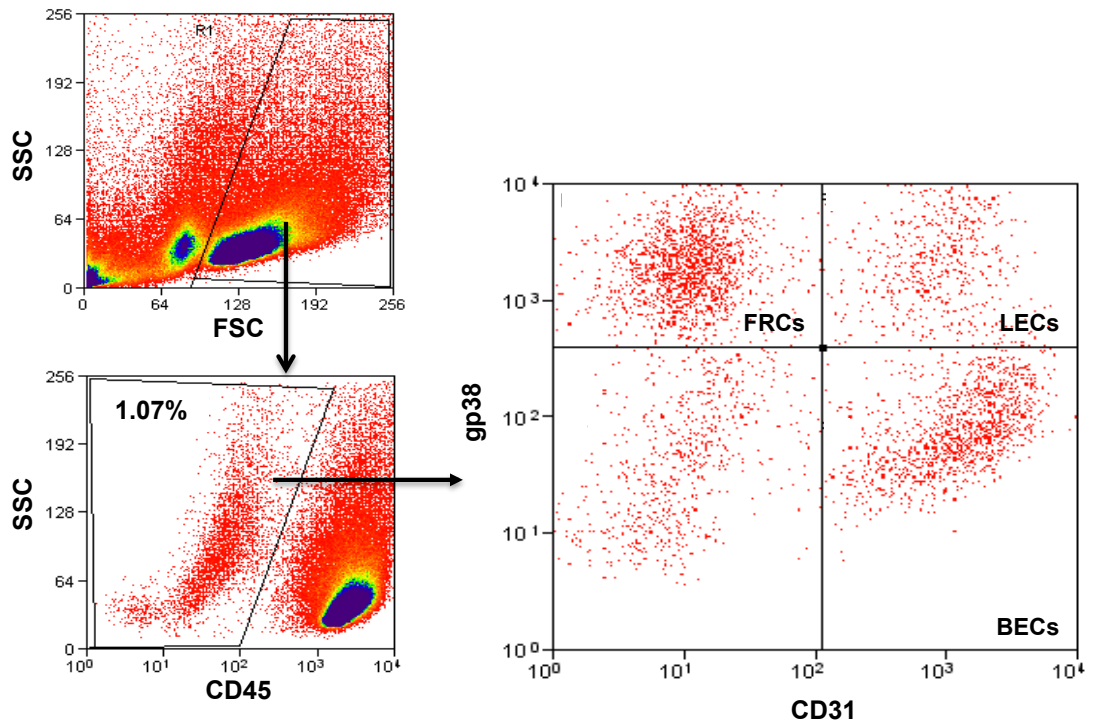


Figure 3.8: Flow cytometry profiles of lymph node stromal subsets freshly isolated from lymph nodes of individual mice.

LNs from B6CD45.1 mice were digested and once a single cell population was obtained, stained for gp38, CD45 and CD31. It is then possible to separate the different subsets, FRCs, LECs, BECs and the double negative population (platelets and FDCs) by flow cytometry.

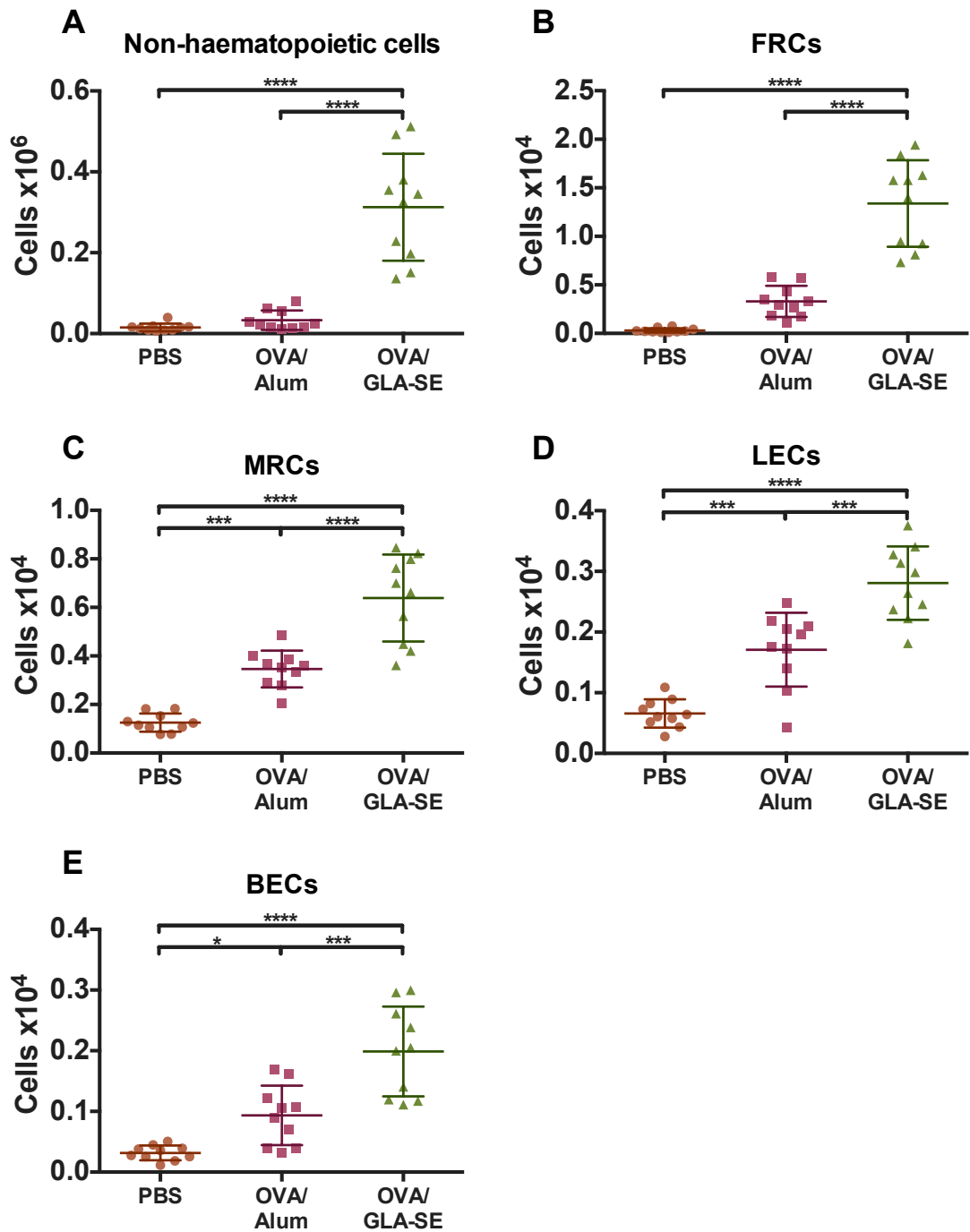


Figure 3.9: Effect of adjuvants on stromal cell and endothelial populations.

Mice were immunized with PBS, OVA/MPL-A+TDM or OVA/GLA-SE and the pLNs were removed and analysed by flow cytometry. Cells were stained with CD45, gp38 and CD31, which is a way to distinguish between the different stromal cell populations. **A:** Non-haematopoietic cells (CD45-), **B:** FRCs (CD45-gp38+CD31-), **C:** MRCs (CD45-gp38+MAdCAM-1+), **D:** LECs (CD45-gp38+CD31+), and **E:** BECs (CD45-gp38-CD31+). AccuCheck counting beads from Invitrogen were used to get an accurate cell count. Data are cell number +/- SEM with N=10 from 2 separate experiments. One-Way ANOVA followed by multiple comparison Tukey's test: *P ≤ 0.05, **P ≤ 0.01, *** P≤0.001, ****P ≤ 0.0001.

3.4. Rapid lymph node hypertrophy

3.4.1. Quantifying immune cell populations

To further understand the mechanisms behind LN enlargement and the differences between adjuvants, a time course experiment of the first three days post stimulation comparing OVA/Alum and OVA/GLA-SE was done. Immune cell types were then analysed by flow cytometry (Figure 3.10). Lymph nodes rapidly undergo LN hypertrophy with significant changes to cellularity occurring in the first 24hrs post stimulation, this process is rapidly accelerated over the following 48hrs with increased numbers of T and B cells. Treatment with OVA/Alum led to no change in T cells but an increase in B cells at 48hrs that resorbs by 72hrs. This correlates with the fact that OVA/Alum stimulates antibody production. OVA/GLA-SE treatment led to an increase in T cells from 12hrs and of B cells from 48hrs. The change in innate immune cell numbers is variable when treated with OVA/GLA-SE, but very little increase is observed with OVA/Alum. OVA/GLA-SE treatment induces an increase in monocytes from 48hrs, of neutrophils and DCs from 12hrs. OVA/GLA-SE is much more potent in inducing immune cell increase and expansion of LNs than OVA/Alum. Although the mechanism of this process is unclear, this indicates that TLR4 ligands have the capacity to rapidly modulate the kinetics of key innate and adaptive cell entry into tissue draining LNs.

3.4.2. Early remodelling of B cell follicles

To analyse the remodelling of LNs, the time course experiment comparing OVA/Alum and OVA/GLA-SE was analysed by immunohistochemistry for B and T cells (Figure 3.11) and quantified in Cell Profiler (Figure 3.12) to understand the remodelling process dynamics. OVA/Alum induces an increase in LN size with no remodelling and an increase in distinct B cell follicle size. Quantification by Cell Profiler showed that OVA/GLA-SE administration leads to increased LN size, more follicles and a larger follicle area by 72hrs compared to OVA/Alum treatment. There is no difference in the increase in T cell zone area upon either treatment. By day seven, the process of nascent follicle formation was complete, with multiple small follicular structures. Over the first 72hrs post OVA/GLA-SE stimulation, there was a rapid loss of B cell follicular structure with the B cells forming a ring like structure and a complete loss of B cell follicles.

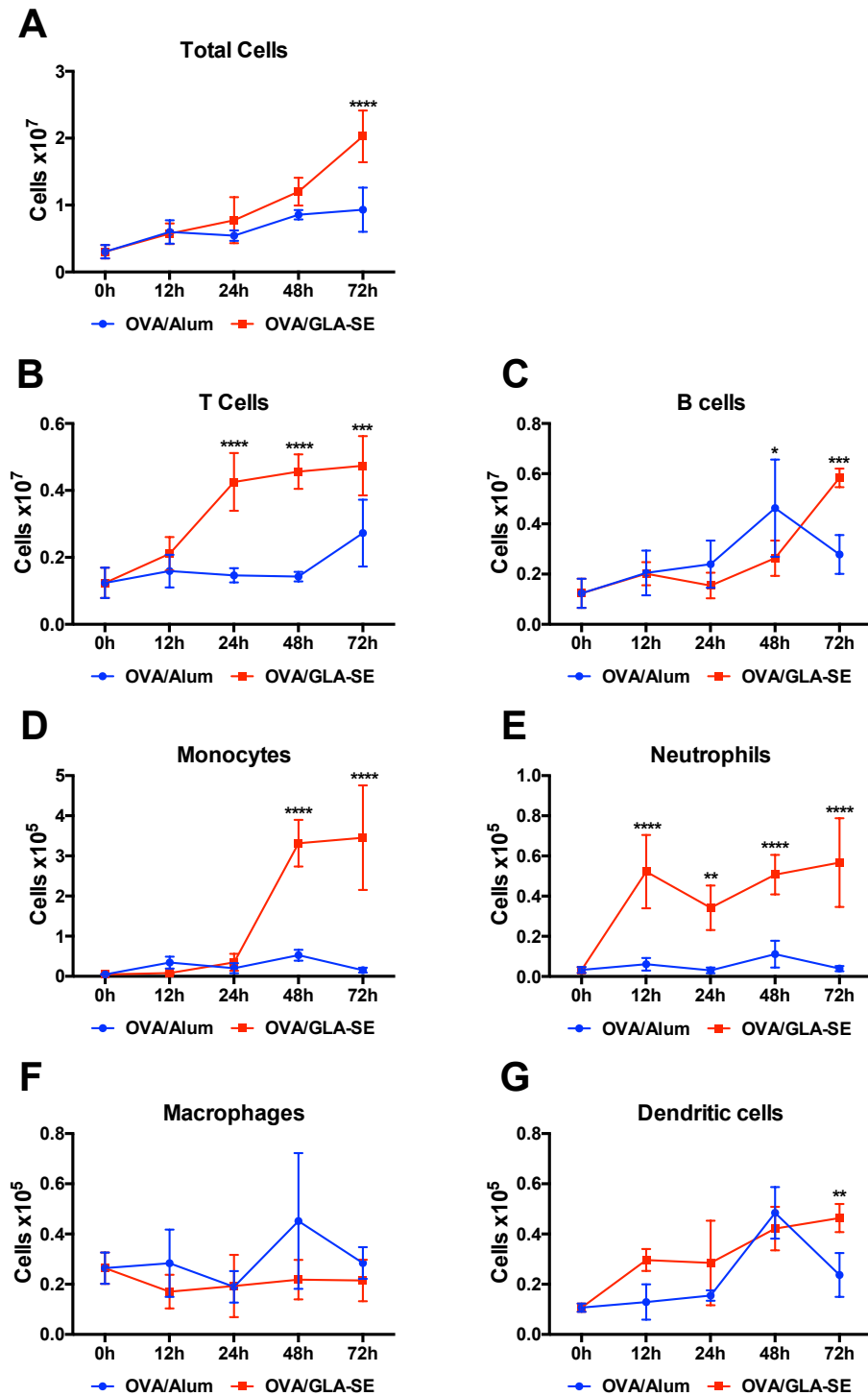


Figure 3.10: Time course of OVA/GLA-SE vs. OVA/Alum and the effect on immune cell types.

Mice were immunized with OVA/Alum or OVA/GLA-SE and the popliteal LNs were removed, stained and analysed by flow cytometry. **A:** Total cells, **B:** T cells (CD3+), **C:** B cells (CD19+), **D:** Monocytes (CD11b+Ly6G-Ly6Chigh), **E:** Neutrophils (CD11b+Ly6G+Ly6Cint), **F:** Macrophages (CD169+), and **G:** Dendritic cells (CD11c+MHCII+). AccuCheck counting beads from Invitrogen were used to get an accurate cell count. N=5 per time point. Data are cell number +/- SEM. Two-Way ANOVA followed by multiple comparison Tukey's test: *P ≤ 0.05, **P ≤ 0.01, *** P≤0.001, ****P ≤ 0.0001. OVA/Alum compared to OVA/GLA-SE at each time point.

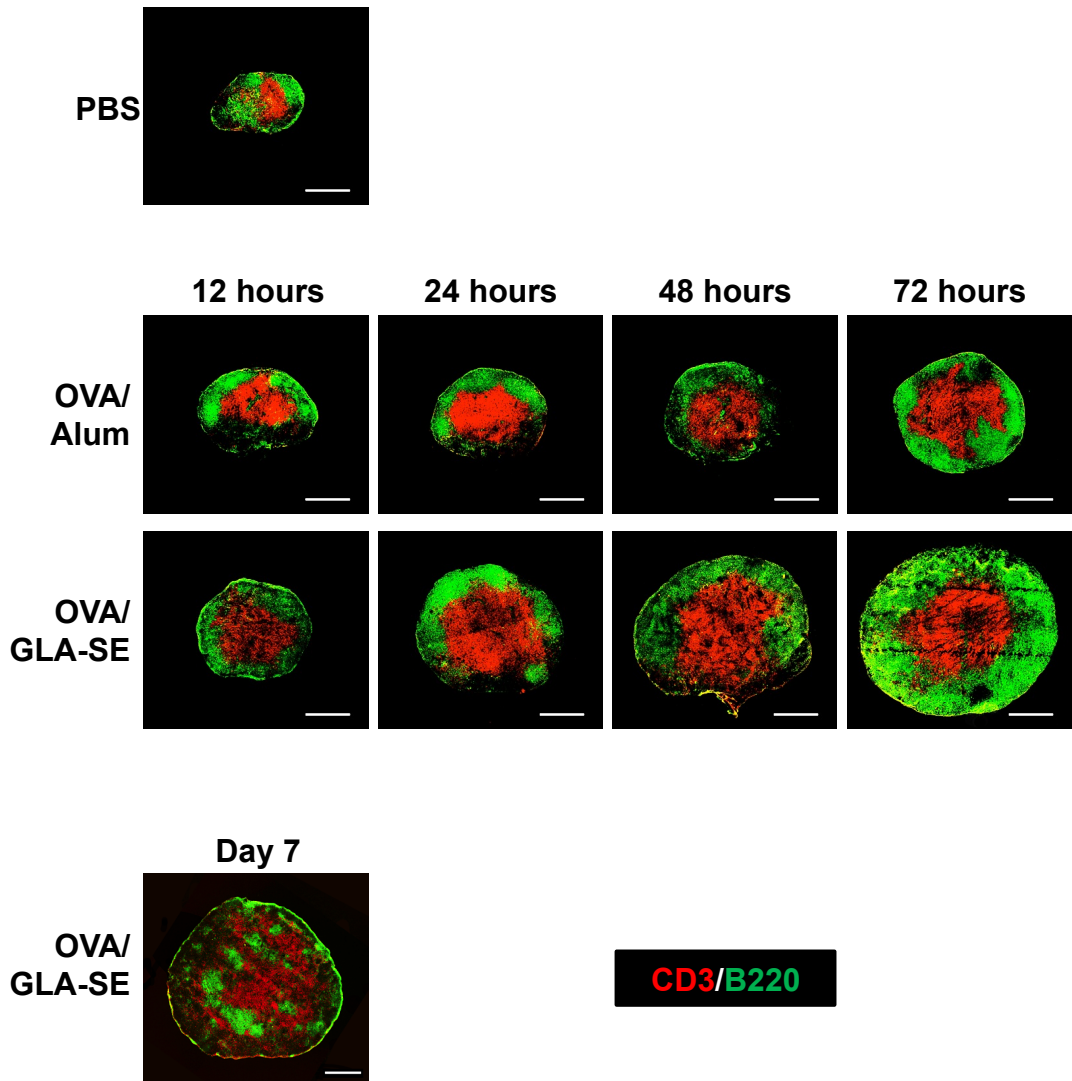


Figure 3.11: LN architecture at different time points.

Frozen sections of the popliteal LN from PBS, OVA/Alum and OVA/GLA-SE immunized mice at different time points were stained with antibodies against CD3 (T cells), and B220 (B cells). N=5 mice, 2 slides/LN, representative image was chosen. Scale bar = 500 μ m.

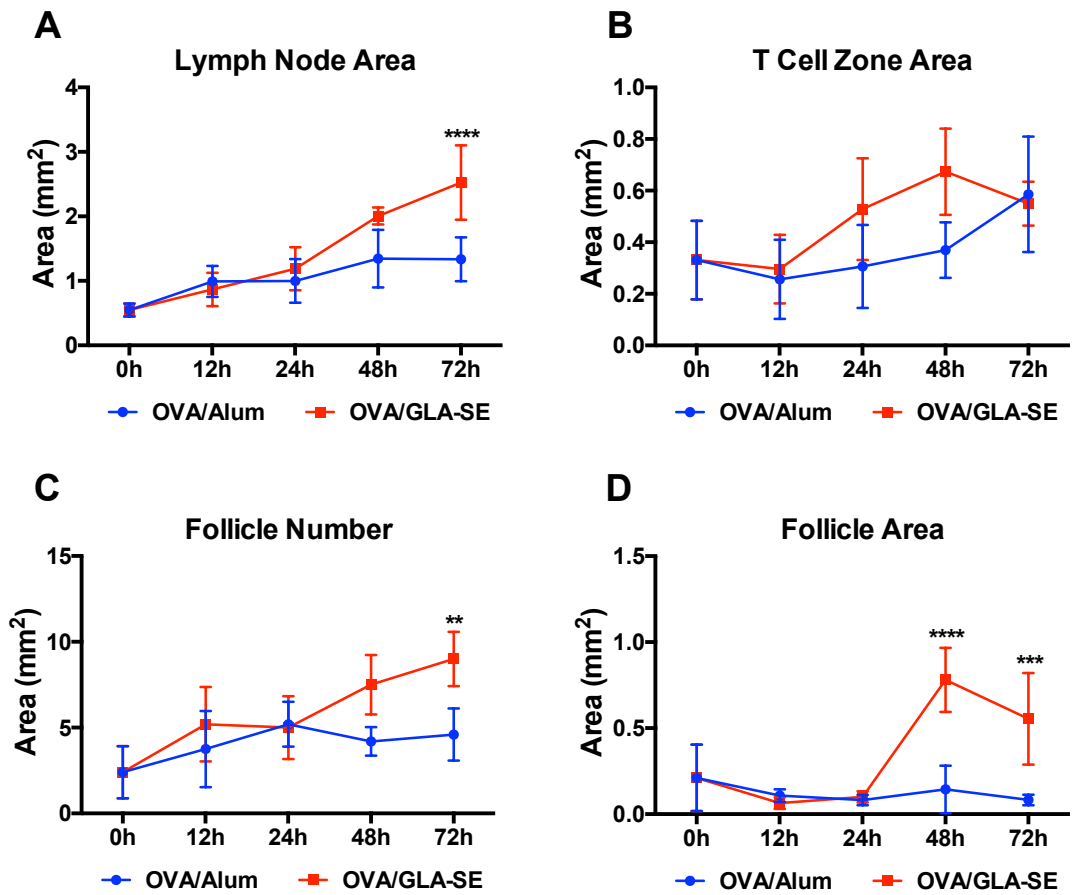


Figure 3.12: Quantification of histology results with Cell Profiler.

Immunizations with OVA in combination with different adjuvants induce dynamic change of the LN. Frozen sections of the popliteal LN from PBS, OVA/Alum or OVA/GLA-SE immunized mice were stained with antibodies against CD3 and B220. Images obtained were then run through a Cell Profiler pipeline to get the **A**: Lymph node area, **B**: T cell zone area, **C**: Follicle number, and **D**: Follicle area. N=5. Two-Way ANOVA followed by multiple comparison Tukey's test: * $P \leq 0.05$, ** $P \leq 0.01$, *** $P \leq 0.001$, **** $P \leq 0.0001$. OVA/Alum compared to OVA/GLA-SE at each time point.

3.4.3. Effect of treatment on stromal architecture

FDCs produce the chemoattractant CXCL13 that has a key role in B cell recruitment and retention in LNs. The remodelling process might involve a loss of FDCs. To quantify FDC networks, LNs were stained with FDCM2 in mice administered with OVA/GLA-SE and OVA/Alum along with the reticular and vascular networks (Figure 3.13 and Figure 3.14). The stromal architecture mirrors that of the B and T cell zones (Figure 3.11). In the GLA-SE injected mice during the first 48hrs condensed FDC networks dissolve, even though there was no loss of FDCM2 staining, rather by 72hrs a scattered population of stromal cells form a ring like structure around the LN. This process was not observed in the OVA/Alum injected mice. Although remodelling of vascular networks was observed demonstrating initiation of lymphangiogenesis 72hrs post stimulation, there is no evidence for a relationship between the vascular remodelling and B follicle remodelling.

3.4.4. Quantifying stromal cell populations

Stromal cells were quantified by flow cytometry (Figure 3.15). Stromal cells increase very little when the mice were treated with OVA/Alum; however, from 48hrs, non-haematopoietic cells, FRC and BEC numbers significantly increased when treated with OVA/GLA-SE.

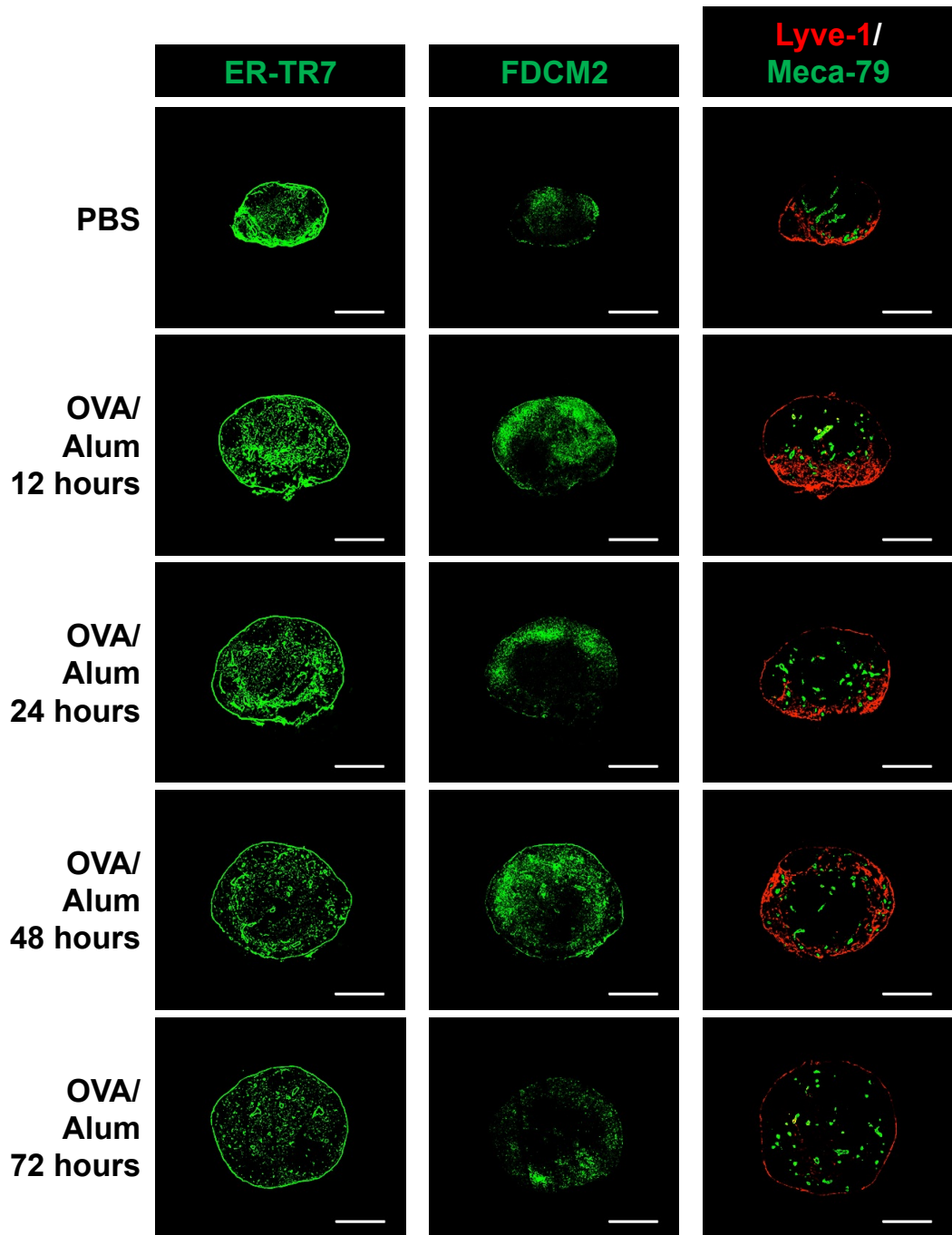


Figure 3.13: Stromal network architecture in mouse LN when treated with OVA/Alum.

Frozen sections of the popliteal LN from PBS, and OVA/Alum immunized mice at different time points were stained with antibodies against ERTR7 (Reticular network), FDCM2 (FDCs), Lyve-1 (Lymphatic vessels) and Meca-79 (HEVs). N=5 mice, 2 slides/LN, representative image was chosen. Scale bar = 500 μ m.

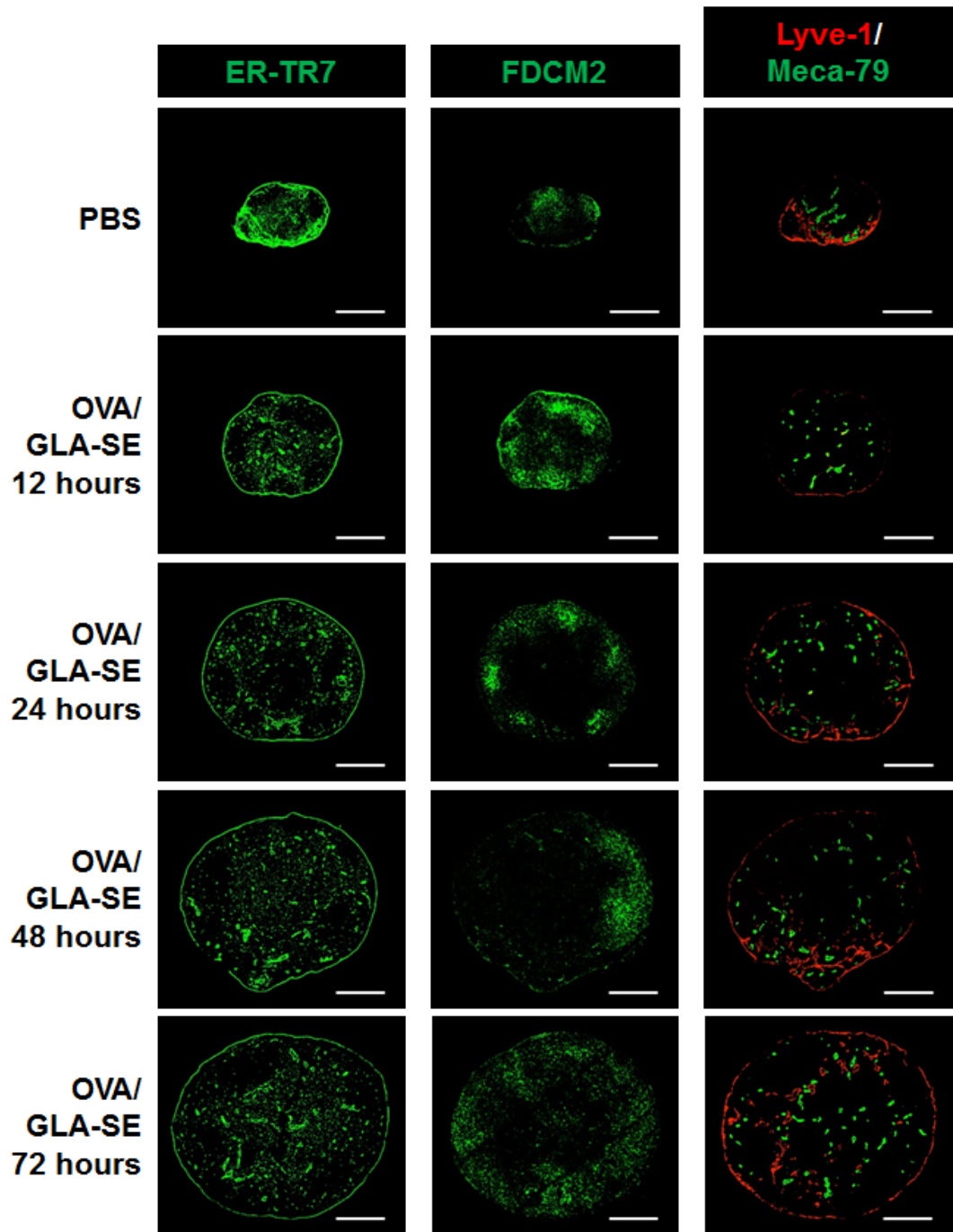


Figure 3.14: Stromal network architecture in mouse LN when treated with OVA/GLA-SE.

Frozen sections of the popliteal LN from PBS, and OVA/GLA-SE immunized mice at different time points were stained with antibodies against ERTR7 (Reticular network), FDCM2 (FDCs), Lyve-1 (Lymphatic vessels) and Meca-79 (HEVs). N=5 mice, 2 slides/LN, representative image was chosen. Scale bar = 500 μ m.

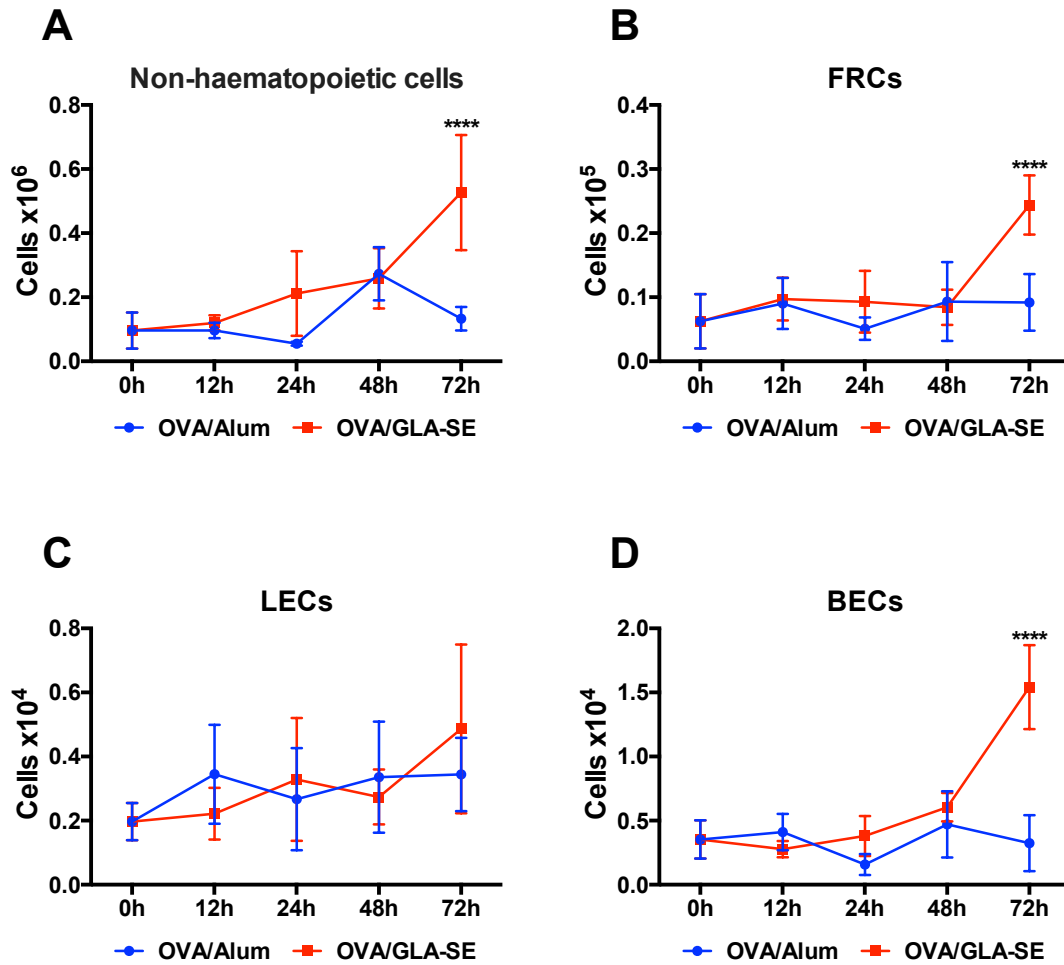


Figure 3.15: Time course of OVA/GLA-SE vs. OVA/Alum and the effect on stromal cell types.

Mice were immunized with OVA/Alum or OVA/GLA-SE and the popliteal LNs were removed, stained and analysed by flow cytometry. **A:** Non-haematopoietic cells (CD45⁻), **B:** FRCs (CD45-CD31-gp38⁺), **C:** LECs (CD45-CD31+gp38⁺), and **D:** BECs (CD45-CD31+gp38⁻). AccuCheck counting beads from Invitrogen were used to get an accurate cell count. N=5 per time point. Data are cell number +/- SEM. Two-Way ANOVA followed by multiple comparison Tukey's test: *P ≤ 0.05, **P ≤ 0.01, *** P≤0.001, ****P ≤ 0.0001. OVA/Alum compared to OVA/GLA-SE at each time point.

3.5. Role of lymphocytes in LN expansion

LN stroma provides signals that promote the survival, migration and organisation of LNs. To determine if lymphocytes are required to drive the stromal remodelling process, Rag^{-/-} mice were primed with antigen/adjuvants for 48hrs. LNs were stained with ER-TR7, Lyve-1 and Meca-79 for the reticular network, the lymphatic vessels and the HEVs respectively (Figure 3.16). The LNs were larger with increased numbers of HEVs and migration of lymphatic vessels into the cortex. In addition, stromal populations were analysed by flow cytometry. Treatment led to an increase in total cellularity, LECs and BECs. There is no change upon treatment to FRCs. This indicates a requirement for lymphocytes in FRC proliferation. These results are consistent with previous findings [89] where, they observed that FRCs numbers closely followed the number of lymphocytes during LN expansion and that the initiation of LN swelling is lymphocyte independent.

3.6. Role of CD11c expressing cells in LN expansion

DCs have an essential role in antigen presentation, adjuvants have been shown to induce DC activation and migration to draining LNs. Migratory DCs are also thought to initiate the hypertrophy process by trafficking antigen and inflammatory signals to LNs. CD11c is expressed at high levels by DCs and at lower levels by subcapsular macrophages. To analyse the effect of these CD11c expressing cells in the remodelling process, 24hrs post DTR injection, CD11c-iDTR mice were treated with OVA/GLA-SE for 48hrs (Figure 3.17). The DTR injection led to a significant reduction in DC numbers (Figure 3.17A). It has previously been shown that macrophages are also depleted in these mice [198]. Treatment with OVA/GLA-SE led to a non-significant increase in total cellularity, non-haematopoietic cells, FRCs and LECs but no change was observed in the other cell types. A significant increase in BEC numbers was observed.

To distinguish between DCs and macrophages, as both are depleted with DTR, bone marrow chimeras were established, as macrophages are radioresistant. This would have enabled the depletion of DCs but not macrophages. However, this experiment didn't work as the DCs were still present in high numbers and no difference was observed when compared to WT mice (data not shown).

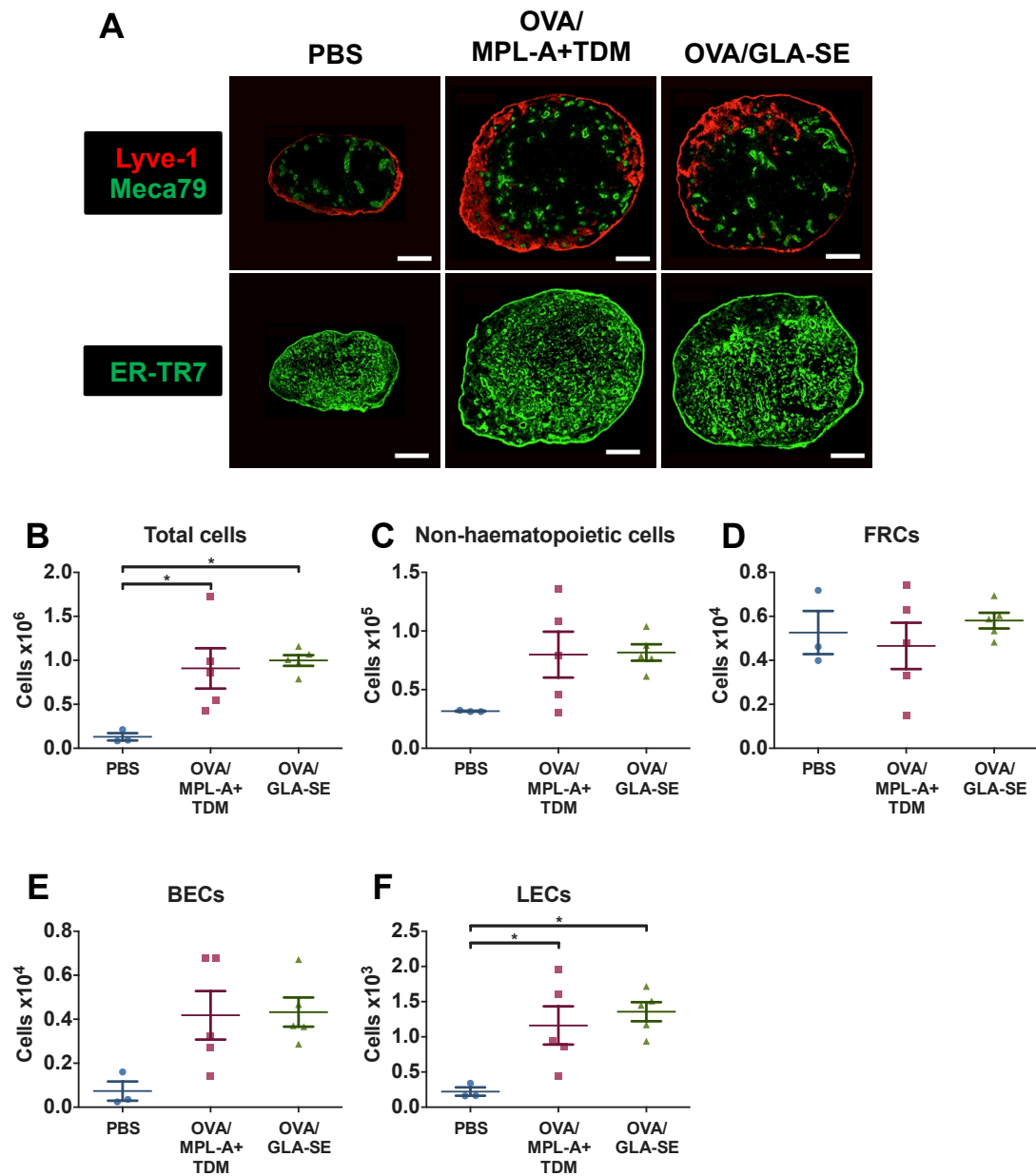


Figure 3.16: Architecture of the reticular network in $Rag^{-/-}$ mouse LNs, and the dynamic remodelling when treated with antigen/adjuvant.

$Rag^{-/-}$ mice were treated with OVA/MPL-A+TDM or OVA/GLA-SE for 48hrs. **A:** Frozen sections of the popliteal LN from PBS, OVA/MPL-A+TDM, or OVA/GLA-SE immunized mice were stained with antibodies against ER-TR7 (reticular network), Lyve-1 (lymphatic vessels) and Meca-79 (HEVs). Scale bar = 200 μ m. **B:** Total cells, **C:** Non-haematopoietic cells, **D:** FRCs, **E:** BECs, and **F:** LECs. AccuCheck counting beads from Invitrogen were used to get an accurate cell count. Data are cell number \pm SEM with N=5 mice. One-Way ANOVA followed by multiple comparison Tukey's test: * $P \leq 0.05$, ** $P \leq 0.01$, *** $P \leq 0.001$, **** $P \leq 0.0001$.

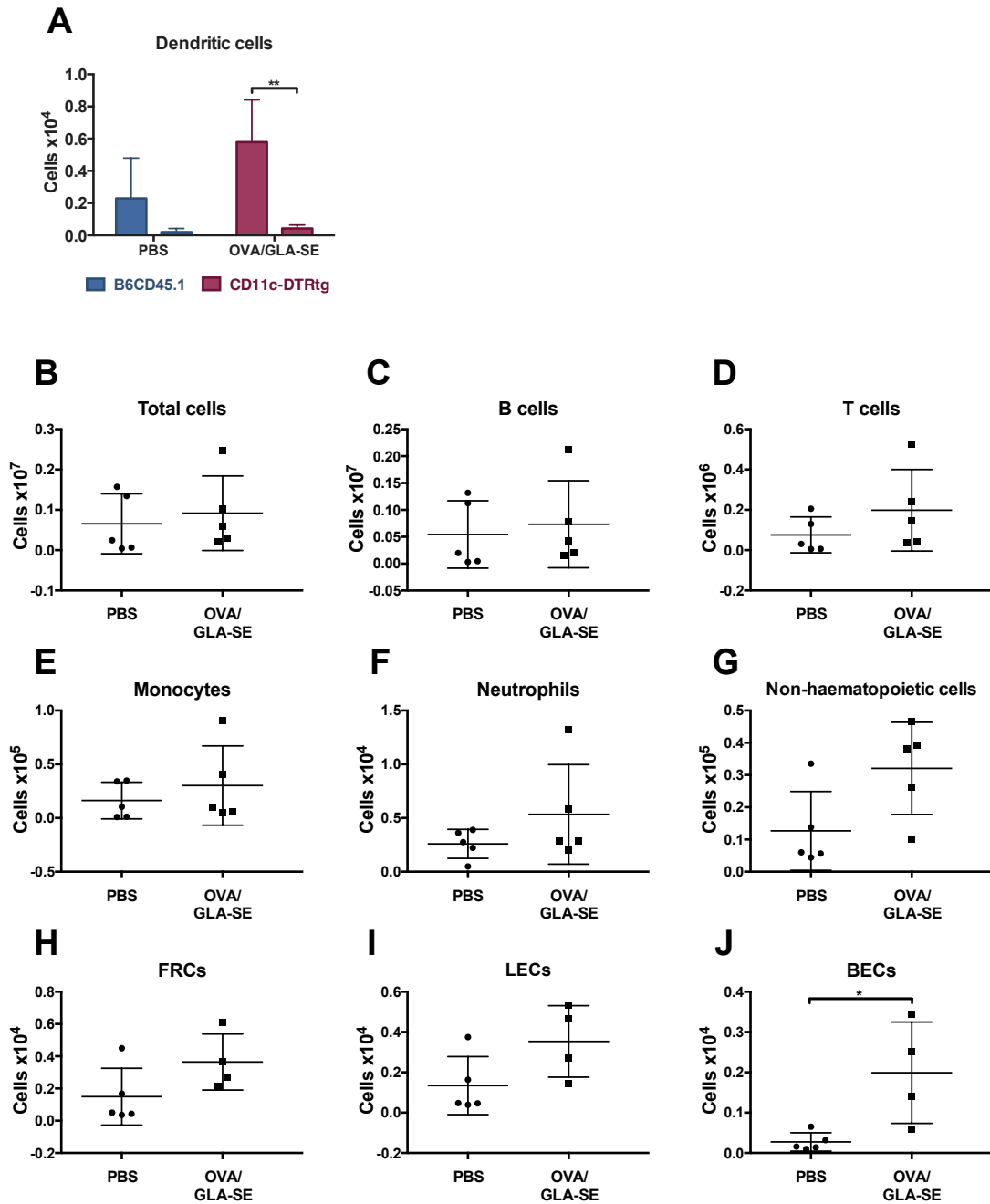


Figure 3.17: CD11c expressing cell effect on remodelling when treated with antigen/adjuvant.

24hrs post DTR injection, mice were treated with OVA/GLA-SE for 48hrs. **A:** Dendritic cells in WT vs. CD11c-DTR mice, **B:** Total cells, **C:** B cells (CD19+), **D:** T cells (CD3+), **E:** Monocytes (CD11b+Ly6G-Ly6Chigh), **F:** Neutrophils (CD11b+Ly6G+Ly6Cint), **G:** Non-haematopoietic cells (CD45-), **H:** FRCs (CD45-CD31-gp38+), and **I:** LECs (CD45-CD31+gp38+), and **J:** BECs (CD45-CD31+gp38-). AccuCheck counting beads from Invitrogen were used to get an accurate cell count. Data are cell number +/- SEM with N=5 mice. One or Two-Way ANOVA followed by multiple comparison Tukey's test: * $P \leq 0.05$, ** $P \leq 0.01$, *** $P \leq 0.001$, **** $P \leq 0.0001$.

3.7. Summary of findings

- To investigate LN remodelling, an effective and reproducible model was established.
- Treatment with TLR4 agonist adjuvants proved to be effective in initiating LN remodelling and hypertrophy compared to Alum and other adjuvants.
- Treatment with GLA-SE leads to rapid increase in immune and stromal cells leading to rapid enlargement of LNs.
- Lymphocytes were shown to not be indispensable for the initiation of hypertrophy in LNs but are necessary for the expansion of FRCs.
- Mice depleted of CD11c expressing cells showed a diminished response to adjuvants.

3.8. Discussion

3.8.1. TLR4 adjuvants drive LN hypertrophy and remodelling

The mechanisms driving tissue remodelling in secondary lymphoid tissues upon initiation of immune responses are unknown. Understanding the timing and molecular mechanisms leading to stromal cell reorganization will help generate therapeutics and vaccination strategies that can control and regulate immune responses. Although adjuvants have been used to boost immune responses for nearly 100 years, the mechanisms of action are still not well understood. More recently adjuvants containing PAMPs have been developed based on their potency in stimulating immune responses. After testing several different adjuvants, TLR4 agonist adjuvants were found to be the most effective in inducing LN remodelling with new follicular structures in the paracortex. TLR4 agonists were also found to be the most efficient in inducing rapid hypertrophy of the LN with a rapid increase in cells, both stromal and immune. The results obtained showed that immunization with TLR4 agonist adjuvants leads to rapid LN remodelling. Immunizations induce rapid hypertrophy and B cell follicle remodelling. The new follicle formation and changes in B and T cell zones mirrored the stromal networks. New vascular networks with lymphangiogenesis and HEV growth were observed enabling to accommodate the rapid influx and increase of cells in the LN. Different adjuvants were compared and TLR4 agonists appeared to drive drastic changes in LN architecture compared to all others investigated. It is also interesting to note that Alum which has been used in vaccines commonly since 1926 doesn't lead to

LN remodelling or new follicular structures forming but to bigger B cell follicles. The difference in potency of these two adjuvants needs to be investigated. Previous studies using different models lead to LN hypertrophy and varying degrees of remodelling [11, 68, 82, 98].

3.8.2. Immunization leads to changes to LN structure and cell numbers

One mechanism by which adjuvants may accelerate and potentiate immune responses is through increasing immune cell recruitment to tissue draining LNs. This increase in the influx of cells into the LN is key in the initiation of the immune response, as it brings all cell types in close contact. Upon treatment with different TLR4 containing adjuvants it was possible to show a dramatic increase both in size and cellularity of the draining LN. Surprisingly, this involved not just an increase in lymphocyte and dendritic cells but also large-scale expansion in stromal cell populations, indicating that adjuvants either, directly through TLR expression on stromal cells, or indirectly through immune cells, drive this expansion process. Histological and FACS analysis of LN architecture and cells indicated that TLR4 stimulation leads to changes in LN structure with B cell follicles forming in the paracortex and an increase in all cell types. This increase in cells is required for an efficient immune response. Stromal cells increase in numbers to adapt to the large numbers of immune cells in the LN that are entering the LN and proliferating. Changes in LN architecture differ according to the adjuvant just as it would depending on the pathogen. These changes in LN architecture leads to cells being released from their compartments and new interactions can be formed which are critical for an efficient immune response. This efficient immune response is even more important when it comes to vaccination as an adjuvant that can drive new architecture efficiently could be driving a different set of immune memory than Alum. This is important to address as Alum has limitations such as the fact that it drives a very polarized T_H2 response.

3.8.3. TLR4 adjuvants drive a dissolution of B cell follicles

Upon treatment with TLR4 adjuvants, an increase in the number of B cell follicles was observed with the remodelling process leading to new follicular structures appearing in the paracortex. This could reflect the plethora of different cell types in a LN that TLR4 agonists can directly stimulate. During a time course experiment, a LN expansion stage was observed followed by, at 72hrs post immunization, a ring-like structure forming with a loss of B cell follicles. Following this ring forming around the LN, by seven days

post-treatment, new follicular structures had formed in the paracortex of the LN mirroring the structure observed after a long-term treatment. The mechanisms behind the formation of new B cell follicles following immunization are still unknown. The first step of this process is the dissolution of the B cell follicle structure. A possible explanation is that the signals that form the B cell follicles are lost leading to this disintegration. FDC differentiation and maturation into cells producing CXCL13 requires LT β R and TNF α from B cells. This dissolution could be linked to a change in any of these signals. Either FDCs differentially express CXCL13 leading to B cells being released from the B cell follicles or B cells lose expression of TNF α leading to loss of B cell follicles.

3.8.4. Initiation of LN expansion

Treatment with OVA/GLA-SE and OVA/MPL-A+TDM of Rag deficient mice, lacking T and B lymphocytes, led to an increase in both the blood and lymphatic endothelial cell networks but not of the FRC network that supports lymphocyte homeostasis and migration. These results are similar to findings [89] where FRCs numbers closely follow lymphocyte numbers during LN swelling. Expansion of FRCs is dependent on the increase in lymphocytes entering the LN during an immune response. However, lymphocytes are not necessary for the increase in new lymphatic and vasculature networks. DCs are required for this rapid expansion of the vasculature network. This indicates that during an immune response after immunization the first step in LN hypertrophy is dependent on APCs, namely DCs. These innate cells are critical in the first steps of LN expansion. By interacting with stromal cells, DCs stimulate the growth and proliferation of BECs that compose HEVs [68, 82]. Lymphocytes can then be recruited into the LN at a higher frequency through the new lymphatic vessels and HEVs. This correlates with our results, where in the absence of lymphocytes in Rag^{-/-} mice there is increased blood and lymphatic vasculature but no change in the reticular network. Therefore, the LN microenvironment and architecture is shaped by the cells it supports. It has previously been speculated that this process is an IL-7/IL-7-receptor dependent process [199] whereby IL-7 is crucial in new LN architecture forming. It would be interesting to investigate the outcome of mice where IL-7 is removed during an antigen/adjuvant-mediated immune response.

The results obtained with depleted DCs are similar to results from other studies. In mice depleted of DCs, treatment with the water-and-oil emulsion OVA/Montanide reduced

lymphocyte trapping and lymphocyte expansion, as well as a reduction in the number and proliferation of FRCs [89]. They also addressed the question of whether the transfer of migratory DCs was sufficient to trigger FRC expansion in DTR-treated mice. FRC expansion and LN swelling was observed when they transferred LPS-matured Bone Marrow Dendritic Cells (BMDCs). It has also been shown that migratory DCs transmit signals to LN resident DCs, which leads to FRC expansion [82, 194]. They also showed that as LN expand; BECs undergo rapid growth that is dependent on DCs and VEGF, which is in part produced by FRCs. A model was proposed where migratory DCs transmit a signal to LN-resident DCs, which then triggers vasculature changes leading to T cell trapping, which is critical for FRC expansion [89]. This model correlates with the results obtained here. This illustrates that DCs and macrophages are important in the initiation of the immune response, but also have a key role in regulating the stromal cell expansion phase. The molecular basis that drives this proliferation process leading to LN expansion and remodelling is unknown. It is also important to note that other cell types such as macrophages are depleted in CD11c DTR mice [198]. DCs are critical in the initiation phase of LN expansion as their absence led to no increase in any cell types. Lymphocytes and stromal cells are required for the expansion phase following initiation by DCs. These results indicate that the cellular process governing LN expansion involves a multitude of cell types, and it is the interactions between different cell types in the LN microenvironment that drive this process.

3.8.5. Conclusion

TLR4 adjuvants lead to LN hypertrophy and remodelling. It is necessary to investigate the mechanisms behind this change in architecture. Results here indicated that Alum as an adjuvant does not lead to new follicle formation and to very little changes in LN architecture and diminished hypertrophy compared to treatment with TLR4 agonists. Therefore, Alum was used as a comparator to investigate how GLA-SE leads to these changes in LN architecture. Different mechanisms and cell types were investigated to elucidate the phenotype observed in remodelled LNs. A microRNA, miR-132 was analysed in its role in LN remodelling.

Chapter 4: miR-132 is a regulator of the immune response

4.1. Introduction

4.1.1. Macrophages in LNs

Macrophages are defined as phagocytic cells that internalize and degrade pathogens and then secrete factors that alert the adaptive immune cells. LN macrophages are bone marrow derived and their development depends on Colony Stimulating Factor-1 (CSF-1) [200]. Resident macrophages can be found in LNs and are sub-divided into Subcapsular Sinus Macrophages (SSMs) and Medullary Sinus Macrophages (MSMs). In reactive LNs, a third population of macrophages can be found, tingible body macrophages that are specialized in the phagocytosis of apoptotic cells in GCs [201].

Just beneath the capsule, on the outer margin of LN's cortex is an area called the Subcapsular Sinus. SSMs are found lining the SCS and are normally immobile and extend into B cell follicles through dendrite-like protrusions [52]. SSMs express CD11b and CD169 as well as low levels of CD11c, which is why macrophages are depleted from LNs in CD11c-DTR mice. They also do not express the markers SIGN-R1 and F4/80 [201]. These cells are capable of quickly capturing lymph-borne antigens but have a diminished phagocytic capacity thus they have taken on a very specialised role distinct from other tissue macrophage populations [51]. Upon the capture of antigen on their surface, SSMs transport antigen along their projections that enter the B cell follicles. There, cognate B cells are able to recognize the antigen through their BCR [202]. In the case of opsonized antigen, follicular non-cognate B cells can take up antigen through the complement receptors 1 and 2 and transport the complexes to FDCs in the light zone of GCs. This process is essential for GC formation and in driving development of high affinity B cells [51]. Lymphotoxin produced by B cells is essential for macrophage development and maintenance [203]. SSM numbers are reduced when B cells are absent, or in the absence of B-cell produced lymphotoxin and increased when lymphotoxin is overexpressed [201]. SSMs are subject to infections by various viruses. For example, in mice, many SSMs are infected by systemic Vesicular Stomatitis Virus (VSV) thereby preventing VSV spread to the periphery. Depletion of SSMs leads to the spread of VSV to the central nervous system. Macrophages produce IFN- α , which is essential in preventing the spread of VSV [204]. SSMs have also been shown to be permissive to dengue virus, vaccinia virus and the parasite *Toxoplasma*

gondii [204-206].

In contrast, MSMs are located in the medulla that is composed of LECs and reticular strands. Macrophages in this area are attached to the sinus and reticular fibres in the lumen [207]. MSMs are characterized by their expression of CD11b, CD169, but also express F4/80, SIGN-R1, Macrophage Receptor with Collagenous Structure (MARCO), Mannose Receptor (MR) and Lyve-1 [201]. SIGN-R1 is a receptor for bacterial dextrans such as pneumococcal polysaccharide of *Streptococcus pneumoniae*. MARCO belongs to the scavenger receptor family and binds unopsonised bacteria. These receptors along with the localization in the medulla suggest that the role of medullary sinus macrophages is antigen clearance in the lymph, enabling the prevention of pathogens spreading from draining LNs and entering blood circulation. In the hours following subcutaneous injection of labelled antigen, label accumulation occurs in lymph exposed MSMs. Due to the large amount of antigen that these cells internalize and their large lysosomes and high vesicle numbers, these cells are described as highly phagocytic. Imaging studies have shown that MSMs often contain apoptotic polymorphonuclear cells such as eosinophils [201, 208].

4.1.2. Role of LN MRCs

MRCs as novel stromal cells were first described in 2012 [61]. A layer of reticular cells can be found in the SCS on the outer region of B cell follicles. Phenotypically these cells resemble FRCs; however, they express CXCL13, RANK-L and MAdCAM-1 but not CCL19 and CCL21 or the FDC markers CD21/35 indicating that these cells are a distinct population and most closely resemble LTo mesenchymal cells that are found in the developing LN anlagen [60]. MRCs support the recognition of antigen entering the LN through the lymph. In the outer area of follicles, MRCs mediate antigen transport to B cells and FDCs [48, 209]. MRCs express CXCL13, ICAM-1 and VCAM-1 promoting interstitial migration of follicular B cells on the scaffold they create. Thus, MRCs promote interaction between macrophages expressing antigen on their surface and B cells [51, 61, 210]. During an immune response, LNs undergo rapid remodelling through changes in stromal cells. Fate-mapping studies have shown that MRCs serve as a potential precursor that can give rise to FDCs, providing a pool of cells that can rapidly generate new secondary structures in LNs [62].

4.1.3. MicroRNAs effect on the immune response in LNs

MicroRNAs are short non-coding RNA sequences. They act by binding to the 3'UTR region of complementary mRNAs leading to their degradation or inhibition of their translation. miRNAs have been shown to be important in haematopoiesis regulation. The tightly regulated process of haematopoiesis and the development of all blood cell lineages is ensured by miRNAs. miR-223 is a microRNA that has been shown to have an important role in B cell differentiation through the down-regulation of LMO2. In the different stages of peripheral B cell maturation, the miRNAs expression patterns changes drastically to regulate the diverse differentiation stages [211]. GC B cells require specific gene expression that is regulated by different miRNAs [212, 213]. MicroRNAs have also been shown to play a key role in T cell differentiation [214]. MicroRNAs are also known to be involved in different diseases. miR-15 and miR-16 are deleted or down-regulated in patients with Chronic Lymphocytic Leukemia [215]. Certain microRNAs that are necessary for lymphocyte differentiation can also be deregulated leading to pathologies. The cluster miR-17-92 is involved in B cell maturation during a GC reaction but has also been shown to have a role in B cell lymphomas [211, 216]. As B cells are the key producers of antibodies and play an indispensable role in adaptive immunity it is critical that their regulation be tightly controlled. The balance between normal immune function and pathologies is regulated from B cell differentiation to the production of specific antibodies. It has been shown that loss of the Dicer microRNA processing protein results in a block of the transition between pro-B and pre-B cells as well as antibody diversity and B cell survival [217]. The transition between pro-B cell and pre-B cell is regulated by miR-150 and miR-34a that target c-Myb and Foxp1 respectively [218, 219]. miR-181 and miR-155 regulate class switching and somatic hypermutation by regulating Activation-Induced Cytidine Deaminase (AICDA) [220, 221].

4.1.4. miR-132 in regulating the immune response

The miR-132/212 cluster has been shown to be a key regulator of the immune response. This cluster regulates haematopoietic cell differentiation and function [222], the antiviral immune response [184], wound healing inflammation and proliferation [223], and immune cell function [180, 224, 225]. The miR-132/miR-212 cluster regulates haematopoietic stem cell cycling and survival through autophagy. It has been shown that over-expression and deletion of miR-132 can both lead to defects in haematopoiesis

[222]. Recent studies have shown that miR-132 has a role in pathological angiogenesis [226] as well as in the proliferation and invasion of tumours [227, 228]. miR-132 is deregulated in certain types of B cell cancers such as Chronic Lymphocytic Leukemia [229, 230]. miR-132 also plays a role in B cell development through the targeting of SOX4 and induces apoptosis in B cells [231]. SOX4 is known to have a key role in cell fate and has also been shown to be up-regulated in different human cancers including breast cancer and prostate cancer [232-234]. Down-regulation of miR-132 in breast cancer inhibits proliferation, invasion and metastasis through targeting HN1 [228]. By inhibiting its target Sox4, miR-132 inhibits invasion of lung cancer cells [235].

TLRs are key in recognizing pathogenic invaders such as LPS or peptidoglycan. Upon receptor triggering, signalling leads to cytokine and chemokine production through activation of the NF κ -B pathway leading to the triggering of the immune response to clear the infection. TLR signalling pathways have to be tightly regulated to control the onset and termination of the immune response in order to avoid over-inflammation leading to pathologies or damage. MicroRNAs have emerged as regulators of TLR signalling. miR-146a has been shown to have a key role in endotoxin tolerance through the regulation of the adaptor molecules IRAK1 and TRAF6, though this doesn't completely extinguish cytokine production [236, 237]. Molecules of the pathway directly targeted by the miR-132/miR-212 cluster have yet to be elucidated. By targeting AChE, miR-132 limits inflammation in mouse brains [180]. miR-132 targets p300, which modulates the immune response induced by infection with Kaposi's sarcoma-associated herpesvirus [184]. Stimulation of cells with TLR2 agonists leads to an increase in the expression of miR-132/miR-212, which have been shown to be critical in the modulation of TLR2-induced tolerance [224].

4.1.5. Summary

Macrophages and MRCs line the SCS and present the first line of defence as they scan lymph-borne antigen and present it to B cells and FDCs. Their role in the remodelling process of LNs during an immune response is still poorly understood. The miR-132/miR-212 cluster has been linked to various aspects of inflammation and is known to regulate TLR4 signalling. TLR4 is expressed on various cell types in the LN. Thus, we hypothesised that miR-132 is important in the regulation of LN remodelling during a response to a TLR4 adjuvant.

4.1.6. Aims

- Investigate the role of TLR4 on stromal cells.
- Determine the effect of TLR4 stimulation of different cell types.
- Investigate the role of miR-132 in LN remodelling and architecture and the kinetics behind this.
- Investigate the potential mechanisms leading to the difference in remodelling.
- Determine what happens after a long-term treatment of 6 months.
- Investigate the stromal and haematopoietic contributions to LN remodelling.

4.2. Stroma responds to TLR stimulation

4.2.1. Expression of TLRs by stromal cells

The Immunological Genome Project (Immgen) developed a gene expression microarray database for cells of the mouse's immune system [69]. Preliminary analysis from the Data Browser indicates that some TLRs are expressed by FRCs, BECs, and LECs (TLR2 and TLR4), as well as key components of the TLR signalling pathways such as MyD88 (Figure 4.1).

4.2.2. Enzymatic isolation of mouse LN stromal cells

LN stromal cells were isolated as previously described by Fletcher et al. using a reproducible low mortality enzymatic digestion protocol [188]. It is then possible to distinguish the different major subsets of LN stroma by using the markers CD45, podoplanin (gp38) and CD31. Additionally, MRCs can be identified and isolated by using MAdCAM-1 as a marker, and the FDC population using the CD21/35 marker. After digestion, it is possible to plate the cells and culture them and after three passages a pure population of FRCs that express podoplanin is obtained (Figure 4.2).

4.2.3. TLR4 expression in FRCs

To validate that TLR4 expression can be found at least on an mRNA level, gene expression was analysed by RT-qPCR after treatment of FRCs with LPS at different time points (Figure 4.3). An increase in TLR4 was observed upon treatment and though its expression stays up-regulated at all time points, there is a slow decrease in expression. This indicates that these molecules are expressed and the presence of the ligand induces an up-regulation of the receptor.

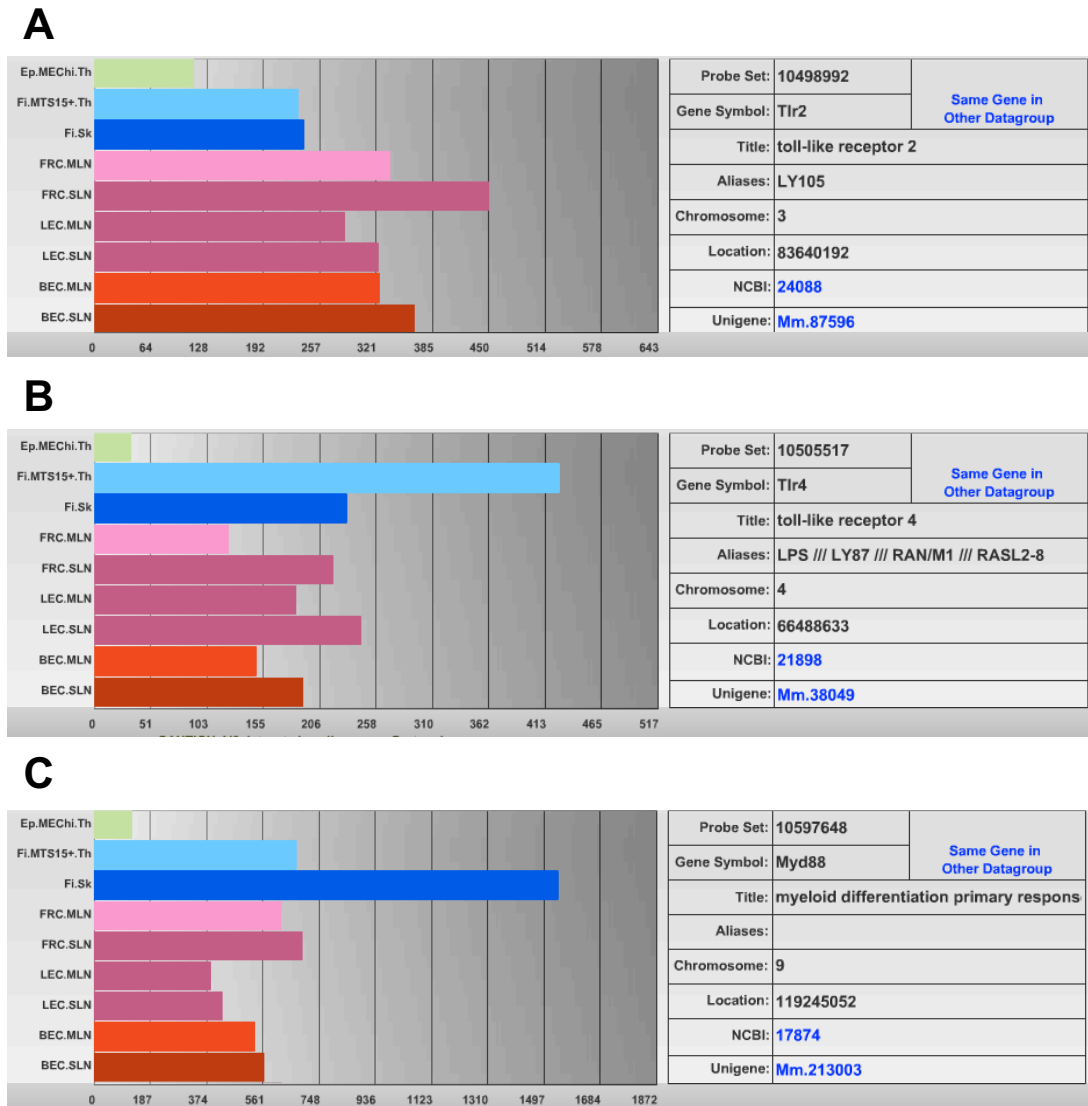


Figure 4.1: Expression of Toll Like Receptors by stromal cells.
A: TLR2, B: TLR4, and C: Myd88 expression as shown on the data browser of the Immgen website.

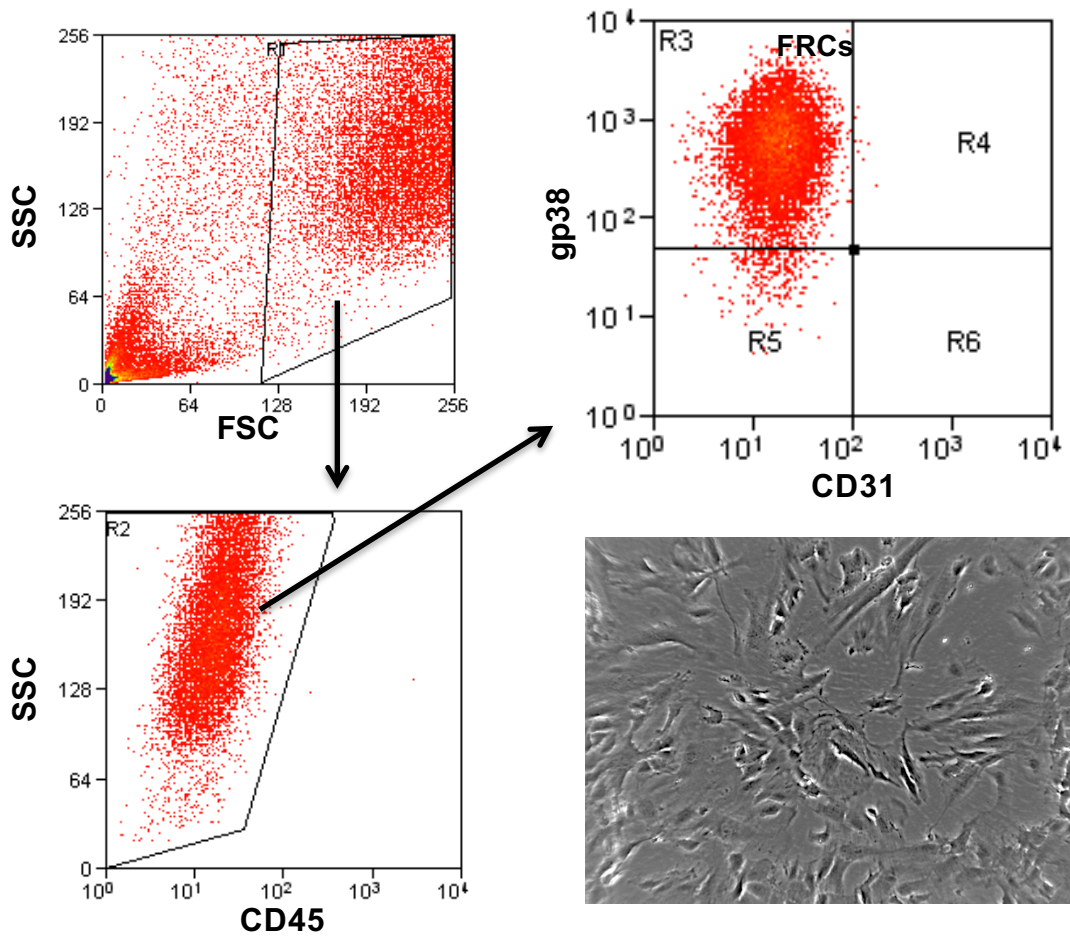


Figure 4.2: Flow cytometry profiles of lymph node stromal subsets freshly isolated from lymph nodes of individual mice after culturing.

LN from B6CD45.1 mice were digested and once a single cell population was obtained, cultured *in vitro* and then stained for gp38, CD45 and CD31. It is then possible to separate the different subsets, FRCs, LECs, BECs and the double negative population (platelets and FDCs) by flow cytometry. Here only a pure population of FRCs was observed that is gp38⁺ and CD31⁻.

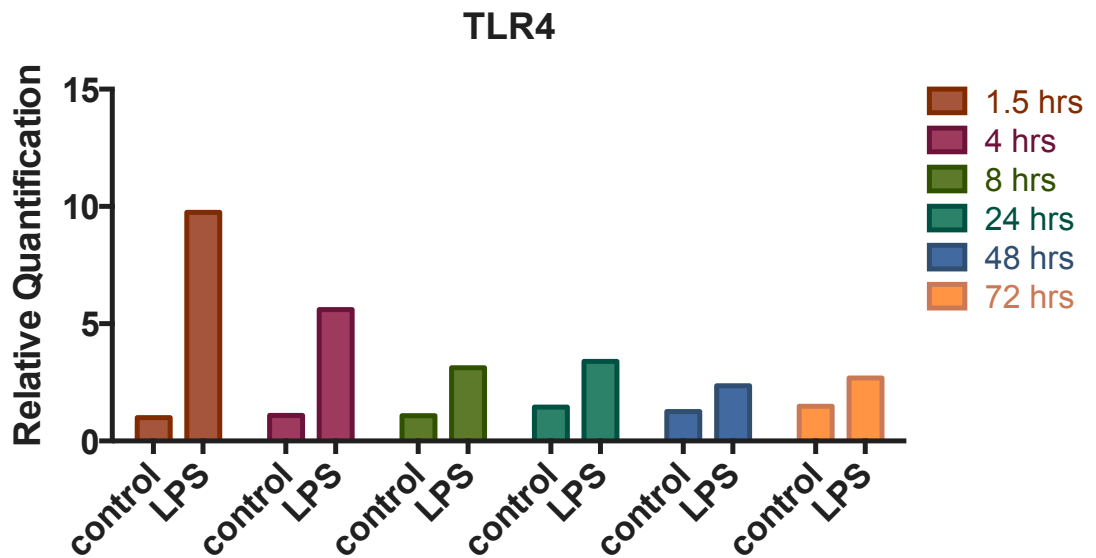


Figure 4.3: LPS treatment effect on TLR4 expression in FRCs.

TLR4 mRNA expression was analysed from isolated FRCs treated for 1.5, 4, 8, 24, 48 or 72 hours with $1\mu\text{g/ml}$ of LPS. Cells were lysed, total RNA was isolated, retro-transcribed into cDNA and analysed by RT-qPCR. Expression values were then normalized to the HPRT internal standard values. Data is shown as relative values. Three technical repeats from one biological experiment.

4.2.4. FRCs respond to a wide range of TLR agonists

FRCs were isolated from WT mice and cultured, then treated for 5hrs with a panel of TLR agonists from Invivogen. PAM3CK4 is a synthetic lipopeptide that mimics bacterial lipoprotein; its recognition is mediated by TLR2 that cooperates with TLR1 to activate the NF- κ B pathway. HKLM is a TLR2 agonist and is a heat-killed preparation of an intracellular Gram-positive bacterium. Poly(I:C) is a synthetic analogue of dsRNA and therefore is a TLR3 agonist. LPS-EK from *E.coli* is a TLR4 agonist. ST-FLA is flagellin from *S.typhimurium* and is a TLR5 agonist. FSL-1 is a synthetic lipoprotein that is recognized by TLR6 and TLR2. ssRNA40 is a protected single-stranded RNA oligonucleotide that is recognized by TLR8 in humans and TLR7 in mice. ODN1826 is a synthetic oligonucleotide containing unmethylated CpG dinucleotides that induce strong immunostimulatory effects through TLR9.

Response to FRC stimulation was determined by RT-qPCR by measuring the gene expression of pro-inflammatory cytokines TNF α , IL-1 β and IL-6. TLR1, TLR2, TLR4, TLR6 and TLR9 stimulation led to an increased expression of these cytokines by FRCs (Figure 4.4).

4.2.5. TLR mediated gene expression in FRCs

LNs from WT, TLR4^{-/-} and Myd88^{-/-} were digested and grown as a monolayer. FRCs were treated with PBS, OVA/MPL-A+TDM or OVA/GLA-SE for 5hrs, the cells were lysed and TNF α , IL-1 β and IL-6 mRNA expression levels were analysed by RT-qPCR (Figure 4.5). WT FRCs are able to generate a strong response to stimuli, by expressing abundant TNF α , IL-1 β and IL-6, that is significant when treated with OVA/MPL-A+TDM. Although GLA-SE is very potent *in vivo*, it doesn't have the same efficacy *in vitro*. FRCs that are deficient for either TLR4 or MyD88 were unable to generate a response and no up-regulation was observed, thus inflammatory cytokine production by FRCs in response to adjuvants is TLR mediated.

These results demonstrate that stromal cells can respond directly to TLR4 ligands *in vitro* and likely respond to TLR4 ligands directly *in vivo*.

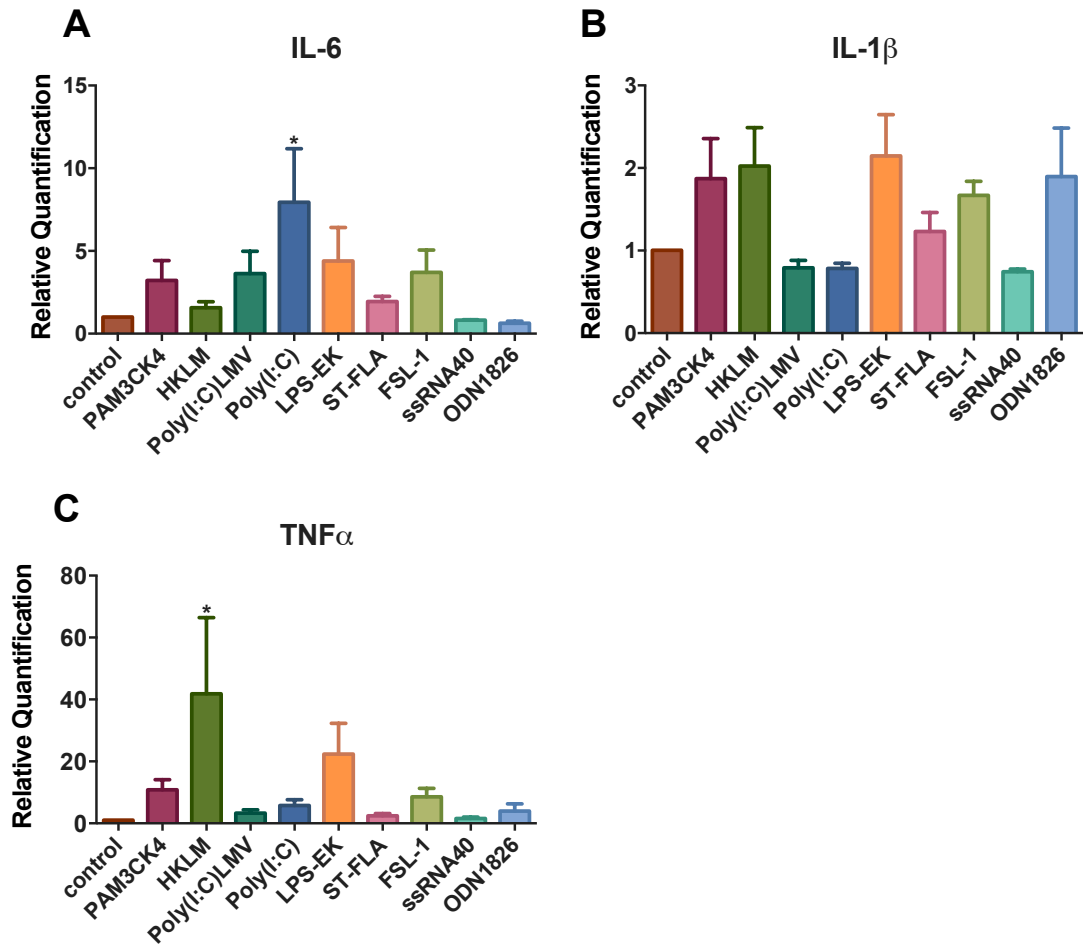


Figure 4.4: Effect of different TLR agonists on cultured FRCs' gene expression.

LN from the mice were digested and plated. Isolated FRCs were treated with a panel of TLR agonists for 5hrs, cells were lysed, total RNA was isolated, retrotranscribed into cDNA and analysed by RT-qPCR. **A:** IL-6, **B:** IL-1 β , and **C:** TNF α . Expression values were then normalized to the HPRT internal standard values. Data is shown as relative values. From 3 separate experiments. One-Way ANOVA followed by multiple comparison Dunnett's test (compared to control): *P \leq 0.05, **P \leq 0.01, *** P \leq 0.001, ****P \leq 0.0001.

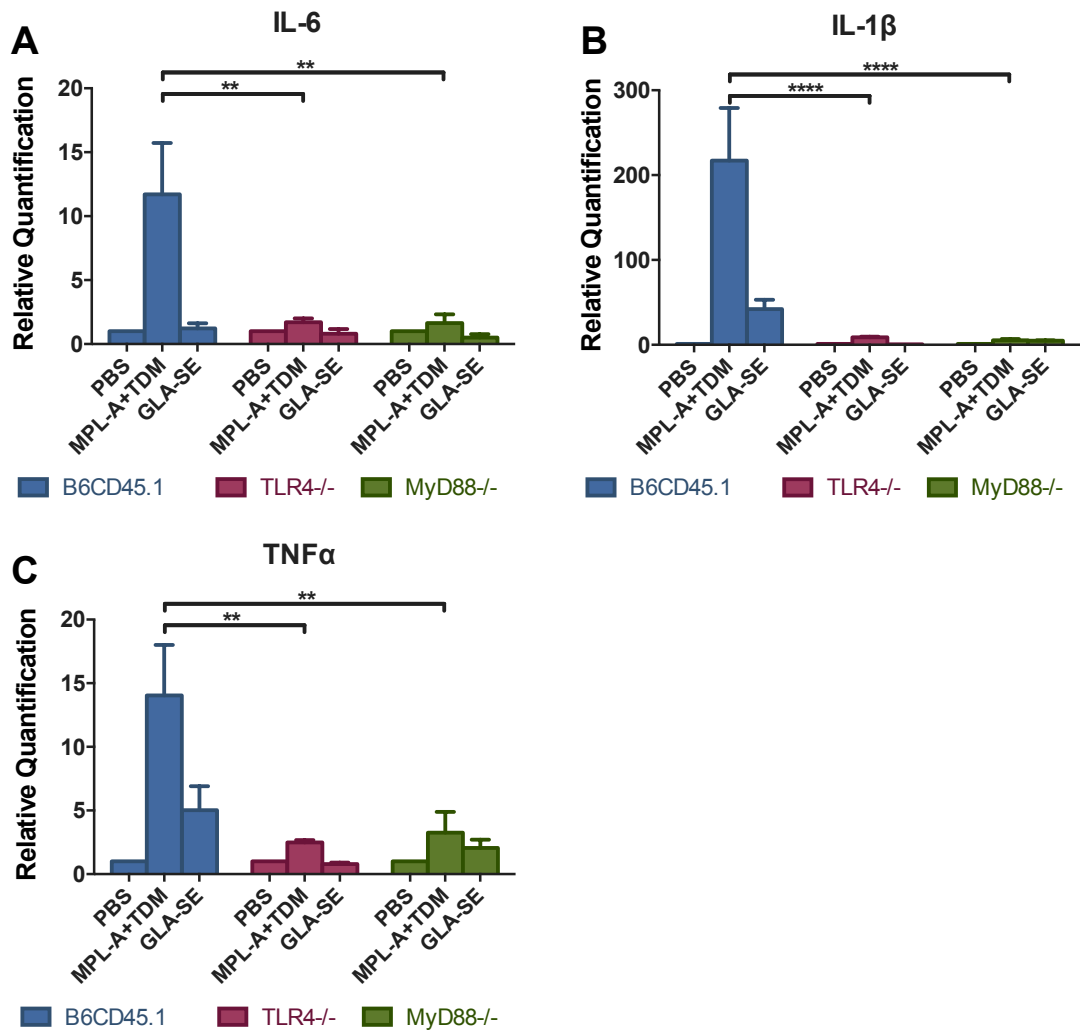


Figure 4.5: FRC response is TLR mediated.

LNs from WT, TLR4^{-/-} and Myd88^{-/-} mice were digested and plated. The cells were treated with TLR4 agonists, OVA/MPL-A+TDM and OVA/GLA-SE for 5 hours, cells were lysed, total RNA was isolated, retrotranscribed into cDNA and analysed by RT-qPCR. **A:** IL-6, **B:** IL-1β, and **C:** TNFα. Expression values were then normalized to the HPRT internal standard values. Data is shown as relative values. From 3 separate experiments. Two-Way ANOVA followed by multiple comparison Tukey's test: *P ≤ 0.05, **P ≤ 0.01, *** P ≤ 0.001, ****P ≤ 0.0001.

4.3. TLR4 signalling regulates cytokines and miR-132 expression

4.3.1. Gene expression in FRCs

Mice were treated for 12hrs with either OVA/MPL-A or OVA/GLA-SE after which FRCs were sorted to analyse expression changes at early time points. IL-1 β , TNF α and miR-132 expression was analysed by RT-qPCR (Figure 4.6). Treatment with both OVA/MPL-A+TDM and OVA/GLA-SE leads to an expansion of FRCs, therefore this cell type was analysed. An increase in all of the genes analysed was observed in FRCs. The increase in miR-132 mirrored the increase in the different inflammatory factors. This led to an interest in miR-132 as a regulator of FRCs and of the enlargement and remodelling process LNs go through. Further analysis was done from total LNs after 24 days of treatment and there is a significant 2.5-fold increase upon immunization.

miR-132 became the focus of this project, as it is known to be expressed in immune and stromal cells alike and to be involved in inflammation.

4.3.2. LPS treatment of isolated B cells

To study the changes in gene expression, B cells were isolated from WT and miR-132^{-/-} mice and treated with LPS, for 3hrs, 6hrs and 24hrs. miR-132 is up-regulated in WT mice from 3hrs. There is no difference between WT and miR-132^{-/-} B cells concerning the three genes analysed, IL-1 β , IL-6 and TNF α (Figure 4.7).

4.3.3. Decreased response in miR-132^{-/-} FRCs to TLR stimulation

Cultured FRCs from WT and miR-132^{-/-} mice were treated with TLR4 agonist adjuvants. A small decrease was observed in the production by miR-132^{-/-} FRCs of TNF α and IL-1 β (Figure 4.8).

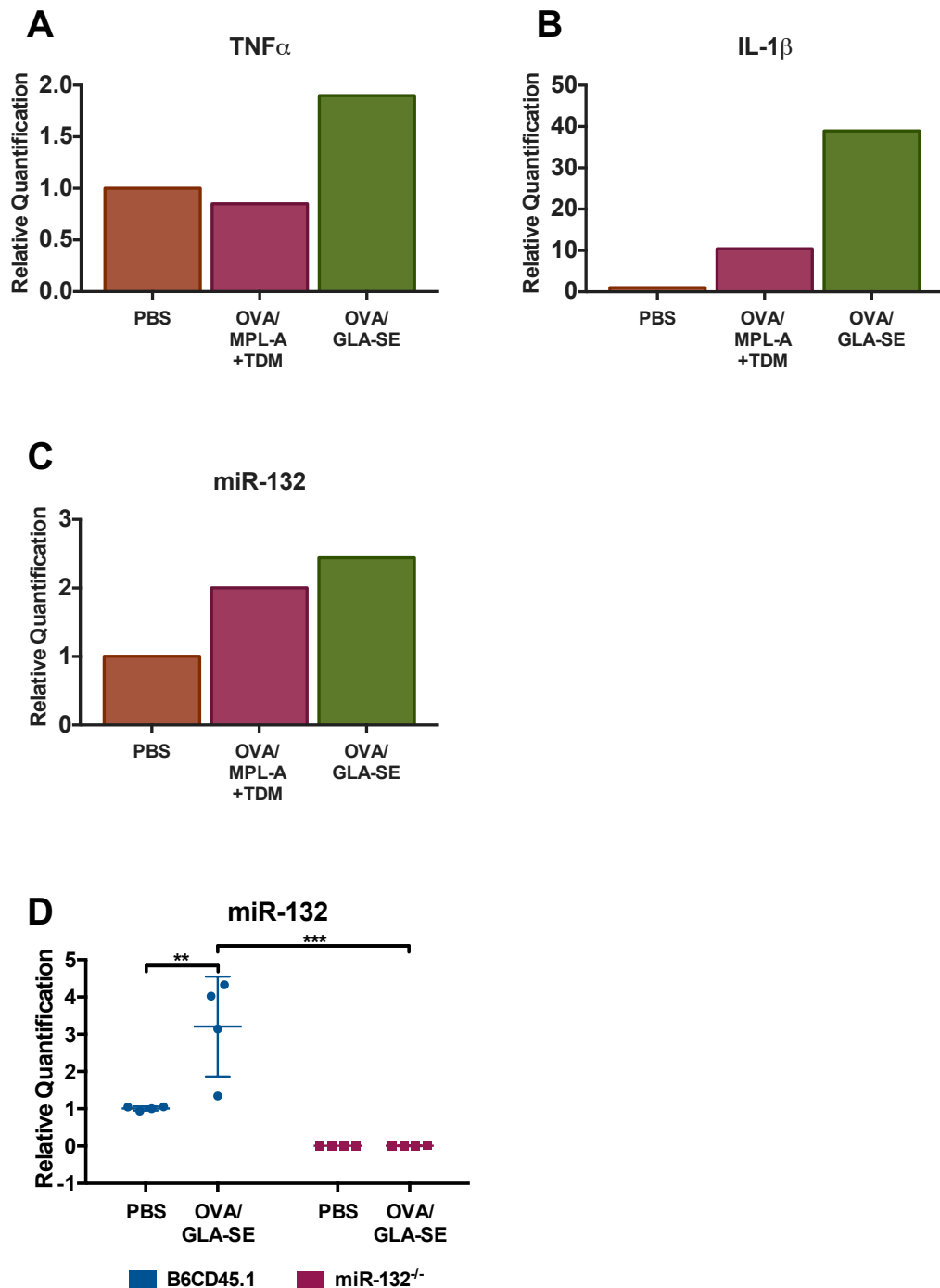


Figure 4.6: Effect of TLR4-agonist adjuvants on isolated FRCs gene expression or on total LN.

A-C: Mice were immunized with PBS, OVA/MPL-A+TDM or OVA/GLA-SE for 12hrs and the popliteal LNs were removed and FRCs were sorted by MOFLO. **A:** TNF α , **B:** IL1- β , and **C:** miR-132 mRNA and miRNA expression were analysed from FRCs.

D: Mice were immunized for 24 days and then total LN was digested. Cells were lysed, miR-132 was isolated, retro-transcribed into cDNA and analysed by RT-qPCR. Expression values were then normalized to the HPRT or RNU6 internal standard values. Data is shown as relative values. Two-Way ANOVA followed by multiple comparison Tukey's test: *P \leq 0.05, **P \leq 0.01, *** P \leq 0.001, ****P \leq 0.0001.

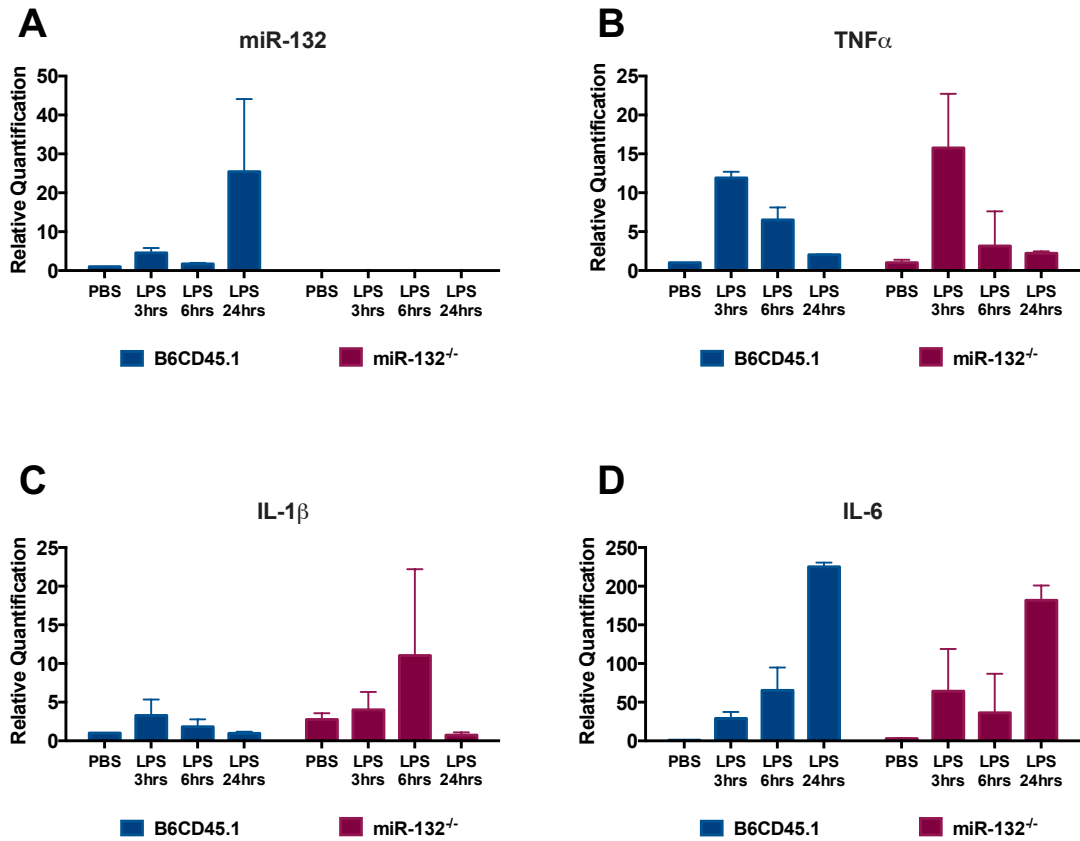


Figure 4.7: Role of miR-132 in B cells response to adjuvants.

B cells were isolated from mice using the MACS separation columns. The cells were treated with LPS for 3hrs, 6hrs and 24hrs. Cells were then lysed, total RNA was isolated, retro-transcribed into cDNA and expression was analysed by RT-qPCR. **A:** miR-132, **B:** TNF α , **C:** IL-1 β , and **D:** IL-6. Expression values were then normalized to the HPRT internal standard values. Data from 2 separate experiments with 2 technical repeats. Data is shown as relative values.

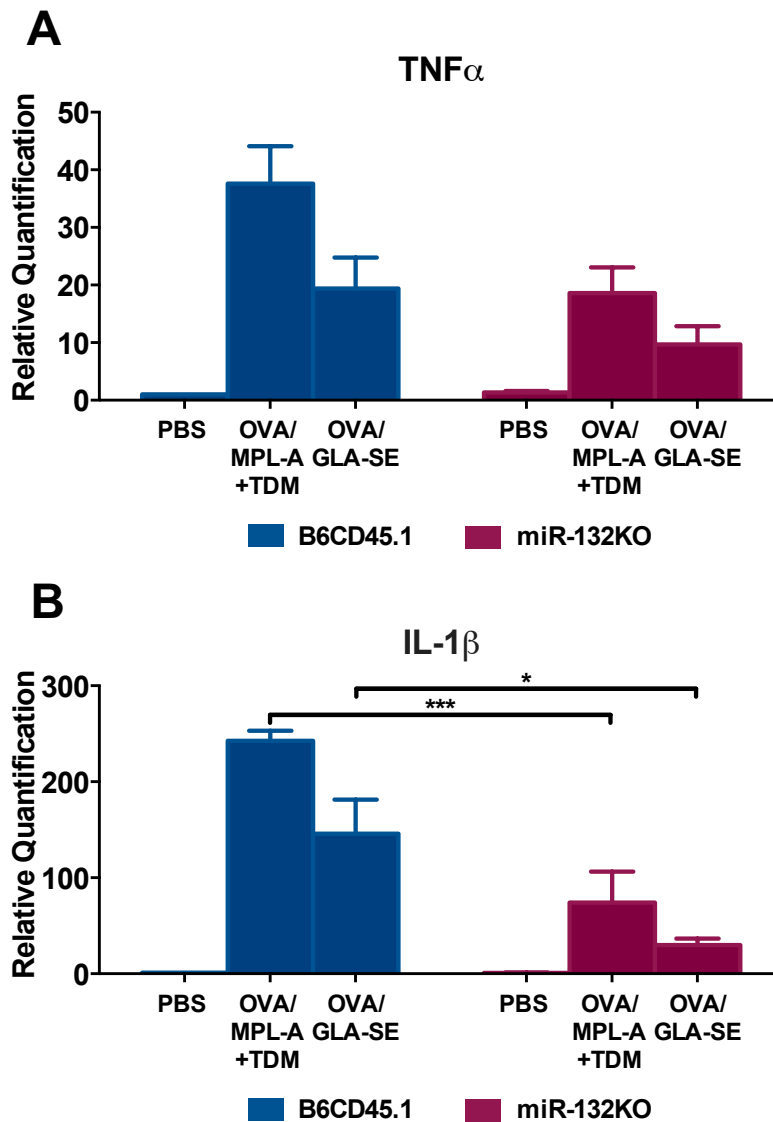


Figure 4.8: Effect of TLR4-agonist adjuvants on WT or miR-132^{-/-} cultured FRCs gene expression.

LNs from the mice were digested and plated. The cells were treated with OVA/MPL-A+TDM and OVA/GLA-SE for 5hrs, cells were lysed, total RNA was isolated, retro-transcribed into cDNA and analysed by qPCR. **A**: TNF α , and **B**: IL1 β . Expression values were then normalized to the HPRT internal standard values. Data is shown as relative values. From 3 separate experiments. Two-Way ANOVA followed by multiple comparison Tukey's test: *P \leq 0.05, **P \leq 0.01, *** P \leq 0.001, ****P \leq 0.0001.

4.4. Loss of miR-132 modulates LN structure

To better understand the role of miR-132, untreated miR-132^{-/-} mice were analysed and compared to WT mice (Figure 4.9). Frozen sections of pLNs were stained with B220 and CD3 to stain for B cells and T cells respectively. From these histology results, it can be observed that the miR-132^{-/-} pLNs are bigger and less organized than the WT pLNs. The B cell follicles are bigger and the separation between B and T cell zones is no longer distinct. The differences observed between WT and miR-132^{-/-} LNs indicate a potential role for miR-132 in B cell follicle function and remodelling.

4.5. Adjuvant induced hypertrophy in miR-132^{-/-} mice

4.5.1. Treatment induces an increase in immune cells

Long-term experiments (prime + boost at day 21) were performed to quantify LN cell populations directly comparing GLA-SE with Alum. Immunizations with both adjuvants lead to increased total cellularity that is significantly higher in OVA/GLA-SE treated mice. There is a significant difference in the number of B cells in miR-132^{-/-} mice. There is no difference between total T cells or CD4 T cells between WT and miR-132^{-/-} mice, but there are significantly less CD8 T cells in miR-132^{-/-} mice upon treatment (Figure 4.10). There is no difference in the increase of DCs upon treatment in either WT or miR-132^{-/-} mice. NK cells were increased upon treatment but there were significantly more NK cells in miR-132^{-/-} mice upon treatment both with Alum and GLA-SE (Figure 4.11).

4.5.2. miR-132 regulates B cell follicle remodelling

Immunization with both OVA/Alum and OVA/GLA-SE leads to an enlargement of pLNs in miR-132^{-/-} and WT mice (Figure 4.12). The difference that can be observed is that treatment of miR-132^{-/-} mice doesn't induce remodelling as in WT mice. LNs got bigger with larger B cell follicles, which resembles more a treatment with Alum than with GLA-SE. Mice lacking miR-132 are not able to remodel in the same way.

The images obtained in Figure 4.12 were quantified by using Cell Profiler image analysis software (www.cellprofiler.org). When treated with OVA/Alum, both miR-132^{-/-} and WT mice have bigger LNs but the difference between the two isn't significant. However, treatment with OVA/GLA-SE leads to significantly bigger WT LNs than miR-132^{-/-}. Treatment with OVA/GLA-SE in WT mice leads to an increase in the number of follicles that is bigger than in miR-132^{-/-} mice, but the follicle area is

significantly bigger in miR-132^{-/-} mice. Treatment induced a significant increase in follicle area in miR-132^{-/-} mice but the number of follicles didn't increase as much as WT mice (Figure 4.13).

B cell subsets were quantified by flow cytometry. There is a significant increase in the number of follicular B cells and in activated B cells in miR-132^{-/-} mice.

4.5.3. Role of miR-132 in stromal remodelling

The stromal network mirrors the B and T cell distribution and follows the organization observed in Figure 4.12. Treatment induced an invasion of the LNs by lymphatic and blood vasculature growth in both WT and miR-132^{-/-} mice (Figure 4.14).

Treatment with OVA/GLA-SE led to an increase in all stromal cell types quantified (Figure 4.15). This increase in cellularity is significantly larger in miR-132^{-/-} mice for FRCs and BECs. These results lead to the conclusion that miR-132 deficient mice are able to induce LN swelling mirrored by stromal cell expansion. However, miR-132 is necessary for remodelling and also seems to serve as a brake on B cell expansion.

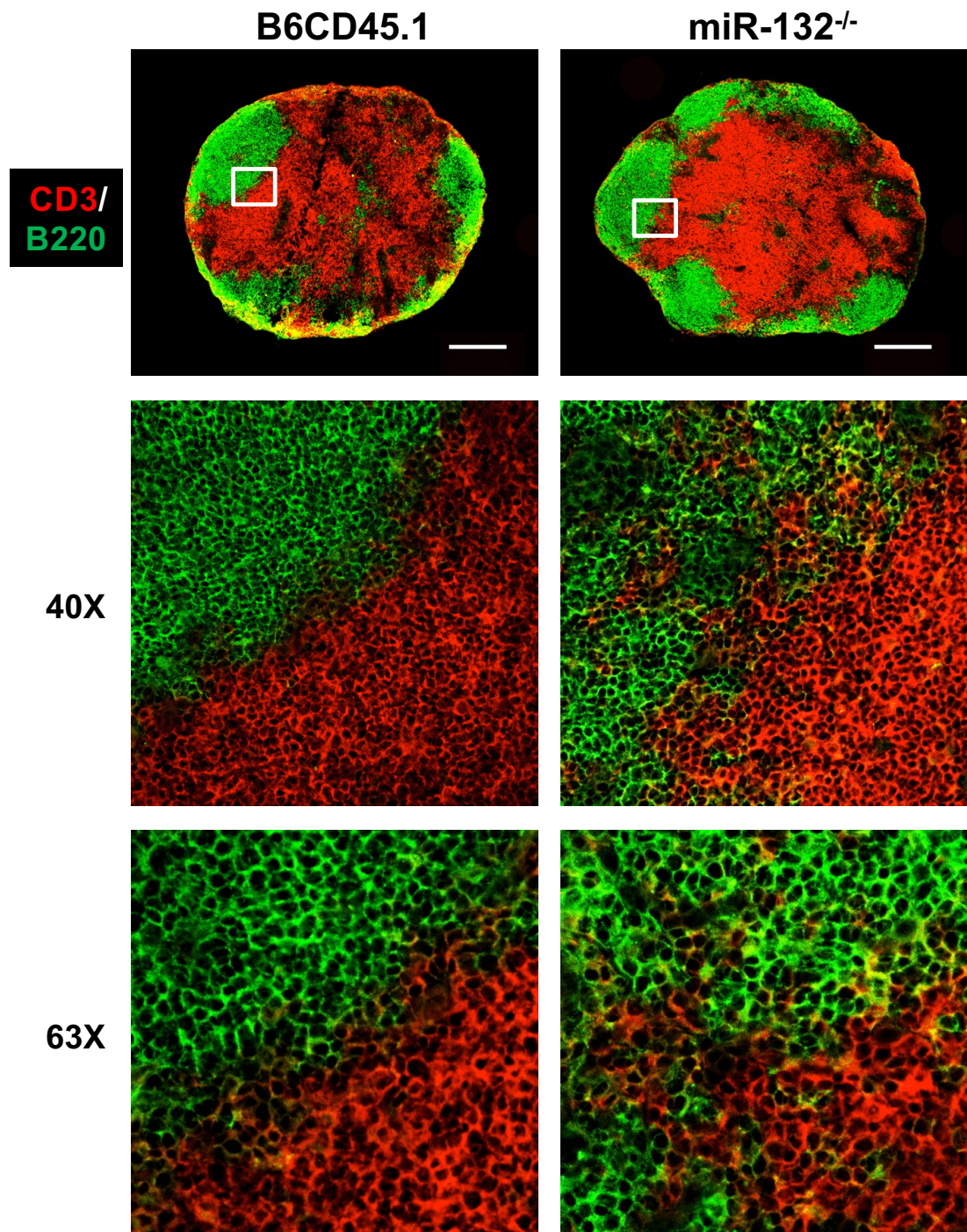


Figure 4.9: Comparison of WT and miR-132^{-/-} naïve LNs.

LNs from 3 independent WT and 3 miR-132^{-/-} mice were removed; a pLN from each mouse was used for histology. Frozen sections of the pLNs from WT and miR-132^{-/-} mice were stained with antibodies against CD3 (T cells) and B220 (B cells). Scale bar = 200µm. A closer look was taken at the B and T cell boundary at 40X and 63X.

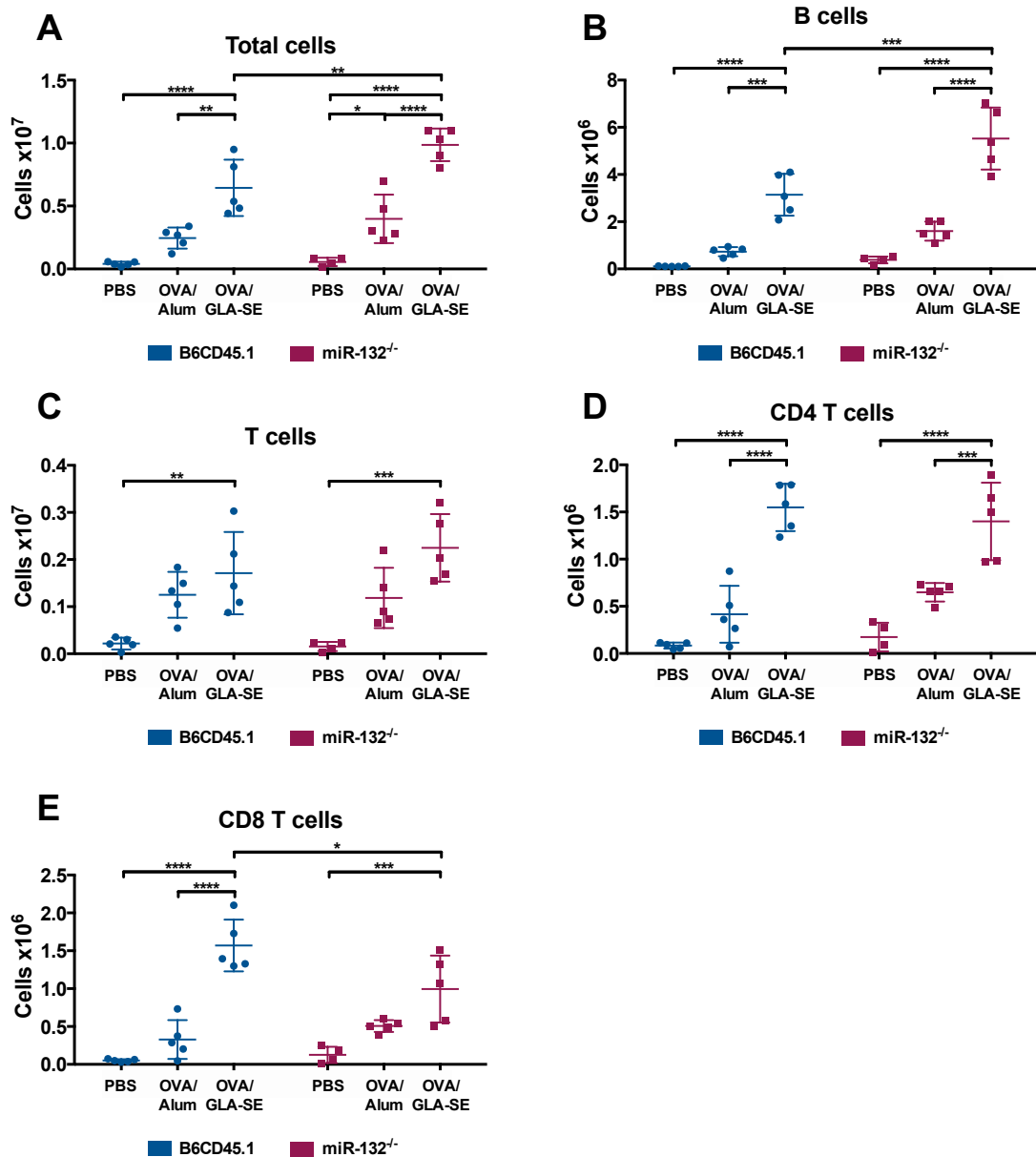


Figure 4.10: Effect of adjuvants on adaptive cell populations in WT and miR-132^{-/-} mice at day 24.

Mice were immunized with PBS, OVA/Alum or OVA/GLA-SE and the popliteal LNs were removed and analysed via flow cytometry. **A:** Total cells, **B:** B cells (CD19+), **C:** T cells (CD3+), **D:** CD4 T cells (CD4+), and **E:** CD8 T cells (CD8+). AccuCheck counting beads from Invitrogen were used to get an accurate cell count. N=5. 3 separate experiments. Two-Way ANOVA followed by multiple comparison Tukey's test: *P ≤ 0.05, **P ≤ 0.01, *** P≤0.001, ****P ≤ 0.0001.

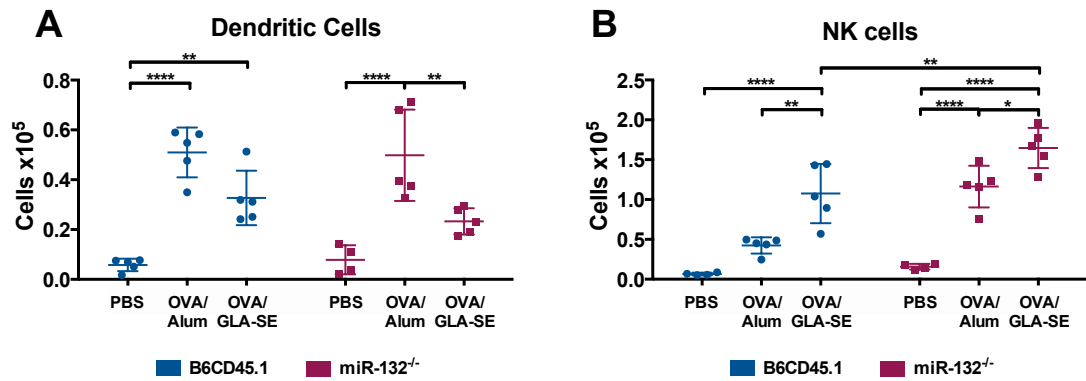


Figure 4.11: Effect of adjuvants on innate cell populations in WT and miR-132^{-/-} mice at day 24.

Mice were immunized with PBS, OVA/Alum or OVA/GLA-SE and the pLNs were removed and analysed via flow cytometry. **A:** Dendritic cells (CD11c+MHCII+), and **B:** NK cells (NK1.1+). AccuCheck counting beads from Invitrogen were used to get an accurate cell count. N=5. 3 separate experiments. Two-Way ANOVA followed by multiple comparison Tukey's test: *P ≤ 0.05, **P ≤ 0.01, *** P≤0.001, ****P ≤ 0.0001.

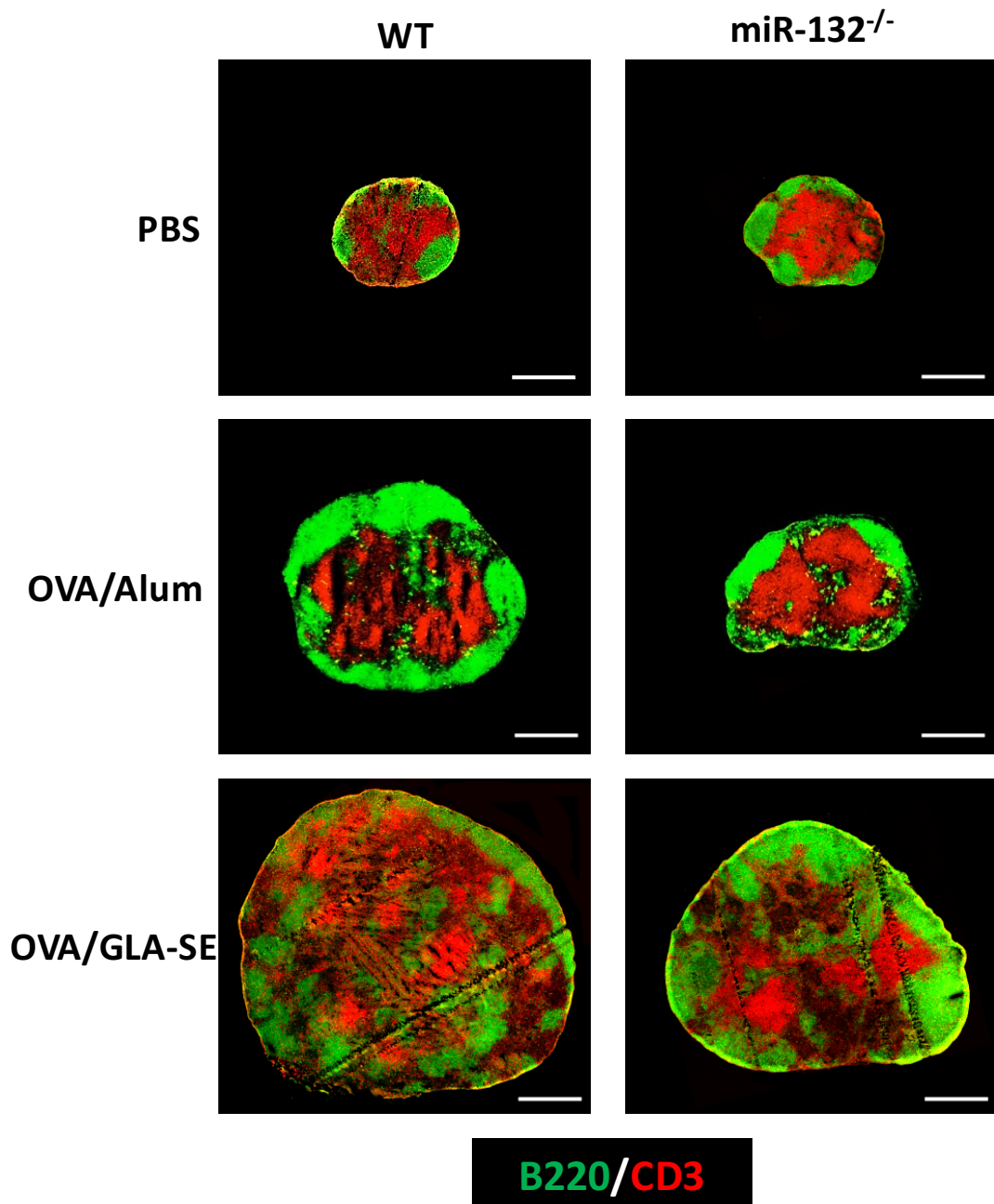


Figure 4.12: B and T cell zones in WT vs. miR-132^{-/-} mouse LN.

Frozen sections of the popliteal LN from PBS, OVA/Alum or OVA/GLA-SE immunized WT or miR-132^{-/-} mice were stained with antibodies against CD3 (T cells), and B220 (B cells). N=20 mice, 5 separate experiments, 2 slides/LN, representative image was chosen. Scale bar = 500 μ m.

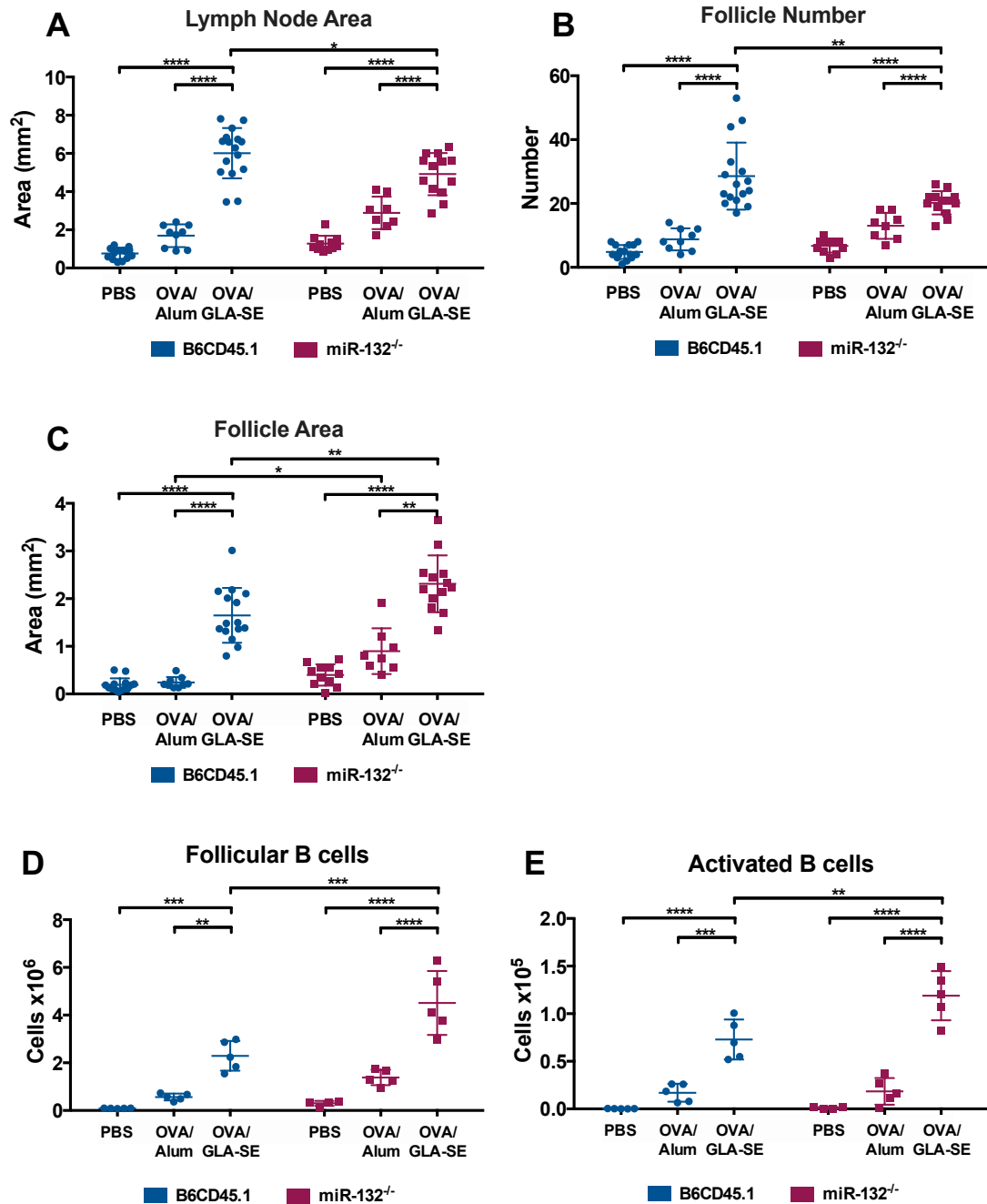


Figure 4.13: Quantification of histology results with Cell Profiler.

A-C: Frozen sections of the pLN from PBS, OVA/Alum or OVA/GLA-SE immunized mice were stained with antibodies against CD3 (T cells) and B220 (B cells). Images obtained were then run through a Cell Profiler pipeline to get the **A:** Lymph node area, **B:** Number of follicles, and **C:** Follicle area.

D-E: Mice were immunized with PBS, OVA/Alum or OVA/GLA-SE and the popliteal LNs were removed and analysed by flow cytometry. **D:** Follicular B cells (CD19+IgD+CD95-), and **E:** Activated B cells (CD19+IgD-CD95+GL7+).

Data from multiple experiments. N=8, N=15 or N=5. Two-Way ANOVA followed by multiple comparison Tukey's test: *P ≤ 0.05, **P ≤ 0.01, *** P≤0.001, ****P ≤ 0.0001.

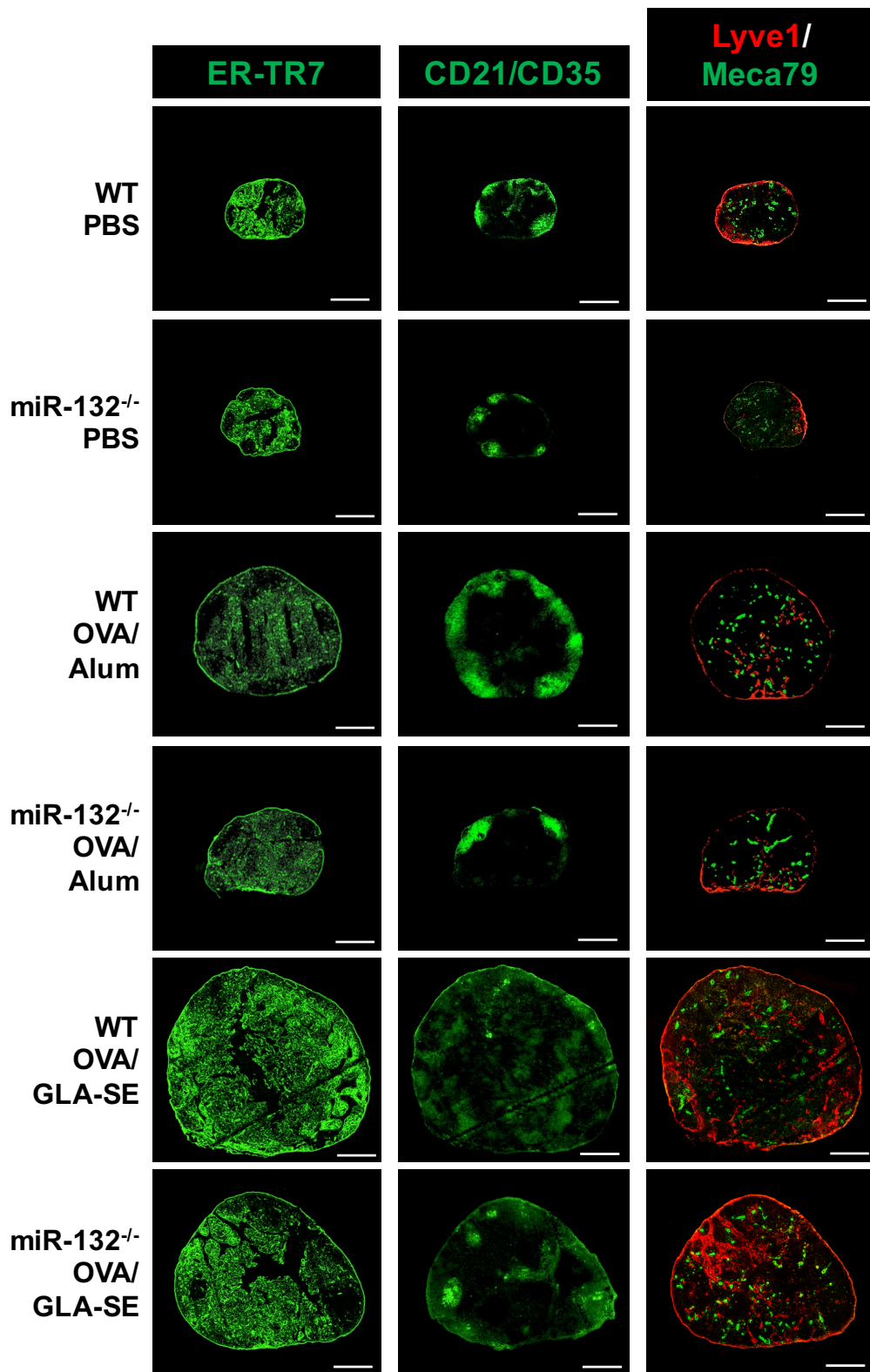


Figure 4.14: Architecture of the stromal network in WT vs. miR-132^{-/-} mouse LNs.

Frozen sections of the popliteal LN from PBS, OVA/Alum or OVA/GLA-SE immunized WT or miR-132^{-/-} mice were stained with antibodies against CD21/CD35 (FDCs), ER-TR7 (reticular network), Lyve-1 (lymphatic vessels) and Meca-79 (HEVs). N=20 mice, 5 separate experiments, 2 slides/LN, representative image was chosen. Scale bar = 500 μ m.

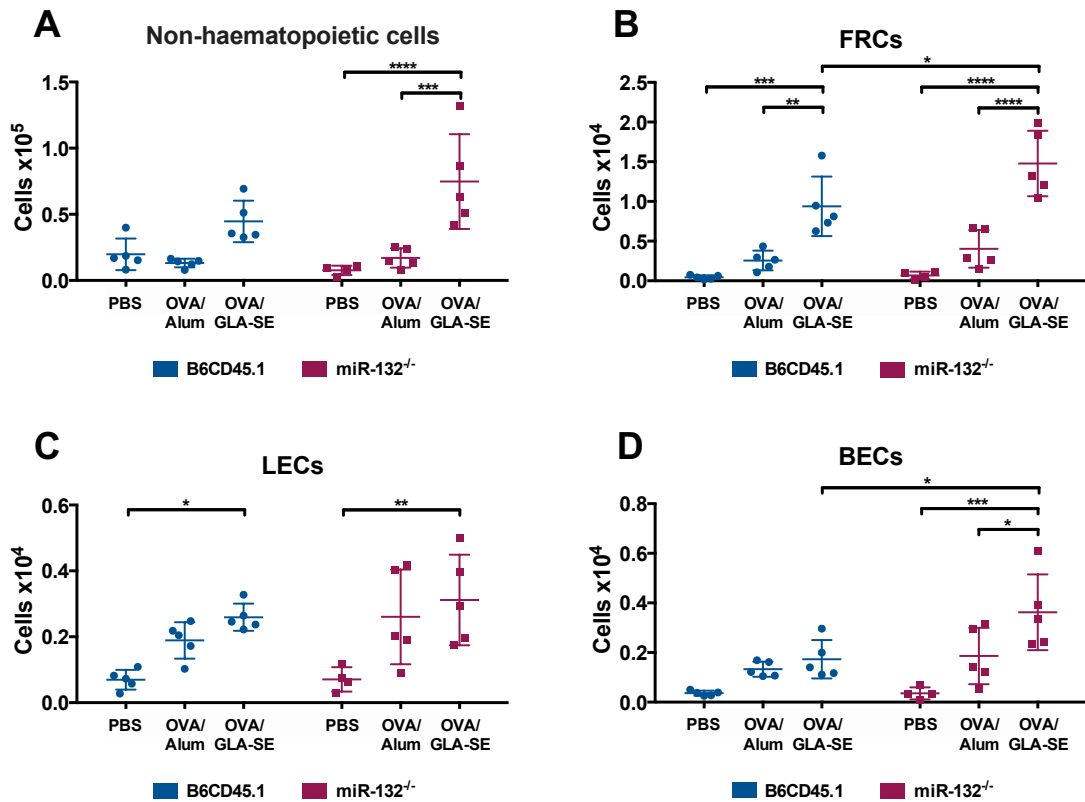


Figure 4.15: Effect of adjuvants on stromal cell populations in WT and miR-132^{-/-} mice at day 24.

Mice were immunized with PBS, OVA/Alum or OVA/GLA-SE and the popliteal LNs were removed and analysed by flow cytometry. **A:** Non-haematopoietic cells (CD45⁻), **B:** FRCs (CD45-CD31-GP38⁺), **C:** LECs (CD45-CD31+GP38⁺), and **D:** BECs (CD45-CD31+GP38⁻). AccuCheck counting beads from Invitrogen were used to get an accurate cell count. N=5. 3 separate experiments. Two-Way ANOVA followed by multiple comparison Tukey's test: *P ≤ 0.05, **P ≤ 0.01, *** P≤0.001, ****P ≤ 0.0001.

4.6. Remodelling kinetics in miR-132^{-/-} mice

4.6.1. Dissolution of LN architecture

Short immunizations of three or seven days with OVA/GLA-SE were administered to WT or miR-132^{-/-} mice. Cell types were analysed by flow cytometry (Figure 4.16). Treatment with OVA/GLA-SE led to a significant increase in total cellularity in miR-132^{-/-} mice. Immunization led to the same increase in T cells and in T_{FR} cells. However, there were significantly more B cells and T_{FH} cells in miR-132^{-/-} mice by seven days post immunization.

Analysis of WT mice showed that key steps in the remodelling process occurred during the first 72hrs. To further understand the mechanisms behind follicular remodelling, early time points of the immune response to OVA/GLA-SE were analysed using immunohistochemistry (Figure 4.17). By seven days of response to the adjuvant, WT LNs are remodelled and there are B cell follicles found in the paracortex, whereas miR-132^{-/-} mice still possess distinct B cell follicles found only in the cortex. This phenotype resembles that observed after a long-term treatment.

The images obtained were analysed using Cell Profiler (Figure 4.18). When treated with OVA/GLA-SE for three and seven days, both miR-132^{-/-} and WT mice have bigger LNs. At three days, treatment induced significantly larger LNs in miR-132^{-/-} mice but by seven days the LNs are the same size between WT and miR-132^{-/-} mice. Treatment with OVA/GLA-SE at seven days in WT mice leads to an increase in the number of follicles that is bigger than in miR-132^{-/-} mice, but the follicle area is significantly bigger in miR-132^{-/-} mice at three days.

4.6.2. Normal stromal networks in miR-132^{-/-} mice

Based on the failure of B cell follicle remodelling in miR-132^{-/-} mice the FDC network, lymphatic and HEV networks were compared during OVA/GLA-SE mediated remodelling. In WT mice GLA-SE induces rapid increase in LN size and leads to the dissolution of organized follicular structures resulting in the loss of organized FDC network (see FDCM2 staining at 72hrs). Immunohistochemistry results indicate that follicular structures are maintained in the miR-132 deficient mice at 72hrs (Figure 4.19). Stromal cell types were analysed by flow cytometry (Figure 4.20). Treatment led to the same increase in stromal cell populations. Stromal remodelling is normal and the phenotype observed is not related to the vascularisation.

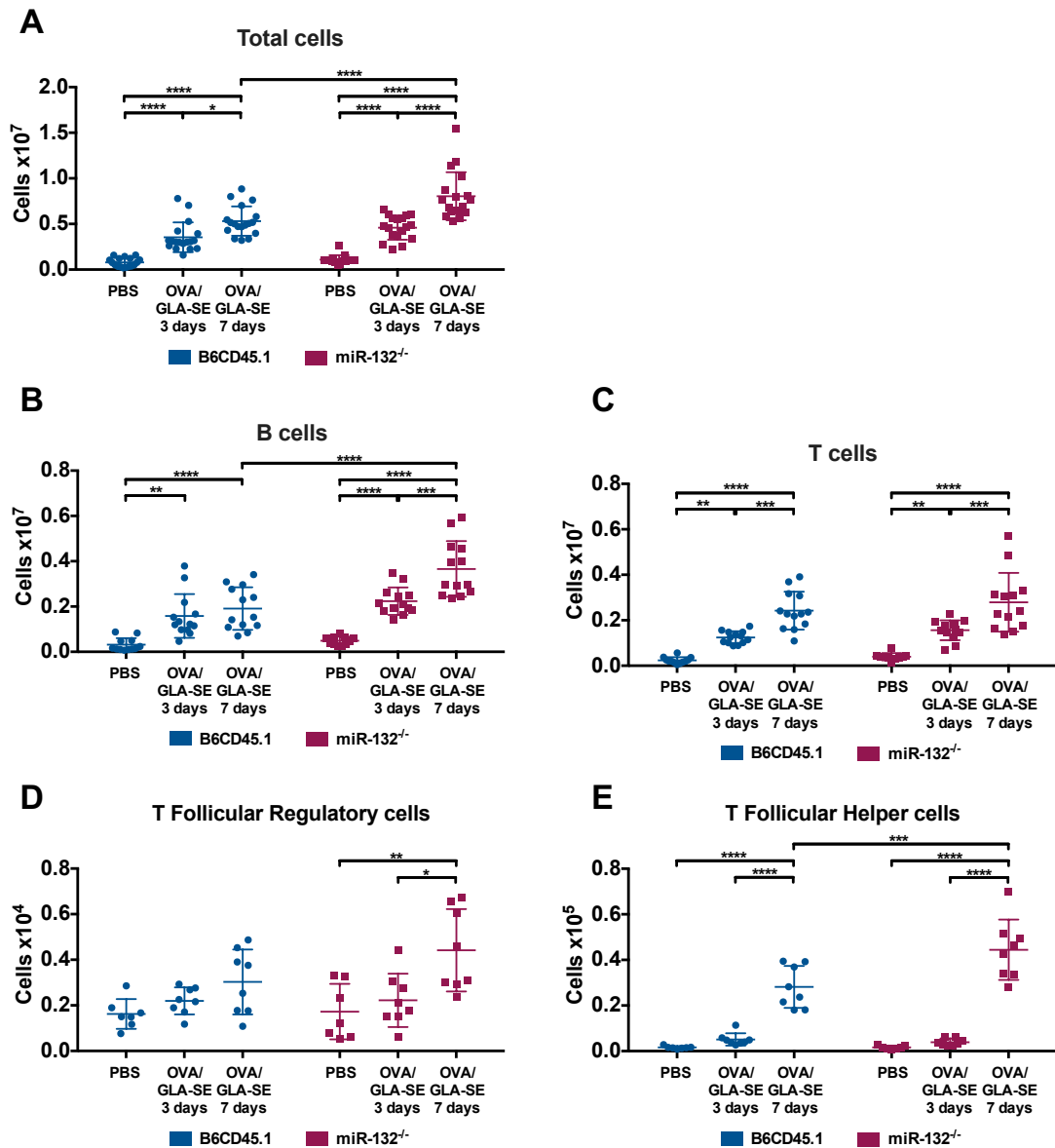


Figure 4.16: Effect of adjuvants on immune cell populations in WT and miR-132^{-/-} mice at days 3 and 7.

Mice were immunized with PBS, or OVA/GLA-SE for 3 or 7 days and the popliteal LNs were removed and analysed by flow cytometry. **A:** Total cells, **B:** B cells (CD19+), **C:** T cells (CD3+), **D:** T Follicular Regulatory Cells (CD4+PD1+CXCR5+Foxp3+CD44+), and **E:** T Follicular Helper Cells (CD4+PD1+CXCR5+Foxp3-CD44+). AccuCheck counting beads from Invitrogen were used to get an accurate cell count. N=10 or N=15 from 3 separate experiments. Two-Way ANOVA followed by multiple comparison Tukey's test: *P ≤ 0.05, **P ≤ 0.01, *** P≤0.001, ****P ≤ 0.0001.

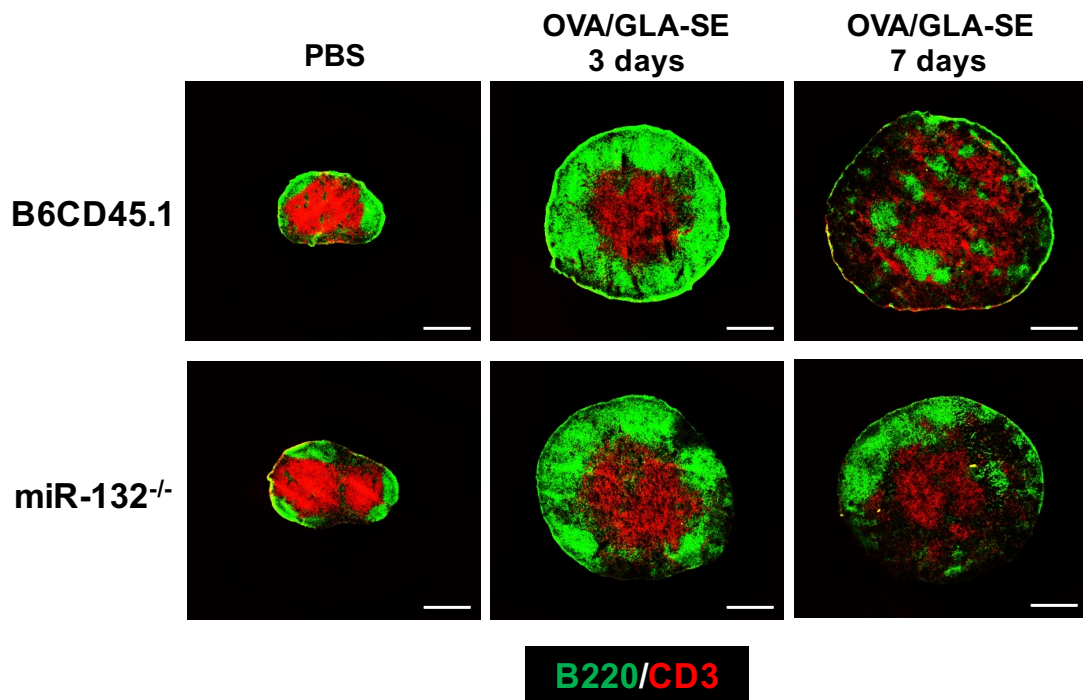


Figure 4.17: LN architecture when treated with antigen/adjuvant complex at days 3 and 7.

Immunizations with OVA in combination with GLA-SE in WT or miR-132^{-/-} mice for 3 or 7 days. Frozen sections of the popliteal LN from PBS, or OVA/GLA-SE immunized mice were stained with antibodies against CD3 (T cells), and B220 (B cells). N=5 mice, from 3 separate experiments. Representative image was chosen. Scale bar = 500 μ m.

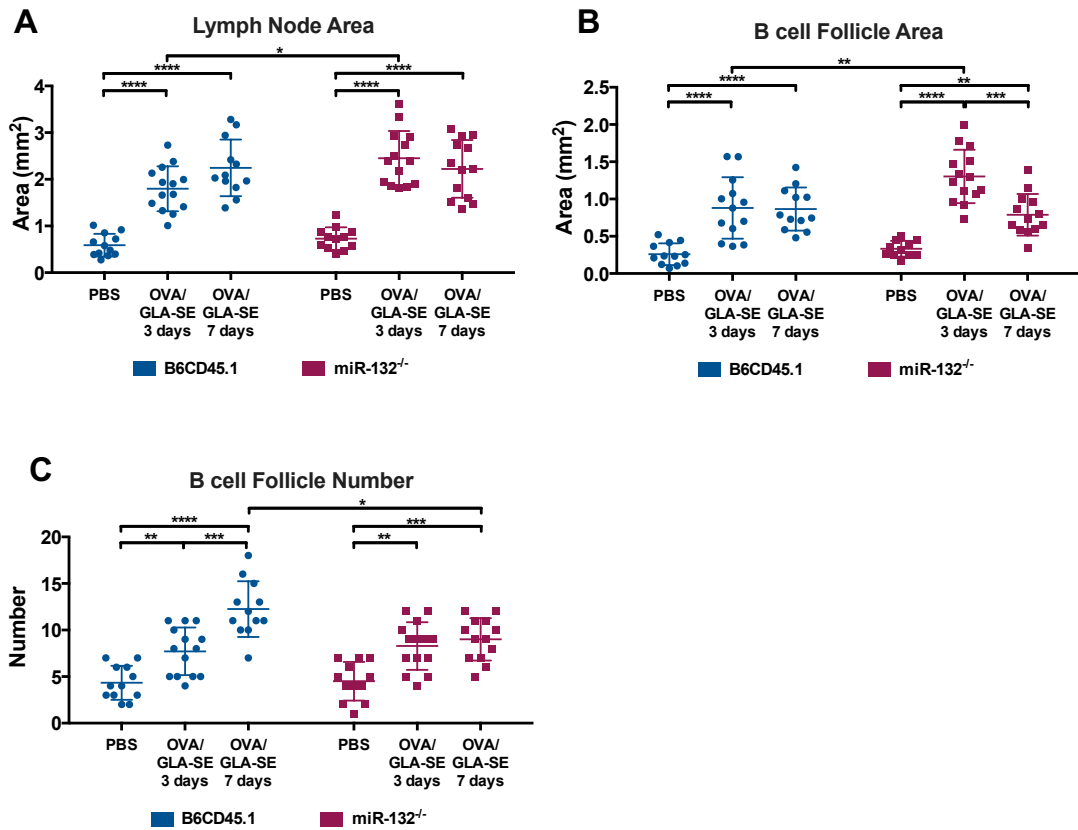


Figure 4.18: Quantification of histology results with Cell Profiler.

Immunizations with OVA in combination with GLA-SE in WT or miR-132^{-/-} mice for 3 or 7 days. Frozen sections of the popliteal LN from PBS, or OVA+GLA-SE immunized mice were stained with antibodies against CD3 (T cells), B220 (B cells). Images obtained were then run through a Cell Profiler pipeline to get the **A**: Lymph node area, **B**: B cell Follicle Area, and **C**: B cell Follicle number. Data from 3 separate experiments. N=18. Two-Way ANOVA followed by multiple comparison Tukey's test: *P ≤ 0.05, **P ≤ 0.01, *** P ≤ 0.001, ****P ≤ 0.0001.

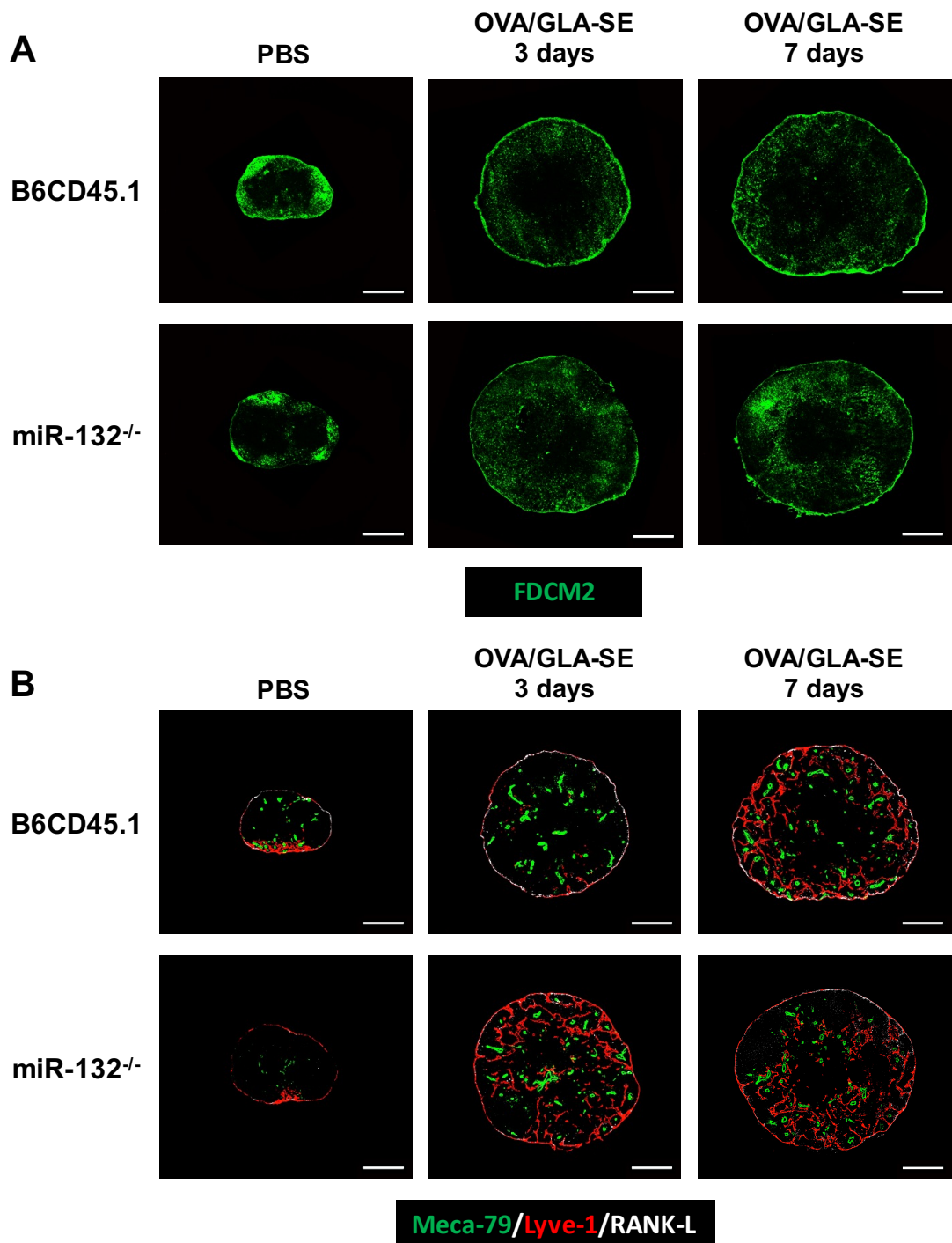


Figure 4.19: LN stroma network when treated with antigen/adjuvant complex at days 3 and 7.

Immunizations with OVA in combination with GLA-SE in WT or miR-132^{-/-} mice for 3 or 7 days. Frozen sections of the popliteal LN from PBS, or OVA/GLA-SE immunized mice were stained with antibodies against **A:** FDCM2 (FDCs), and **B:** RANK-L (MRCs), Lyve-1 (lymphatic vessels) and Meca-79 (HEVs). N=5 mice, from 3 separate experiments. Representative image was chosen. Scale bar = 500 μ m.

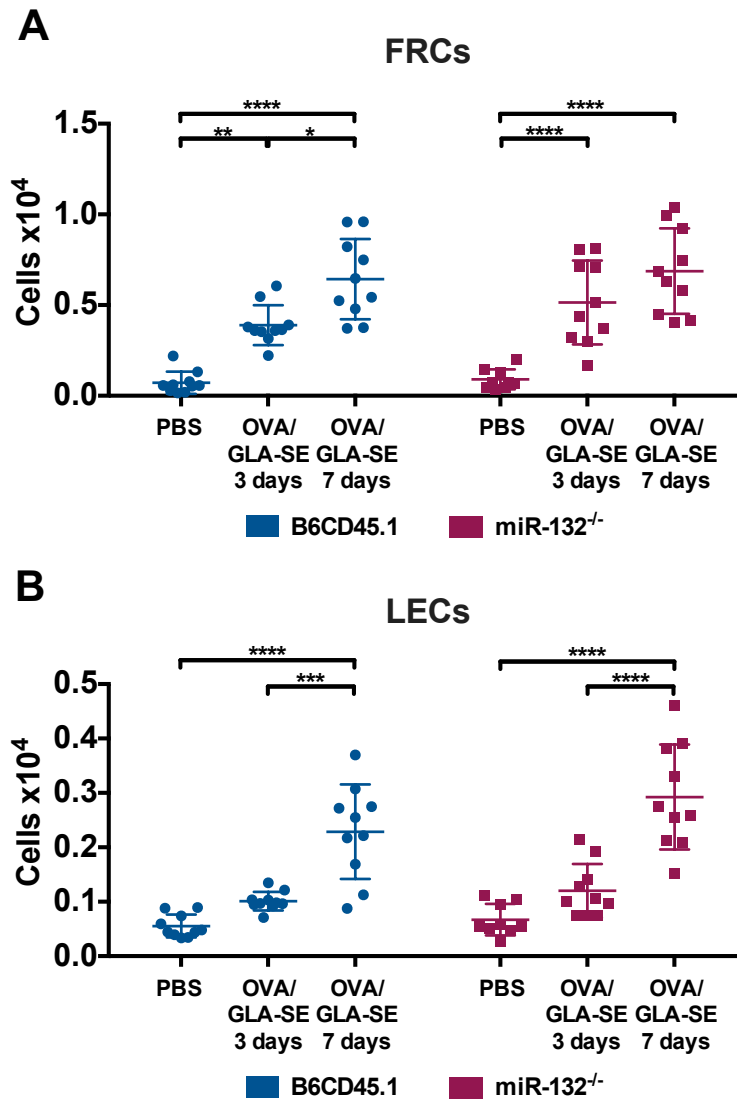


Figure 4.20: Effect of adjuvants on stromal cell populations in WT and miR-132^{-/-} mice at days 3 and 7.

Mice were immunized with PBS, or OVA/GLA-SE for 3 or 7 days and the popliteal LNs were removed and analysed by flow cytometry. **A:** FRCs (CD45⁻ gp38⁺CD31⁻), and **B:** LECs (CD45⁻gp38⁺CD31⁺). AccuCheck counting beads from Invitrogen were used to get an accurate cell count. N=10 from 3 separate experiments. Two-Way ANOVA followed by multiple comparison Tukey's test: *P ≤ 0.05, **P ≤ 0.01, *** P≤0.001, ****P ≤ 0.0001.

4.7. Immunization effect on macrophages

Antigen/Adjuvant immunization led to changes in macrophages localization (Figure 4.21A). Treatment with OVA/Alum led to an increase in SSMs into the LN where they interact with DCs both in WT and miR-132^{-/-} mice. OVA/GLA-SE treatment seems to lead to a reduction in SSM numbers, there are almost no more SSMs found and they are not interacting with dendritic cells.

Macrophages were quantified by flow cytometry (Figure 4.21B-C). There was an increase in macrophages upon treatment with both OVA/Alum and OVA/GLA-SE but the increase in cellularity is significantly lessened in miR-132^{-/-} mice treated with OVA/GLA-SE than with OVA/Alum. There is no difference in SSM numbers but there are more MSMs in the miR-132^{-/-} mice when treated with OVA/Alum (Figure 4.21D). miR-132 does not appear to modulate macrophage migration or function.

4.8. Marginal reticular cell network remodelling

MRCs are a specialised stromal cell population that have a lineage relationship with FDCs. MRCs were sorted three days post PBS or OVA/GLA-SE immunization. OVA/GLA-SE treatment led to a 2-fold increase in miR-132 expression in WT mice (Figure 4.22A).

Immunizations with both adjuvants lead to increased MRCs cellularity that is significantly higher in OVA/GLA-SE treated mice after prime and boost (at day 24). This increase in cellularity is significantly larger in miR-132^{-/-} mice for MRCs (Figure 4.22B).

Immunohistochemistry analysis of MRC localisation was done at day 24 (prime and boost) post immunization. At a resting state MRCs are found under the floor of the SCS. Treatment led to changes in the location of MRCs. MRCs in both treatments are found inside the LN and not just around it. miR-132^{-/-} mice treated with OVA/GLA-SE have more MRCs and enter the LN more (Figure 4.23). MRCs migrate upon adjuvant administration and this is modulated differentially in miR-132^{-/-} mice.

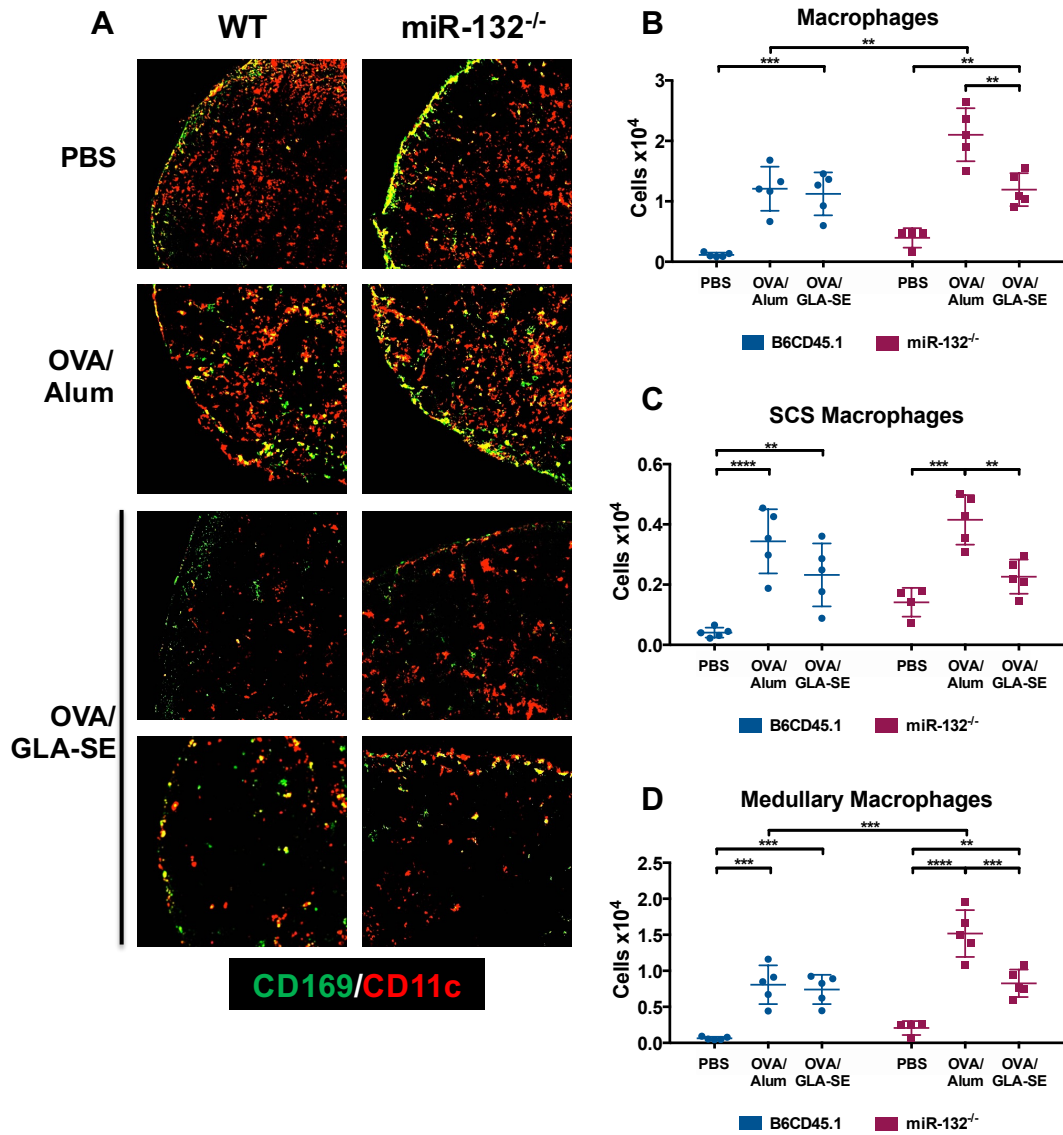


Figure 4.21: Close up of the architecture in mouse LNs when treated with antigen/adjuvant at day 24.

A: Immunizations with OVA/Alum or OVA/GLA-SE in WT or miR-132^{-/-} mice. Frozen sections of the popliteal LN from PBS, OVA/Alum or OVA/GLA-SE immunized mice were stained with antibodies, CD169 (Macrophages), CD11b (DCs). N=5 mice, representative image was chosen.

B-D: Mice were immunized with PBS, OVA/Alum or OVA/GLA-SE and the pLNs were removed and analysed by flow cytometry. **B:** Macrophages (CD169+), **C:** SCS Macrophages (CD169+SIGNR1-), and **D:** Medullary Macrophages (CD169+SIGNR1+). AccuCheck counting beads from Invitrogen were used to get an accurate cell count. N=5. 3 separate experiments. Two-Way ANOVA followed by multiple comparison Tukey's test: *P ≤ 0.05, **P ≤ 0.01, *** P≤0.001, ****P ≤ 0.0001.

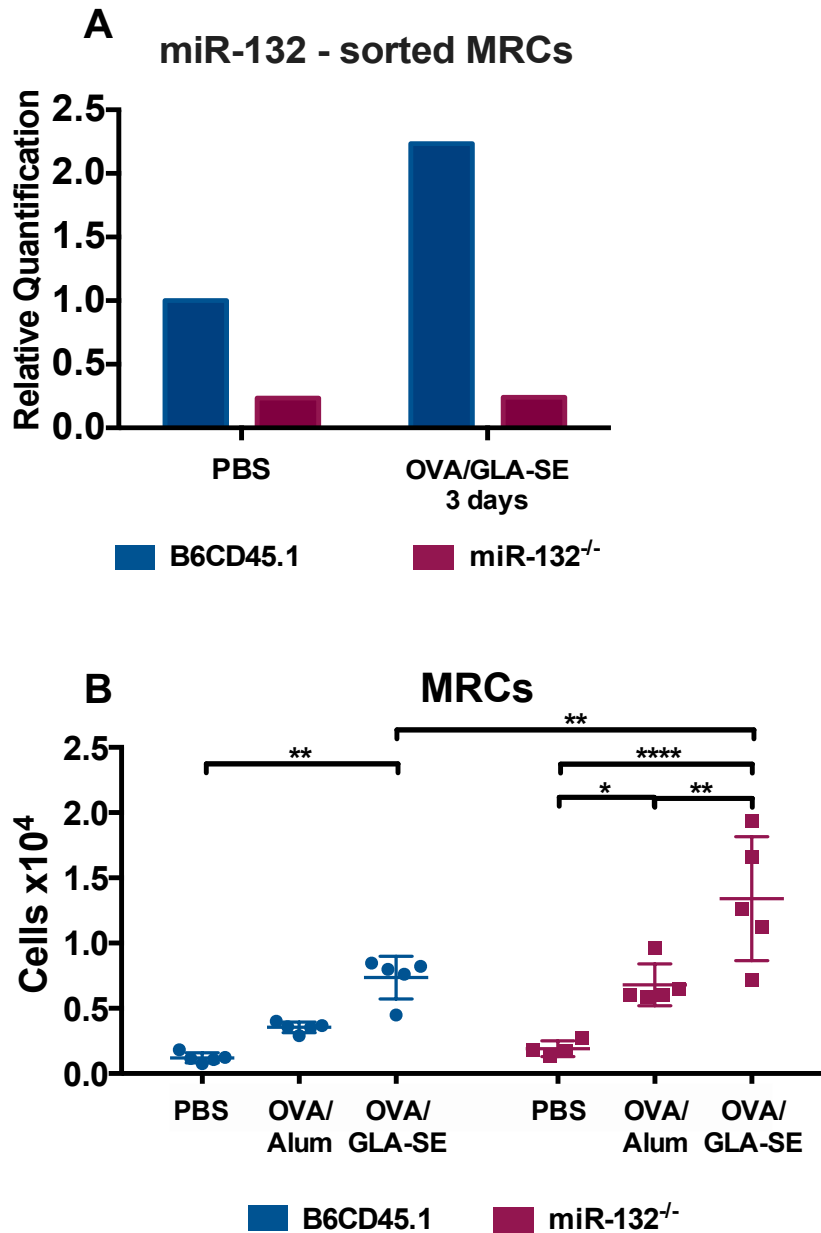


Figure 4.22: Effect of adjuvants on miR-132 expression in MRCs and on MRC expansion in WT and miR-132^{-/-} mice.

A: Mice were immunized with PBS, or OVA/GLA-SE for 3 days and the popliteal LNs were removed and MRCs were sorted by MOFLO. Cells were lysed, total RNA was isolated, retro-transcribed into cDNA and miR-132 expression analysed by RT-qPCR. Expression values were then normalized to the RNU6 internal standard values. Data is shown as relative values. **B:** MRCs (CD45-CD31-GP38+MAdCAM-1+) were quantified by flow cytometry at day 24 post immunization. AccuCheck counting beads from Invitrogen were used to get an accurate cell count. N=5. 3 separate experiments. Two-Way ANOVA followed by multiple comparison Tukey's test: *P ≤ 0.05, **P ≤ 0.01, *** P ≤ 0.001, ****P ≤ 0.0001.

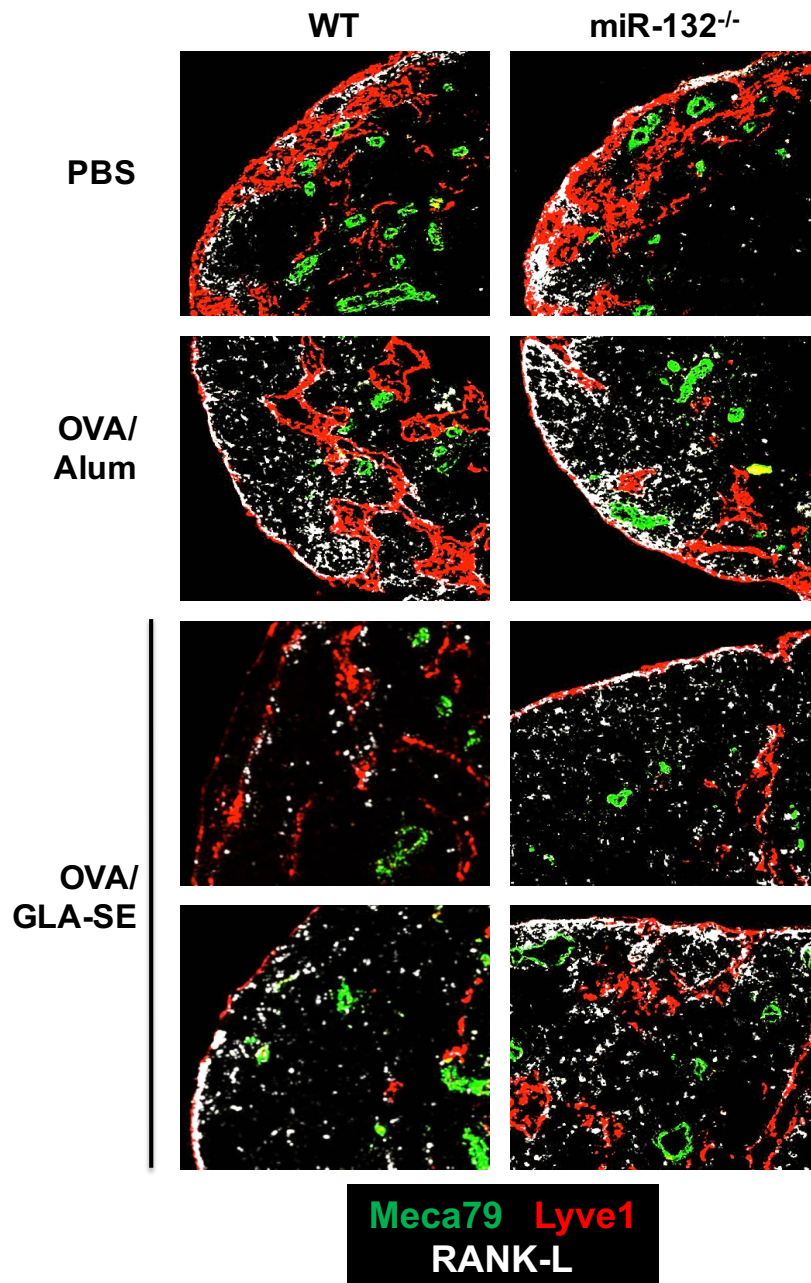


Figure 4.23: Close up of the architecture in mouse LNs when treated with antigen/adjuvant at day 24.

Immunizations with OVA/Alum or OVA/GLA-SE in WT or miR-132^{-/-} mice. Frozen sections of the popliteal LN from PBS, OVA/Alum or OVA/GLA-SE immunized mice were stained with antibodies, RANK-L (MRCs), Lyve-1 (lymphatic vessels) and Meca-79 (HEVs). N=5 mice, representative image was chosen.

4.9. MRC differentiation into FDCs

MRCs during immune responses can differentiate into FDCs through down-regulation of RANK-L and MAdCAM-1, followed by an up-regulation of CD21/CD35 and CXCL13. The kinetics and gene expression of MRCs was quantified. At three and seven days post immunization, cell populations were quantified by flow cytometry (Figure 4.24). MRCs, MRCs expressing CD21/35 and FDCs are increased in numbers upon OVA/GLA-SE immunization. There are significantly more of these cell types at three days post immunization in miR-132^{-/-} mice compared to WT mice. This number decreases by seven days.

A hypothesis to explain the ring-like structure that appears in WT mice at three days post treatment was that there was a drop in CXCL13 production. To test this, CXCL13 and CXCL12 expression was analysed in total LNs (Figure 4.25A-B). There is an increase upon OVA/GLA-SE treatment in CXCL13 expression in both WT and miR-132^{-/-} mice. This increase is mirrored by a significant decrease in CXCL12 expression in total LN. CXCL12 and CXCL13 expression was then analysed in sorted MRCs after three days of OVA/GLA-SE immunization (Figure 4.25C-D). Treatment led to an 8-fold increase in CXCL12 and a 15-fold increase in CXCL13 expression in WT mice. In miR-132^{-/-} mice, treatment led to a 2-fold increase in both CXCL12 and CXCL13 expression.

CXCR5 expression was then analysed by flow cytometry (Figure 4.26). Interestingly treatment led to no increase in CXCR5 MFI in WT mice but to a significant increase in miR-132 deficient mice, which might explain the difference in phenotype observed.

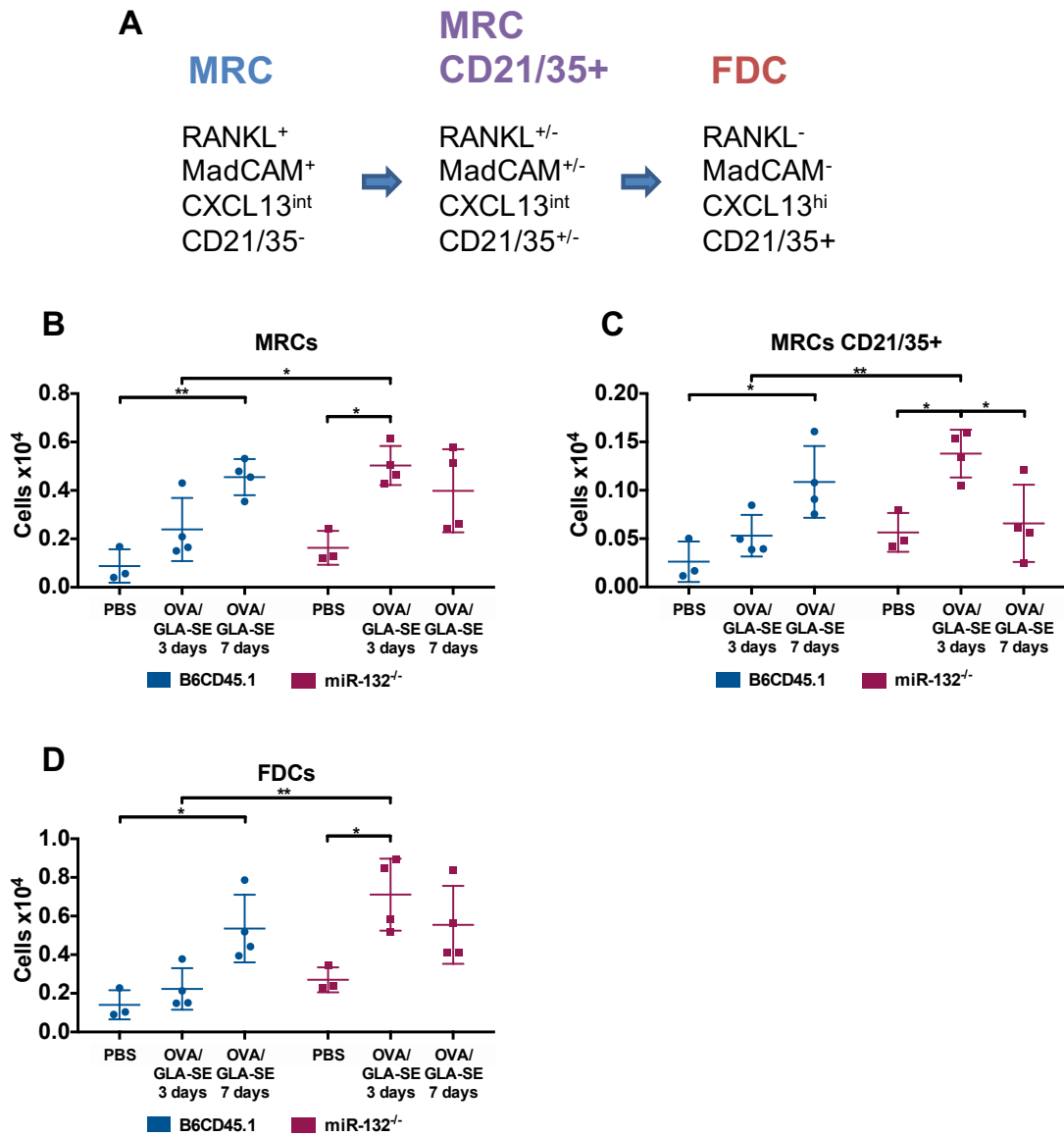


Figure 4.24: Quantification of MRC kinetics.

Mice were immunized with PBS, or OVA/GLA-SE for 3 or 7 days and analysed by flow cytometry. **A:** Schematic showing the MRC differentiation into FDCs. **B:** MRCs (CD45-gp38+MAdCAM1+CD21/35⁻), **C:** MRCs CD21/35⁺ (CD45-gp38+MAdCAM1+CD21/35⁺), and **D:** FDCs (CD45-gp38+MAdCAM1-CD21/35⁺). N=4. Two-Way ANOVA followed by multiple comparison Tukey's test: *P ≤ 0.05, **P ≤ 0.01, *** P ≤ 0.001, ****P ≤ 0.0001.

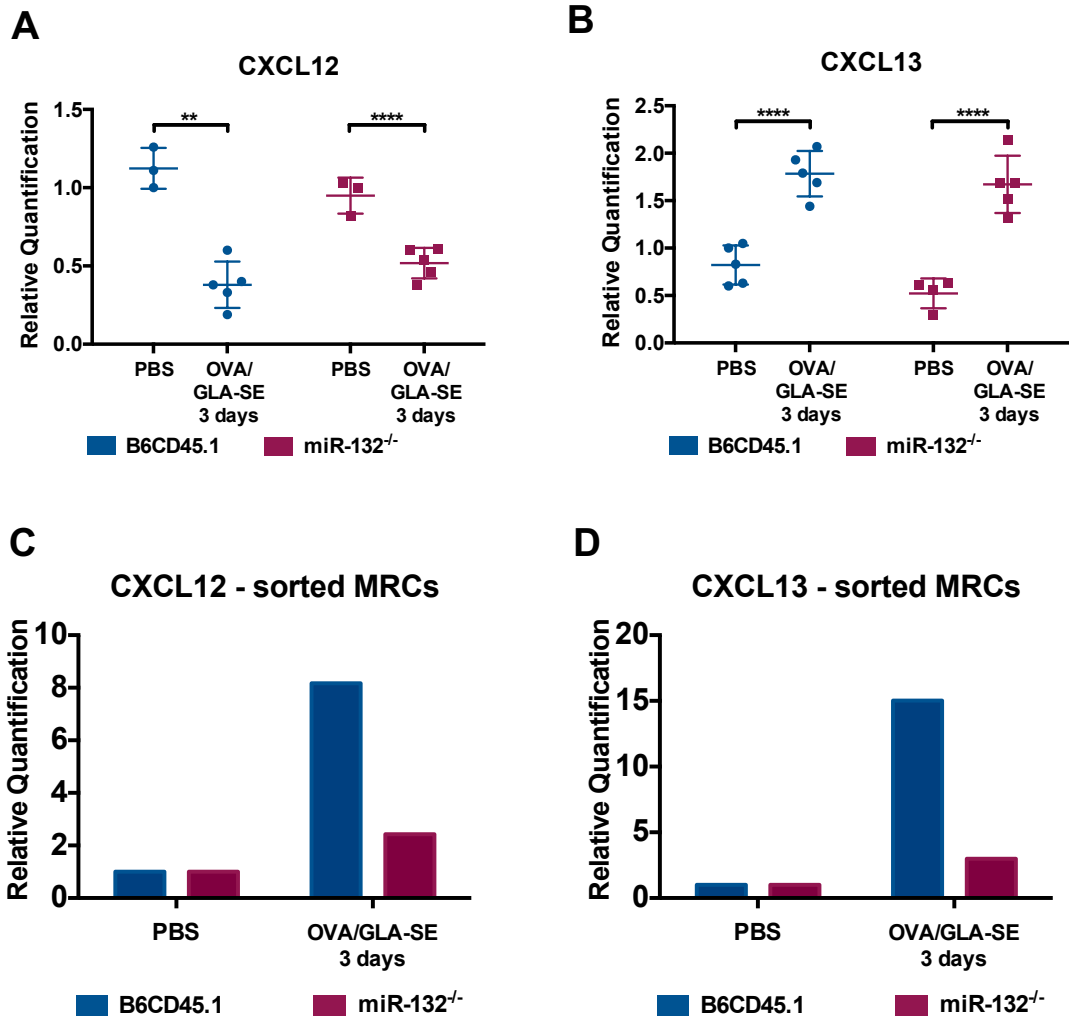


Figure 4.25: Investigating CXCL12 and CXCL13 expression in total LNs and in MRCs.

Mice were immunized with PBS, or OVA/GLA-SE for 3 days and total RNA was isolated or MRCs were sorted on the MOFLO. Cells were then lysed, total RNA was isolated, retro-transcribed into cDNA and expression was analysed by qPCR. **A-B:** **A:** CXCL13 in total LN, and **B:** CXCL12 in total LN. Expression values were then normalized to the HPRT internal standard values. Two-Way ANOVA followed by multiple comparison Tukey's test: * $P \leq 0.05$, ** $P \leq 0.01$, *** $P \leq 0.001$, **** $P \leq 0.0001$. $N=4$ or 5 . **C-D:** **C:** CXCL12 in sorted MRCs, and **D:** CXCL13 in sorted MRCs. Expression values were then normalized to the HPRT internal standard values. $N=1$.

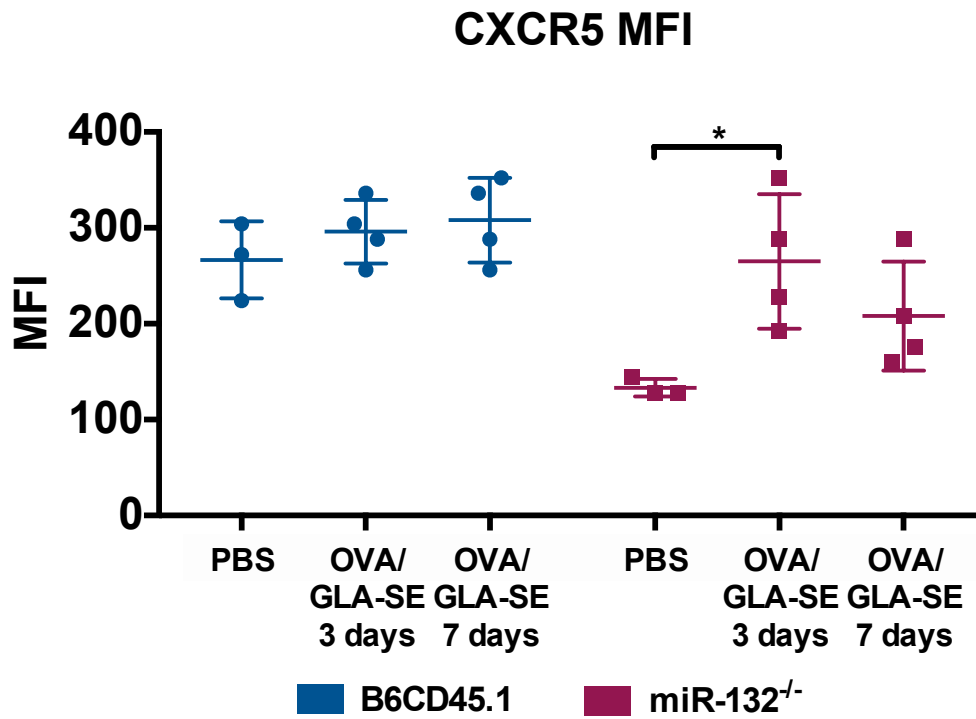


Figure 4.26: Investigating CXCR5 expression in B cells by flow cytometry. Mice were immunized with PBS, or OVA/GLA-SE for 3 or 7 days and analysed by flow cytometry. CXCR5 MFI. N=4. Two-Way ANOVA followed by multiple comparison Tukey's test: *P ≤ 0.05, **P ≤ 0.01, *** P≤0.001, ****P ≤ 0.0001.

4.10. Role of TNF α in follicle structure

B cell distribution in WT mice at three days treatment closely resembles that found in TNF α /TNFR deficiency and that found in the neonatal LN prior to B cell follicle formation. To test this hypothesis, TNF α was inhibited in mice and after three days, LNs were analysed. No changes in structure were observed in these mice (Figure 4.27A). However, these results are inconclusive as there was no control done to make sure that TNF α was efficiently inhibited in the mice during the course of treatment. TNF α expression was analysed in BMDCs post TLR4 stimulation, no difference was observed between WT and miR-132^{-/-} mice (Figure 4.27B). TNF α expression after three days of treatment with OVA/GLA-SE is identical to untreated mice (Figure 4.27C). This indicates that although TNF α production by B cell is required for initial follicle formation it is not required for the maintenance of existing B cell follicles, indicating that TNF α is involved in the differentiation of FDCs and CXCL13 up-regulation but not the maintenance of CXCL13 expression, thus TNF α is unlikely to have a key role in the observed phenotype.

4.11. Analysis of miR-132 mediated transcription

4.11.1. Dendritic cell regulation by miR-132

Bone Marrow Derived Cells (BMDCs) from WT and miR-132^{-/-} mice were cultured and treated with LPS, OVA/MPL-A+TDM or OVA/GLA-SE for 1.5hrs and RNA expression was then analysed by RT-qPCR (Figure 4.28). When treated with TLR4 agonists, MMP-9 is over-expressed in both WT and miR-132KO mice. However, this expression is lower in miR-132 deficient BMDCs. HTRA1 is a serine protease which has the potential to cleave immobilized chemokine fields, anchored to glycoproteins, that helps guide and shape DC's migration [238]. Up-regulation of HTRA1 by FRCs along with T cells and DCs is expected since this protease could be capable of modulating LN microenvironment through potential cleavage of extracellular matrix and bound chemokine that are secreted by FRCs and enable T cells and DCs to migrate. Treatment induced an up-regulation of HTRA1 in both WT and miR-132^{-/-} BMDCs. IL-22 is an inflammatory cytokine of the IL-10 family that helps initiate innate immune responses. Previous work showed that mice lacking IL-22 share a similar phenotype to miR-132 deficient mice. IL-22 Binding Protein (IL-22BP) regulates IL-22 by binding to the cytokine, this inhibits the effects of IL-22 and helps control inflammation. No

changes were observed in IL-22BP expression upon treatment.

4.11.2. Treatment effect on gene expression in total LNs

To analyse the changes in gene expression after treatment, mice were treated long-term with PBS or OVA/GLA-SE in WT or miR-132^{-/-} mice. pLNs were digested and FRCs, LECs, BECs, B cells, T cells and DCs were sorted on the MoFlo (Beckman Coulter). The differences in IL-22BP expression are not significant, but treatment induces a down-regulation of the protein, and when untreated IL-22BP is expressed at a higher level in miR-132^{-/-} mice than in WT mice. The increase in HTRA1 is significantly larger in miR-132^{-/-} mice in B cells and T cells (Figure 4.29).

4.12. Remodelling at 6 months post boost

4.12.1. LN structure 6 months post boost

To determine the dynamic remodelling process, mice were immunized (prime and boost) and LNs were analysed six months later (Figure 4.30). Immunohistochemistry analysis was done followed by quantification with Cell Profiler. Six months post immunization; LNs have not yet reverted back to the untreated state but are the same size as controls. This showed that B cell remodelling is not permanent but LNs do not revert back to their original unprimed state even after six months, indicating that aspects of the remodelling process are permanent or take longer to resorb.

4.12.2. LN structure 3 day boost post 6 months post boost

To further determine the effect of time on the remodelling process, mice were immunised (prime and boost) and six months later mice were immunised for a further three days (Figure 4.31). LNs are bigger but there is no follicle remodelling, there is no difference between WT and miR-132^{-/-} mice.

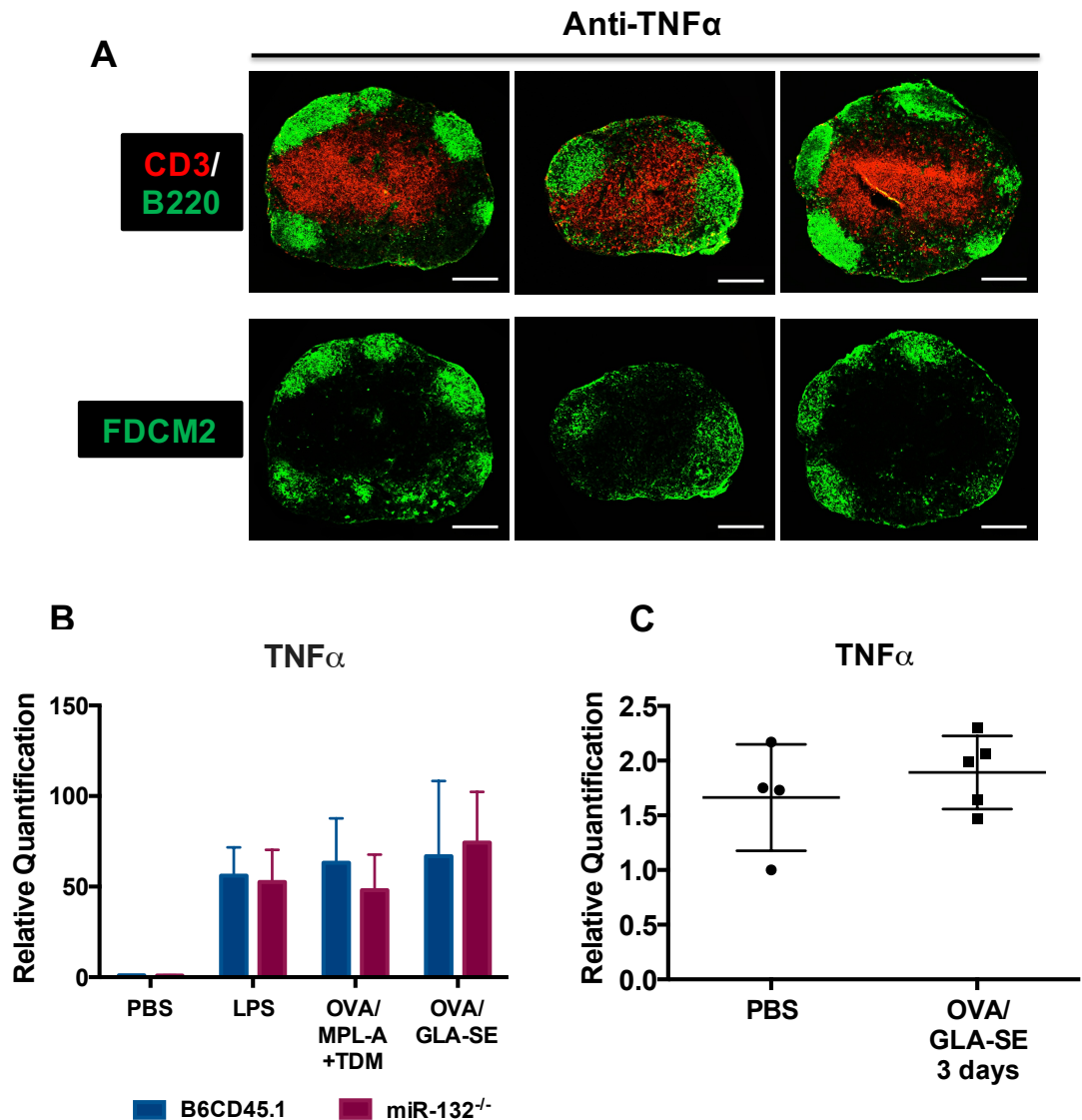


Figure 4.27: Role of TNF α in regulating the remodelling process.

A: Mice were treated with an anti-TNF α antibody for 3 days. LNs were removed and frozen sections of the popliteal LN were stained for CD3 (T cells), B220 (B cells) and FDCM2 (FDCs). Scale bar = 200 μ m, N=5, 2 slides/LN, representative image was chosen. **B:** BM was flushed from WT and miR-132^{-/-} mice and seeded in the presence of GM-CSF. After 12 days and after obtaining a pure population of BMDCs, the cells were treated for 1.5 hours with PBS as a control and with a series of TLR4 agonist adjuvants. Cells were lysed, total RNA was isolated, retro-transcribed into cDNA and TNF α expression was analysed by RT-qPCR. **C:** Effect of 3 days of OVA/GLA-SE treatment on TNF α expression. Total LN cells were isolated from mice, cells were then lysed, total RNA was isolated, retro-transcribed into cDNA and TNF α and CXCL13 expression was analysed by RT-qPCR. Expression values were then normalized to the HPRT internal standard values. Student t test: *P \leq 0.05, **P \leq 0.01, *** P \leq 0.001, ****P \leq 0.0001.

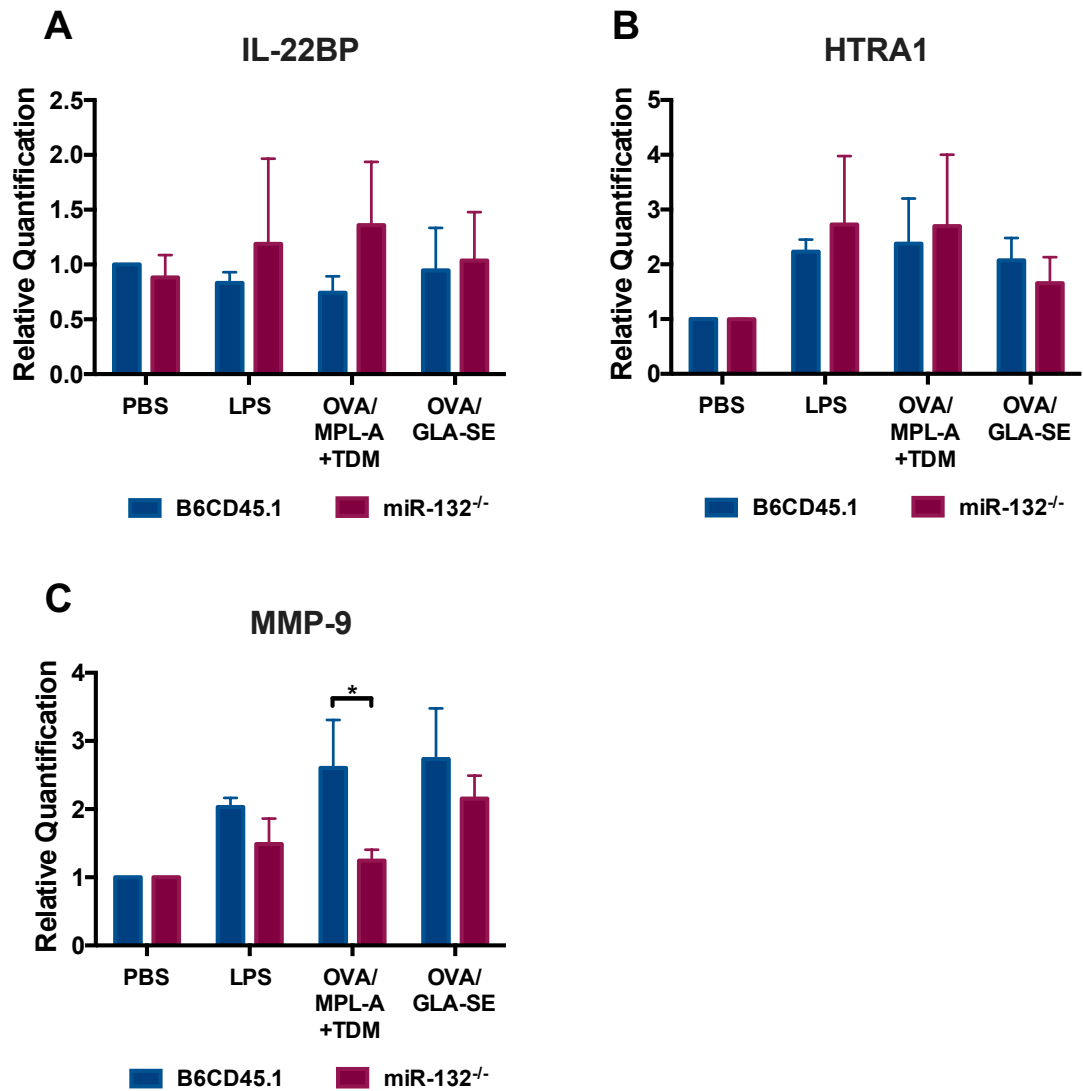


Figure 4.28: Role of miR-132 in Bone Marrow DCs response to adjuvants.

BM was flushed from WT and miR-132^{-/-} mice and seeded in the presence of GM-CSF. After 12 days and after obtaining a pure population of BMDCs, the cells were treated for 1.5 hours with PBS as a control and with a series of TLR4 agonist adjuvants. Cells were lysed, total RNA was isolated, retro-transcribed into cDNA and expression was analysed by RT-qPCR. **A:** IL22-BP **B:** HTRA1 and **C:** MMP-9. Expression values were then normalized to the HPRT internal standard values. Data is shown as relative values. Data from 3 separate experiments. One-Way ANOVA followed by multiple comparison Tukey's test: *P ≤ 0.05, **P ≤ 0.01, *** P ≤ 0.001, ****P ≤ 0.0001.

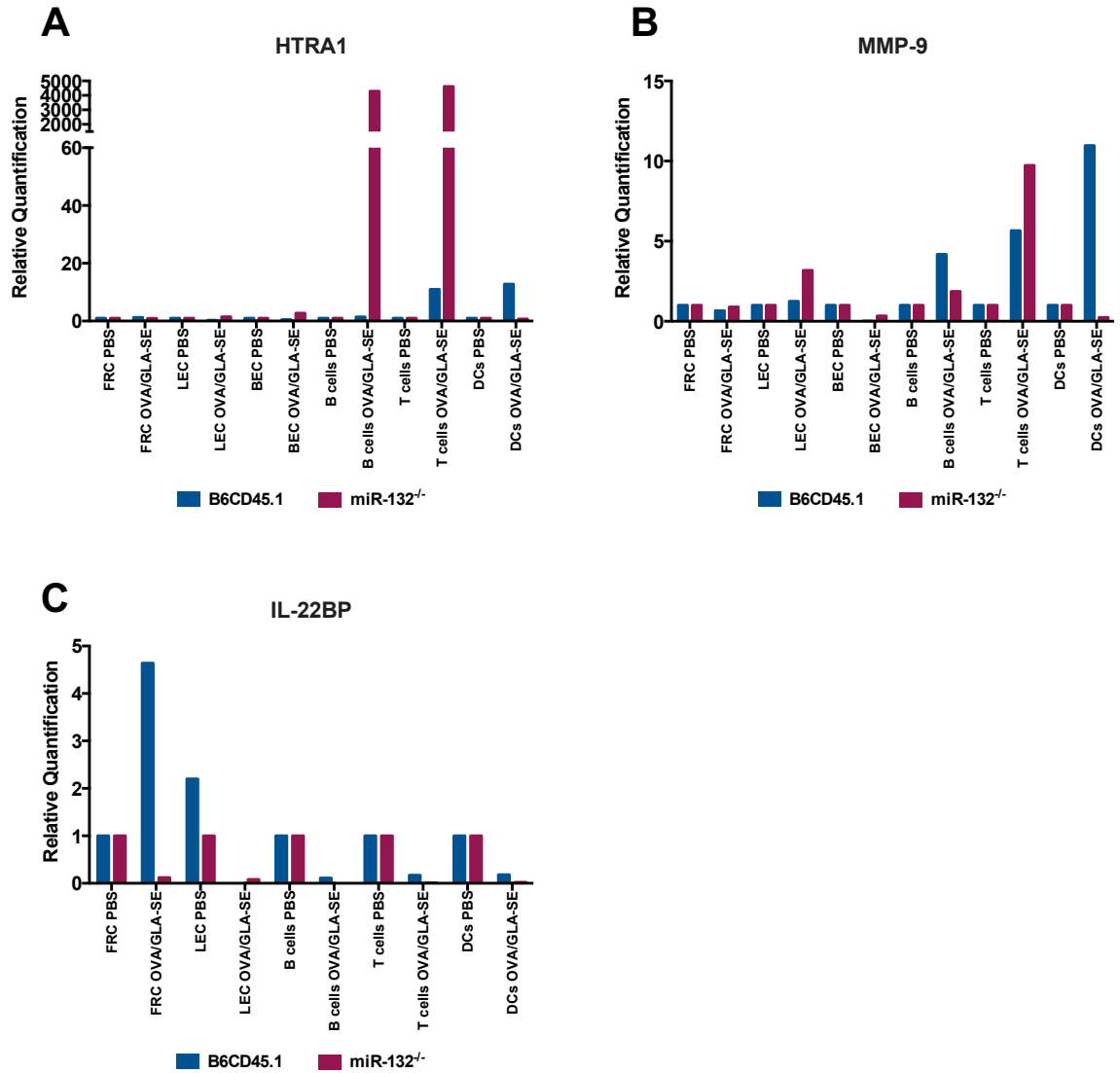


Figure 4.29: Role of miR-132 in stromal and immune cells' response to adjuvants.

Mice were immunized with PBS, or OVA/GLA-SE following the long-term model and cells were isolated from mice using the MOFLO sorter. Cells were then lysed, total RNA was isolated, retro-transcribed into cDNA and expression was analysed by RT-qPCR. N=1. **A:** HTRA1, **B:** MMP-9, and **C:** IL-22BP. Expression values were then normalized to the HPRT internal standard values.

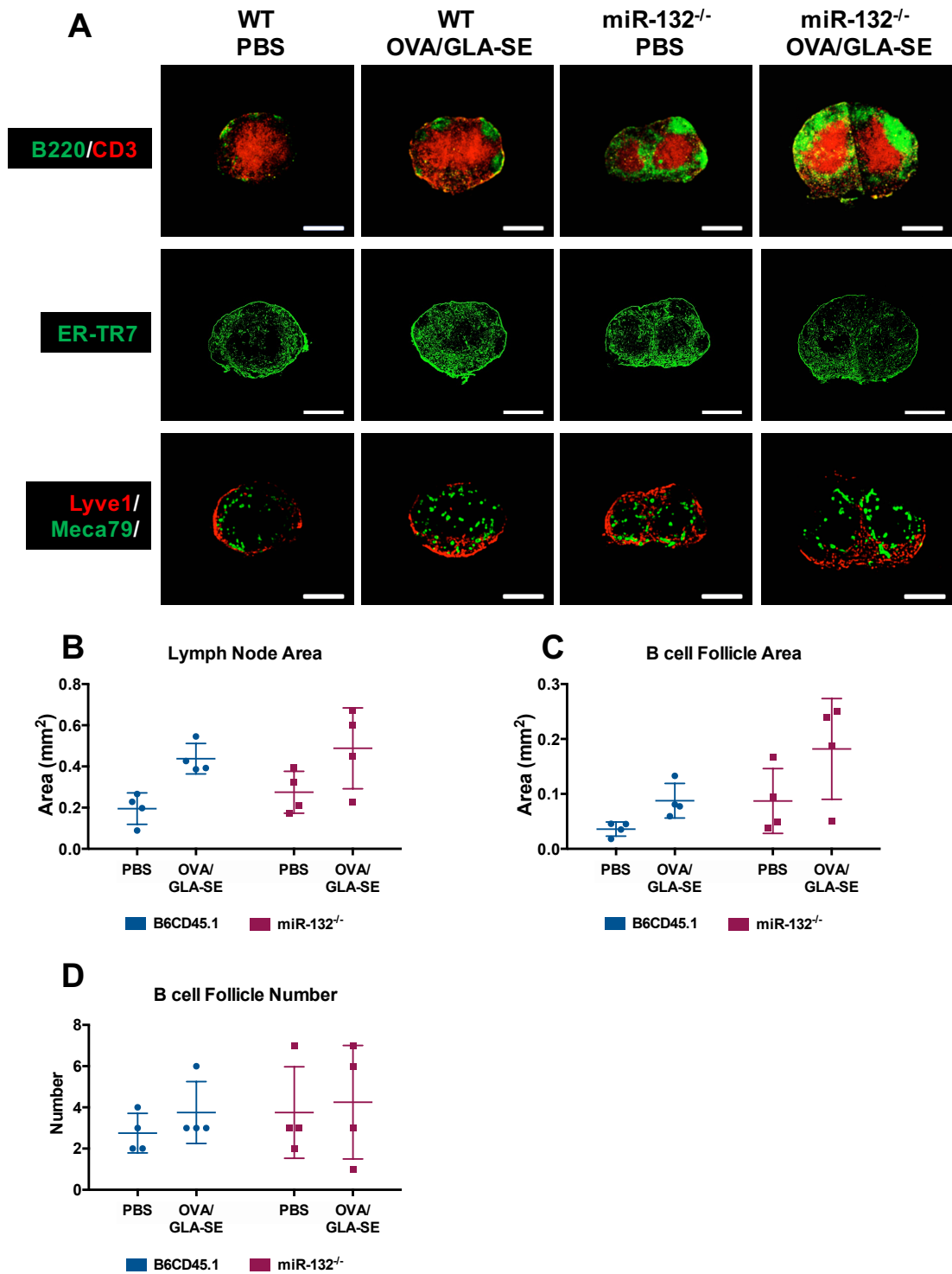


Figure 4.30: Analysis of LNs 6 months post immunization.

WT and miR-132^{-/-} mice were immunized and boosted 21 days later. After which LNs were removed 6 months later. The popliteal LNs were removed and analysed by immunohistochemistry. **A:** Frozen sections of the popliteal LN from PBS, or OVA/GLA-SE immunized mice were stained with antibodies against CD3 (T cells), B220 (B cells), ER-TR7 (Reticular network), Lyve-1 (lymphatic vessels), and Meca-79 (HEVs). Images were then quantified by Cell Profiler. **B:** Lymph Node area, **C:** Follicle Area, and **D:** Follicle number. N=4 mice, 2 slides/LN, representative image was chosen. Scale bar = 500 μ m.

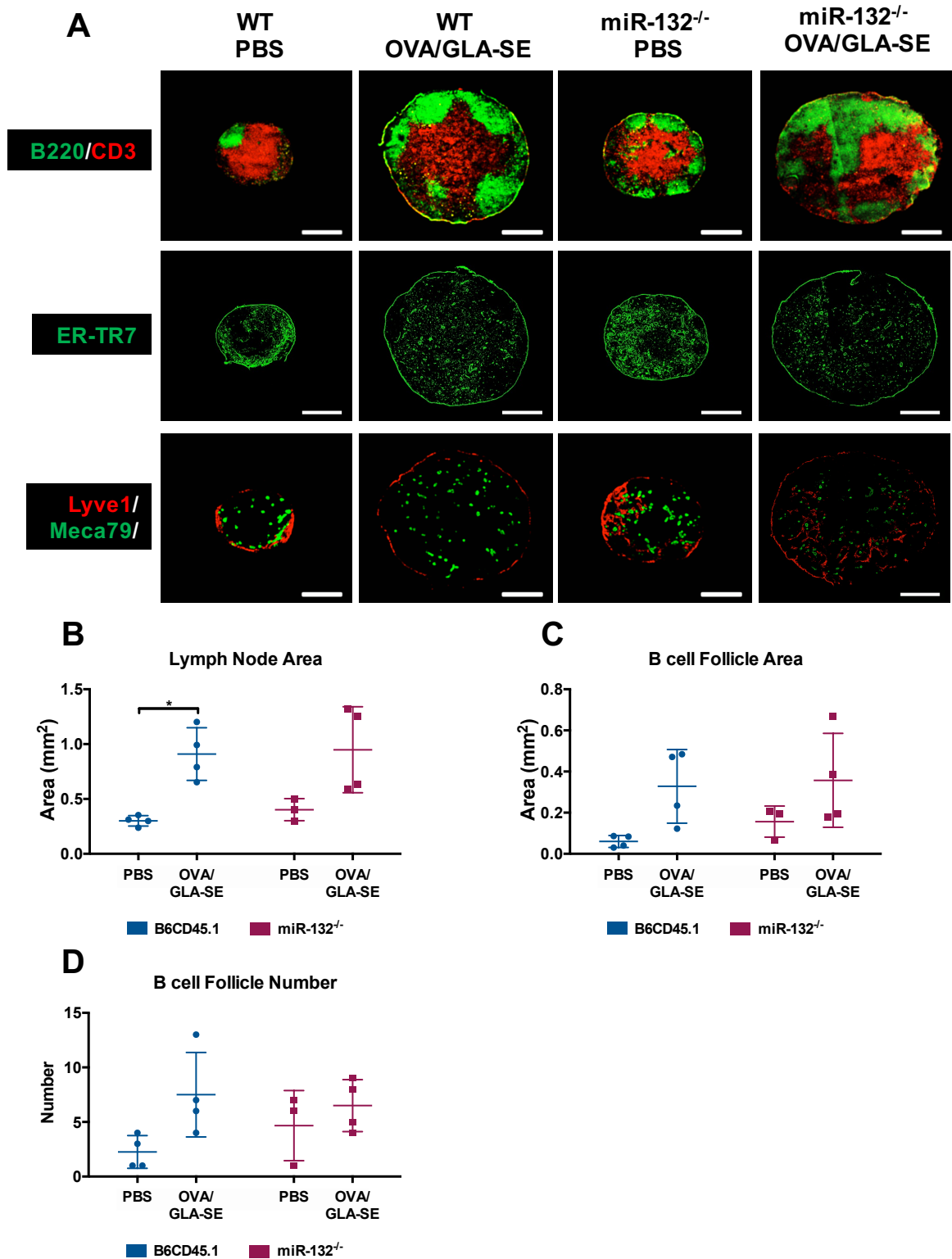


Figure 4.31: Analysis of LNs boosted for 3 days 6 months post immunization.

WT and miR-132^{-/-} mice were immunized and boosted 21 days later. After which LNs were boosted again 6 months later for a further 3 days. The popliteal LNs were removed and analysed by immunohistochemistry. **A:** Frozen sections of the popliteal LN from PBS, or OVA/GLA-SE immunized mice were stained with antibodies against CD3 (T cells), B220 (B cells), ER-TR7 (Reticular network), Lyve-1 (lymphatic vessels), and Meca-79 (HEVs). Images were then quantified by Cell Profiler. **B:** Lymph Node area, **C:** Follicle Area, and **D:** Follicle number. N=4 mice, 2 slides/LN, representative image was chosen. Scale bar = 500 μ m.

4.13. Haematopoietic and stromal contribution to remodelling

To understand the stromal and haematopoietic contribution of miR-132, reciprocal BM chimeras were set up. Irradiated miR-132^{-/-} mice reconstituted with WT BM, possess stromal cells that are miR-132 deficient but the haematopoietic cells are WT. This would enable the analysis of the stromal contribution. In contrast, irradiated WT mice were reconstituted with miR-132^{-/-} BM, which would mean that stromal cells are WT but the haematopoietic cells are deficient for miR-132. This would enable the analysis of the haematopoietic contribution. There is no difference in the increase in cellularity in either stromal cells or B and T cells upon treatment between the two different conditions (Figure 4.32).

Histology from the two reciprocal chimera experiments were done and no clear pattern came out of it. The phenotype is intermediate between WT and miR-132^{-/-} mice. The phenotype between the two chimeras is very similar whether PBS or OVA/GLA-SE treated (Figure 4.33). Images were then quantified by Cell Profiler, in both chimeras treatment induced an increase in LN size and in follicle number. Treatment induced a smaller follicle area in WT mice reconstituted with miR-132^{-/-} BM. This would mean that miR-132 is necessary in haematopoietic cells to have an increase in follicle area that we observe in miR-132^{-/-} mice. The controls for this experiment, that is WT reconstituted with WT and miR-132^{-/-} reconstituted with miR-132^{-/-} were not done. These results must therefore be considered as preliminary and the experiment repeated with the proper controls.

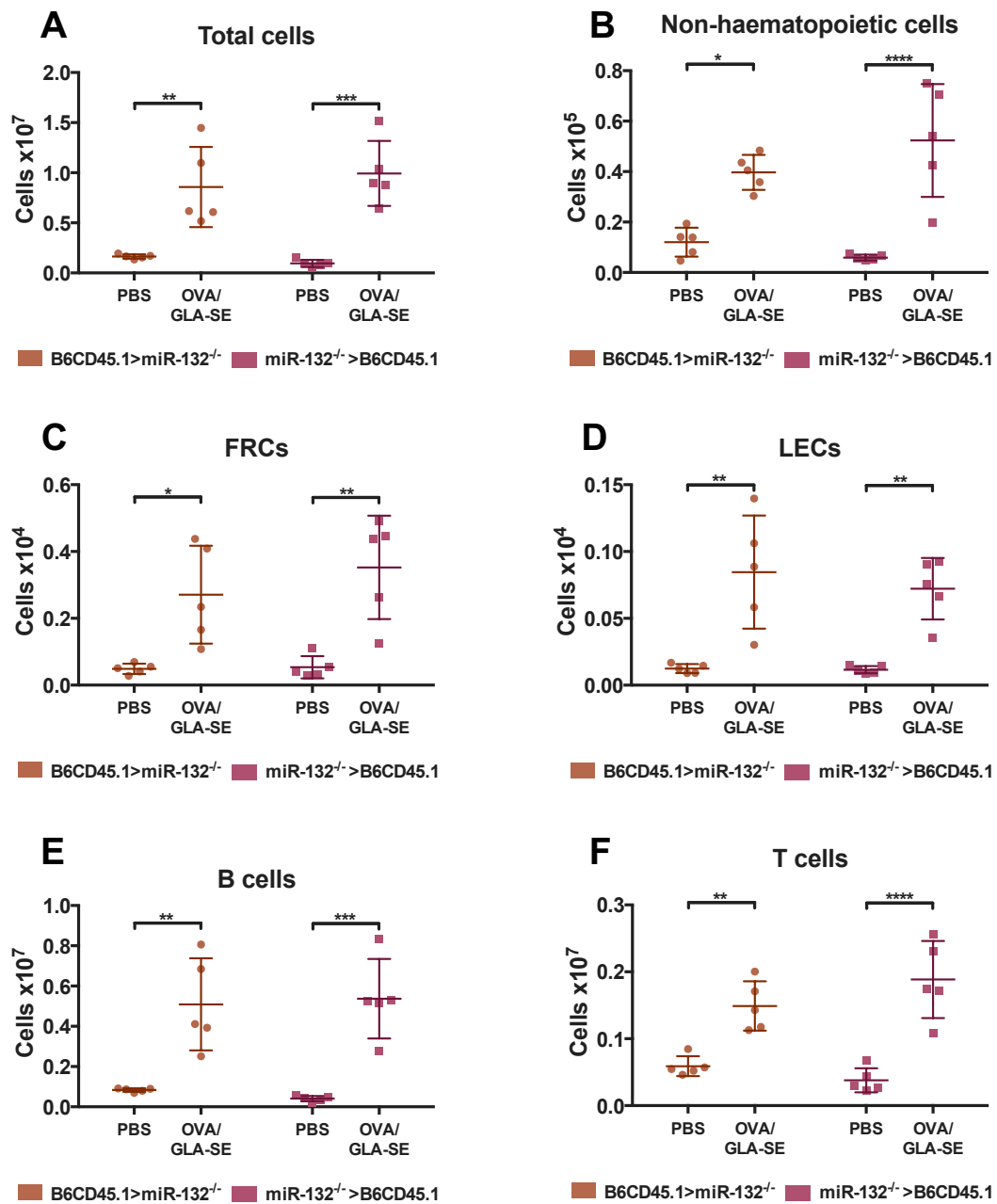


Figure 4.32: Flow cytometry on reciprocal Bone Marrow Chimeras to study the stromal vs. haematopoietic contribution of miR-132.

Mice were irradiated and then reconstituted with bone marrow. miR-132^{-/-} mice were reconstituted with WT BM and WT mice with miR-132^{-/-} BM. After 8 weeks, mice were immunized with PBS, or OVA/GLA-SE following the long-term model and the popliteal LNs were removed and analysed by flow cytometry. **A:** Total cells, **B:** Non-haematopoietic cells (CD45⁻), **C:** FRCs (CD45-CD31-gp38⁺), **D:** LECs (CD45-CD31+gp38⁺), **E:** B cells (CD19⁺), and **F:** T cells (CD3⁺). AccuCheck counting beads from Invitrogen were used to get an accurate cell count. N=5 from 2 separate experiments. Two-Way ANOVA followed by multiple comparison Tukey's test: *P ≤ 0.05, **P ≤ 0.01, *** P≤0.001, ****P ≤ 0.0001.

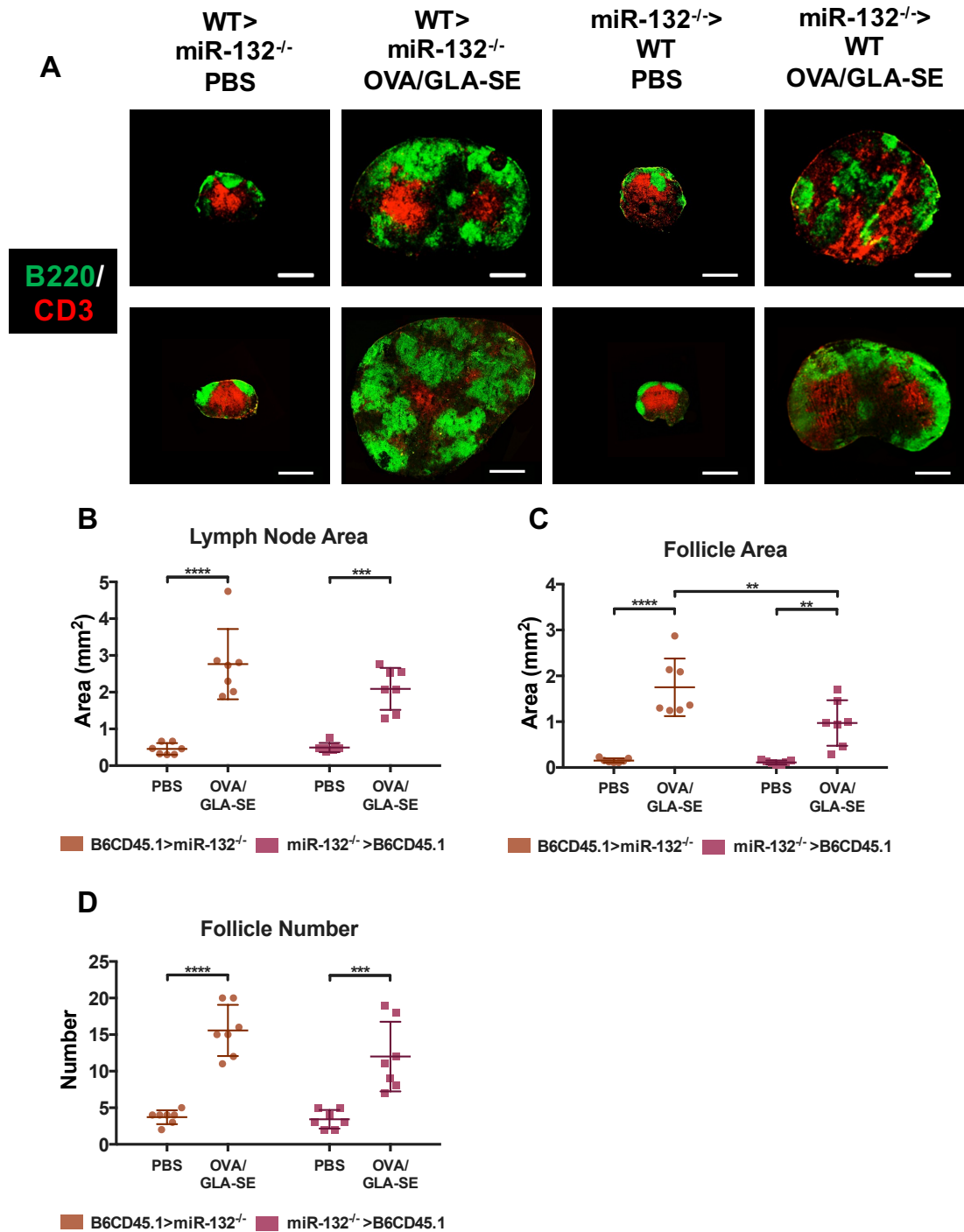


Figure 4.33: Histology on reciprocal Bone Marrow Chimeras to study the stromal vs. haematopoietic contribution of miR-132.

Mice were irradiated and then reconstituted with bone marrow. miR-132^{-/-} mice were reconstituted with WT BM and WT mice with miR-132^{-/-} BM. After 8 weeks, mice were immunized with PBS, or OVA/GLA-SE following the long-term model and the popliteal LNs were removed and analysed by immunohistochemistry. **A:** Frozen sections of the popliteal LN from PBS, or OVA+GLA-SE immunized mice were stained with antibodies against CD3 (T cells), and B220 (B cells). Images were then quantified by Cell Profiler. **B:** Lymph Node area, **C:** Follicle Area, and **D:** Follicle number. N=7 mice, 2 separate experiments, 2 slides/LN, representative image was chosen. Scale bar = 500µm.

4.14. Summary of findings

- Stromal cells respond to TLR agonists *in vitro* and *in vivo*.
- Induction of TLR4 signalling regulates cytokines and miR-132 expression.
- miR-132 deficiency leads to an altered LN structure in naïve mice but also following TLR4 adjuvant immunization. This remodelling is not dependent on blood and lymphatic vasculature.
- miR-132^{-/-} mice do not have the same remodelling kinetics as WT mice. There is no ring-like structure forming around the LN or new follicular structures appearing in the paracortex.
- Immunization of WT and miR-132^{-/-} mice showed that miR-132 does not regulate macrophage migration and localization.
- MRCs migrate upon immunization and this is modulated in miR-132^{-/-} mice.
- miR-132^{-/-} mice have a deficiency in CXCL12 and CXCL13 production which is mirrored by an up-regulation of CXCR5 in B cells.
- LN remodelling is not a TNF α -dependent process.
- The remodelling process is not permanent but LNs do not revert back to naïve resting state after 6 months.
- BM chimeras illustrated that the remodelling process is dependent both on stromal and haematopoietic cells.

4.15. Discussion

4.15.1. Stromal cells respond to TLR stimulation

Traditionally PRRs including TLRs are thought to be expressed by innate immune cells and barrier epithelium. Analysis of TLR4 mediated remodelling in Rag deficient mice in Chapter 3 indicated a key role for stromal cells in the remodelling process. The role of stromal cells in this process is still poorly understood. Data from the pre-existing gene expression database Immgen showed that FRCs, LECs and BECs express multiple TLRs, and the associated adapter molecule MyD88. *In vitro* cultured FRCs were treated with specific TLR agonists leading to the production of pro-inflammatory cytokines in response to stimulation. Treatment of FRC cultures with the TLR4 ligand LPS regulates TLR4 expression. By using FRCs from WT, TLR4^{-/-} or Myd88^{-/-}, it was possible to demonstrate that FRC stimulation is TLR mediated as response was dampened in the knockout mice. Our results obtained here demonstrate that stromal cells, namely FRCs

respond to TLR4 ligands. These results are key, as it has been believed that TLR4 signalling was critical in immune cells. Here we showed that TLR4 signalling occurs *in vitro* in FRCs further indicating that stromal cells have a key role in LN remodelling.

4.15.2. miR-132 is up-regulated in LNs upon stimulation

It has been shown that miR-132 has a key role in immune and stromal cells in regulating inflammation. miR-132 is also one of the microRNAs to have been linked to the TLR4 signalling pathway. To identify a pathway that regulates stromal cell activation, miR-132 expression was analysed. Adjuvant treatment of mice led to an increase in TNF α and IL-1 β expression, this increased expression is mirrored by the increase in miR-132. This illustrates that as there is an immune response linked to TLR4 signalling leading to production of inflammatory factors, there is also an up-regulation of miR-132. This is expected as miR-132 serves as a brake to over-inflammation by inhibiting the TLR4 signalling pathway and TLR4 induced genes. Stimulation of FRCs from WT and miR-132^{-/-} mice showed that TLR4 stimulation drives inflammatory factor production but this production is lessened in the case of IL-1 β . These results are surprising as miR-132 is expected to dampen inflammation, so absence of this microRNA would lead to a higher expression of these inflammatory molecules. This indicates that miR-132 may have a differential role in FRCs than that of inhibiting inflammation such as regulating the production of certain molecules or their ability to respond to TLR4 stimulation. A similar experiment was done with isolated B cells and their response to TLR4 stimulation. No clear difference in cytokine production was observed between WT and miR-132^{-/-} B cells. miR-132 deficiency in B cells does not alter these cells' ability to respond to TLR4 stimulation. Even though miR-132 expression is regulated in cells both *in vitro* and *in vivo* and the expression correlates with cytokine production, deficiency does not alter cytokine production. miR-132's effect on architecture was then analysed to investigate the role it might have in LN structure.

4.15.3. miR-132 deficiency leads to changes in LN structure

To determine the role of miR-132 in LN development and function, which is currently unknown, LN structure was analysed. Analysis of miR-132 deficient mice showed distinct differences to littermate controls. This might in part be due to a failure to fully down-regulate immune responses to the endogenous bacterial flora in mice. LNs from miR-132 deficient mice are increased in size, with larger B cell follicles and a less

distinct separation between B and T cell zones. This could be due to differences in B and T cell gene expression or changes to the LN microenvironment. The difference observed between miR-132 deficient mice and WT mice indicates a role for miR-132 in B cell follicle function and remodelling. miR-132 is one of the many microRNAs to have been linked to B cell maturation and function. Here we observed a clear phenotype in untreated mice. Therefore further studies were done to try and elucidate the role of miR-132 in the changes in architecture.

To investigate if miR-132 affects the LN hypertrophy and remodelling process, immune cells, both innate and adaptive, were quantified. Treatment led to increase in all cell types observed; therefore miR-132 does not alter recruitment of cells to the LN. However, there was more B cells and CD8 T cells in miR-132^{-/-} mice illustrating that miR-132 does have a role in regulating B cells during hypertrophy. How these changes alter LN remodelling was then investigated to determine if miR-132 regulates B cell follicle remodelling. Differential remodelling was observed in miR-132^{-/-} mice compared to WT mice. *In vivo* experiments showed LN expansion but a decrease in tissue remodelling. LNs from miR132^{-/-} mice were not as large upon stimulation as LNs from WT mice, but possessed larger B cell follicles restricted to the LN cortex rather than smaller ones found in the paracortex. Although miR-132 does not appear to regulate B cell response to TLR4 stimulation, it does have a role in LN remodelling and hypertrophy, as mice lacking miR-132 do not remodel as WT mice. miR-132 regulates LN remodelling. How B cell remodelling affects other stromal cell populations was then investigated. Stromal cell networks, both FRC and FDC mirror the changes in LN architecture in B and T cell zones. Vasculature remodelling is the same between both miR-132^{-/-} and WT mice illustrating that the changes in architecture observed are not dependent on changes in vasculature.

Previous work in Chapter 3 illustrated that in WT mice the key steps in the remodelling process occurred during the first 72hrs. Therefore, the kinetics of remodelling was compared between WT and miR-132^{-/-} mice. The ring-like structure that was observed in WT mice was absent in miR-132 mice. By seven days of treatment, the phenotype resembled that after a long-term treatment. WT LN had small B cell follicles in the paracortex while miR-132^{-/-} mice had big B cell follicles limited to the cortex. This illustrates that B cell follicles fail to dissociate in the absence of miR-132, which leads to bigger follicles that stay in their compartment rather than migrating into the paracortex. Absence of miR-132 does not alter inflammatory molecule production but

does alter LN architecture and leads to differential structure.

Based on the failure of B cell follicles to dissociate, the effect on stromal cell networks was investigated. There were no changes in stromal cell number increase upon treatment for short period and the stromal cell networks mirrored the B and T cell architecture and there were no changes in vasculature. The differences observed in LN architecture between WT and miR-132^{-/-} mice are not due to changes in stromal cells but appear to be in B cells from early on in the immune response.

There is a clear phenotype in miR-132^{-/-} mice. The LN remodelling process that we observed in WT mice is altered in miR-132^{-/-} mice. miR-132 appears to be regulating B cell follicle formation by having a role in the dissociation of these rigid compartments in response to immunization. How this affects the immune response to immunization still needs to be investigated.

4.15.4. Macrophage and MRC migration in miR-132^{-/-} mice

The SCS is a region of the LN that is critical in the initiation of the immune response. SSMs have been shown to migrate down towards B cell follicles during an immune response to present antigen. SSMs dynamics have a key role in regulating immune responses, thus they were analysed in the miR-132 deficient mice. SSMs were analysed by histology, to study their positioning in the LN. Treatment with OVA/GLA-SE led to there being less macrophages on the SCS and they appeared to have migrated into the LN in both WT and miR-132^{-/-} mice. Treatment with Alum led to more total macrophages and MSMs in mice deficient in miR-132. However, treatment with the TLR4 agonist, GLA-SE led to no change in macrophage numbers. miR-132 does not modulate macrophage migration or numbers upon immunization. Macrophages are important in the initiation of the immune response namely in activating B cells by presenting antigen. However the changes observed in the different LN architecture in mice lacking miR-132 is not due to changes in macrophage numbers or their localization. Another element that needs investigating is the interaction between macrophages and B cells to analyse if miR-132 could be regulating antigen presentation and interactions between these cells.

MRCs are a specialised stromal cell population that have a lineage relationship with FDCs. Therefore, the distribution and number of MRCs was quantified. miR-132 is up-regulated in MRCs upon GLA-SE treatment and after 24 days of treatment there are more MRCs in miR-132^{-/-} mice than WT mice. To further investigate this, MRCs were

analysed by histology and it was shown that in WT mice there are more MRCs upon adjuvant treatment than in untreated mice. However, in miR-132 deficient mice there appear to be more MRCs still in the SCS but also more that have entered the LN. MRCs migrate in response to adjuvants and this is modulated in miR-132 deficient mice. MRCs express CXCL13 and adhesion markers promoting B cell migration in B cell follicles and their interaction with macrophages. As there are more MRCs in mice lacking miR-132, this microRNA could modulate MRC numbers in order to alter interactions with the increased number of B cells leading to the dissolution of B cell follicles that we observed by 3 days.

4.15.5. MRC differentiation and potential mechanisms of remodelling

MRCs have been shown to be precursor cells for FDCs during an immune response [62]. MRCs differentiate into FDCs through loss of RANK-L, up-regulation of CD21/CD35 and CXCL13. The kinetics and gene expression of MRCs was therefore quantified. At three days of OVA/GLA-SE treatment in miR-132^{-/-} mice there are more MRCs, MRCs expressing CD21/35 and FDCs. CXCL12 and CXCL13 expression in total LNs were quantified. An increase in CXCL13 and a decrease in CXCL12 were observed that was the same between WT and miR-132^{-/-} mice. However, the increase in CXCL12 and CXCL13 was dampened in miR-132^{-/-} mice compared to WT mice. Deficiency in miR-132 leads to more MRCs but they express less chemokines that regulate B cell positioning. To further analyse this change, CXCR5 expression on B cells was investigated. miR-132^{-/-} mice had less CXCR5 than WT mice in untreated mice, CXCR5 expression increased upon treatment in miR-132^{-/-} mice to levels similar to that of WT mice. This shows that in miR-132^{-/-} mice there is an increase in CXCR5 that is not observed in WT mice. miR-132 plays a role in CXCR5 expression in B cells either in the expression on the surface or in the internalization and degradation process of this receptor. Absence of miR-132 leads to a deficiency in chemokine production by MRCs even though there are more MRCs. The phenotype observed of B cell dissolution could also be affected by changes in CXCR5 expression on B cells.

miR-132 has multiple targets that might also regulate the remodelling process. Thus several potential targets of miR-132 were analysed. The targets analysed showed no difference upon treatment between WT and miR-132^{-/-} BMDCs. However there was an increase in miR-132^{-/-} B and T cells of HTRA1, which might be a key regulator of chemokine gradients crucial for T cells and DCs [14, 238]. Transcriptional control of

HTRA1 appears to occur through miR-132 control, which might modulate chemokine gradients controlling the localised microenvironment.

4.15.6. TNF α is critical in B cell follicle formation but not remodelling

TNF α has been shown to be critical in B cell follicle formation in the LN anlagen. Therefore, we investigated if TNF α has a role in the remodelling process. Blocking TNF α does not induce changes in B cell follicle structure. This indicates that even though it is crucial in the development of B cell follicles it is not required for new follicle formation. Treatment of BMDCs with TLR4 led to the same increase in TNF α in WT and miR-132^{-/-} mice. Three days treatment with GLA-SE led to no changes in TNF α in total LN of WT mice. These results indicate that the remodelling process is unlikely to be driven by TNF α . However, deficiency in TNF α might alter the remodelling process. To investigate this WT mice would have to be treated with anti-TNF α during treatment with GLA-SE and LN architecture observed.

4.15.7. LN structure 6 months after immunization

To determine the stability of the remodelling process mice were treated and LN architecture was analysed six months later with or without a boost. Restimulation of WT and miR-132^{-/-} mice after 6 months for a further 3 days led to a rapid increase in LN size but no difference in the remodelling process between them. The LNs appeared to be more reactive to restimulation. LNs analysed after 6 months of immunization were small but had not returned to the naive resting state. This illustrates that changes in LN structure and remodelling are not permanent even though after 6 months LNs have not reverted back to resting state. This could mean either that LNs never go back to their naïve state or that it takes longer to go back to resting state. It is possible that for a time LNs stay in a slightly activated state ready for a secondary infection.

4.15.8. Stromal and haematopoietic contribution of miR-132

In our model miR-132 appears to be crucial in both stromal and immune cell regulation. Chimeras were set up to determine which component was necessary for the changes in phenotype observed in miR-132 deficient mice. Quantification of stromal cells and immune cells showed no difference between WT and miR-132^{-/-} mice. Imaging showed that in both types of chimeras there was an intermediate phenotype between WT and miR-132^{-/-} mice. The only change observed was that in WT mice reconstituted with miR-132^{-/-} haematopoietic cells there is a lessened follicle area. The increase in follicle

area that was observed in miR-132^{-/-} mice appears to be dependent on miR-132 expression in stromal cells. From these results it appears that the phenotype observed of LN architecture is mediated by both haematopoietic and stromal cells which is consistent with the changes observed both in MRCs and CXCR5 expression in B cells.

4.15.9. Conclusion

miR-123 has shown to be a key regulator in the LN hypertrophy and remodelling process. There is a clear difference in LN architecture between WT and miR-132^{-/-} mice illustrating that there might be an altered immune response. These changes in LN architecture upon TLR4 stimulation are dependent on miR-132 expression both in stromal and haematopoietic cells. miR-132 is crucial in LN remodelling but the mechanism behind these changes in architecture are due to various different factors and cell types that are regulated by miR-132. Through analysis of GC formation and activated B cells but also of antibody production, the functionality of these changes in architecture were investigated.

Chapter 5: Consequence of TLR4 mediated remodelling on the immune response

5.1. Introduction

5.1.1. Effect of LN hypertrophy on B cell follicles

LNs are indispensable organs for the generation of an adaptive immune response to antigen encounter in peripheral tissues. LNs are highly organized structures with distinct B and T cell zones. There are two types of stromal cells described in the cortex, FDCs and MRCs [5]. FDCs express CD21/35 and FDCM2 and are capable of displaying opsonized antigen to B cells. FDCs also secrete CXCL13 and BAFF, which are critical in the recruitment and survival of B cells, respectively [52]. CXCL13 is an important chemokine in the generation of GCs [50]. LN expansion during an immune response is due to an increase in adaptive and innate immune cells and the underlying stromal cell networks. LN remodelling serves as a scaffold for the increased entry of lymphocytes and DCs into the organ [3, 5]. In inflamed LNs, the follicles grow and start to migrate into the T cell zone. Stromal cells that are in this zone are then converted into CXCL13 expressing cells through a $LT\beta$ pathway. These cells were dubbed versatile stromal cells as they lose CXCL13 expression after resolution of inflammation and follicle withdrawal as B and T cell zones return to their original limits [74]. GCs are structures that appear in follicles during an immune response when B cells encounter antigen and are subsequently activated and then driven to proliferate. GCs likely result from the expansion and differentiation of FDCs. Activated B cells drive the formation of the light zone and proliferating B cells drive dark zone formation, in addition to attracting more naïve B cells, thus increasing chances of a cell being capable of recognizing antigen.

5.1.2. GC formation

GCs are composed of a light zone that is orientated to antigen entry points close to the SCS and a dark zone that is close to the T cell zone [239]. The dark zone contains a multitude of large proliferating B cells with low expression of surface immunoglobulin called centroblasts. Due to the presence of FDCs the light zone contains less B cells that express surface immunoglobulin called centrocytes [240]. B cells in GCs have similar migration patterns as naïve B cells but possess dendrite like structures enabling them to probe for antigen with a greater surface [241, 242]. In GCs, B cells go through clonal

expansion, class switch recombination, somatic hypermutation, and affinity maturation [49]. These GC structures are critical in the production of B cell effector and memory cells. The classic GC model is that B cells in the dark zone undergo quick cellular division, class switch recombination, and somatic hypermutation. B cells then migrate into the light zone where with the help of T_{FH} cells they go through antigen selection [240]. Since this model was developed, studies using *in vivo* tracking of B cells have shown that B cells migrate dynamically in both directions between the light zone and the dark zone [33, 241, 242]. Somatic hypermutation is the process of random point mutations appearing in the V regions of the immunoglobulin genes of B cells. Class switching is the process whereby the type of immunoglobulin converts through recombinations in the constant region of the antibody heavy chain while the variable region stays the same. This process doesn't affect the affinity of antibodies but leads to changes the functional properties of immunoglobulin [243]. AICDA encodes for a DNA-editing deaminase (AID) involved in somatic hypermutation and class-switching of immunoglobulin genes [244, 245]. AICDA expression gives an idea of antibody specificity. B cells undergo cellular proliferation and antigen selection in both these zones. Upon antigen encounter, B cells up-regulate CCR7 expression enabling the migration to the T cell zone boundary following CCL19 and CCL21 gradients. In this zone, B cells interact with CD4 T_H cells [246]. B cells entering the follicle seed the GC reaction and rapidly divide forming the two zones. In the dark zone, B cells express the chemokine receptor CXCR4 and migrate to this area through CXCL12 signalling by stromal cells. CXCR4 down-regulation in dark zone B cells leads to migration towards the light zone following the CXCL13 gradient binding to CXCR5 on B cells [74, 247]. After class switch recombination, and somatic hypermutation, B cells are selected for antigen reactivity [248]. B cells are selected for antigen recognition by the BCR and also T_{FH} presentation in the light zone.

T_{FH} cells are characterised as being CXCR5 high enabling them to migrate to the T cell zone/B cell follicle border following CXCL13 gradients [249]. T_{FH} differentiation happens after T cell and DC interactions with the production of IL-6, IL-12 and the co-stimulatory molecule inducible co-stimulator (ICOS). These signals are indispensable for the transcription of B-cell lymphoma 6 (Bcl6), which is critical for the differentiation into T_{FH} cells [250, 251]. Transcription factor achaete-scute complex homolog 2 (Ascl-1) expression induces expression of CXCR5 on T_{FH} cells. Full differentiation into GC T_{FH} cells is mediated by interaction of precursor T_{FH} cells with B

cells mediated by ligation of CD84 and Ly108 and supported by SLAM-Associated Protein (SAP), an intracellular adaptor molecule [252]. GC B cells compete for interaction with T_{FH} cells. T_{FH} cells in turn provide survival and differentiation signals to high affinity B cells through CD40/CD40L interaction and production of cytokines such as IL-21 and IL-4 [253]. B cells pick up antigen presented by FDCs on their mutated BCR and present it in turn to MHCII found on T_{FH} cells. Only high affinity B cells are able to interact with T_{FH} cells leading to high affinity plasma cells and memory cells [254]. B cells that do not obtain a signal through their BCR and through CD40 undergo apoptosis [33].

T_{FR} cells are also found in GCs. These cells are very similar to T_{FH} cells but do not express molecules to help B cells such as IL-21 and CD40 ligand. T_{FR} cells appear during an immune response and the peak numbers are between days 11 and 17, compared to 7 and 11 for T_{FH} cells. Studies suggest that T_{FR} cells limit the size of germinal centres [255]. Figure 5.1 illustrates the germinal centre reaction [256].

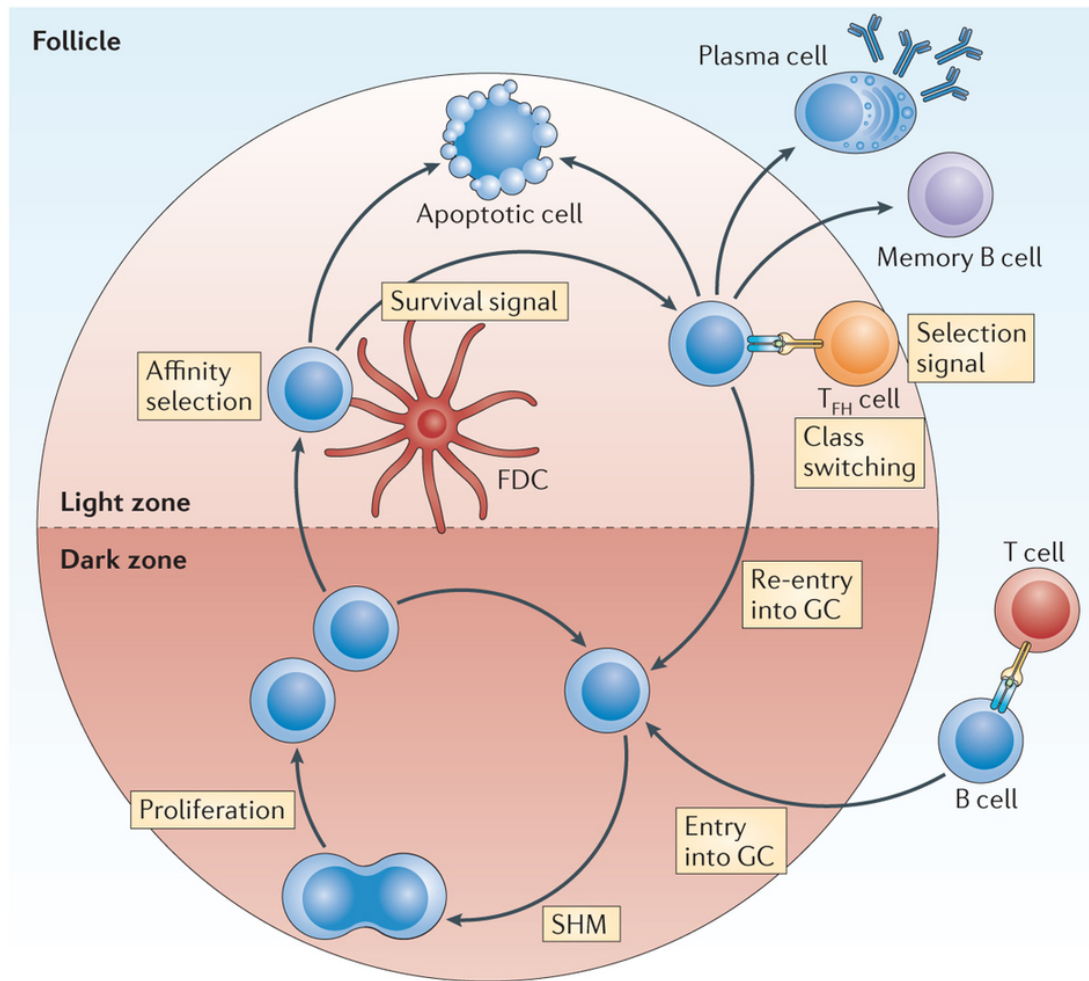


Figure 5.1: The Germinal Centre reaction.

Representation of B cell maturation in germinal centres. At the border between follicle and T cell zone, B cells receive stimulatory signals by presenting antigen to T helper cells. Cells then enter the dark zone where they undergo somatic hypermutation and cell proliferation. Cells then migrate into the light zone where the mutated BCR is selected by exposure to antigen by FDCs. If there is high affinity, B cells receive survival signals and receive further signals from T_{FH} cells and go through class switching. B cells then either re-enter the dark zone, exit as memory cells or as plasma cells. Adapted from Heesters, B.A. et al., *Nature Reviews Immunology*, 2014.

5.1.3. Plasma cells and antibody production

A population of differentiated B cells called plasma cells produces antibodies [257]. There are two types of antibody producing cells, plasmablasts that are short lived and produce low affinity antibodies and plasma cells that are produced from T-cell dependent GC reactions that can produce high affinity antibodies for weeks. Plasmablasts can be found three days after the start of the immune response, whereas plasma cells appear later at about six days [258]. Plasma cells are distinguished by expression of syndecan-1 on their surface and a rough endoplasmic reticulum [259]. Plasma cells differentiate through the transcriptional repressor Blimp-1, which inhibits most B cell pathways, and the GC specific genes AICDA and Bcl6. The transcription factor XBP1 is essential in the survival of plasma cells from the stress put on the endoplasmic reticulum due to high antibody production [257, 260]. The medulla is the part of the LN that contains the least immune cells in resting conditions. However, during an immune response, the medulla is colonized by the plasma cells generated. During an immune response, LN medulla is remodelled in a B-cell and $LT\beta R$ dependent way [86]. This migration from the GCs to the medulla is chemokine dependent, namely CXCL12 that binds to CXCR4 on plasma cells [261]. Plasma cells there produce antigen specific antibodies that are sent into the circulation in large quantities helping to clear the pathogen [262, 263]. It is suggested that cells in the medulla, either myeloid or stromal, under inflammatory conditions, produce IL-6 and A Proliferation-Inducing Ligand (APRIL) that promote plasma cell recruitment and survival [264]. This plasma niche is created upon inflammatory conditions in the medulla following LN expansion. Egress from the medulla of long-lived plasma cells is critical for their survival and is dependent on S1P expression [21, 265].

Antibodies are fundamental components of the adaptive immune system, they protect against infection through binding of pathogens participating in their inactivation. This binding also recruits different immune cells and the complement [266]. Antibodies can either be produced as cell-surface bound or secreted. Antibodies possess a Y structure with two identical binding sites at the arms of the structure. They are composed of a light chain and a heavy chain held together by non-covalent and covalent bonds. In the mammalian immune system, there are 5 classes of antibodies, IgA, IgD, IgE, IgG and IgM that have their own type of heavy chain. The class of antibody produced is determined by class switching that occurs in the GC. IgM is the first type of antibody made by immature B cells; mature B cells possess both IgM and IgD. IgG is the major

type of antibody found in the blood. IgA is the most common antibody found in secretions such as saliva and respiratory and intestinal secretions as well as mucosal surfaces. IgE is critical for the secretion of histamine by eosinophils [267-269].

5.1.4. Summary

GCs are key structures required for the clearance of pathogens by the adaptive immune system. GCs develop during an immune response and lead to the production of high affinity memory B cells and plasma cells. This is done through migration between the light zone and the dark zone where the B cells undergo proliferation, class-switching and somatic hypermutation. B cells recognize antigen on FDCs and present it to T_{FH} cells, triggering their differentiation into high affinity effector cells. Plasma cells then migrate to the medulla in a CXCL12-dependent way. There they produce antibodies and secrete them into circulation. Cell egress from there happens where they enter the circulation or go to the bone marrow following S1P gradients. Antibody production is one of the key ways used here to measure the effect of LN structure changes on the immune response, namely the measure of T_H1 versus T_H2 antibodies.

We hypothesize that since miR-132 deficiency during TLR4 agonist adjuvant immunization results in changes in cell numbers and in LN structure, the phenotype observed leads to functional changes. These functional changes in the adjuvant efficacy were measured by analysing key cell types in GC development and antibody production and affinity.

5.1.5. Aims

- Determine the effect of miR-132 deficiency on GC formation and the associated cell types.
- Investigate effect of miR-132 deficiency in antibody production both at long-term treatments and short term.
- Investigate the effect of miR-132 in haematopoietic or stromal cells on antibody production.

5.2. Adjuvant effect on AICDA expression in total LNs

Treatment with OVA/GLA-SE leads to an increase in AICDA in both mouse strains. This over-expression is significantly greater in miR-132^{-/-} mice, potentially driving higher affinity immune responses and promoting the class switching of antibodies during the response (Figure 5.2).

5.3. Immune cell analysis

Follicular and activated B cells were quantified by flow cytometry at day 24 (Figure 5.3). Treatment induces a significant increase in both WT and miR-132^{-/-} mice compared to the PBS control. There is a significant difference in the total number of B cells, follicular B cells and activated B cells in the miR-132^{-/-} mice.

B cells, T_{FR} cells and T_{FH} cells were analysed by flow cytometry at three days and seven days post treatment (Figure 5.4). Treatment with OVA/GLA-SE led to a significant increase in B cells in miR-132^{-/-} mice at seven days compared to WT mice. Treatment led to the same increase in T_{FR} cells in both WT and miR-132^{-/-} mice. However, there were significantly more T_{FH} cells in miR-132^{-/-} mice which is interesting as they are critical for the creation and maintenance of GCs [29]. This is even more noteworthy as immunohistochemistry results indicate that germinal centres are formed by seven days post immunization in miR-132 deficient mice but are absent in WT mice (Figure 5.5).

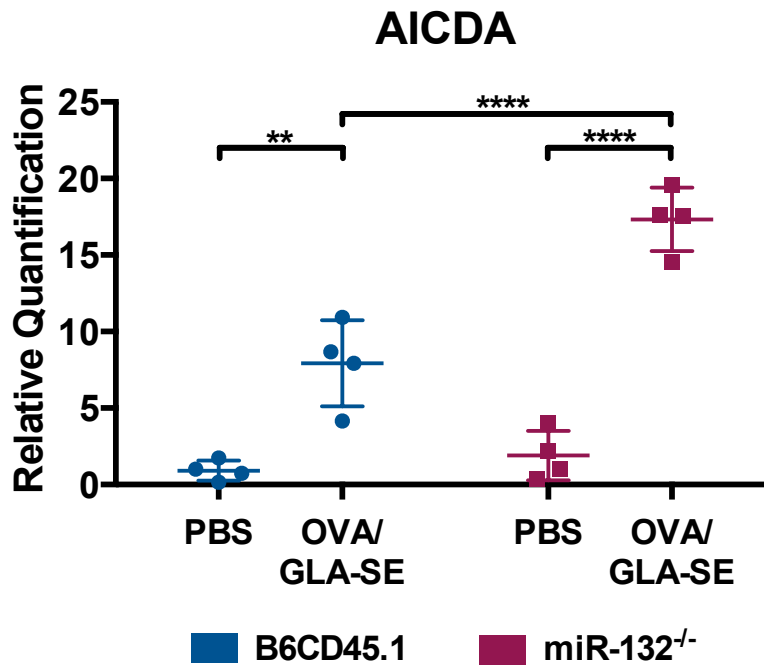


Figure 5.2: Effect of TLR4-agonist adjuvant on AICDA expression in WT and miR-132^{-/-} mice.

Thirty 10 μ m sections were taken from LN imaged earlier from the long-term treatment study after taking care to remove as much OCT as possible. Total RNA was then isolated from the sections, retro-transcribed into cDNA and AICDA expression was analysed by qPCR. Expression values were then normalized to the HPRT internal standard values. Data is shown as relative values. N=4. Two-Way ANOVA followed by multiple comparison Tukey's test: *P \leq 0.05, **P \leq 0.01, *** P \leq 0.001, ****P \leq 0.0001.

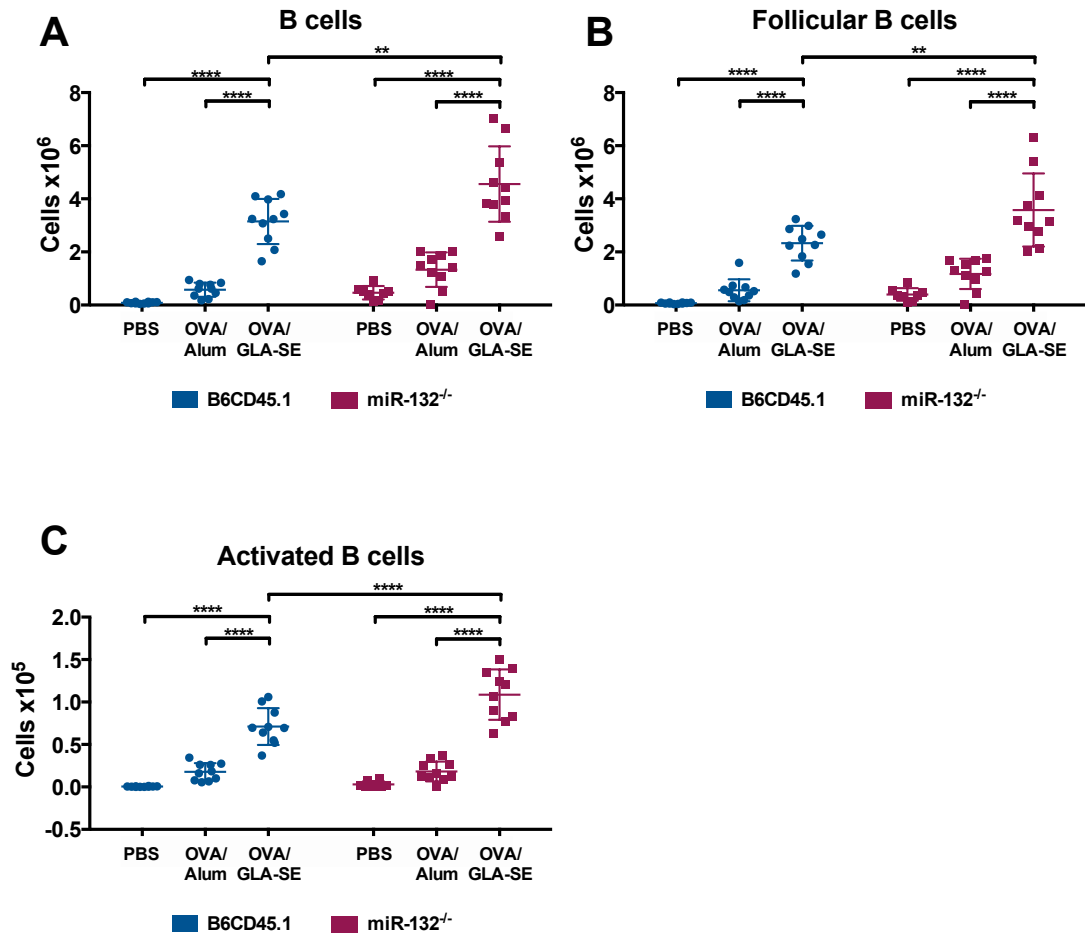


Figure 5.3: Effect of adjuvants on B cell populations in WT and miR-132^{-/-} mice at day 24.

Mice were immunized with PBS, OVA/Alum or OVA/GLA-SE and the popliteal LNs were removed and analysed by flow cytometry. **A:** B cells (CD19+), **B:** Follicular B cells (CD19+IgD+CD95-), and **C:** Activated B cells (CD19+IgD-CD95+GL7+). AccuCheck counting beads from Invitrogen were used to get an accurate cell count. N=10. 2 separate experiments. Two-Way ANOVA followed by multiple comparison Tukey's test: *P ≤ 0.05, **P ≤ 0.01, *** P≤0.001, ****P ≤ 0.0001.

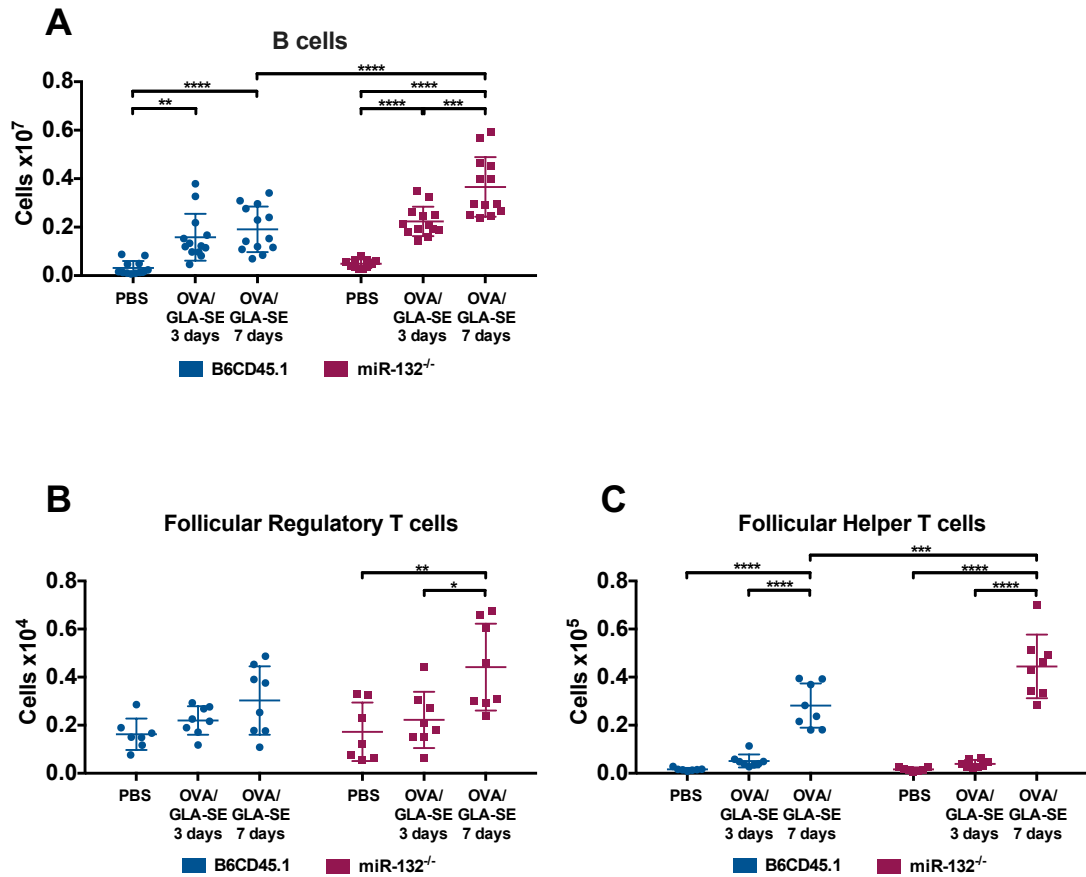


Figure 5.4: Effect of adjuvants on cell populations in WT and miR-132^{-/-} mice at days 3 and 7.

Mice were immunized with PBS, or OVA/GLA-SE for 3 or 7 days and the popliteal LNs were removed and analysed by flow cytometry. **A:** B cells (CD19+), **B:** Follicular Regulatory T Cells (CD4+PD1+CXCR5+ Foxp3+CD44+), and **C:** Follicular Helper T Cells (CD4+PD1+CXCR5+Foxp3-CD44+). AccuCheck counting beads from Invitrogen were used to get an accurate cell count. N=10 or N=15 from 3 separate experiments. Two-Way ANOVA followed by multiple comparison Tukey's test: *P ≤ 0.05, **P ≤ 0.01, *** P≤0.001, ****P ≤ 0.0001.

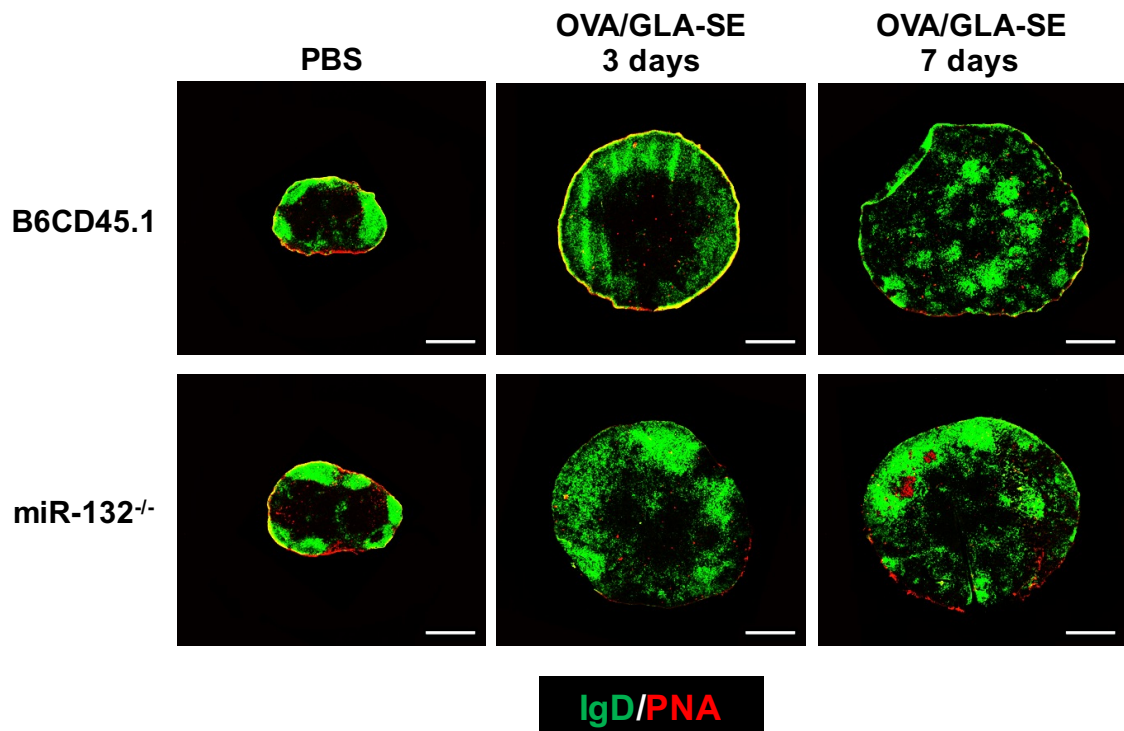


Figure 5.5: Germinal centre formation post immunization in WT and miR-132^{-/-} mice.

Immunizations with OVA in combination with GLA-SE in WT or miR-132^{-/-} mice for 3 or 7 days. Frozen sections of the popliteal LN from PBS, or OVA/GLA-SE immunized mice were stained with antibodies against IgD (naïve B cells) and PNA (GCs). N=5 mice, from 3 separate experiments. Representative image was chosen. Scale bar = 500 μ m.

5.4. OVA specific antibody production

5.4.1. Antibody titration at day 24

Adjuvants are used in order to induce high titre, high affinity antibody responses. Therefore, antibody production was compared between WT and miR-132 deficient mice when primed and boosted with either OVA/Alum or OVA/GLA-SE. Antibody titration and avidity was determined (Figure 5.6). These results indicate a profound role for both TLR4 agonists and miR-132 in regulating the type and avidity of the response. In comparison to Alum, GLA-SE produces both a strong IgG2c (T_H1) response and higher avidity response in both WT and miR-132^{-/-} mice. miR-132 deficiency leads to a loss in IgG1 (T_H2) and a corresponding polarization to an IgG2c (T_H1) response. Despite the LN remodelling that occurred in Alum treated miR-132^{-/-} mice, a near total inhibition of IgG1 antibody response occurred. To further pursue these results, different antibodies were analysed in the serum, IgA and IgE. There was no difference in these immunoglobulins between WT and miR-132^{-/-} mice upon treatment either with OVA/Alum or OVA/GLA-SE.

5.4.2. Rapid antibody production post treatment

Antibody production was compared between WT and miR-132^{-/-} mice when primed with OVA/GLA-SE for three or seven days. Antibody titration was determined (Figure 5.7). In miR-132^{-/-} mice at seven days there are significantly more specific IgG, IgG1 and IgG2c antibodies than in WT mice. This correlates with the fact that there were GCs at seven days in miR-132^{-/-} mice as shown in the PNA staining in Figure 5.4 and an increased number of T_{FH} cells. Inhibiting miR-132 could be a novel way of getting specific B cells.

5.4.3. Antibodies at 6 months, 3 days post boost

To further understand the immune response dynamics, mice were primed and six months after boosted for three days and the OVA-specific antibodies were analysed (Figure 5.8). Due to the memory response, a quick production of OVA-specific antibodies was expected. Treatment led to an increase in total IgG in both WT and significantly in miR-132^{-/-} mice. There is significantly less IgG1 in miR-132^{-/-} mice post treatment compared to WT mice but there is no difference in the increase in IgG2c.

5.4.4. Antibody production in chimeras

Irradiated miR-132^{-/-} mice reconstituted with WT BM, possess stromal cells that are miR-132 deficient but the haematopoietic cells are WT. This would enable the analysis of the stromal contribution. In contrast, irradiated WT mice were reconstituted with miR-132^{-/-} BM, which would mean that stromal cells are WT but the haematopoietic cells are deficient for miR-132. This would enable the analysis of the haematopoietic contribution. To further determine the immune response, antibody titres were determined (Figure 5.9). There is no difference in antibody titres between the chimeras upon treatment, consistent with what was observed in the structural analysis of the LNs (Chapter 4).

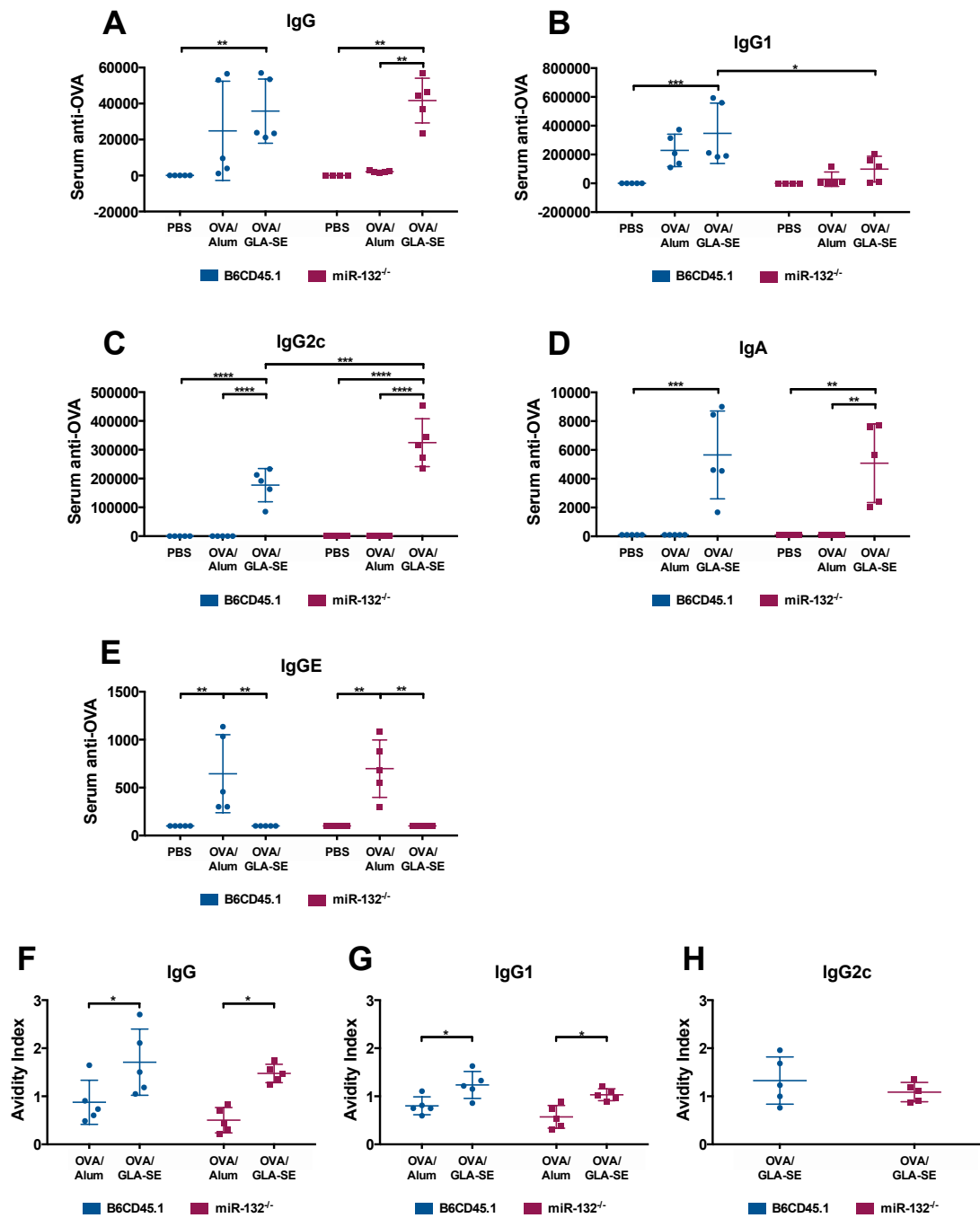


Figure 5.6: Antibody titration and avidity in WT and miR-132^{-/-} mice.

Mice were immunized with PBS, OVA/Alum, or OVA/GLA-SE and the serum was analysed for OVA-specific antibodies. **A-E**: IgG, IgG1, IgG2c, IgA and IgE antibody titration, and **F-H**: IgG, IgG1 and IgG2c antibody avidity. N=5. Representative graphs from 2 separate experiments. Two-Way ANOVA followed by multiple comparison Tukey's test: *P ≤ 0.05, **P ≤ 0.01, *** P≤0.001, ****P ≤ 0.0001.

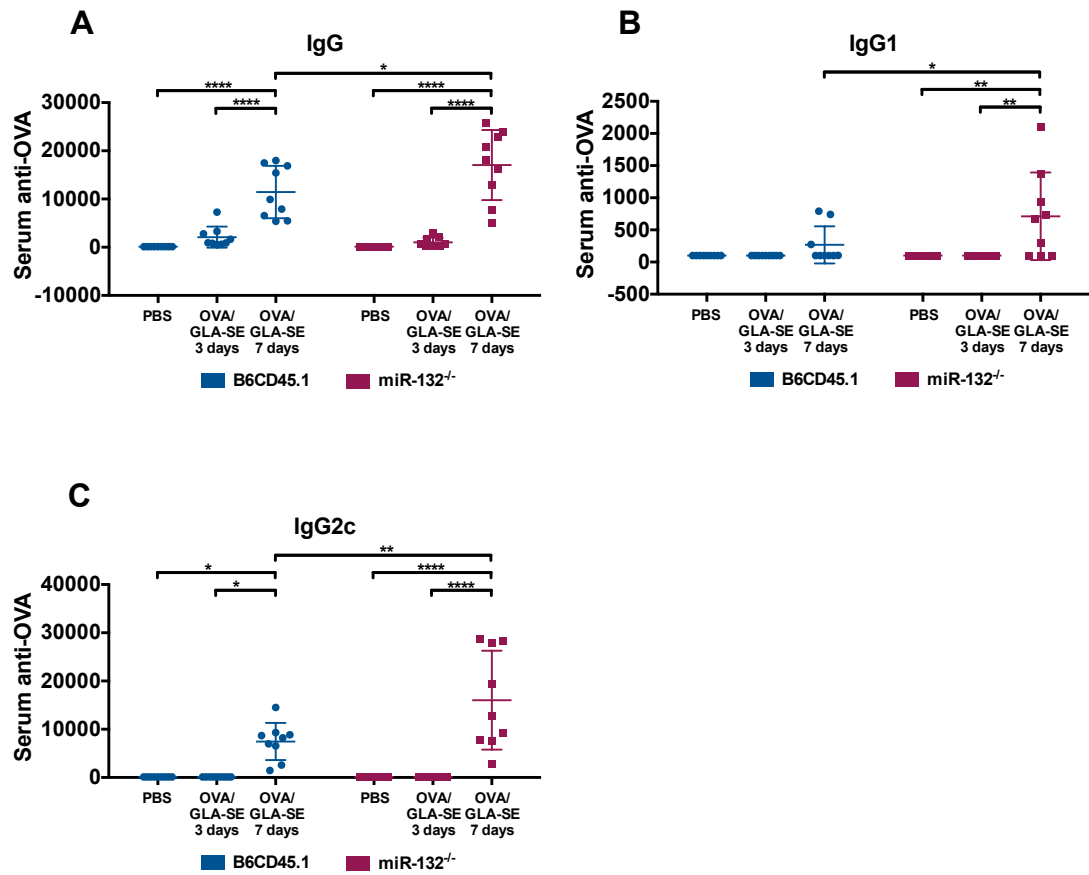


Figure 5.7: Antibody production in WT and miR-132^{-/-} mice after 3 or 7 days of OVA/GLA-SE treatment.

Mice were immunized with PBS, or OVA/GLA-SE and the serum was analysed for OVA-specific antibodies. **A:** IgG, **B:** IgG1, and **C:** IgG2c antibody titration. N=9 from 2 separate experiments. Two-Way ANOVA followed by multiple comparison Tukey's test: * $P \leq 0.05$, ** $P \leq 0.01$, *** $P \leq 0.001$, **** $P \leq 0.0001$.

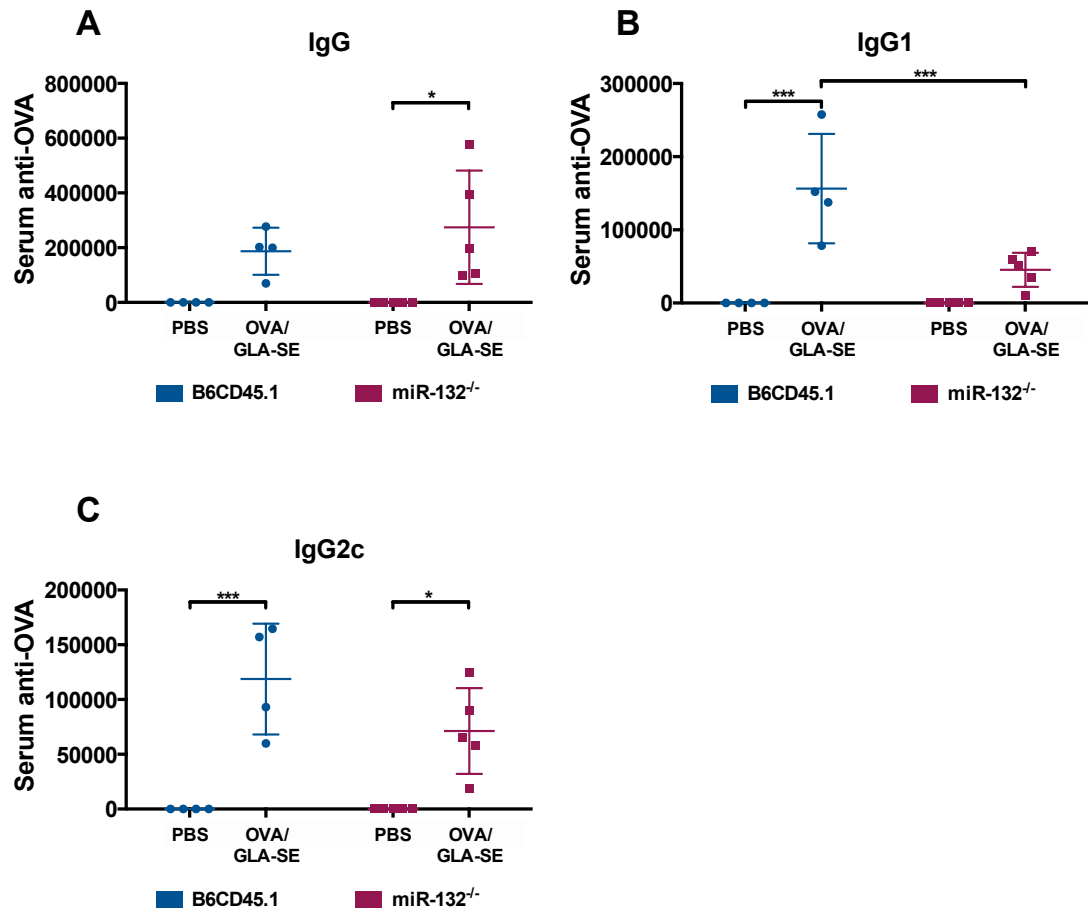


Figure 5.8: Antibody production in 6 month prime and boost mice.

Mice were injected with PBS or OVA/GLA-SE for 3 weeks then boosted and left for 6 months after which the mice were boosted again for a further 3 days. The serum was analysed for OVA-specific antibodies. **A:** IgG, **B:** IgG1, and **C:** IgG2c antibody titration. N=5. Two-Way ANOVA followed by multiple comparison Tukey's test: * $P \leq 0.05$, ** $P \leq 0.01$, *** $P \leq 0.001$, **** $P \leq 0.0001$.

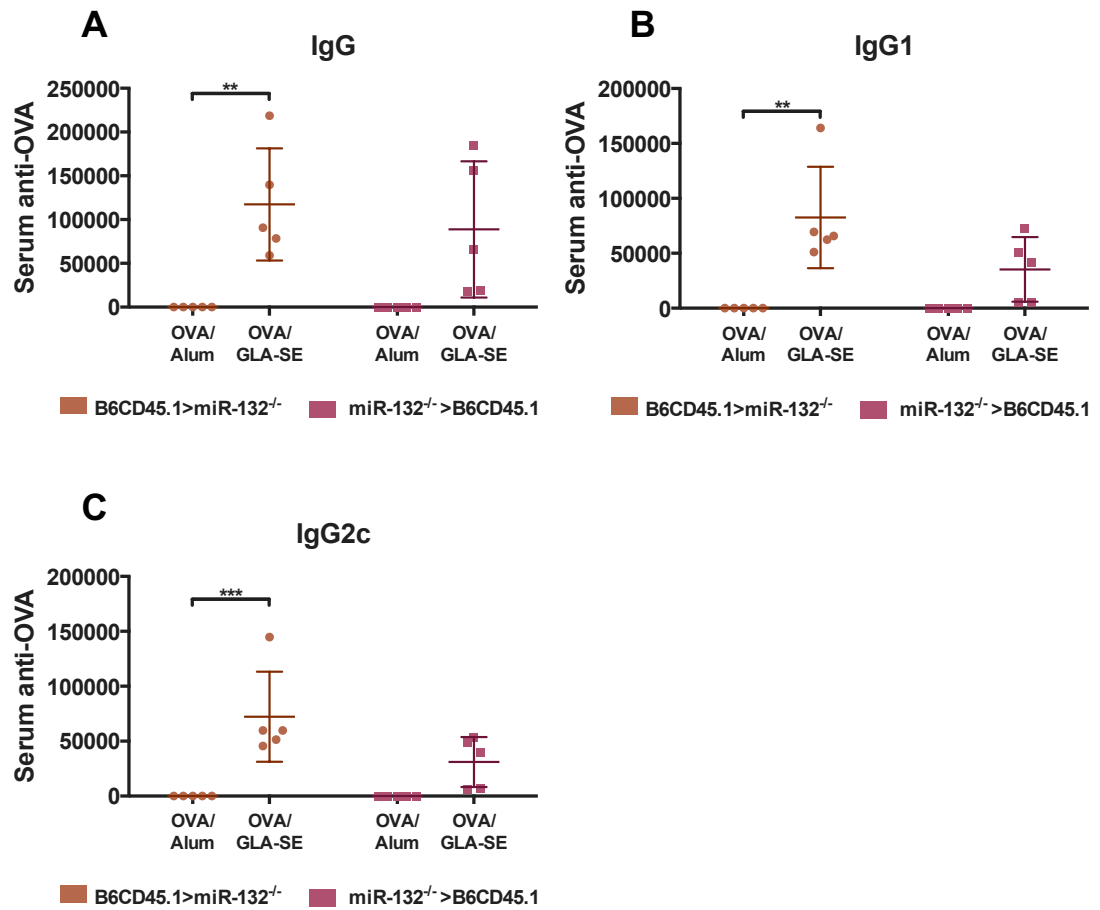


Figure 5.9: Antibody production in reciprocal bone marrow chimeras.

Mice were irradiated and then reconstituted with BM. miR-132^{-/-} mice were reconstituted with WT BM and WT mice with miR-132^{-/-} BM. After 8 weeks, mice were immunized with PBS, or OVA/GLA-SE following the long-term model and the serum was analysed for OVA-specific antibodies. **A:** IgG, **B:** IgG1, and **C:** IgG2c antibody titration. N=5. Two-Way ANOVA followed by multiple comparison Tukey's test: *P ≤ 0.05, **P ≤ 0.01, *** P≤0.001, ****P ≤ 0.0001.

5.5. Summary of findings

- Treatment with OVA/GLA-SE leads to an increase in AICDA expression that is greater in miR-132^{-/-} mice than WT mice.
- There were more activated B cells and T_{FH} cells in miR-132^{-/-} mice compared to WT mice upon OVA/GLA-SE treatment.
- At seven days post-treatment there are GCs in miR-132^{-/-} mice that are absent in WT mice.
- There is a rapid increase in antibody production upon treatment in miR-132^{-/-} mice. After a long-term OVA/GLA-SE treatment there is a polarization of the response towards T_H1 in miR-132^{-/-} mice.
- After six months of immunization and a further three days of OVA/GLA-SE treatment, there is a rapid production of antibodies, but no difference between WT and miR-132^{-/-} mice.
- Chimeras showed that presence of miR-132 is necessary in both stromal and haematopoietic cells for the polarization towards a T_H1 immune response

5.6. Discussion

5.6.1. GLA-SE treatment leads to an increase in AICDA and specific cell types

Previous results (Chapter 3 and 4) have shown that miR-132 has a crucial role in the remodelling process. LN structure after GLA-SE treatment was altered in miR-132^{-/-} mice. Thus the role of architectural remodelling on functional changes in the type of immune response generated following antigen/adjuvant administration was investigated. AICDA is an enzyme that controls the process of somatic hypermutation and class switching and it is a surrogate marker for antibody responses as it regulates the affinity and isotype during the immune response. There was a significantly higher AICDA expression in miR-132^{-/-} mice compared to control mice after a long-term OVA/GLA-SE treatment. The next steps were to investigate antibody production and avidity to address the question of whether this increase in AICDA translates into differences in the antibody response in miR-132^{-/-} mice.

To understand the dynamics of immune responses to the defined antigen OVA; B cell subsets were analysed by flow cytometry. miR-132^{-/-} mice had increased numbers of all subsets including follicular B cells and activated B cells after OVA/GLA-SE treatment

compared to WT mice. This indicates that miR-132 is either directly, by acting on B cell function, or indirectly through modulating LN structure, regulating B cell responses in the LN. To further investigate the effect of miR-132 and TLR4 treatment, cell types were analysed after short-term treatments during which time OVA/GLA/SE treatment induces follicular remodelling. Though there was no difference in the increase of T_{FR} cells upon treatment between WT and miR-132^{-/-} mice, there were more B cells and T_{FH} cells by seven days of OVA/GLA-SE treatment in miR-132^{-/-} mice in addition to differences in the remodelling process quantified in Chapter 4. T_{FH} cells are indispensable for the proper generation of GCs. Therefore if there are more T_{FH} cells and B cells as well as activated B cells in miR-132^{-/-} mice, the early formation of larger GCs might be a compound effect. The function of T_{FH} cells in the miR-132 deficient mice remains to be investigated. This could be done through investigating their markers and the cytokines they produce to determine if miR-132 could be regulating their function directly and potentiating the GC reaction.

The mechanism driving these changes in T_{FH} and B cell activation is unclear but might involve changes in cytokine and chemokine expression patterns in the LN. The cell type responsible for this is unknown. To further investigate the effect of different cell types and miR-132 in antibody production, chimeras were set up and serum collected. Results obtained demonstrated that miR-132 is necessary in both haematopoietic and stromal cells to regulate OVA-specific antibody production. miR-132 in stromal cells alone or haematopoietic cells was not enough to polarize the response towards T_H1 as observed in miR-132^{-/-} mice indicating that it is a combination of both structural changes and B and T_{FH} dynamics that lead to this faster T_H1 response.

5.6.2. miR-132 deficiency leads to a rapid formation of GCs and production of antibodies

miR-132^{-/-} and WT mice were treated for three and seven days and histology was analysed for GCs. At three days, there is no ring-like structure of B cells in the paracortex in miR-132^{-/-} mice compared to WT mice. By seven days, miR-132^{-/-} mice had LNs that were significantly larger, but no B cell follicular remodelling had occurred. At seven days post OVA/GLA-SE treatment, there were more GCs found in miR-132^{-/-} mice and none were found in control mice, miR-132^{-/-} mice also had higher titres of both IgG1 and IgG2c and total IgG. miR-132^{-/-} draining LNs had accelerated GC formation but also contained increased numbers of B cells and T_{FH} cells than WT mice. Inhibiting miR-132 leads to a rapid formation of GCs, more B cells and T_{FH} cells

and faster production of OVA-specific antibodies. Inhibiting miR-132 in conjunction with vaccination could drive the response to a quicker production of specific antibodies to the antigen. Thus driving faster higher affinity antibody responses to diseases where resolution is essential to pathogen/toxin clearance.

5.6.3. Absence of miR-132 leads to a polarization of the immune response

Antibody titration and avidity was investigated comparing WT and miR-132^{-/-} mice. These results indicate a profound role for both TLR4 agonists and miR-132 in regulating the production of specific antibodies and avidity of the response; however, using a simple antigen the full effects were not possible to measure. In comparison to Alum, GLA-SE produces both a strong IgG2c (T_H1) response and higher avidity response in both WT and miR-132^{-/-} mice. miR-132 deficiency leads to a decrease in IgG1 (T_H2) and a corresponding polarization to an IgG2c (T_H1) response. Alum is known to induce a strong T_H2 response; however, despite the changes in LN structure in Alum treated miR-132 deficient mice, a near total lack of IgG1 antibody response occurred. This indicates that the mechanism controlling the T_H1 switch is not in itself a miR-132 driven process. Thus miR-132 inhibition in conventional Alum based vaccines is not a useful method to modulate the type of response. However, inhibiting miR-132 could be a novel way to further polarize the immune response towards T_H1 responses during vaccination with TLR4 adjuvants. A preliminary experiment using miR-132 LNA inhibitor was performed, but the inhibitor-dosing regimen in mice still needs to be optimized, as no difference was observed to the control (data not shown). This is likely to be pharmacodynamics problem that requires optimisation to replicate the miR-132^{-/-} mouse phenotype.

5.6.4. miR-132 has no role on the memory response

To investigate the effect of miR-132 on long-term memory response to repeated immunization, mice were immunized, left for six months and boosted for a further three days. There is a rapid production of antibodies after treatment with OVA/GLA-SE in both WT mice and miR-132^{-/-} mice. There is no difference in changes in total IgG or IgG2c but less IgG1 in miR-132^{-/-} mice compared to WT mice. miR-132 does seem to have an effect on the memory response, although there is an increase in antibody production as in WT mice, there is less IgG1. This has interesting implications to the potency of miR-132 inhibition in skewing the memory response, thus miR-132 inhibition has the potential to have long-term effects on the immune response. The

molecular and cellular mechanisms of this process are not known, it is possible that miR-132 modulates the memory cell niche biasing the response, or modifies memory T cells.

5.6.5. Conclusion

These results indicate that miR-132 regulates the kinetics of GC formation and the type of antibodies produced. Inhibition of miR-132 may be a way to super-potentiate T_H1 immune responses that provide protection against intracellular pathogens. miR-132 is critical in the proper development of LN structure changes in response to TLR4 agonist adjuvant immunization and inhibiting it could be a way of manipulating the immune response to get early antibody secretion but also to push the immune response towards T_H1 responses. Likewise transient overexpression of miR-132 might induce additional structural changes or GC reactions potentially modifying the diversity of the immune response.

Chapter 6: General Discussion

6.1. Summary of findings and relevance

6.1.1. TLR4 adjuvants induce rapid LN remodelling

Historically, mechanisms driving adjuvant efficacy have been thought to be driven by APC maturation and function. However, unlike Alum that works in a NLRP3 inflammasome dependent process, TLR stimulation has the potential to drive the activation of many different cell types at both the site of vaccine delivery and in the draining LN. This project was based on the previous finding that repeated CFA delivery that possesses potent TLR stimulatory capacity, drives large scale LN remodelling although the molecular and cellular mechanisms driving this process are unknown (summarised in Figure 1.6). Due to the toxicity and excessive inflammation that prevents CFA use in humans and multiple administrations into mice an alternative model was developed using GLA-SE, a potent TLR4 agonist. This also enabled the investigation of LN remodelling using an adjuvant that has been proven in clinical trials to have significant potency without uncontrolled toxic inflammation. The remodelling induced by GLA-SE involved a rapid increase in all cell types including innate and adaptive immune cells and the underlying stromal cell networks. This increase was mirrored by an increase in the production of different cytokines, chemokines and extracellular matrix as well as the induction of miR-132 expression. Signalling induced by this adjuvant drove rapid new B cell follicle formation involving B cell follicle dissolution and formation of large numbers of new follicles in the LN cortex.

6.1.2. MiR-132 is a regulator of the immune response to adjuvants

An increase in miR-132 expression was observed post treatment in LNs. miR-132 is known to be up-regulated upon TLR4 stimulation and regulate genes driving inflammation. miR-132^{-/-} mice were found to have an altered architecture in naïve LN with an intermingling of B and T cell zones. Immunization with TLR4 adjuvants led to a different LN architecture compared to WT. Dissolution of B cell follicles was not observed in miR-132^{-/-} mice and there were no new B cell follicles in the paracortex. Instead, B cell follicles increased in size but remained in the cortex. The mechanisms behind this process were investigated but no clear mechanism could be identified as miR-132 regulates a plethora of genes from cytokines to proteases. It was shown that there are more MRCs and MRCs differentiating into FDCs in miR-132^{-/-} mice. These

MRCs express less chemokines in miR-132^{-/-} mice compared to WT mice. A differential expression of CXCR5 was also observed in miR-132^{-/-} mice. This altered chemokine and chemokine receptor expression could explain why no B cell follicle dissolution occurs in the absence of miR-132 as B cells are guided differently. This could also explain why bone marrow chimeras indicate that both radiation sensitive (B and T cells, DCs) and insensitive cells (stromal cells, endothelium, macrophages, innate lymphoid cells, memory T cells) are involved in process of LN reorganisation.

6.1.3. Consequence of LN remodelling on the immune response

As the process of LN remodelling upon TLR4 adjuvant immunization was altered in miR-132^{-/-} mice, the potential function effect was investigated. To elucidate the role of remodelling antibody production and cell types required for GC reactions were characterised. Both B cells and TFH cells were increased in miR-132^{-/-} mice after treatment compared to controls and large GCs appeared after only seven days of treatment, prior to formation in WT mice. Correlating with accelerated GC formation rapid production of antibodies was also observed in miR-132^{-/-} mice concurrent with polarization of the immune response towards T_H1 and additional AICDA expression. This indicates that inhibiting miR-132 could lead to more efficient vaccines and aids in identifying targets that might improve the function of adjuvants by targeting selective pathways using small molecules or agonistic proteins.

6.2. Conclusion and schematic of miR-132 role in remodelling

We have shown that TLR4 agonist adjuvants are potent in inducing LN remodelling. These adjuvants have also been shown to be very efficient in generating an immune response to vaccination and are currently in clinical vaccine trials. Through investigating the cellular and molecular mechanisms behind LN remodelling we showed that it involved an increase in both immune and stromal cell types, cytokines and miR-132. In WT mice by three days post-delivery, B cell follicle dissolution was observed and by seven days complete remodelling was observed with new follicle formation in the LN paracortex surrounded by T cell stroma (illustrated in Figure 6.1). Using miR-132^{-/-} mice it was possible to show this microRNA had an essential role in regulating changes in LN structure following OVA/GLA-SE immunization. There were increased numbers of MRCs, B cells and T_{FH} cells in mice lacking miR-132 compared to WT mice as well as changes in chemokine expression. By three days of treatment of miR-132^{-/-} mice, the B cell follicles did not dissolve, rather B cell follicles got bigger and

were restricted to the marginal zone in the cortex. By seven days of OVA/GLA-SE treatment there were significantly increased B cell follicles that possessed large GCs. These changes in architecture observed led to an accelerated production of antibodies in miR-132^{-/-} mice and to polarisation towards a T_H1 immune response. This is illustrated in Figure 6.2. Inhibiting miR-132 could be a novel way of regulating the immune response during vaccination to get a rapid induction and polarization towards T_H1 antibody response.

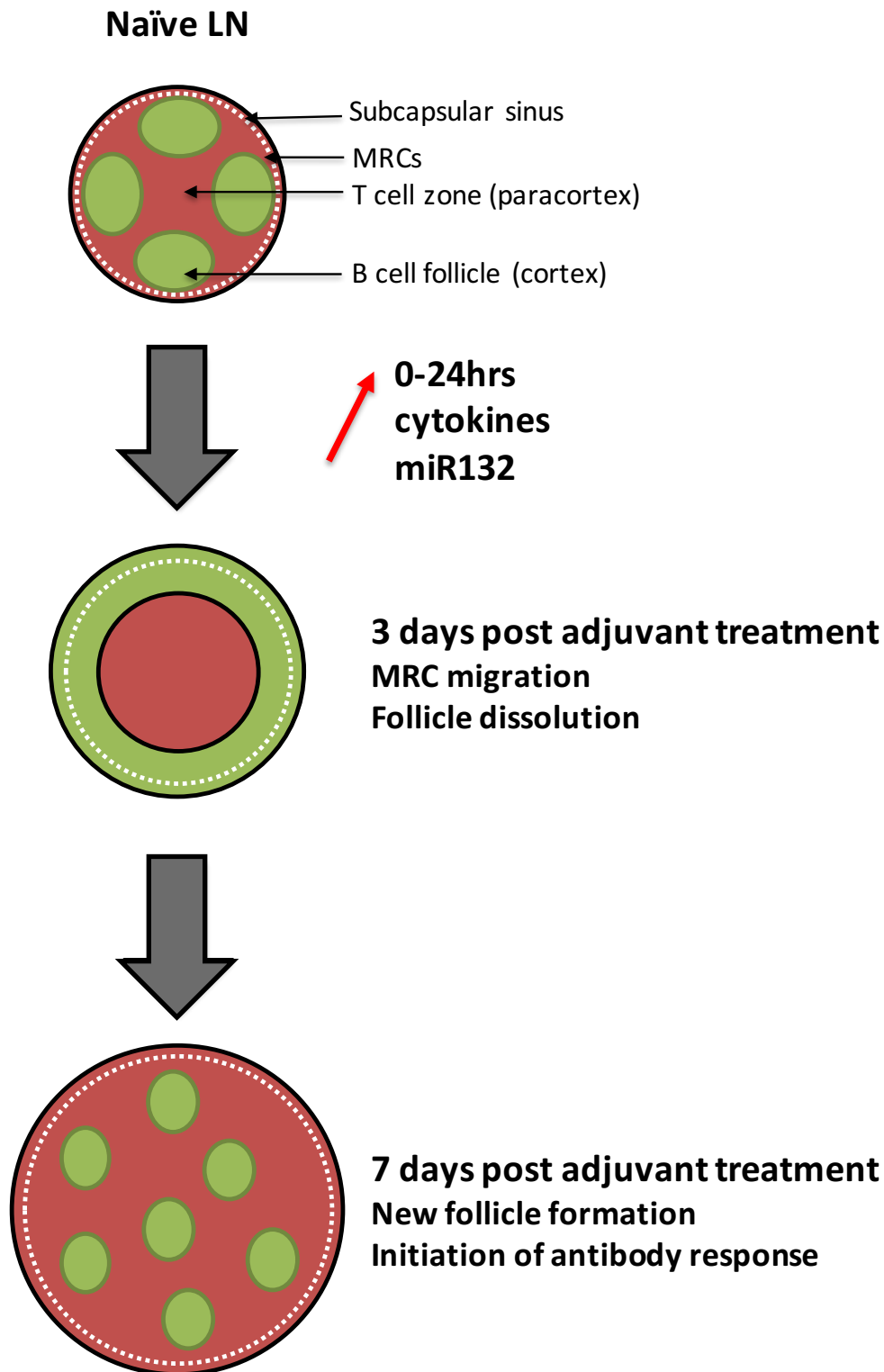


Figure 6.1: Schematic of changes to LN structure in WT mice upon OVA/GLA-SE treatment.

The structure of a naïve LN is tightly regulated by stromal cells; however, during immunization with TLR4 agonists there is an increase in cytokine and miR-132 production and a rapid increase in LN size with a ring-like structure of B cells forming in the cortex. After 7 days of treatment, LNs are remodelled with B cell follicles found in the paracortex.

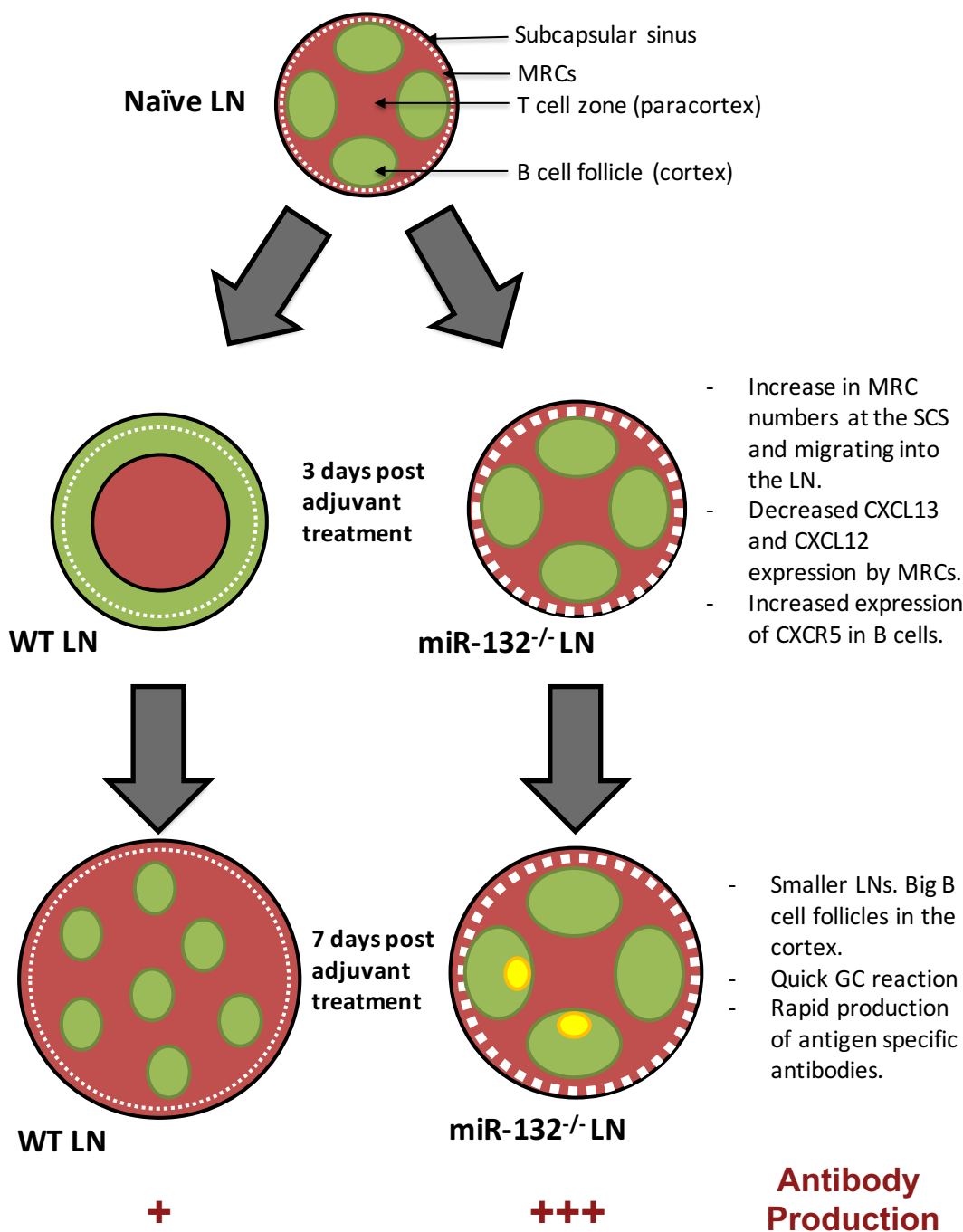


Figure 6.2: Schematic of changes to LN structure in WT mice upon OVA/GLA-SE treatment.

In WT mice, remodelling of LNs starts with a dissolution of B cell follicles leading to at 7 days post immunization new follicles forming in the paracortex. However, in the absence of miR-132 there are more MRCs migrating into the LN but they produce less CXCL13 and CXCL12 while B cells up-regulate CXCR5. At 3 days the LNs do not have dissolution of B cell follicles but they get bigger. By 7 days there are big B cell follicles in the cortex with a rapid GC reaction and increased production of antigen specific antibodies.

6.3. Outstanding questions and future work

6.3.1. Role of MRCs

The results obtained showed a clear role of MRCs in the LN remodelling process. A rapid increase in MRC numbers was observed that correlated with histology results where there were increased number of MRCs in the SCS and entering the LN in miR-132^{-/-} mice compared to WT mice. These histological results still need to be quantified in order to be certain that what was observed does in fact coincide with there being more MRCs entering the cortex of the LN. An automated pipeline in Cell Profiler to quantify the observations is currently being developed.

6.3.2. MiR-132 effect on the breadth of the immune response

An aspect that still needs investigation is the effect of miR-132 deficiency on the breadth of the immune response. An experiment has been completed in vivo and serum is in the process of being analysed using influenza epitope protein arrays. Control and miR-132 deficient mice were treated with OVA/adjuvant then with influenza, or with influenza/adjuvant to examine the diversity of response. This should enable the determination of whether miR-132 inhibition could lead to a more diverse lower affinity immune response.

6.3.3. Effect of miR-132 inhibition on other microRNAs

miR-132 has a profound effect on LN remodelling upon immunization. However, there are many different miRNAs that collectively regulate cellular function, multiple different miRNAs are regulated through TLR signalling and most miRNAs have multiple targets. Therefore, why does the absence of a single microRNA lead to such a distinct phenotype when there is strong evidence for redundancy in miRNA-mediated regulation of transcription? Although miR-132 has multiple direct targets, most of the key changes observed are not direct target genes of miRNA-132 and lack target sequences. Therefore, the more likely interpretation is that miR-132 acts mostly indirectly through regulation of master regulatory proteins that control transcription of genes that regulate tissue remodelling. Strong evidence shows that miR-132 can negatively regulate EP300 in endothelial cells, a core protein involved in the transcription of many genes [184]. Recently, miR-132 has been shown to regulate expression of the RISC Component Ago 2 (AGO2) a regulator of the miRNA-mediated gene silencing and miRNA biogenesis machinery [270]. miR-132's unique role in the

remodelling process likely arises from its capacity to act as a master regulator of mechanisms driving the inflammatory cascade. We speculate that the processes that occur in early inflammation induce a “stop and wait” signal preventing tissue remodelling. Subsequent induction of miR-132 turns off this signal permitting cell migration and remodelling to occur (Figure 6.3A). In miR-132^{-/-} mice this “stop and wait” signal is not appropriately turned off delaying the tissue remodelling process due to a failure of miR-132 to shut down inflammation in stromal cells (Figure 6.3B). This delay in shut down results in a failure of MRC migration and B cell follicle dissolution driving large and faster GCs with increased number of B cells and TFH cells leading to the early antibody formation observed in miR-132^{-/-} mice. We speculate that MRCs and DCs differentially migrate due to the high levels of TLR4 agonist in the SCS of the LNs driving high levels of miR-132 up-regulation. Interestingly the inflammatory “stop and wait” phenotype is found in number of tissues including the skin where initial inflammation inhibits wound closure, likely benefitting the host by allowing time for macrophages and DCs to sense and respond to pathogen infection. Data from the Coles laboratory indicates that this process has a key role in the inflammatory pathology observed in non-healing chronic wounds in humans, where inflammation appears not to stop and dermal fibroblasts and keratinocytes fail to migrate in the wound closure process.

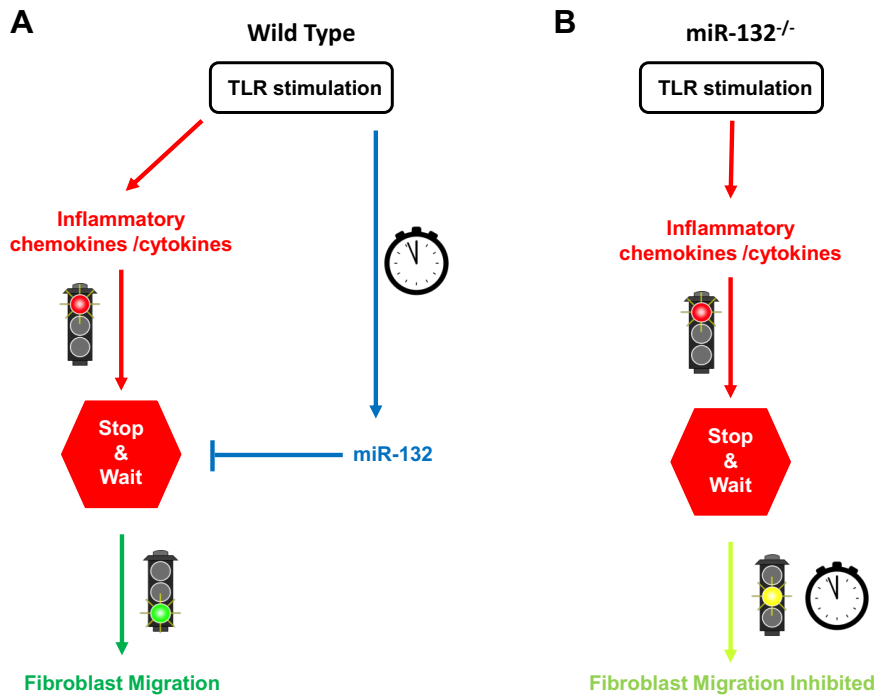


Figure 6.3: The “stop and wait” model.

TLR stimulation leads to an initial inflammation that activates cytokine and chemokine production by stromal fibroblasts (Marginal Reticular Cells) inhibiting cell migration. miR-132 is rapidly upregulated down modulating inflammation and permitting migration to predominate over inflammation. In the absence of miR-132, inflammation predominates over migration driving enhanced B cell recruitment and retention within follicles and blocking.

6.3.4. TLR4 as a target

The specificity of this phenotype to TLR4 over other PRR stimulation is unknown. That is if the phenotype observed in LN remodelling is a general principle of all TLRs or intracellular detection by Stimulator of Interferon Genes (STING). Different TLR and STING agonists are being developed for use as next generation adjuvants for the efficient induction of T_H1 antibody responses, and efficient CTL induction to therapeutically treat chronic viral infection and cancer. LN architecture and the molecular mechanisms following immunization needs to be characterised in response to a range of TLR adjuvants. This would determine if the mechanism behind miR-132 is a generalised phenomenon or specific to TLR4 and provide new insights into novel agonist and antagonist approaches for adjuvant formation.

6.3.5. Determining which cell types are indispensable in LN remodelling

Using TLR4^{-/-} and MyD88^{-/-} mice and developing chimeras it would be possible to determine whether the expression of TLR4 on radiation sensitive or on resistant components drives LN remodelling. This would provide new insights into the different cell types required for LN architecture formation and remodelling. Radiation chimeras are inherently difficult to interpret as radiation sensitivity depends on the capacity of a cell to repair cell damage, this process is deficient in lymphocytes, and other sensitive cells like dendritic cells are short lived when they are activated. Radiation is inherently inflammatory and depletes existing pools of host DCs. In contrast macrophages are long-lived cells and are radiation resistant. Recent evidence shows that Innate Lymphoid Cells are also radiation resistant. Therefore, development of tissue and cell specific knock outs of miR-132, TLR4, MyD88 and other signalling components will provide more precise information for their individual roles in the inflammatory processes.

To further determine which cell types are involved and determine miR-132's role in different cell types, Rag^{-/-} mice were injected with WT LN cells, miR-132^{-/-} LN cells, WT B cells and miR-132^{-/-} T cells or miR-132^{-/-} B cells and WT T cells. This experiment was repeated twice and both times there were very few cells found in the LNs with no follicular structures. It has previously been observed in the Coles' laboratory that HEVs are deficient in Rag^{-/-} mice leading to poor trafficking into the host LNs by the donor cells. This is likely very inefficient in the pLNs. It has been shown that transfer of cells into neonatal mice leads to efficient LN reconstitution even in mice deficient in the

common gamma chain providing an alternative model to understand stromal cell function without using radiation chimeras [43].

6.3.6. How do changes in LN help develop better adjuvants?

It has already been shown that TLR4 adjuvants are potent adjuvants, which has led to the use of different formulations of MPL-A by GSK: AS04 in Fendrix and Cervarix, and AS01 in Mosquirix. We have demonstrated that one of the outcomes of vaccines is massive LN remodelling driving changes to stroma networks, and vasculature within the LNs. It was possible to identify methods to modulate LN remodelling by determining the molecular mechanism driving this process. This would enable the modulation of the timing and type of immune response and provide potential insights into how the diversity of the immune response might be modulated. The effect observed in LNs following TLR treatment could explain how the “shock and kill” approach works in the eradication of HIV. Survival of HIV-infected individuals has increased through the use of anti-retroviral therapy but it does not lead to a full eradication of the virus that will remain in the body. The “shock and kill” approach involves reactivating latent HIV transcription in memory CD4+ T cells, which would lead to immune clearance and infected cell death. A study using a TLR9 agonist stimulated strong antiviral responses to HIV as well as enhanced HIV transcription [271]. The increase in LN size and drastic remodelling observed in the case of treatment with the TLR4 agonist GLA-SE could explain how these TLR agonists are working in the “shock and kill” method for eradication of latent HIV.

Definitions

AChE	Acetylcholinesterase
Ago2	Argonaute 2
AICD	Antigen Induced Cell Death
AICDA	Activation-Induced Cytidine Deaminase
AID	DNA-editing deaminase
Alum	Aluminium
AP	Alkaline phosphatase
APC	Antigen Presenting Cell
APRIL	A Proliferation-Inducing Ligand
ASC	Apoptosis-associated Speck-like protein containing CARD
Ascl-1	Achaete-scute complex homolog 2
BAFF	B cell Activating Factor
Bcl6	B-cell lymphoma 6
BCR	B Cell Receptor
BEC	Blood Endothelial Cell
BM	Bone marrow
BMDC	Bone Marrow Derived Cell
BSA	Bovine Serum Albumin
BSF	Biological Services Facility
CFA	Complete Freund's Adjuvant
CLEC-2	C-type Lectin receptor

CR1/CR2	Complement Receptor 1 and 2
CREB	cAMP-Response Element Binding protein
CSF-1	Colony Stimulating Factor-1
Ct	Threshold cycles
CTL	Cytotoxic T Lymphocyte
DAMP	Damage Associated Molecular Patterns
DAPI	4',6'-diamidino-2-phenylindole
DC	Dendritic Cell
dsRNA	Double-stranded RNA
DTR	Diphtheria Toxin Receptor
DTx	Diphtheria toxin
EDTA	Ethylenediaminetetraacetic Acid
ELISA	Enzyme-Linked Immunosorbent Assay
ER-TR7	Reticular Fibroblasts and Reticular Fibres
FACS	Fluorescence-Activated Cell Sorting
FCS	Foetal Calf Serum
FDC	Follicular Dendritic Cell
FRC	Fibroblastic Reticular Cell
FSC	Forward scatter
GC	Germinal Centre
GLA-SE	Glucopyranosyl Lipid Adjuvant-Stable oil in water Emulsion
GM-CSF	Granulocyte Macrophage Colony-Stimulating Factor

gp38	Podoplanin
GSK	Glasko Smith Kline
HB-EGF	Heparin-Binding Epidermal-like Growth Factor
HBV	Hepatitis B Virus
HCMV	Human Cytomegalovirus
HEV	High Endothelial Venule
Hprt	Hypoxanthine phosphoribosyltransferase
ICAM	Intercellular Adhesion Molecule
ICOS	Co-stimulatory molecule inducible co-stimulator
IDRI	Infectious Disease Research Institute
IFA	Incomplete Freund's Adjuvant
IFN	Interferon
IL-7	Interleukin-7
iLN	Inguinal LN
Immgen	Immunological Genome Project
IRF3	Interferon Regulatory Factor 3
ISCOM	Immune Stimulating Complexes
LCMV	Lymphocytic Choriomeningitis Virus
LEC	Lymphatic Endothelial Cell
LFA-1	Lymphocyte Function-associated Antigen-1
LN	Lymph Node
LPB	LPS Binding Protein

LPS	Lipopolysaccharide
LRR	Leucine-Rich Repeat
LTi	Lymphoid Tissue inducer cell
LTo	Lymphoid Tissue organizer
LTα1β2	Lymphotoxin α 1 β 2
LTβR	Lymphotoxin β Receptor
MAdCAM-1	Mucosal Vascular Addressin Cell Adhesion Molecule-1
MARCO	Macrophage Receptor with Collagenous Structure
MHCII	Major Histocompatibility Complex II
miRNA	MicroRNA
MMP-9	Matrix metalloproteinase 9
MPL-A	Monophosphoryl Lipid-A
MR	Mannose Receptor
MRC	Marginal Reticular Cell
MSM	Medullary Sinus Macrophage
MyD88	Myeloid Differentiation Factor 88
NK	Natural killer cell
NLRP3	NLR family, Pyrin Domain containing 3
OVA	Ovalbumin
PACT	Protein Activator of PKR
PAMP	Pathogen-Associated Molecular Pattern
PAZ	Piwi Argonaut and Zwiille

PBS	Phosphate Buffered Saline
PBS/T	PBS/0,05% Tween
PFA	Paraformaldehyde
pLN	popliteal LN
PMA	Phorbol 12-myristate 13-acetate
PNAd	Peripheral Node Addressin
PRR	Pattern Recognition Receptor
qPCR	quantitative PCR
RANK-L	Receptor Activator of Nuclear Factor kappa-B ligand
REST	Repressor Element 1 Silencing Transcription factor
RISC	RNA-Induced Silencing Complex
Rnu6	U6 small nuclear RNA
rRNA	Ribosomal RNA
RT	Reverse Transcriptase
S1P	Sphingosine-1-Phosphate
S1PR1	Sphingosine-1-Phosphate Receptor 1
SAP	SLAM-associated protein
SCS	Subcapsular Sinus
SEM	Standard Error of the Mean
siRNA	Small interfering RNA
SLA-SE	Second generation lipid adjuvant – stable oil in water emulsion
SLO	Secondary Lymphoid Organ

snRNA	Small nuclear RNA
SSC	Side scatter
SSM	Subcapsular Sinus Macrophage
STAT4	Signal Transducer and Activator of Transcription 4
STING	Stimulator of Interferon Genes
T_{CM}	Central Memory T cell
TCR	T Cell Receptor
TDM	Trehalose Dicorynomycolate
T_{EM}	Effector Memory T cell
T_{FH}	Follicular Helper T cell
T_{FR}	Follicular Regulatory T cell
T_H	T Helper cell
TIR	Toll/Interleukin-1 Receptor-like
TIV	Inactivated Influenza Vaccine
TLR	Toll-Like Receptor
TNFα	Tumor Necrosis Factor α
TRAM	TRIF-Related Adapter Molecule
TRBP	Tar RNA Binding Protein
T_{reg}	Regulatory T cell
TRIF	TIR-domain-containing adapter inducing interferon- β
tRNA	Transfer RNA
VCAM	Vascular Cell Adhesion Molecule

VEGF	Vascular Endothelial Growth Factor
VSV	Systemic Vesicular Stomatitis Virus
W/OE	Formulated oil-in-water emulsion
WT	Wild-type

Bibliography

1. Girard, J.P., C. Moussion, and R. Forster, *HEVs, lymphatics and homeostatic immune cell trafficking in lymph nodes*. *Nat Rev Immunol*, 2012. **12**(11): p. 762-73.
2. Sainte-Marie, G., *The lymph node revisited: development, morphology, functioning, and role in triggering primary immune responses*. *Anat Rec (Hoboken)*, 2010. **293**(2): p. 320-37.
3. Allen, C.D. and J.G. Cyster, *Follicular dendritic cell networks of primary follicles and germinal centers: phenotype and function*. *Semin Immunol*, 2008. **20**(1): p. 14-25.
4. Link, A., et al., *Fibroblastic reticular cells in lymph nodes regulate the homeostasis of naive T cells*. *Nat Immunol*, 2007. **8**(11): p. 1255-65.
5. Bajenoff, M., et al., *Stromal cell networks regulate lymphocyte entry, migration, and territoriality in lymph nodes*. *Immunity*, 2006. **25**(6): p. 989-1001.
6. Forster, R., et al., *CCR7 coordinates the primary immune response by establishing functional microenvironments in secondary lymphoid organs*. *Cell*, 1999. **99**(1): p. 23-33.
7. Luther, S.A., et al., *Differing activities of homeostatic chemokines CCL19, CCL21, and CXCL12 in lymphocyte and dendritic cell recruitment and lymphoid neogenesis*. *J Immunol*, 2002. **169**(1): p. 424-33.
8. Gunn, M.D., et al., *A B-cell-homing chemokine made in lymphoid follicles activates Burkitt's lymphoma receptor-1*. *Nature*, 1998. **391**(6669): p. 799-803.
9. Katakai, T., *Marginal reticular cells: a stromal subset directly descended from the lymphoid tissue organizer*. *Front Immunol*. **3**: p. 200.
10. Katakai, T., et al., *A novel reticular stromal structure in lymph node cortex: an immuno-platform for interactions among dendritic cells, T cells and B cells*. *Int Immunol*, 2004. **16**(8): p. 1133-42.
11. Katakai, T., et al., *Lymph node fibroblastic reticular cells construct the stromal reticulum via contact with lymphocytes*. *J Exp Med*, 2004. **200**(6): p. 783-95.
12. Gretz, J.E., et al., *Sophisticated strategies for information encounter in the lymph node: the reticular network as a conduit of soluble information and a highway for cell traffic*. *J Immunol*, 1996. **157**(2): p. 495-9.
13. Miyasaka, M. and T. Tanaka, *Lymphocyte trafficking across high endothelial venules: dogmas and enigmas*. *Nat Rev Immunol*, 2004. **4**(5): p. 360-70.
14. Majumdar, R., M. Sixt, and C.A. Parent, *New paradigms in the establishment and maintenance of gradients during directed cell migration*. *Curr Opin Cell Biol*, 2014. **30**: p. 33-40.
15. Mionnet, C., et al., *High endothelial venules as traffic control points maintaining lymphocyte population homeostasis in lymph nodes*. *Blood*, 2011. **118**(23): p. 6115-22.
16. Tal, O., et al., *DC mobilization from the skin requires docking to immobilized CCL21 on lymphatic endothelium and intralymphatic crawling*. *J Exp Med*, 2011. **208**(10): p. 2141-53.
17. Weber, M., et al., *Interstitial dendritic cell guidance by haptotactic chemokine*

- gradients*. Science, 2013. **339**(6117): p. 328-32.
18. Ulvmar, M.H., et al., *The atypical chemokine receptor CCRL1 shapes functional CCL21 gradients in lymph nodes*. Nat Immunol, 2014. **15**(7): p. 623-30.
 19. Grigorova, I.L., et al., *Cortical sinus probing, SIP1-dependent entry and flow-based capture of egressing T cells*. Nat Immunol, 2009. **10**(1): p. 58-65.
 20. Pham, T.H., et al., *Lymphatic endothelial cell sphingosine kinase activity is required for lymphocyte egress and lymphatic patterning*. J Exp Med, 2010. **207**(1): p. 17-27.
 21. Kabashima, K., et al., *Plasma cell SIP1 expression determines secondary lymphoid organ retention versus bone marrow tropism*. J Exp Med, 2006. **203**(12): p. 2683-90.
 22. Medzhitov, R. and C.A. Janeway, Jr., *Innate immunity: impact on the adaptive immune response*. Curr Opin Immunol, 1997. **9**(1): p. 4-9.
 23. Parish, C.R. and E.R. O'Neill, *Dependence of the adaptive immune response on innate immunity: some questions answered but new paradoxes emerge*. Immunol Cell Biol, 1997. **75**(6): p. 523-7.
 24. Guermonprez, P., et al., *Antigen presentation and T cell stimulation by dendritic cells*. Annu Rev Immunol, 2002. **20**: p. 621-67.
 25. Tan, J.K. and H.C. O'Neill, *Maturation requirements for dendritic cells in T cell stimulation leading to tolerance versus immunity*. J Leukoc Biol, 2005. **78**(2): p. 319-24.
 26. Kapsenberg, M.L., *Dendritic-cell control of pathogen-driven T-cell polarization*. Nat Rev Immunol, 2003. **3**(12): p. 984-93.
 27. MacLeod, M.K., J.W. Kappler, and P. Marrack, *Memory CD4 T cells: generation, reactivation and re-assignment*. Immunology, 2010. **130**(1): p. 10-5.
 28. MacLeod, M.K., et al., *CD4 memory T cells: what are they and what can they do?* Semin Immunol, 2009. **21**(2): p. 53-61.
 29. Fazilleau, N., et al., *Follicular helper T cells: lineage and location*. Immunity, 2009. **30**(3): p. 324-35.
 30. Zhang, S., H. Zhang, and J. Zhao, *The role of CD4 T cell help for CD8 CTL activation*. Biochem Biophys Res Commun, 2009. **384**(4): p. 405-8.
 31. Stinchcombe, J.C. and G.M. Griffiths, *The role of the secretory immunological synapse in killing by CD8+ CTL*. Semin Immunol, 2003. **15**(6): p. 301-5.
 32. Goodnow, C.C., et al., *Control systems and decision making for antibody production*. Nat Immunol, 2010. **11**(8): p. 681-8.
 33. Allen, C.D., T. Okada, and J.G. Cyster, *Germinal-center organization and cellular dynamics*. Immunity, 2007. **27**(2): p. 190-202.
 34. Mebius, R.E., *Organogenesis of lymphoid tissues*. Nat Rev Immunol, 2003. **3**(4): p. 292-303.
 35. Drayton, D.L., et al., *Lymphoid organ development: from ontogeny to neogenesis*. Nat Immunol, 2006. **7**(4): p. 344-53.
 36. van de Pavert, S.A., et al., *Chemokine CXCL13 is essential for lymph node initiation and is induced by retinoic acid and neuronal stimulation*. Nat Immunol, 2009. **10**(11): p. 1193-9.

37. Eberl, G., et al., *An essential function for the nuclear receptor RORgamma(t) in the generation of fetal lymphoid tissue inducer cells*. Nat Immunol, 2004. **5**(1): p. 64-73.
38. Mebius, R.E., et al., *The fetal liver counterpart of adult common lymphoid progenitors gives rise to all lymphoid lineages, CD45+CD4+CD3- cells, as well as macrophages*. J Immunol, 2001. **166**(11): p. 6593-601.
39. Vondenhoff, M.F., et al., *LTbetaR signaling induces cytokine expression and up-regulates lymphangiogenic factors in lymph node anlagen*. J Immunol, 2009. **182**(9): p. 5439-45.
40. Kim, D., et al., *Regulation of peripheral lymph node genesis by the tumor necrosis factor family member TRANCE*. J Exp Med, 2000. **192**(10): p. 1467-78.
41. van de Pavert, S.A. and R.E. Mebius, *New insights into the development of lymphoid tissues*. Nat Rev Immunol, 2010. **10**(9): p. 664-74.
42. Schmutz, S., et al., *Cutting edge: IL-7 regulates the peripheral pool of adult ROR gamma+ lymphoid tissue inducer cells*. J Immunol, 2009. **183**(4): p. 2217-21.
43. Coles, M.C., et al., *Role of T and NK cells and IL7/IL7r interactions during neonatal maturation of lymph nodes*. Proc Natl Acad Sci U S A, 2006. **103**(36): p. 13457-62.
44. Roozendaal, R. and R.E. Mebius, *Stromal cell-immune cell interactions*. Annu Rev Immunol, 2011. **29**: p. 23-43.
45. Cupedo, T., et al., *Induction of secondary and tertiary lymphoid structures in the skin*. Immunity, 2004. **21**(5): p. 655-67.
46. Endres, R., et al., *Mature follicular dendritic cell networks depend on expression of lymphotoxin beta receptor by radioresistant stromal cells and of lymphotoxin beta and tumor necrosis factor by B cells*. J Exp Med, 1999. **189**(1): p. 159-68.
47. Fu, Y.X., et al., *B lymphocytes induce the formation of follicular dendritic cell clusters in a lymphotoxin alpha-dependent fashion*. J Exp Med, 1998. **187**(7): p. 1009-18.
48. Bajenoff, M. and R.N. Germain, *B-cell follicle development remodels the conduit system and allows soluble antigen delivery to follicular dendritic cells*. Blood, 2009. **114**(24): p. 4989-97.
49. Cyster, J.G., et al., *Follicular stromal cells and lymphocyte homing to follicles*. Immunol Rev, 2000. **176**: p. 181-93.
50. Wang, X., et al., *Follicular dendritic cells help establish follicle identity and promote B cell retention in germinal centers*. J Exp Med, 2011. **208**(12): p. 2497-510.
51. Phan, T.G., et al., *Immune complex relay by subcapsular sinus macrophages and noncognate B cells drives antibody affinity maturation*. Nat Immunol, 2009. **10**(7): p. 786-93.
52. Cyster, J.G., *B cell follicles and antigen encounters of the third kind*. Nat Immunol, 2010. **11**(11): p. 989-96.
53. Acton, S.E., et al., *Podoplanin-rich stromal networks induce dendritic cell motility via activation of the C-type lectin receptor CLEC-2*. Immunity, 2012. **37**(2): p. 276-89.

54. Malhotra, D., A.L. Fletcher, and S.J. Turley, *Stromal and hematopoietic cells in secondary lymphoid organs: partners in immunity*. Immunol Rev, 2013. **251**(1): p. 160-76.
55. Scandella, E., et al., *Restoration of lymphoid organ integrity through the interaction of lymphoid tissue-inducer cells with stroma of the T cell zone*. Nat Immunol, 2008. **9**(6): p. 667-75.
56. Cremasco, V., et al., *B cell homeostasis and follicle confines are governed by fibroblastic reticular cells*. Nat Immunol, 2014. **15**(10): p. 973-81.
57. Denton, A.E., et al., *Fibroblastic reticular cells of the lymph node are required for retention of resting but not activated CD8+ T cells*. Proc Natl Acad Sci U S A, 2014. **111**(33): p. 12139-44.
58. Bajénoff, M., *Stromal cells control soluble material and cellular transport in lymph nodes*. Frontiers in Immunology. **3**.
59. Sixt, M., et al., *The conduit system transports soluble antigens from the afferent lymph to resident dendritic cells in the T cell area of the lymph node*. Immunity, 2005. **22**(1): p. 19-29.
60. Katakai, T., et al., *Organizer-like reticular stromal cell layer common to adult secondary lymphoid organs*. J Immunol, 2008. **181**(9): p. 6189-200.
61. Katakai, T., *Marginal reticular cells: a stromal subset directly descended from the lymphoid tissue organizer*. Front Immunol, 2012. **3**: p. 200.
62. Jarjour, M., et al., *Fate mapping reveals origin and dynamics of lymph node follicular dendritic cells*. J Exp Med, 2014. **211**(6): p. 1109-22.
63. Mueller, S.N. and R.N. Germain, *Stromal cell contributions to the homeostasis and functionality of the immune system*. Nat Rev Immunol, 2009. **9**(9): p. 618-29.
64. Mueller, S.N., et al., *Regulation of homeostatic chemokine expression and cell trafficking during immune responses*. Science, 2007. **317**(5838): p. 670-4.
65. Lee, J.W., et al., *Peripheral antigen display by lymph node stroma promotes T cell tolerance to intestinal self*. Nat Immunol, 2007. **8**(2): p. 181-90.
66. Johnson, L.A., et al., *An inflammation-induced mechanism for leukocyte transmigration across lymphatic vessel endothelium*. J Exp Med, 2006. **203**(12): p. 2763-77.
67. Turley, S.J., A.L. Fletcher, and K.G. Elpek, *The stromal and haematopoietic antigen-presenting cells that reside in secondary lymphoid organs*. Nat Rev Immunol, 2010. **10**(12): p. 813-25.
68. Chyou, S., et al., *Fibroblast-type reticular stromal cells regulate the lymph node vasculature*. J Immunol, 2008. **181**(6): p. 3887-96.
69. Malhotra, D., et al., *Transcriptional profiling of stroma from inflamed and resting lymph nodes defines immunological hallmarks*. Nat Immunol. **13**(5): p. 499-510.
70. Marsland, B.J., et al., *CCL19 and CCL21 induce a potent proinflammatory differentiation program in licensed dendritic cells*. Immunity, 2005. **22**(4): p. 493-505.
71. Yanagawa, Y. and K. Onoe, *CCL19 induces rapid dendritic extension of murine dendritic cells*. Blood, 2002. **100**(6): p. 1948-56.

72. Yanagawa, Y. and K. Onoe, *CCR7 ligands induce rapid endocytosis in mature dendritic cells with concomitant up-regulation of Cdc42 and Rac activities*. Blood, 2003. **101**(12): p. 4923-9.
73. Bannard, O., et al., *Germinal center centroblasts transition to a centrocyte phenotype according to a timed program and depend on the dark zone for effective selection*. Immunity, 2013. **39**(5): p. 912-24.
74. Mionnet, C., et al., *Identification of a new stromal cell type involved in the regulation of inflamed B cell follicles*. PLoS Biol, 2013. **11**(10): p. e1001672.
75. Podgrabinska, S., et al., *Inflamed lymphatic endothelium suppresses dendritic cell maturation and function via Mac-1/ICAM-1-dependent mechanism*. J Immunol, 2009. **183**(3): p. 1767-79.
76. Lukacs-Kornek, V., et al., *Regulated release of nitric oxide by nonhematopoietic stroma controls expansion of the activated T cell pool in lymph nodes*. Nat Immunol, 2011. **12**(11): p. 1096-104.
77. Siegert, S. and S.A. Luther, *Positive and negative regulation of T cell responses by fibroblastic reticular cells within paracortical regions of lymph nodes*. Front Immunol, 2012. **3**: p. 285.
78. Mueller, S.N., et al., *Viral targeting of fibroblastic reticular cells contributes to immunosuppression and persistence during chronic infection*. Proc Natl Acad Sci U S A, 2007. **104**(39): p. 15430-5.
79. Bogdan, C., et al., *Fibroblasts as host cells in latent leishmaniosis*. J Exp Med, 2000. **191**(12): p. 2121-30.
80. Davis, K.J., et al., *Pathology of experimental Ebola virus infection in African green monkeys. Involvement of fibroblastic reticular cells*. Arch Pathol Lab Med, 1997. **121**(8): p. 805-19.
81. Steele, K.E., A.O. Anderson, and M. Mohamadzadeh, *Fibroblastic reticular cell infection by hemorrhagic fever viruses*. Immunotherapy, 2009. **1**(2): p. 187-97.
82. Chyou, S., et al., *Coordinated regulation of lymph node vascular-stromal growth first by CD11c+ cells and then by T and B cells*. J Immunol, 2011. **187**(11): p. 5558-67.
83. Bajenoff, M., et al., *Highways, byways and breadcrumbs: directing lymphocyte traffic in the lymph node*. Trends Immunol, 2007. **28**(8): p. 346-52.
84. Tomei, A.A., et al., *Fluid flow regulates stromal cell organization and CCL21 expression in a tissue-engineered lymph node microenvironment*. J Immunol, 2009. **183**(7): p. 4273-83.
85. Angeli, V., et al., *B cell-driven lymphangiogenesis in inflamed lymph nodes enhances dendritic cell mobilization*. Immunity, 2006. **24**(2): p. 203-15.
86. Abe, J., et al., *B cells regulate antibody responses through the medullary remodeling of inflamed lymph nodes*. Int Immunol, 2012. **24**(1): p. 17-27.
87. Bankovich, A.J., L.R. Shiow, and J.G. Cyster, *CD69 suppresses sphingosine 1-phosphate receptor-1 (S1P1) function through interaction with membrane helix 4*. J Biol Chem, 2010. **285**(29): p. 22328-37.
88. Shiow, L.R., et al., *CD69 acts downstream of interferon-alpha/beta to inhibit S1P1 and lymphocyte egress from lymphoid organs*. Nature, 2006. **440**(7083): p. 540-4.

89. Yang, C.Y., et al., *Trapping of naive lymphocytes triggers rapid growth and remodeling of the fibroblast network in reactive murine lymph nodes*. Proc Natl Acad Sci U S A, 2014. **111**(1): p. E109-18.
90. Acton, S.E., et al., *Dendritic cells control fibroblastic reticular network tension and lymph node expansion*. Nature, 2014. **514**(7523): p. 498-502.
91. Junt, T., et al., *Expression of lymphotoxin beta governs immunity at two distinct levels*. Eur J Immunol, 2006. **36**(8): p. 2061-75.
92. Tumanov, A.V., et al., *Dissecting the role of lymphotoxin in lymphoid organs by conditional targeting*. Immunol Rev, 2003. **195**: p. 106-16.
93. Junt, T., et al., *Antiviral immune responses in the absence of organized lymphoid T cell zones in plt/plt mice*. J Immunol, 2002. **168**(12): p. 6032-40.
94. Junt, T., et al., *Impact of CCR7 on priming and distribution of antiviral effector and memory CTL*. J Immunol, 2004. **173**(11): p. 6684-93.
95. Kursar, M., et al., *Differential requirements for the chemokine receptor CCR7 in T cell activation during Listeria monocytogenes infection*. J Exp Med, 2005. **201**(9): p. 1447-57.
96. Mori, S., et al., *Mice lacking expression of the chemokines CCL21-ser and CCL19 (plt mice) demonstrate delayed but enhanced T cell immune responses*. J Exp Med, 2001. **193**(2): p. 207-18.
97. Yasuda, T., et al., *Chemokines CCL19 and CCL21 promote activation-induced cell death of antigen-responding T cells*. Blood, 2007. **109**(2): p. 449-56.
98. St John, A.L. and S.N. Abraham, *Salmonella disrupts lymph node architecture by TLR4-mediated suppression of homeostatic chemokines*. Nat Med, 2009. **15**(11): p. 1259-65.
99. Poltorak, A., et al., *Defective LPS signaling in C3H/HeJ and C57BL/10ScCr mice: mutations in Tlr4 gene*. Science, 1998. **282**(5396): p. 2085-8.
100. Janssens, S. and R. Beyaert, *Role of Toll-like receptors in pathogen recognition*. Clin Microbiol Rev, 2003. **16**(4): p. 637-46.
101. Park, B.S., et al., *The structural basis of lipopolysaccharide recognition by the TLR4-MD-2 complex*. Nature, 2009. **458**(7242): p. 1191-5.
102. Lizundia, R., et al., *Host species-specific usage of the TLR4-LPS receptor complex*. Innate Immun, 2008. **14**(4): p. 223-31.
103. Doyle, S.L. and L.A. O'Neill, *Toll-like receptors: from the discovery of NFkappaB to new insights into transcriptional regulations in innate immunity*. Biochem Pharmacol, 2006. **72**(9): p. 1102-13.
104. Zepp, F., *Principles of vaccine design-Lessons from nature*. Vaccine. **28 Suppl 3**: p. C14-24.
105. Moser, M. and O. Leo, *Key concepts in immunology*. Vaccine, 2010. **28 Suppl 3**: p. C2-13.
106. Garlapati, S., *Do we know the Th1/Th2/Th17 determinants of vaccine response?* Expert Rev Vaccines, 2012. **11**(11): p. 1307-10.
107. Saltzman, W.M., et al., *DNA vaccines methods and protocols*, in *Methods in molecular medicine 127*. 2006, Humana Press: Totowa, N.J. p. xv, 384 p.
108. Cockburn, W.C., *The use of mixed diphtheria-pertussis-tetanus antigens*. Bull

- World Health Organ, 1955. **13**(3): p. 409-22.
109. Ramon, G., *Sur l'augmentation anormale de l'antitoxine chez les chevaux producteurs de serum antidiptérique*. Bull. Soc. Centr. Med. Vet, 1925. **101**: p. 227-234.
 110. Glenny AT, P.C., Waddington H, Wallace V. , *The antigenic value of toxoid precipitated by potassium-alum*. J. Path. Bacteriol, 1926. **29**: p. 38-45.
 111. Opie, E.L. and J. Freund, *An Experimental Study of Protective Inoculation with Heat Killed Tubercle Bacilli*. J Exp Med, 1937. **66**(6): p. 761-88.
 112. O'Neill, L.A., *How Toll-like receptors signal: what we know and what we don't know*. Curr Opin Immunol, 2006. **18**(1): p. 3-9.
 113. Coffman, R.L., A. Sher, and R.A. Seder, *Vaccine adjuvants: putting innate immunity to work*. Immunity. **33**(4): p. 492-503.
 114. Gupta, R.K., et al., *Adjuvant properties of aluminum and calcium compounds*. Pharm Biotechnol, 1995. **6**: p. 229-48.
 115. Marrack, P., A.S. McKee, and M.W. Munks, *Towards an understanding of the adjuvant action of aluminium*. Nat Rev Immunol, 2009. **9**(4): p. 287-93.
 116. Mannhalter, J.W., et al., *Modulation of the human immune response by the non-toxic and non-pyrogenic adjuvant aluminium hydroxide: effect on antigen uptake and antigen presentation*. Clin Exp Immunol, 1985. **61**(1): p. 143-51.
 117. Kool, M., et al., *Alum adjuvant boosts adaptive immunity by inducing uric acid and activating inflammatory dendritic cells*. J Exp Med, 2008. **205**(4): p. 869-82.
 118. Schnare, M., et al., *Toll-like receptors control activation of adaptive immune responses*. Nat Immunol, 2001. **2**(10): p. 947-50.
 119. Gavin, A.L., et al., *Adjuvant-enhanced antibody responses in the absence of toll-like receptor signaling*. Science, 2006. **314**(5807): p. 1936-8.
 120. Eisenbarth, S.C., et al., *Crucial role for the Nalp3 inflammasome in the immunostimulatory properties of aluminium adjuvants*. Nature, 2008. **453**(7198): p. 1122-6.
 121. Li, H., et al., *Cutting edge: inflammasome activation by alum and alum's adjuvant effect are mediated by NLRP3*. J Immunol, 2008. **181**(1): p. 17-21.
 122. Hornung, V., et al., *Silica crystals and aluminum salts activate the NALP3 inflammasome through phagosomal destabilization*. Nat Immunol, 2008. **9**(8): p. 847-56.
 123. Grun, J.L. and P.H. Maurer, *Different T helper cell subsets elicited in mice utilizing two different adjuvant vehicles: the role of endogenous interleukin 1 in proliferative responses*. Cell Immunol, 1989. **121**(1): p. 134-45.
 124. Kopf, M., et al., *Disruption of the murine IL-4 gene blocks Th2 cytokine responses*. Nature, 1993. **362**(6417): p. 245-8.
 125. Jordan, M.B., et al., *Promotion of B cell immune responses via an alum-induced myeloid cell population*. Science, 2004. **304**(5678): p. 1808-10.
 126. Wilson-Welder, J.H., et al., *Vaccine adjuvants: current challenges and future approaches*. J Pharm Sci, 2009. **98**(4): p. 1278-316.
 127. Daemen, T., et al., *Virosomes for antigen and DNA delivery*. Adv Drug Deliv

- Rev, 2005. **57**(3): p. 451-63.
128. Johansson, J., et al., *Identification of adjuvants that enhance the therapeutic antibody response to host IgE*. Vaccine, 2004. **22**(21-22): p. 2873-80.
 129. McNeela, E.A. and K.H. Mills, *Manipulating the immune system: humoral versus cell-mediated immunity*. Adv Drug Deliv Rev, 2001. **51**(1-3): p. 43-54.
 130. Giannini, S.L., et al., *Enhanced humoral and memory B cellular immunity using HPV16/18 L1 VLP vaccine formulated with the MPL/aluminium salt combination (AS04) compared to aluminium salt only*. Vaccine, 2006. **24**(33-34): p. 5937-49.
 131. Behzad, H., et al., *GLA-SE, a synthetic toll-like receptor 4 agonist, enhances T-cell responses to influenza vaccine in older adults*. J Infect Dis, 2012. **205**(3): p. 466-73.
 132. Desbien, A.L., et al., *Squalene emulsion potentiates the adjuvant activity of the TLR4 agonist, GLA, via inflammatory caspases, IL-18, and IFN-gamma*. Eur J Immunol, 2015. **45**(2): p. 407-17.
 133. Anderson, R.C., et al., *Physicochemical characterization and biological activity of synthetic TLR4 agonist formulations*. Colloids Surf B Biointerfaces, 2010. **75**(1): p. 123-32.
 134. Treanor, J.J., et al., *Evaluation of safety and immunogenicity of recombinant influenza hemagglutinin (H5/Indonesia/05/2005) formulated with and without a stable oil-in-water emulsion containing glucopyranosyl-lipid A (SE+GLA) adjuvant*. Vaccine, 2013. **31**(48): p. 5760-5.
 135. Vogel, F.R., *Immunologic adjuvants for modern vaccine formulations*. Ann N Y Acad Sci, 1995. **754**: p. 153-60.
 136. Claassen, E., et al., *Freund's complete adjuvant: an effective but disagreeable formula*. Res Immunol, 1992. **143**(5): p. 478-83; discussion 572.
 137. Feyerabend, S., et al., *Novel multi-peptide vaccination in Hla-A2+ hormone sensitive patients with biochemical relapse of prostate cancer*. Prostate, 2009. **69**(9): p. 917-27.
 138. Leffers, N., et al., *Immunization with a P53 synthetic long peptide vaccine induces P53-specific immune responses in ovarian cancer patients, a phase II trial*. Int J Cancer, 2009. **125**(9): p. 2104-13.
 139. Garcon, N., P. Chomez, and M. Van Mechelen, *GlaxoSmithKline Adjuvant Systems in vaccines: concepts, achievements and perspectives*. Expert Rev Vaccines, 2007. **6**(5): p. 723-39.
 140. Guy, B., *The perfect mix: recent progress in adjuvant research*. Nat Rev Microbiol, 2007. **5**(7): p. 505-17.
 141. Aguilar, J.C. and E.G. Rodriguez, *Vaccine adjuvants revisited*. Vaccine, 2007. **25**(19): p. 3752-62.
 142. Petrovsky, N. and J.C. Aguilar, *Vaccine adjuvants: current state and future trends*. Immunol Cell Biol, 2004. **82**(5): p. 488-96.
 143. Moser, C., et al., *Influenza virosomes as a combined vaccine carrier and adjuvant system for prophylactic and therapeutic immunizations*. Expert Rev Vaccines, 2007. **6**(5): p. 711-21.
 144. Kim, Y.J., et al., *Synthetic studies of complex immunostimulants from Quillaja*

- saponaria: synthesis of the potent clinical immunoadjuvant QS-21Aapi*. J Am Chem Soc, 2006. **128**(36): p. 11906-15.
145. Sanders, M.T., et al., *ISCOM-based vaccines: the second decade*. Immunol Cell Biol, 2005. **83**(2): p. 119-28.
 146. Ishii, K.J. and S. Akira, *Toll or toll-free adjuvant path toward the optimal vaccine development*. J Clin Immunol, 2007. **27**(4): p. 363-71.
 147. Jackson, D.C., et al., *A totally synthetic vaccine of generic structure that targets Toll-like receptor 2 on dendritic cells and promotes antibody or cytotoxic T cell responses*. Proc Natl Acad Sci U S A, 2004. **101**(43): p. 15440-5.
 148. Diwan, M., M. Tafaghodi, and J. Samuel, *Enhancement of immune responses by co-delivery of a CpG oligodeoxynucleotide and tetanus toxoid in biodegradable nanospheres*. J Control Release, 2002. **85**(1-3): p. 247-62.
 149. Ishii, K.J., et al., *CpG-activated Th1.2+ dendritic cells protect against lethal Listeria monocytogenes infection*. Eur J Immunol, 2005. **35**(8): p. 2397-405.
 150. Munoz, J.J., et al., *Biological activities of crystalline pertussigen from Bordetella pertussis*. Infect Immun, 1981. **33**(3): p. 820-6.
 151. Baqar, S., L.A. Applebee, and A.L. Bourgeois, *Immunogenicity and protective efficacy of a prototype Campylobacter killed whole-cell vaccine in mice*. Infect Immun, 1995. **63**(9): p. 3731-5.
 152. Elson, C.O., *Cholera toxin and its subunits as potential oral adjuvants*. Curr Top Microbiol Immunol, 1989. **146**: p. 29-33.
 153. Xiang, Z. and H.C. Ertl, *Manipulation of the immune response to a plasmid-encoded viral antigen by coinoculation with plasmids expressing cytokines*. Immunity, 1995. **2**(2): p. 129-35.
 154. Miyaki, S. and H. Asahara, *Macro view of microRNA function in osteoarthritis*. Nat Rev Rheumatol, 2012. **8**(9): p. 543-52.
 155. Guo, H., et al., *Mammalian microRNAs predominantly act to decrease target mRNA levels*. Nature, 2010. **466**(7308): p. 835-40.
 156. Lagos-Quintana, M., et al., *Identification of novel genes coding for small expressed RNAs*. Science, 2001. **294**(5543): p. 853-8.
 157. Han, J., et al., *The Drosha-DGCR8 complex in primary microRNA processing*. Genes Dev, 2004. **18**(24): p. 3016-27.
 158. Bohnsack, M.T., K. Czaplinski, and D. Gorlich, *Exportin 5 is a RanGTP-dependent dsRNA-binding protein that mediates nuclear export of pre-miRNAs*. RNA, 2004. **10**(2): p. 185-91.
 159. Chendrimada, T.P., et al., *TRBP recruits the Dicer complex to Ago2 for microRNA processing and gene silencing*. Nature, 2005. **436**(7051): p. 740-4.
 160. Kim, V.N., *MicroRNA biogenesis: coordinated cropping and dicing*. Nat Rev Mol Cell Biol, 2005. **6**(5): p. 376-85.
 161. Krol, J., I. Loedige, and W. Filipowicz, *The widespread regulation of microRNA biogenesis, function and decay*. Nat Rev Genet, 2010. **11**(9): p. 597-610.
 162. Yang, J.S., et al., *Widespread regulatory activity of vertebrate microRNA* species*. RNA, 2011. **17**(2): p. 312-26.
 163. Hammond, S.M., *An overview of microRNAs*. Adv Drug Deliv Rev, 2015. **87**: p.

3-14.

164. Gregory, R.I., et al., *Human RISC couples microRNA biogenesis and posttranscriptional gene silencing*. Cell, 2005. **123**(4): p. 631-40.
165. Meister, G., et al., *Human Argonaute2 mediates RNA cleavage targeted by miRNAs and siRNAs*. Mol Cell, 2004. **15**(2): p. 185-97.
166. Ma, J.B., K. Ye, and D.J. Patel, *Structural basis for overhang-specific small interfering RNA recognition by the PAZ domain*. Nature, 2004. **429**(6989): p. 318-22.
167. Parker, J.S., S.M. Roe, and D. Barford, *Crystal structure of a PIWI protein suggests mechanisms for siRNA recognition and slicer activity*. EMBO J, 2004. **23**(24): p. 4727-37.
168. Grimson, A., et al., *MicroRNA targeting specificity in mammals: determinants beyond seed pairing*. Mol Cell, 2007. **27**(1): p. 91-105.
169. Breving, K. and A. Esquela-Kerscher, *The complexities of microRNA regulation: mirandering around the rules*. Int J Biochem Cell Biol, 2010. **42**(8): p. 1316-29.
170. Cheng, H.Y., et al., *microRNA modulation of circadian-clock period and entrainment*. Neuron, 2007. **54**(5): p. 813-29.
171. Hancock, M.L., et al., *MicroRNA-132 is enriched in developing axons, locally regulates Rasaf1 mRNA, and promotes axon extension*. J Neurosci, 2014. **34**(1): p. 66-78.
172. Hanieh, H. and A. Alzahrani, *MicroRNA-132 suppresses autoimmune encephalomyelitis by inducing cholinergic anti-inflammation: a new Ahr-based exploration*. Eur J Immunol, 2013. **43**(10): p. 2771-82.
173. Wanet, A., et al., *miR-212/132 expression and functions: within and beyond the neuronal compartment*. Nucleic Acids Res, 2012. **40**(11): p. 4742-53.
174. Wayman, G.A., et al., *An activity-regulated microRNA controls dendritic plasticity by down-regulating p250GAP*. Proc Natl Acad Sci U S A, 2008. **105**(26): p. 9093-8.
175. Vo, N., et al., *A cAMP-response element binding protein-induced microRNA regulates neuronal morphogenesis*. Proc Natl Acad Sci U S A, 2005. **102**(45): p. 16426-31.
176. Conaco, C., et al., *Reciprocal actions of REST and a microRNA promote neuronal identity*. Proc Natl Acad Sci U S A, 2006. **103**(7): p. 2422-7.
177. Taganov, K.D., et al., *NF-kappaB-dependent induction of microRNA miR-146, an inhibitor targeted to signaling proteins of innate immune responses*. Proc Natl Acad Sci U S A, 2006. **103**(33): p. 12481-6.
178. O'Neill, L.A., F.J. Sheedy, and C.E. McCoy, *MicroRNAs: the fine-tuners of Toll-like receptor signalling*. Nat Rev Immunol, 2011. **11**(3): p. 163-75.
179. Soreq, H. and Y. Wolf, *NeurimmiRs: microRNAs in the neuroimmune interface*. Trends Mol Med, 2011. **17**(10): p. 548-55.
180. Shaked, I., et al., *MicroRNA-132 potentiates cholinergic anti-inflammatory signaling by targeting acetylcholinesterase*. Immunity, 2009. **31**(6): p. 965-73.
181. Ucar, A., et al., *miR-212 and miR-132 are required for epithelial stromal*

- interactions necessary for mouse mammary gland development.* Nat Genet, 2010. **42**(12): p. 1101-8.
182. Molnar, V., et al., *MicroRNA-132 targets HB-EGF upon IgE-mediated activation in murine and human mast cells.* Cell Mol Life Sci, 2012. **69**(5): p. 793-808.
183. Huang, Y., et al., *MicroRNA regulation of STAT4 protein expression: rapid and sensitive modulation of IL-12 signaling in human natural killer cells.* Blood, 2011. **118**(26): p. 6793-802.
184. Lagos, D., et al., *miR-132 regulates antiviral innate immunity through suppression of the p300 transcriptional co-activator.* Nat Cell Biol, 2010. **12**(5): p. 513-9.
185. Magill, S.T., et al., *microRNA-132 regulates dendritic growth and arborization of newborn neurons in the adult hippocampus.* Proc Natl Acad Sci U S A, 2010. **107**(47): p. 20382-7.
186. Buch, T., et al., *A Cre-inducible diphtheria toxin receptor mediates cell lineage ablation after toxin administration.* Nat Methods, 2005. **2**(6): p. 419-26.
187. Kamala, T., *Hock immunization: a humane alternative to mouse footpad injections.* J Immunol Methods, 2007. **328**(1-2): p. 204-14.
188. Fletcher, A.L., et al., *Reproducible isolation of lymph node stromal cells reveals site-dependent differences in fibroblastic reticular cells.* Front Immunol. **2**: p. 35.
189. Soderberg, K.A., et al., *Innate control of adaptive immunity via remodeling of lymph node feed arteriole.* Proc Natl Acad Sci U S A, 2005. **102**(45): p. 16315-20.
190. Arbones, M.L., et al., *Lymphocyte homing and leukocyte rolling and migration are impaired in L-selectin-deficient mice.* Immunity, 1994. **1**(4): p. 247-60.
191. Berlin-Rufenach, C., et al., *Lymphocyte migration in lymphocyte function-associated antigen (LFA)-1-deficient mice.* J Exp Med, 1999. **189**(9): p. 1467-78.
192. Hall, J.G. and B. Morris, *The immediate effect of antigens on the cell output of a lymph node.* Br J Exp Pathol, 1965. **46**(4): p. 450-4.
193. Anderson, A.O. and N.D. Anderson, *Studies on the structure and permeability of the microvasculature in normal rat lymph nodes.* Am J Pathol, 1975. **80**(3): p. 387-418.
194. Webster, B., et al., *Regulation of lymph node vascular growth by dendritic cells.* J Exp Med, 2006. **203**(8): p. 1903-13.
195. Benahmed, F., et al., *Multiple CD11c+ cells collaboratively express IL-1beta to modulate stromal vascular endothelial growth factor and lymph node vascular-stromal growth.* J Immunol, 2014. **192**(9): p. 4153-63.
196. Kumar, V., et al., *Global lymphoid tissue remodeling during a viral infection is orchestrated by a B cell-lymphotoxin-dependent pathway.* Blood. **115**(23): p. 4725-33.
197. Van den Broeck, W., A. Derore, and P. Simoons, *Anatomy and nomenclature of murine lymph nodes: Descriptive study and nomenclatory standardization in BALB/cAnNCrl mice.* J Immunol Methods, 2006. **312**(1-2): p. 12-9.

198. Probst, H.C., et al., *Histological analysis of CD11c-DTR/GFP mice after in vivo depletion of dendritic cells*. Clin Exp Immunol, 2005. **141**(3): p. 398-404.
199. Onder, L., et al., *IL-7-producing stromal cells are critical for lymph node remodeling*. Blood.
200. Gordon, S., *The macrophage: past, present and future*. Eur J Immunol, 2007. **37 Suppl 1**: p. S9-17.
201. Gray, E.E. and J.G. Cyster, *Lymph node macrophages*. J Innate Immun, 2012. **4**(5-6): p. 424-36.
202. Szakal, A.K., K.L. Holmes, and J.G. Tew, *Transport of immune complexes from the subcapsular sinus to lymph node follicles on the surface of nonphagocytic cells, including cells with dendritic morphology*. J Immunol, 1983. **131**(4): p. 1714-27.
203. Moseman, E.A., et al., *B cell maintenance of subcapsular sinus macrophages protects against a fatal viral infection independent of adaptive immunity*. Immunity, 2012. **36**(3): p. 415-26.
204. Honke, N., et al., *Enforced viral replication activates adaptive immunity and is essential for the control of a cytopathic virus*. Nat Immunol, 2012. **13**(1): p. 51-7.
205. Fink, K., et al., *Depletion of macrophages in mice results in higher dengue virus titers and highlights the role of macrophages for virus control*. Eur J Immunol, 2009. **39**(10): p. 2809-21.
206. Schmitz, J.L., et al., *Beta interferon inhibits Toxoplasma gondii growth in human monocyte-derived macrophages*. Infect Immun, 1989. **57**(10): p. 3254-6.
207. Fossum, S. and J.L. Vaaland, *The architecture of rat lymph nodes. I. Combined light and electron microscopy of lymph node cell types*. Anat Embryol (Berl), 1983. **167**(2): p. 229-46.
208. Steer, H.W. and R.A. Foot, *Changes in the medulla of the parathyroid lymph nodes of the rat during acute gastro-intestinal inflammation*. J Anat, 1987. **152**: p. 23-36.
209. Roozendaal, R., et al., *Conduits mediate transport of low-molecular-weight antigen to lymph node follicles*. Immunity, 2009. **30**(2): p. 264-76.
210. Carrasco, Y.R. and F.D. Batista, *B cells acquire particulate antigen in a macrophage-rich area at the boundary between the follicle and the subcapsular sinus of the lymph node*. Immunity, 2007. **27**(1): p. 160-71.
211. Malumbres, R., et al., *Differentiation stage-specific expression of microRNAs in B lymphocytes and diffuse large B-cell lymphomas*. Blood, 2009. **113**(16): p. 3754-64.
212. Basso, K., et al., *Identification of the human mature B cell miRNome*. Immunity, 2009. **30**(5): p. 744-52.
213. Zhang, J., et al., *Patterns of microRNA expression characterize stages of human B-cell differentiation*. Blood, 2009. **113**(19): p. 4586-94.
214. Neilson, J.R., et al., *Dynamic regulation of miRNA expression in ordered stages of cellular development*. Genes Dev, 2007. **21**(5): p. 578-89.
215. Calin, G.A., et al., *Frequent deletions and down-regulation of micro- RNA genes miR15 and miR16 at 13q14 in chronic lymphocytic leukemia*. Proc Natl Acad

- Sci U S A, 2002. **99**(24): p. 15524-9.
216. He, L., et al., *A microRNA polycistron as a potential human oncogene*. Nature, 2005. **435**(7043): p. 828-33.
 217. Koralov, S.B., et al., *Dicer ablation affects antibody diversity and cell survival in the B lymphocyte lineage*. Cell, 2008. **132**(5): p. 860-74.
 218. Rao, D.S., et al., *MicroRNA-34a perturbs B lymphocyte development by repressing the forkhead box transcription factor Foxp1*. Immunity, 2010. **33**(1): p. 48-59.
 219. Xiao, C., et al., *MiR-150 controls B cell differentiation by targeting the transcription factor c-Myb*. Cell, 2007. **131**(1): p. 146-59.
 220. de Yebenes, V.G., et al., *miR-181b negatively regulates activation-induced cytidine deaminase in B cells*. J Exp Med, 2008. **205**(10): p. 2199-206.
 221. Thai, T.H., et al., *Regulation of the germinal center response by microRNA-155*. Science, 2007. **316**(5824): p. 604-8.
 222. Mehta, A., et al., *The MicroRNA-132 and MicroRNA-212 Cluster Regulates Hematopoietic Stem Cell Maintenance and Survival with Age by Buffering FOXO3 Expression*. Immunity, 2015. **42**(6): p. 1021-32.
 223. Li, D., et al., *MicroRNA-132 enhances transition from inflammation to proliferation during wound healing*. J Clin Invest, 2015. **125**(8): p. 3008-26.
 224. Nahid, M.A., et al., *Regulation of TLR2-mediated tolerance and cross-tolerance through IRAK4 modulation by miR-132 and miR-212*. J Immunol, 2013. **190**(3): p. 1250-63.
 225. Nakahama, T., et al., *Aryl hydrocarbon receptor-mediated induction of the microRNA-132/212 cluster promotes interleukin-17-producing T-helper cell differentiation*. Proc Natl Acad Sci U S A, 2013. **110**(29): p. 11964-9.
 226. Anand, S., et al., *MicroRNA-132-mediated loss of p120RasGAP activates the endothelium to facilitate pathological angiogenesis*. Nat Med, 2010. **16**(8): p. 909-14.
 227. Jiang, X., et al., *Upregulation of the miR-212/132 cluster suppresses proliferation of human lung cancer cells*. Oncol Rep, 2015. **33**(2): p. 705-12.
 228. Zhang, Z.G., et al., *MiR-132 prohibits proliferation, invasion, migration, and metastasis in breast cancer by targeting HNI*. Biochem Biophys Res Commun, 2014. **454**(1): p. 109-14.
 229. Pede, V., et al., *CLL cells respond to B-Cell receptor stimulation with a microRNA/mRNA signature associated with MYC activation and cell cycle progression*. PLoS One, 2013. **8**(4): p. e60275.
 230. Tavolaro, S., et al., *Increased chronic lymphocytic leukemia proliferation upon IgM stimulation is sustained by the upregulation of miR-132 and miR-212*. Genes Chromosomes Cancer, 2015. **54**(4): p. 222-34.
 231. Mehta, A., et al., *The microRNA-212/132 cluster regulates B cell development by targeting Sox4*. J Exp Med, 2015. **212**(10): p. 1679-92.
 232. Wang, L., et al., *ERG-SOX4 interaction promotes epithelial-mesenchymal transition in prostate cancer cells*. Prostate, 2014. **74**(6): p. 647-58.
 233. Wang, L., et al., *SOX4 is associated with poor prognosis in prostate cancer and*

- promotes epithelial-mesenchymal transition in vitro*. Prostate Cancer Prostatic Dis, 2013. **16**(4): p. 301-7.
234. Zhang, J., et al., *SOX4 induces epithelial-mesenchymal transition and contributes to breast cancer progression*. Cancer Res, 2012. **72**(17): p. 4597-608.
 235. Li, Y., et al., *miR-132 inhibits lung cancer cell migration and invasion by targeting SOX4*. J Thorac Dis, 2015. **7**(9): p. 1563-9.
 236. Lin, S.C., Y.C. Lo, and H. Wu, *Helical assembly in the MyD88-IRAK4-IRAK2 complex in TLR/IL-1R signalling*. Nature, 2010. **465**(7300): p. 885-90.
 237. Nahid, M.A., M. Satoh, and E.K. Chan, *Mechanistic role of microRNA-146a in endotoxin-induced differential cross-regulation of TLR signaling*. J Immunol, 2011. **186**(3): p. 1723-34.
 238. Schumann, K., et al., *Immobilized chemokine fields and soluble chemokine gradients cooperatively shape migration patterns of dendritic cells*. Immunity, 2010. **32**(5): p. 703-13.
 239. Dogan, I., et al., *Multiple layers of B cell memory with different effector functions*. Nat Immunol, 2009. **10**(12): p. 1292-9.
 240. MacLennan, I.C., *Germinal centers*. Annu Rev Immunol, 1994. **12**: p. 117-39.
 241. Allen, C.D., et al., *Imaging of germinal center selection events during affinity maturation*. Science, 2007. **315**(5811): p. 528-31.
 242. Hauser, A.E., M.J. Shlomchik, and A.M. Haberman, *In vivo imaging studies shed light on germinal-centre development*. Nat Rev Immunol, 2007. **7**(7): p. 499-504.
 243. Stavnezer, J. and C.T. Amemiya, *Evolution of isotype switching*. Semin Immunol, 2004. **16**(4): p. 257-75.
 244. Conticello, S.G., et al., *Evolution of the AID/APOBEC family of polynucleotide (deoxy)cytidine deaminases*. Mol Biol Evol, 2005. **22**(2): p. 367-77.
 245. Muramatsu, M., et al., *Class switch recombination and hypermutation require activation-induced cytidine deaminase (AID), a potential RNA editing enzyme*. Cell, 2000. **102**(5): p. 553-63.
 246. Okada, T., et al., *Antigen-engaged B cells undergo chemotaxis toward the T zone and form motile conjugates with helper T cells*. PLoS Biol, 2005. **3**(6): p. e150.
 247. Allen, C.D., et al., *Germinal center dark and light zone organization is mediated by CXCR4 and CXCR5*. Nat Immunol, 2004. **5**(9): p. 943-52.
 248. Jacob, J., et al., *Intraclonal generation of antibody mutants in germinal centres*. Nature, 1991. **354**(6352): p. 389-92.
 249. Hardtke, S., L. Ohl, and R. Forster, *Balanced expression of CXCR5 and CCR7 on follicular T helper cells determines their transient positioning to lymph node follicles and is essential for efficient B-cell help*. Blood, 2005. **106**(6): p. 1924-31.
 250. Choi, Y.S., et al., *ICOS receptor instructs T follicular helper cell versus effector cell differentiation via induction of the transcriptional repressor Bcl6*. Immunity, 2011. **34**(6): p. 932-46.

251. Nurieva, R.I., et al., *Bcl6 mediates the development of T follicular helper cells*. Science, 2009. **325**(5943): p. 1001-5.
252. Cannons, J.L., et al., *Optimal germinal center responses require a multistage T cell:B cell adhesion process involving integrins, SLAM-associated protein, and CD84*. Immunity, 2010. **32**(2): p. 253-65.
253. Vanderleyden, I., M.A. Linterman, and K.G. Smith, *Regulatory T cells and control of the germinal centre response*. Arthritis Res Ther, 2014. **16**(5): p. 471.
254. Gitlin, A.D., Z. Shulman, and M.C. Nussenzweig, *Clonal selection in the germinal centre by regulated proliferation and hypermutation*. Nature, 2014. **509**(7502): p. 637-40.
255. Linterman, M.A., et al., *Foxp3+ follicular regulatory T cells control the germinal center response*. Nat Med, 2011. **17**(8): p. 975-82.
256. Heesters, B.A., R.C. Myers, and M.C. Carroll, *Follicular dendritic cells: dynamic antigen libraries*. Nat Rev Immunol, 2014. **14**(7): p. 495-504.
257. Calame, K.L., K.I. Lin, and C. Tunyaplin, *Regulatory mechanisms that determine the development and function of plasma cells*. Annu Rev Immunol, 2003. **21**: p. 205-30.
258. Ho, F., et al., *Distinct short-lived and long-lived antibody-producing cell populations*. Eur J Immunol, 1986. **16**(10): p. 1297-301.
259. Smith, K.G., et al., *The phenotype and fate of the antibody-forming cells of the splenic foci*. Eur J Immunol, 1996. **26**(2): p. 444-8.
260. Shaffer, A.L., et al., *Blimp-1 orchestrates plasma cell differentiation by extinguishing the mature B cell gene expression program*. Immunity, 2002. **17**(1): p. 51-62.
261. Hargreaves, D.C., et al., *A coordinated change in chemokine responsiveness guides plasma cell movements*. J Exp Med, 2001. **194**(1): p. 45-56.
262. Cyster, J.G., *Homing of antibody secreting cells*. Immunol Rev, 2003. **194**: p. 48-60.
263. Fooksman, D.R., et al., *Development and migration of plasma cells in the mouse lymph node*. Immunity, 2010. **33**(1): p. 118-27.
264. Mohr, E., et al., *Dendritic cells and monocyte/macrophages that create the IL-6/APRIL-rich lymph node microenvironments where plasmablasts mature*. J Immunol, 2009. **182**(4): p. 2113-23.
265. Pappu, R., et al., *Promotion of lymphocyte egress into blood and lymph by distinct sources of sphingosine-1-phosphate*. Science, 2007. **316**(5822): p. 295-8.
266. Rajewsky, K., *Clonal selection and learning in the antibody system*. Nature, 1996. **381**(6585): p. 751-8.
267. Allison, A.C., *Interactions of antibodies, complement components and various cell types in immunity against viruses and pyogenic bacteria*. Transplant Rev, 1974. **19**(0): p. 3-55.
268. Stavnezer, J., *Antibody class switching*. Adv Immunol, 1996. **61**: p. 79-146.
269. Delphin, S. and J. Stavnezer, *Regulation of antibody class switching to IgE: characterization of an IL-4-responsive region in the immunoglobulin heavy-*

chain germline epsilon promoter. Ann N Y Acad Sci, 1995. **764**: p. 123-35.

270. Leonov, G., et al., *Suppression of AGO2 by miR-132 as a determinant of miRNA-mediated silencing in human primary endothelial cells*. Int J Biochem Cell Biol, 2015. **69**: p. 75-84.
271. Offersen, R., et al., *A novel toll-like receptor-9 agonist, MGN1703, enhances HIV-1 transcription and NK cell-mediated inhibition of HIV-1 infected autologous CD4+ T cells*. J Virol, 2016.